

R-5061

FACILITY FORM 802

N64-27803	
(ACCESSION NUMBER)	
257	
(PAGES)	
CR-58034	
(NASA CR OR TRR OR AD NUMBER)	
	(THRU)
	1
	(CODE)
	29
	(CATEGORY)



ROCKETDYNE • A DIVISION OF NORTH AMERICAN AVIATION INC

257P
NASA CONTRACT: NAS 7-124
FINAL REPORT FEBRUARY 1963

PROPELLION REQUIREMENTS

FOR SUBORBITAL FLIGHTS

In Extraterrestrial Landing Environments

VOLUME II A

OTS PRICE

XEROX

\$

MICROFILM

\$

R-5061

**Propulsion Requirements for
Soft Landing in
Extraterrestrial Environments**

Final Report

February 1963

NAS 7-124

Volume 2 A

**Prepared for
National Aeronautics and Space Administration**

NASA Headquarters

Mr. H. Burlage

Ames Research Center

Mr. H. Hornby

**Prepared by
Advanced Systems Section**

Mart S. Bensky

M. S. Bensky

Responsible Engineer

Approved by:

S. F. Iacobellis

**S. F. Iacobellis
Section Chief
Advanced Systems**

FOREWORD

This document was prepared in compliance with the requirement for the final report for National Aeronautics and Space Administration contract NAS 7-124, "Propulsion Requirements for Soft Landing in Extraterrestrial Environments."

ABSTRACT

Volumes IIA and IIB, "Propulsion Requirements for Soft Landing in Extraterrestrial Environments," present the analyses conducted under NASA Contract NAS 7-124. Landing trajectory concepts applicable to landings on the moon, Mars, Venus, Mercury and the Earth were analyzed to define the required propulsive maneuvers and to determine the optimum characteristics of propulsion systems for performance of these maneuvers. Related investigations presented herein were conducted to determine appropriate interplanetary trajectories upon which to base landing analyses and to evaluate takeoff propulsion requirements.

27803
Author

TABLE OF CONTENTS - VOLUME IIA

	Page
FOREWORD	i
ABSTRACT	i
TABLE OF CONTENTS	ii
INTRODUCTION	1
LANDING MISSION CONCEPTS	2
Factor Affecting Landing Analysis	2
Landing Maneuvers	4
Deceleration Methods	11
EARTH RETURN MISSIONS	17
Atmospheric Entry and Terminal Correction Requirements	17
Propulsive Earth Orbit Establishment and Departure Maneuvers	48
Earth Atmospheric Graze Maneuvers	86
Propulsive/Aerodynamic Deceleration for Direct Earth Landing	104
Earth Terminal Deceleration Phase Systems	140
EARTH-MARS MISSIONS	160
Mars Trajectory Selection	160
Terminal Corrections for Earth-Mars Trajectories	162
Propulsive Mars Orbit Establishment and Departure Maneuvers	176
Mars Orbit Establishment Following an Atmospheric Graze	176
Propulsive/Aerodynamic Braking Maneuver for Mars Entry	192
Mars Terminal Deceleration Phase Systems	192
Mars Propulsive Takeoff and Landing	203

EARTH-VENUS MISSIONS	Page 209
Trajectory Selection	209
Terminal Corrections for Earth-Venus Trajectories	209
Propulsive Venus Orbit Establishment and Departure Maneuvers	222
Venus Orbit Establishment Following an Atmospheric Graze	222
Propulsive/Aerodynamic Braking Maneuver for Venus Entry	229
Venus Terminal Deceleration Phase Systems	229
Venus Takeoff Propulsion Requirements	246
REFERENCES	250

TABLE OF CONTENTS - VOLUME IIB

FOREWORD	i
ABSTRACT	i
TABLE OF CONTENTS	ii
INTRODUCTION	1
LUNAR MISSIONS	2
Initial and Midphase Maneuvers	2
Landing and Takeoff Trajectories	13
Lunar Landing and Takeoff Propulsion Requirements	34
Error Analysis for Lunar Landing-from-Orbit Maneuver	96
Mission Abort	109
Near-Surface Translation	129
Final Descent Phase of a Lunar Landing	153
Touchdown Stability	163

EARTH-MERCURY MISSIONS	Page 174
Transfer Phase	174
Mercury Orbit Establishment	178
Orbital Landing and Takeoff	196
Error Analysis for Mercury Landing-from-Orbit Maneuver	204
ENGINE PARAMETER OPTIMIZATION	216
Selection of Propulsion System Characteristics	216
Effect of Assumptions	220
Propulsion Parameters	223
REFERENCES	242

INTRODUCTION

Presented in this volume are the analyses conducted and results obtained in the study, "Propulsion Requirements for Soft Landing in Extraterrestrial Environments." The study was performed (1) to define the most suitable landing concepts for landings on Mars, Venus, Mercury, Earth and the moon, in order to specify the required propulsive phases, and (2) to determine the optimum characteristics of propulsion systems for these propulsive phases.

Analysis of landings on these bodies entailed initially the selection of appropriate transfer trajectories and consequent planetary arrival conditions; these results provided the applicable initial conditions upon which to base subsequent studies of landing maneuvers. The sequence of maneuvers comprising an extraterrestrial landing operation was dependent primarily on the presence or absence of an atmosphere about the destination body. As a result, the landing maneuver profiles were qualitatively, though not quantitatively, similar for the all-propulsive lunar and Mercury landings, and for the Earth, Mars and Venus landings, which utilized the atmospheres of those bodies for a major part of the required vehicle deceleration.

For a landing mission as defined in this study, the first in the chronological sequence of propulsive and aerodynamic maneuvers considered for terrestrial and extraterrestrial landing phase analyses was the propulsive terminal correction utilized to establish the initial conditions required for safe entry into a planetary atmosphere or deceleration into a prescribed planetocentric circular orbit. This maneuver, in preference to earlier (e.g., midcourse correction) or later (e.g., deceleration into orbit) maneuvers was chosen, first, because it is essential to satisfactory performance of any subsequent maneuvers, and second, because it is the earliest maneuver primarily influenced by the gravitational field of the destination planet.

Subsequent to the terminal correction, the maneuvers considered for planets having atmospheres were: orbit-establishment, with or without aerodynamic drag providing a portion of the required deceleration; direct atmospheric entry; and near-surface deceleration and maneuvering by means of parachute/retrorocket systems. For Mercury and the moon, neither of which has an atmosphere, the maneuvers of interest were direct landing, or alternatively, orbit-establishment and landing-from-orbit, and propulsive near-surface translation and descent.

The basic results of the study were the definition of the propulsive maneuvers associated with landings on each of the destination bodies, and specification of the velocity requirements and optimum propulsion system parameters for these maneuvers.

LANDING MISSION CONCEPTS

FACTORS AFFECTING LANDING ANALYSIS

Transfer Phase and Planetary Environment

A lunar or interplanetary round-trip mission is comprised of a sequence of closely interrelated propulsive and nonpropulsive phases which can be described broadly by the chart in Figure 1. The objective of this program was an investigation of terrestrial and extraterrestrial landings. However, the landing investigations require analyses or review of the mission phases which precede and follow the landing phase to adequately provide data for comprehensive investigation of the landing phase. With the exception of landing-from-orbit and takeoff-to-orbit maneuvers, the trajectory and vehicle characteristics of any portion of an overall space vehicle system cannot be optimized without consideration of other aspects of the vehicle and mission. Therefore, with the discussions of the discrete phases of planetary landings, the necessary descriptions of interplanetary trajectories and planetary takeoff requirements are included.

Representative interplanetary trajectories, related to the landing missions considered, are described as part of a planet-by-planet presentation of extraterrestrial landing and takeoff analyses. For each planet, the landing mission is characterized by a sequence of maneuvers; the nature of these maneuvers is governed primarily by the presence or absence of an atmosphere about the subject planet. For example, a lunar landing must be entirely propulsive and therefore entails a major deceleration phase, either from orbit or from a transfer trajectory, a hover/translation phase and a vertical descent phase, all of which are rocket-powered. The corresponding portions of a Mars landing utilize aerodynamic vehicle drag for most of the required velocity cancellation, parachute drag for further deceleration and maneuvering, and possibly a small rocket for a final small amount of deceleration prior to impact.

Propulsion System

The principal objective of maneuver analysis was the determination of velocity requirements and optimum thrust-to-weight ratios for each of the propulsive maneuvers considered. It should be noted that each of these parameters is affected by propulsion system or vehicle characteristics for which accurate specific values are known only approximately at best.

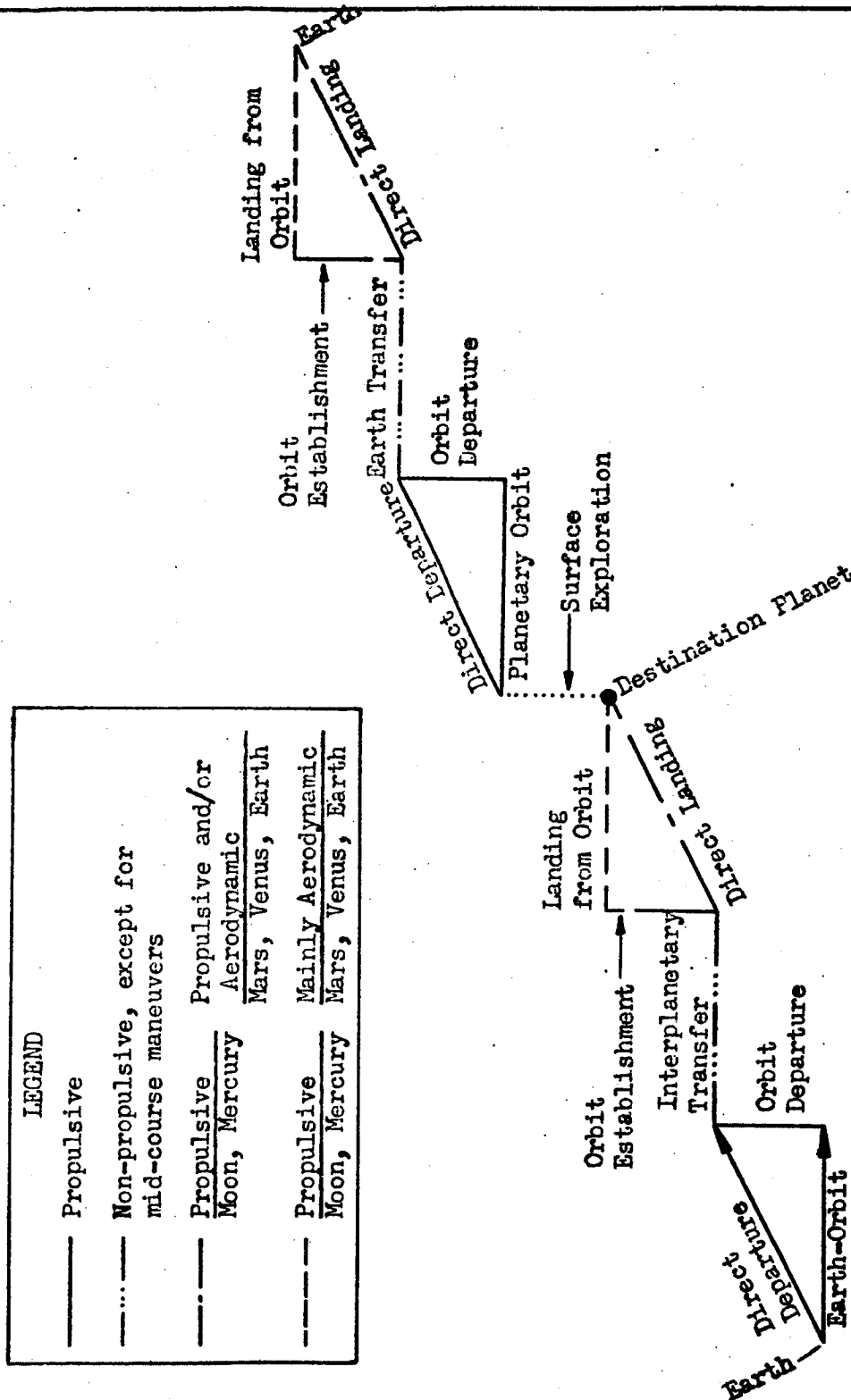


Figure 1 . Interplanetary Missions

Examples of such parameters include specific impulse, interplanetary transfer duration, propellant tank weight and engine weight. Of these, the latter is the most significant in thrust-to-weight (F/W) optimizations, and is therefore treated parametrically in F/W optimization analyses. The others do not generally have sufficient influence on optimum F/W to warrant parametric treatment; fixed values are usually selected for analyses, based on representative engine and vehicle characteristics.

Thus in the data presented, the specific impulse of a propulsion system intended to be representative of an O_2/H_2 system might range between 400 and 440 seconds. The precise value, as indicated in Figure 2, is dependent on chamber pressure, mixture ratio and expansion area ratio (and on combustion efficiency, nozzle efficiency and engine type), but since knowledge of the precise value of specific impulse has negligible bearing on velocity requirements or F/W optimization, the selection of detailed engine operating parameters was reserved for separate study. Similarly, noncryogenic propellants are represented by specific impulse values between 300 and 325 seconds, though in fact the precise value is determined by specific engine characteristics.

LANDING MANEUVERS

The major deceleration phase of an extraterrestrial landing may be accomplished in a single maneuver directly from the approach trajectory or by a sequence of two maneuvers in which the vehicle first decelerates into an orbit about the destination body and subsequently descends to the surface. The approach velocity can range from a value slightly in excess of the local planetocentric parabolic velocity, as in the case of an elliptic Earth-Moon trajectory, to several times parabolic velocity, as for fast, hyperbolic, interplanetary trajectories. Both the type of landing trajectory selected and the type of devices employed for decelerating the vehicle are strongly dependent on the presence or absence of an atmosphere about the destination body.

Direct Landings

A direct landing from supersatellite velocity can be performed in several ways. These trajectories have been divided into three major types:

1. Direct Vertical Landing

For this type of landing, the vehicle approaches the destination planet along a vertical flight path. Propulsion is applied at the correct altitude to brake the vehicle for the landing, or, if the destination planet has an atmosphere, no propulsion is applied and aerodynamic drag slows the vehicle.

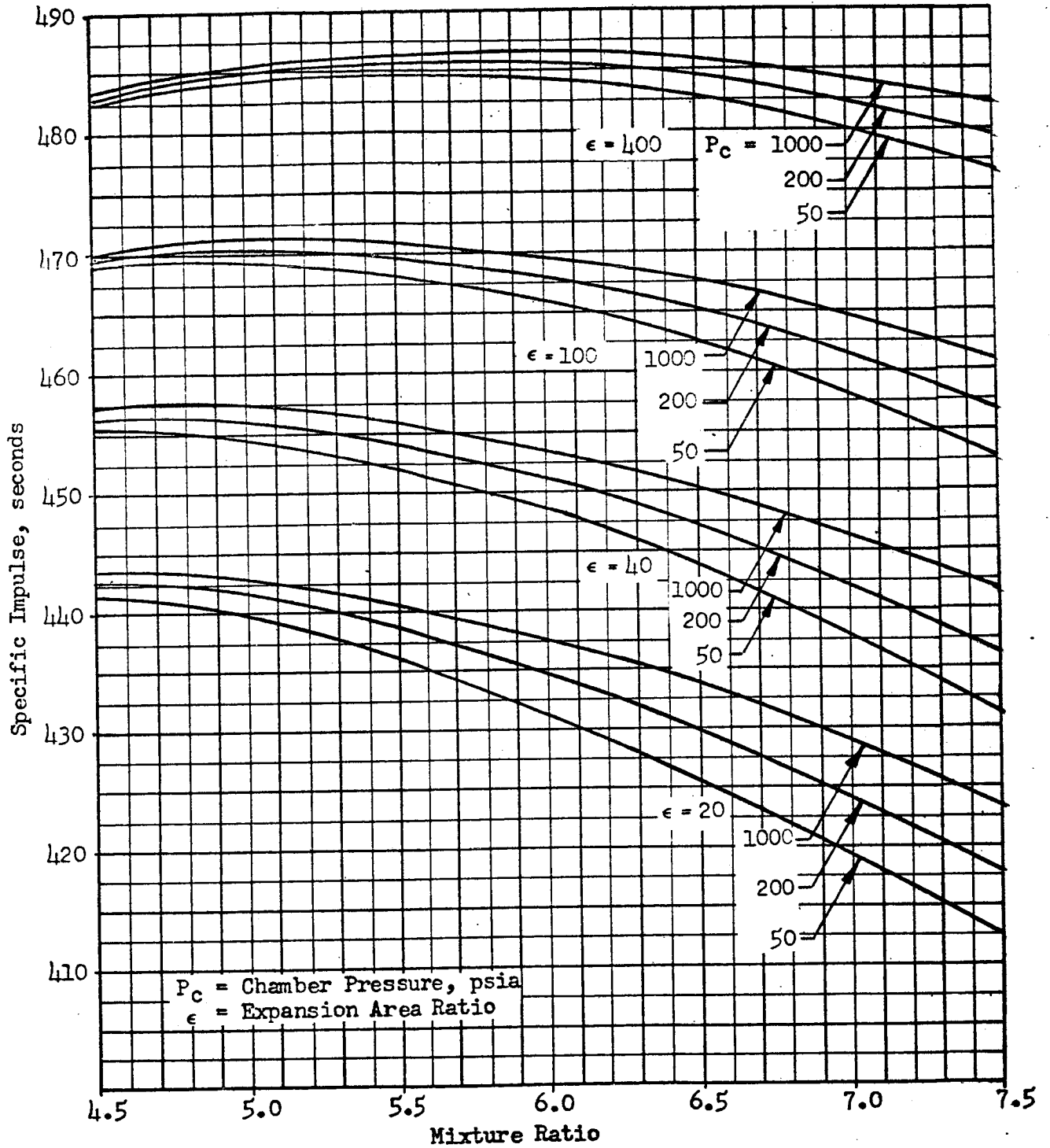


Figure 2. Theoretical Shifting Equilibrium Performance for O_2/H_2
Vacuum Conditions

2. Direct Nonvertical Landing

The vehicle approaches on a parabolic or hyperbolic path which is somewhat displaced from a vertical landing approach trajectory, and would, in the absence of a planetary atmosphere or a propulsive braking phase, bypass, or impact obliquely, the destination planet. Propulsion or aerodynamic braking slows the vehicle for the landing. The nature of the approach flight path is selected to correspond to the characteristics of the landing vehicle.

3. Grazing Approach Landing

This landing trajectory type is for aerodynamic braking only. The approaching vehicle grazes the planetary atmosphere, and then, slowed by drag during the graze, again leaves the atmosphere. Subsequently, the vehicle may circle the planet in an elliptical orbit before again entering the atmosphere or, if it has been slowed sufficiently, reenter after only a short skip out of the atmosphere. One or more grazes may be necessary before the vehicle is slowed to a velocity suitable for the final braking entry.

A summary of aerodynamic and propulsive braking for the three types of landings from supersatellite velocity is presented in Figure 3. Of the three types considered, the direct nonvertical landing appears to be the concept best suited to extraterrestrial soft landings whether propulsive or aerodynamic braking is used.

Orbit Establishment From Supersatellite Velocity

The establishment of a parking orbit from the approach trajectory may be desirable in many missions. This aspect of landing trajectories has been divided into two major types.

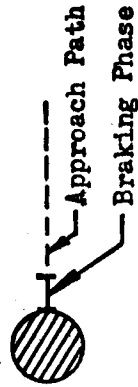
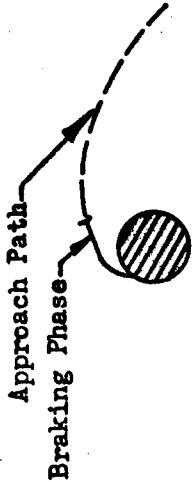
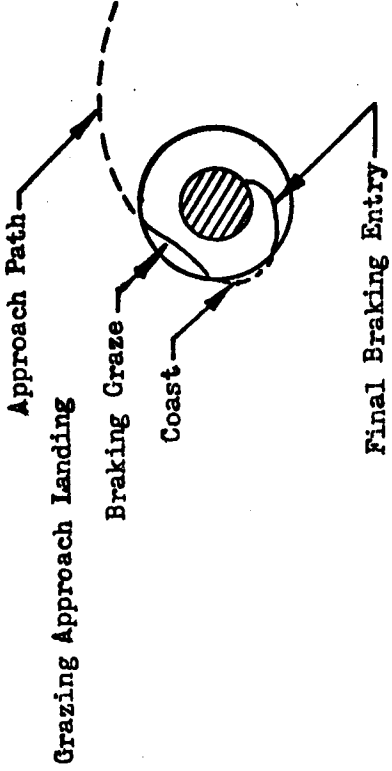
1. Direct Orbit Establishment

In this maneuver the vehicle, when it is in the vicinity of the target planet, is propulsively decelerated to orbit velocity.

2. Grazing Approach Establishment

In this maneuver, the vehicle grazes the atmosphere of the target planet. After the graze, the vehicle, slowed by drag during the graze, leaves the atmosphere. One or more of these grazes can be used to slow the vehicle so that it leaves

Figure 3 Direct Landing Summary

	<p>Direct Vertical Landing</p> 	<p>Direct NonVertical Landing</p> 	<p>Grazing Approach Landing</p> 																
Aerodynamic Braking Heating	<p>The 90-degree entry into the planetary atmosphere has the lowest total heat transfer but very high heat transfer rates. Because of the high heat transfer rates, ablative or heat sink protection would be more suitable than radiation cooling.</p>	<p>High surface temperatures occur (about 5000 R) which make radiation cooling impractical for Earth entry vehicles. Equilibrium and nonequilibrium radiation from hot gas cap may make any type of cooling difficult at hyperbolic velocities. A radiation cooled vehicle may be practical for a Mars entry where a 2500 R surface temperature is required for entry at escape velocity.</p>	<p>Heating rates may be low enough for earth entry at escape velocity so that the vehicle may be radiation cooled at a surface temperature below 4000 R during the graze. If several grazes are used, heat might be absorbed in each graze and radiated away during the flight outside the atmosphere between grazes. Heating during the final entry should be no more severe than that encountered in the graze.</p>																
Deceleration	<p>Very high decelerations. Over 300 G's for an Earth entry and about 18.3 Earth G's for a Mars entry (both from escape velocity).</p>	<p>Planetary landings with less than 10G's maximum deceleration are possible. Lift, even an L/D as low as $\frac{1}{2}$, will substantially lower deceleration over those encountered by a ballistic vehicle.</p>	<p>Deceleration during the graze would be at least $\frac{1}{2}$ G's for an Earth approach at escape velocity for a ballistic vehicle. During final braking entry, the deceleration would be higher (at least 10 G's).</p>																
Guidance	<p>The simple vertical approach should minimize guidance requirements.</p>	<p>Approach corridors decrease markedly as entry velocity increases. Lift and modulated L/D will increase entry corridor width. Guidance accuracy required for Earth entry at parabolic velocity is less severe than ICBM guidance accuracy requirements.</p> <table><tr><td colspan="4">Parabolic Approach Corridor Width (5 G's Maximum)</td></tr><tr><td colspan="4">Earth Landing</td></tr><tr><td>L/D = 0</td><td>L/D = 1</td><td>L/D = 1 Modulated</td><td></td></tr><tr><td>0 Miles</td><td>27 Miles</td><td>34 Miles</td><td></td></tr></table>	Parabolic Approach Corridor Width (5 G's Maximum)				Earth Landing				L/D = 0	L/D = 1	L/D = 1 Modulated		0 Miles	27 Miles	34 Miles		<p>It would be difficult to predict where, after the graze, the vehicle would again enter the atmosphere and therefore landing at a preselected site might be difficult.</p>
Parabolic Approach Corridor Width (5 G's Maximum)																			
Earth Landing																			
L/D = 0	L/D = 1	L/D = 1 Modulated																	
0 Miles	27 Miles	34 Miles																	
Propulsive Braking	<p>The vertical trajectory has high gravity losses unless the vehicle has a high thrust-to-weight ratio.</p>	<p>High ideal velocities are required. Escape velocity from the Earth is about 37,000 ft/sec and from the moon about 8000 ft/sec. Ignition and the blowing of the jet flame back against the vehicle might be problems for propulsive braking in an atmosphere.</p>	<p>This landing concept is for aerodynamic braking only.</p>																
Comments	<p>The only advantage of this concept is simple guidance. Poor abort capability and the high levels of heating rate and deceleration forces generally make this landing concept unsatisfactory.</p>		<p>Deceleration and heating rates are lower than encountered in a direct nonvertical aerodynamic landing, but the landing concept offers less accurate site selection than the direct landing. The grazing approach also has the disadvantages that the coasts between grazes may go through radiation belts which would be harmful for manned vehicles. The direct nonvertical landing concept appears superior to this concept.</p>																

the atmosphere with the approximate velocity of a low altitude planetary orbit. After the final graze, a short propulsive phase is utilized to establish a suitable orbit above the atmosphere.

Further comments on these two orbit-establishment methods are presented in Figure 4 . The grazing approach orbit establishment technique offers higher vehicle payload than does propulsive orbit establishment, since aerodynamic braking devices are generally lighter than propulsion systems for the same task. The grazing approach, however, is applicable only for planets with atmospheres and consequently, in some cases, propulsive orbit establishment must be selected.

Landing-From-Satellite Velocity

The descent-from-orbit phase of landing trajectories has been divided into two major types.

1. Orbit Decay Landing

If the orbit altitude is sufficiently low, the vehicle experiences aerodynamic drag, and the altitude of the orbit is slowly decreased. Subsequently, the vehicle enters dense enough atmosphere to introduce a period of high deceleration, and the vehicle is slowed for landing.

2. Direct Landing

In this landing concept, the vehicle is braked in orbit propulsively to initiate descent. If the planet has an atmosphere, the vehicle can enter the atmosphere and perform an aerodynamic landing.

Further comments on landing from satellite velocity are presented in Figure 5 . Of the two major trajectory types, direct landings would be the type used in most instances. Few applications, if any, would be found for orbit decay because of the difficulty in predicting time and place of descent.

Figure 4 Orbit Establishment Summary

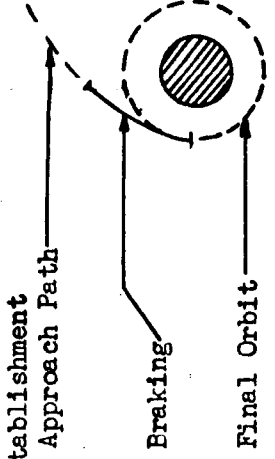
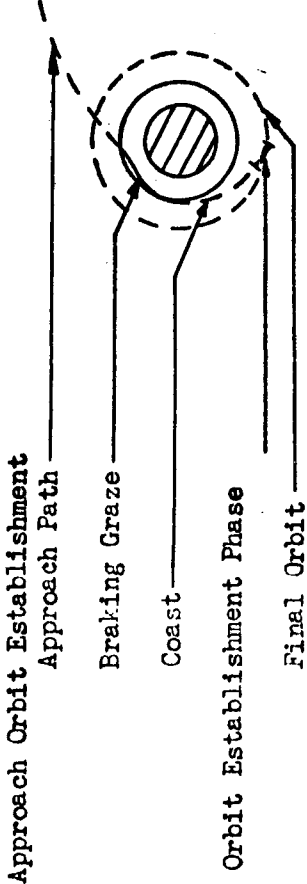
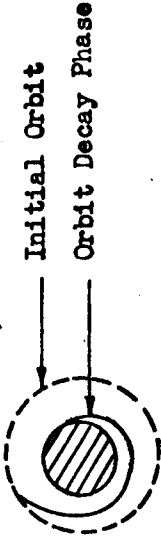
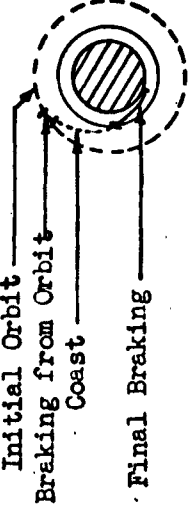
	<p>Direct Orbit Establishment</p>  <p>Approach Path</p> <p>Braking</p> <p>Final Orbit</p>	<p>Grazing Approach Orbit Establishment</p>  <p>Approach Path</p> <p>Braking Graze</p> <p>Coast</p> <p>Orbit Establishment Phase</p> <p>Final Orbit</p>
Aerodynamic Braking	<p>This orbit establishment concept is for propulsive braking only.</p>	<p>Heating rates for a braking graze in the Earth's atmosphere, initiated at escape velocity, may be low enough to allow the vehicle to be radiation-cooled at a surface temperature below 4000°R. Total heat, however, is high and increases rapidly as the entry velocity increases.</p>
Deceleration		<p>Deceleration for the braking graze, began at escape velocity in the Earth's atmosphere, could be limited to less than 10 G's.</p>
Guidance		<p>Errors in the braking graze should easily be correctable in the propulsive orbit establishment phase. If the orbit establishment propulsion capability were limited, however, very narrow entry corridors for the graze would result.</p>
Propulsive Braking	<p>Propulsive braking for establishment of a lunar orbit from an Earth-moon coast requires about 3300 ft/sec at a thrust-to-Earth weight of about 0.1. Establishment of an Earth orbit from a moon-Earth coast requires 10,200 ft/sec at a thrust-to-weight ratio of about 0.5. These ideal velocities indicate that a high percentage of a vehicle weight may be required to provide orbit establishment propulsion.</p>	<p>Propulsion would be required in the orbit injection phase of this orbit establishment concept. The ideal velocity requirement, however, should be low and a low thrust-to-weight (.01 to .1) should be optimum.</p>
Comments	<p>On a planet with little or no atmosphere (Moon, Mercury) this type of orbit establishment must be used. For planets with atmospheres aerodynamic braking should provide substantial payload improvement.</p>	<p>This method should substantially reduce propulsion requirements and provide higher payloads than an all-propulsive orbit establishment maneuver.</p>

Figure 5 Orbital Landing Summary

	<p>Orbit Decay Landing</p> 	<p>Direct Landing</p> 	
<p>Aerodynamic Braking</p> <p>Heating</p>	<p>Most of the heating occurs during the last phase of orbit decay which lasts only a few minutes. An equilibrium surface temperature of about 3600°R would be required to cool a non-lifting body by radiation for an Earth landing. Lift would decrease heating rate. Lower heating would result for a Mars entry (radiation equilibrium temperature equals 1900°R).</p>	<p>The maximum equilibrium surface temperature may not exceed 4000°R for Earth landing. Lift will reduce the maximum heating rate but will increase total heating. High angles of entry into the atmosphere will decrease total heat absorbed but increase maximum heat rate.</p>	
<p>Deceleration</p>	<p>A deceleration of less than 10 G's is experienced by a non-lifting body when entering from Earth orbit. Lift would lower the peak deceleration.</p>	<p>Deceleration will be at least 10 G's for an Earth landing for a ballistic vehicle. A lifting vehicle will have substantially less deceleration. Deceleration will increase as the entry angle into the atmosphere is increased.</p>	
<p>Guidance</p>	<p>The final orbit decay phase is preceded by a long period, possibly many revolutions, in which the satellite orbit decays gradually. It would be difficult to predict this long decay accurately enough to control landing site.</p>	<p>No problems should be encountered in this type of landing.</p>	
<p>Propulsive Braking</p>	<p>This landing concept is for aerodynamic braking only.</p>	<p>A propulsive phase is required for the braking from orbit when an aerodynamic entry is used. For a planet with no atmosphere, propulsion must also be used for the final braking. If desirable, the coast could be eliminated and only one propulsive phase, which brings the vehicle from orbit to the surface, could be used.</p>	
<p>Comments</p>	<p>The long period of gradual decay and the difficulty in predicting landing site would probably rule out this landing concept.</p>		

DECELERATION METHODS

Aerodynamic Landing

Determining a suitable entry corridor (Figure 6) is required for analysis of the landing trajectory for an aerodynamic landing vehicle. The entry corridor can be defined either by the use of entry angle (angle of the vehicle velocity vector when the vehicle is at a specified altitude above the atmosphere) or by virtual periapsis (the periapsis that the entry conic would have if there were no planetary atmosphere). The undershoot boundary (lowest periapsis or highest entry angle) and the overshoot boundary (highest periapsis or lowest entry angle) are the boundaries of the entry corridor, and the entry corridor is defined by an entry angle range or by a corridor depth (the difference between the virtual periapsis of the overshoot and undershoot boundaries).

If a vehicle enters into the atmosphere at too shallow an entry angle, it will not be slowed sufficiently to remain within the atmosphere. The entry angle of the overshoot boundary must therefore be high enough to prevent skipping out of the atmosphere. Entry on the overshoot boundary results in a higher total heat transfer to the vehicle than do steeper entries. The overshoot boundary entry angle must therefore also be high enough to prevent too high a total heat transfer to the vehicle.

On the undershoot boundary, the vehicle enters the atmosphere at a steeper angle than on the overshoot boundary. This results in higher decelerations and higher heat transfer rates. The undershoot boundary is therefore selected so that vehicle deceleration and heat transfer rate limits are not exceeded.

The entry corridor for a lifting vehicle is wider than that of a ballistic vehicle. Negative lift, up to an approximate lift-to-drag ratio (L/D) of 0.5, will increase the overshoot boundary height and positive lift, up to an L/D of approximately 2, will decrease the undershoot boundary height. A modulated L/D would further decrease the undershoot boundary.

The use of a vehicle bank angle to provide for lateral maneuvering increases heating rate and deceleration for an aerodynamic vehicle. For normal entry maneuvering, the effects should not be inordinately large since the correction required to arrive in the desired landing plane will probably be made propulsively while approaching the planet.

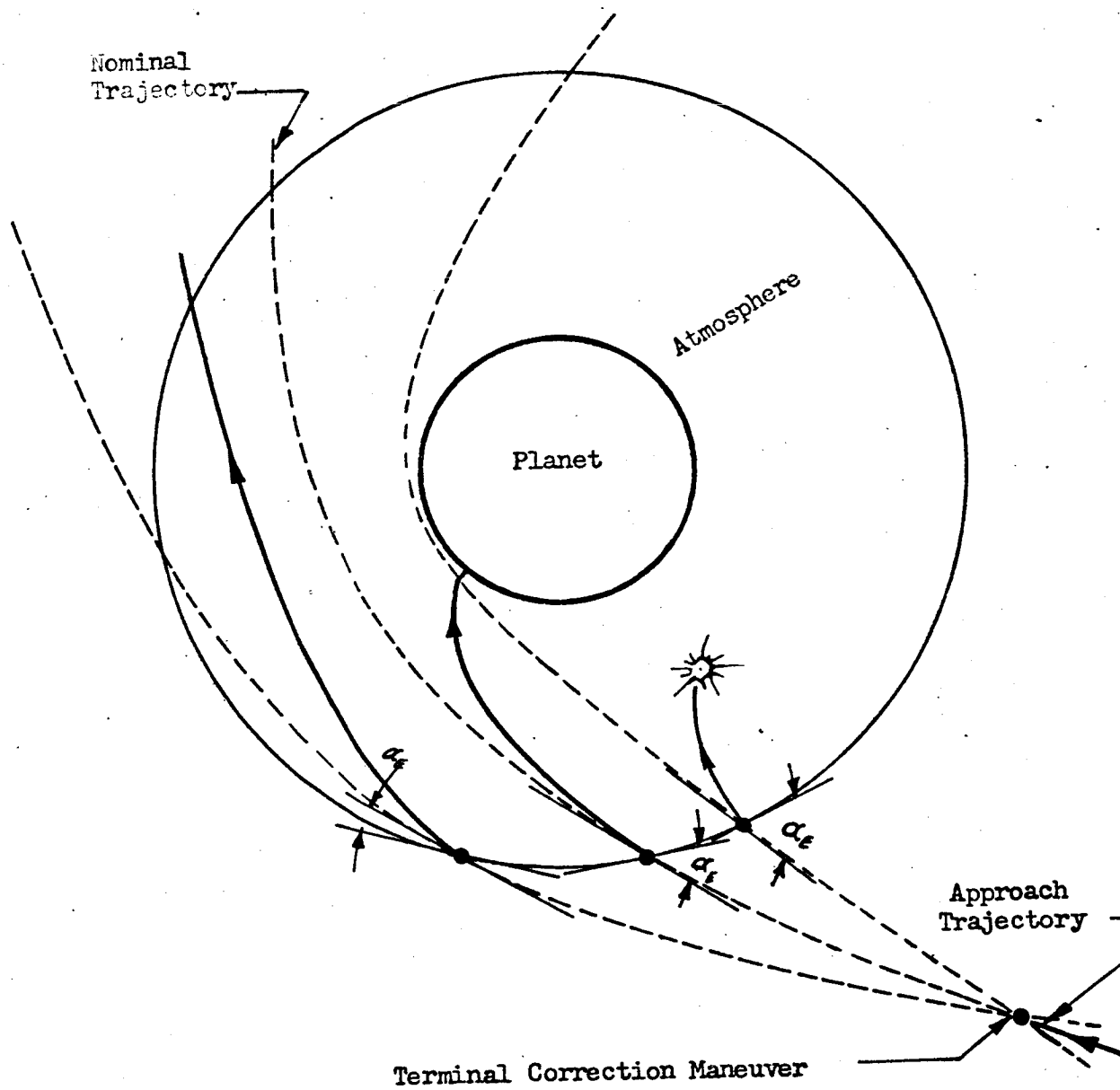


Figure 6. Entry Variations Resulting from Terminal Correction Maneuver Errors

During entry into a planetary atmosphere, an aerodynamic braking vehicle experiences high heating rates. Heating rates are strongly influenced by entry velocity, increasing rapidly as entry velocities become greater. Vehicles entering at satellite velocity experience convective heating primarily. During hyperbolic entry, however, radiation and nonequilibrium radiation dominate heat transfer. Since heating rates increase rapidly with high vehicle entry velocity, propulsive braking before entering the atmosphere may be required to reduce aerodynamic heating. Vehicle deceleration during aerodynamic braking also increases with vehicle entry velocity. For a vehicle with a specified peak-deceleration limit, therefore, a propulsive braking phase before entry may also be required.

The planets, Earth, Mars, and Venus are of interest in the study of aerodynamic braking. Since much more information is available for Earth aerodynamic entries than for the planets Mars and Venus, a comparison of the entry problems for these planets with Earth entry is of interest. In Table 1 (Reference 1) a comparison is made of total heating (q), maximum heating rate (\dot{q}), maximum deceleration (G), and entry corridor width (h) for the three planets.

TABLE 1

	Satellite Entry			Parabolic Entry			
	G	\dot{q}	q	G	h	\dot{q}	q
Earth	1	1	1	1	1	1	1
Mars	0.4	0.1	0.2	1	12	0.5	0.2
Venus	0.9	0.8	0.9	1	1	0.9	1

In Table 1 it is indicated that the aerodynamic entry problems for Earth and Venus are similar. Entry at Mars, however, is less difficult than at either Earth or Venus because the atmosphere of Mars has a lower density variation with altitude than the atmospheres of Venus and Earth; in addition, the lower gravity of Mars reduces the problems associated with an aerodynamic landing.

Propulsive Landing

Analysis of propulsive landing maneuvers entails primarily that ideal velocity requirements be determined for the type of trajectory selected; this quantity is dependent upon the vehicle thrust-to-weight ratio, the

vehicle thrust orientation program, and the type of propulsion system being considered. From consideration of the ideal velocity requirements for the landing maneuver and the effect of the landing maneuver on propulsion system design (thrust level, throttling requirement, restart capability), vehicle design (maximum deceleration, velocity at vehicle impact), and guidance requirements, suitable systems can be selected. A tangential thrust program is an efficient method of velocity reduction and is reasonable choice for most propulsive braking maneuvers. Engine operation at maximum thrust (no throttling) minimizes gravity losses during the propulsive maneuver and consequently would be used in most propulsive braking maneuvers. Restarts should be avoided whenever possible to increase system reliability.

Combined Propulsive and Aerodynamic Landing

During entry into a planetary atmosphere at supersatellite velocity, vehicles experience high heating rates and decelerations. To reduce heating and/or deceleration, it may be necessary (or desirable from the payload standpoint) for a propulsive phase to precede the aerodynamic entry.

As the vehicle approaches the planetary atmosphere, it will increase in velocity due to the acceleration caused by the planetary gravity field. A vehicle-velocity reduction of magnitude, ΔV , decreases vehicle energy by the greatest amount if it is applied at the highest possible vehicle velocity. A propulsive phase should, therefore, occur when the vehicle has its highest velocity, or just before aerodynamic braking begins. The propulsive phase of a combined propulsive-aerodynamic landing therefore takes place just above the planetary atmosphere. After the propulsive braking phase, the propulsive braking system would probably be jettisoned and the remaining conventional aerodynamic vehicle would enter the planetary atmosphere.

For a combined propulsive aerodynamic braking, an optimization must be conducted to determine the distribution of the total vehicle velocity reduction between the propulsive and aerodynamic phases. Except for this optimization, each phase should not appreciably influence the other.

Review

The following tables review the trajectory concepts and propulsion applications for extraterrestrial landings.

TABLE 2

LANDING ON PLANETS WITH NO ATMOSPHERE

<u>Trajectory Concept</u>	<u>Potential Propulsion Phases</u>
1. Direct Nonvertical Landing from Supersatellite Velocity	Approach Trajectory Correction Major Braking Near Surface Maneuvering
2. Direct Orbit Establishment from Supersatellite Velocity	Approach Trajectory Correction Major Braking Orbit Correction
3. Direct Landing from Satellite Velocity	Deorbiting Major Braking Near Surface Maneuvering

TABLE 3

LANDING ON PLANETS WITH ATMOSPHERE

<u>Trajectory Concept</u>	<u>Vehicle Type</u>	<u>Potential Propulsion Phases</u>
1. Direct Nonvertical Landing from Supersatellite Velocity	Lifting Body of Ballistic	Approach Trajectory Correction Braking (Prior to Aerodynamic Entry to Reduce Heating and/or Deceleration)
2. Grazing Approach Orbit Establishment	Lifting Body	Approach Trajectory Correction Braking (Prior to Aerodynamic Entry to Reduce Heating and/or Deceleration) Orbit Establishment (After Graze) Orbit Correction

TABLE 3
(Continued)

3.	<u>Trajectory Concept</u>	<u>Vehicle Type</u>	<u>Potential Propulsion Phases</u>
3.	Direct Landing-from Satellite Velocity	Ballistic Airplane	Deorbiting Deorbiting Propulsion for Conventional Aircraft Flight Below Orbital Velocity

EARTH RETURN MISSIONS

ATMOSPHERIC ENTRY AND TERMINAL CORRECTION REQUIREMENTS

The trajectory of a space vehicle approaching a planet defines the conditions at atmospheric entry, and determines if propulsive maneuvers are required to facilitate safe aerodynamic entry. If the entry conditions are unacceptable, the trajectory of the vehicle must be altered through use of a terminal correction to provide the correct conditions.

Particular return-to-Earth missions were selected for investigation of terminal corrections. For this investigation, a specific vehicle configuration and an entry-corridor characteristic of that configuration were selected and defined. The required change in the planetary approach path was studied to determine 1) the magnitude of velocity increment to perform a terminal correction 2) the optimum range at which to apply the corrective maneuver and 3) the deviation from nominal entry conditions resulting from errors encountered in executing terminal corrections.

Earth-Return Missions Description

To provide atmospheric entry conditions encompassing the range that can presently be anticipated for interplanetary missions of the near future, three round-trip missions, two to Mars and one to Venus, were selected. Neither the outbound nor the return phases of any of the three missions were selected to minimize the energy requirements. Instead velocity requirements were compromised to achieve relatively short mission times. Further, the return phases of the three missions were intentionally biased toward presenting a wide range of arrival velocities at Earth. Trajectory details for the missions are presented in Table 4. A more detailed discussion of mission selection is presented in conjunction with the sections devoted to each of the destination planets. The six trajectories for the three missions are numbered for convenient reference in subsequent areas in the analysis.

Atmospheric Entry

The major factors determining the role an atmosphere plays in a space mission are the entry velocity, incident angle at which a vehicle enters the atmosphere and the vehicle design. (For analysis purposes, a specific altitude above the effective atmosphere was defined to provide a basis for specification of entry corridor parameters; for Earth this altitude is

TABLE 4
TRAJECTORIES SELECTED FOR TERMINAL ANALYSIS STUDY

Mission	Trajectory Number	Phase	Launch Date	Trip Time Days	Destination Stay Time Days	Total Mission Time, Days	Hyperbolic Departure Hyperbolic Arrival, ft./sec
Mars (A)	1.	Earth-Mars	19 May 1971	170	5		9,700 11,000
	2.	Mars-Earth	10 Nov 1971	278		453	23,200 43,500
Mars (B)	3.	Earth-Mars	6 June 1971	80	2		20,500 34,400
	4.	Mars-Earth	26 Aug 1971	110		192	41,300 29,000
Venus	5.	Earth-Venus	5 April 1965	265	5		23,800 15,900
	6.	Venus-Earth	31 Dec 1965	86		356	20,300 12,650

400,000 feet.) If the entry angle is too high for the entry velocity, an "undershoot" occurs where the atmospheric entry results in a higher deceleration rate than allowable. At the other extreme, too shallow an entry angle results in an "overshoot" where the atmospheric deceleration is insufficient, thus allowing the space vehicle to skip out of the atmosphere (Figure 7). There are particular combinations of velocity and entry angle, for a given vehicle design, that define an entry corridor suitable for aerodynamic landing.

Entry Vehicle. Aerodynamic landing vehicle configurations (Figure 8) are of three major types; ballistic (Mercury Capsule), lifting bodies, and airplane (Dyna-soar). The ballistic configuration has no lift. Lifting bodies have L/D values up to approximately 1.5, and the airplane is capable of somewhat higher L/D values (about 2 for Dyna-soar).

The ballistic vehicle, with its blunt shape, lends itself to the use of an ablative heat shield. Also relatively blunt are the lifting bodies which would also probably be cooled by this method. The airplane configuration, because of its high wing area, would probably require heavy heat shields if ablative cooling were used. A major portion of the vehicle would have to be radiation cooled for this type of vehicle to be practical. Airplane-type vehicles could be flown and landed like conventional aircraft, and for this reason, may find applications where heating is not too severe.

Analyses conducted by General Dynamics/Astronautics, using simulated reentry trajectories, were made to define those trajectories that are within specified maximum deceleration g limits. In these analyses, three entry vehicles, shown in Figure 9, were selected as representative of the spectrum of possible configurations. The relation between payload and entry-vehicle weight (air-frame structure, not including heat shield or payload) is shown in Figure 10 based on preliminary calculations.

The ballistic coefficient or wing loading for the vehicle was 50 lb/ft². The drag vehicle followed a ballistic path. The modified drag (Egger's) body used values of L/D up to 0.5 and $C_{L(max)}$ up to 0.3. Lift modulation was not applied for this preliminary investigation. The lifting vehicles analyzed were flown at a fixed attitude for discrete intervals along the trajectory as follows:

<u>Boundary</u>	<u>Interval</u>	<u>Attitude</u>
Undershoot	Entry to $\alpha = 0$	+ $(L/D)_{max}$
	$\alpha = 0$ to Surface	- $(L/D)_{max}$
Overshoot	Entry to Circular Velocity	- $(C_L)_{max}$
	Circular Velocity to Surface	+ $(L/D)_{max}$

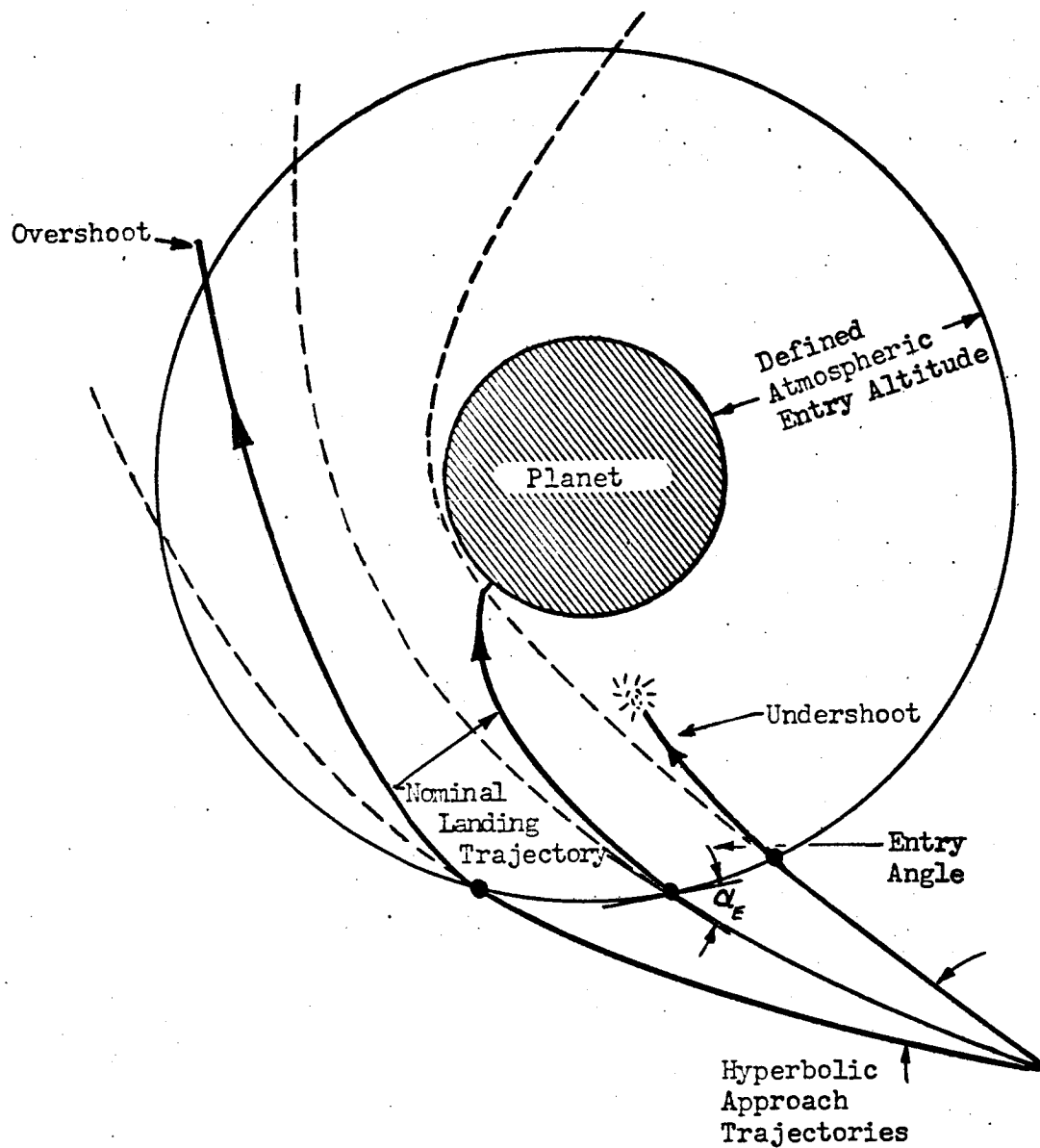
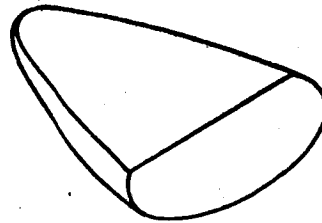
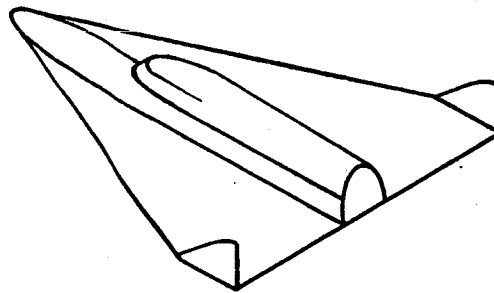


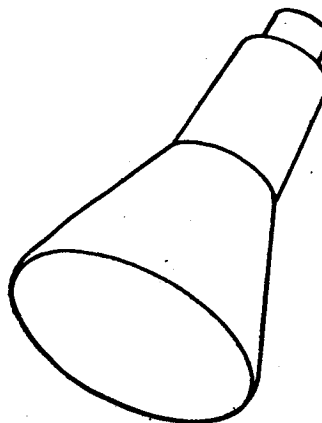
Figure 7 Entry into Planetary Atmosphere



Lifting Body



Airplane



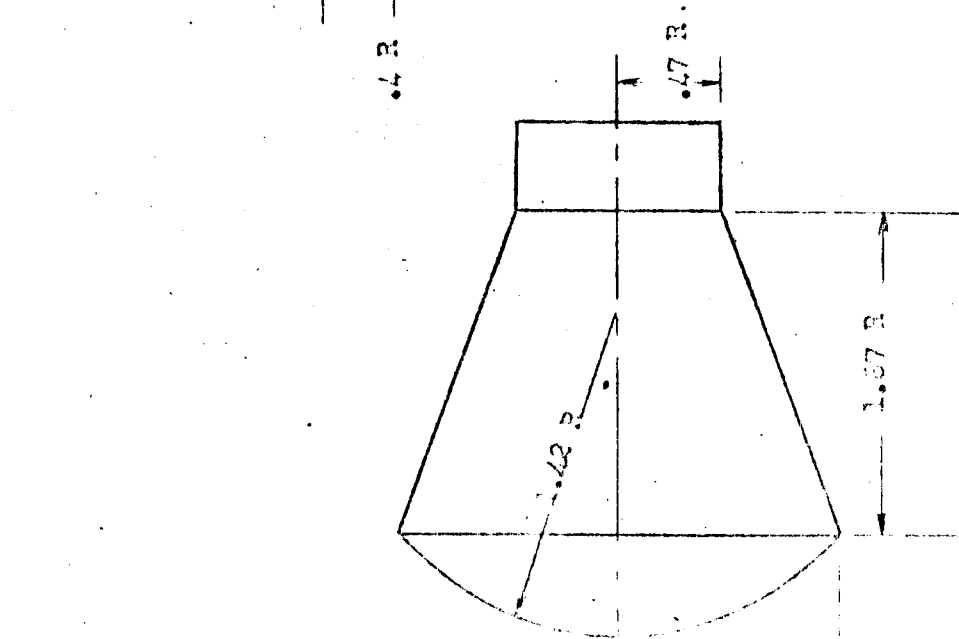
Ballistic

Figure 8 . Aerodynamic Vehicle Configurations

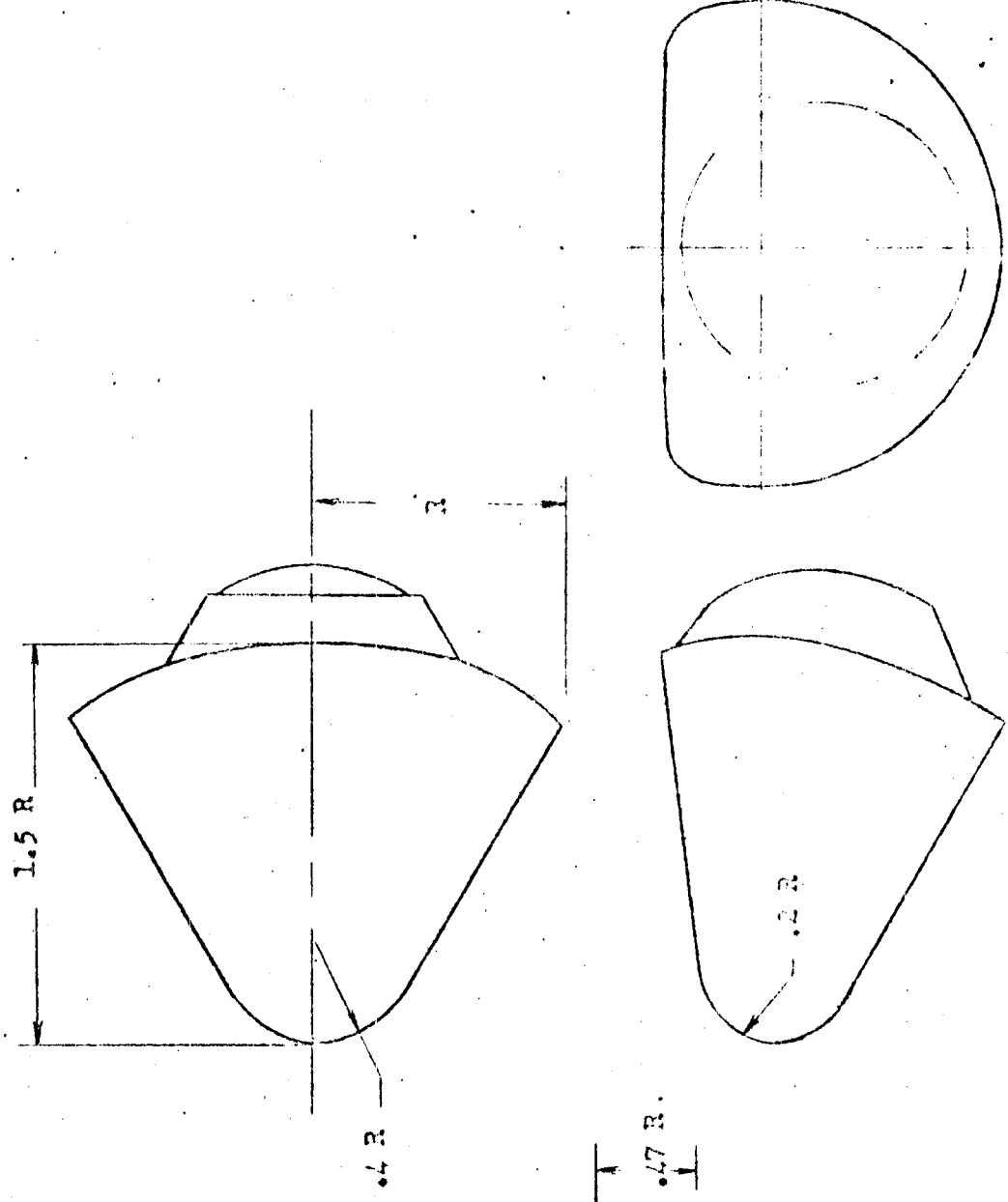
DRAG

MODIFIED DRAG

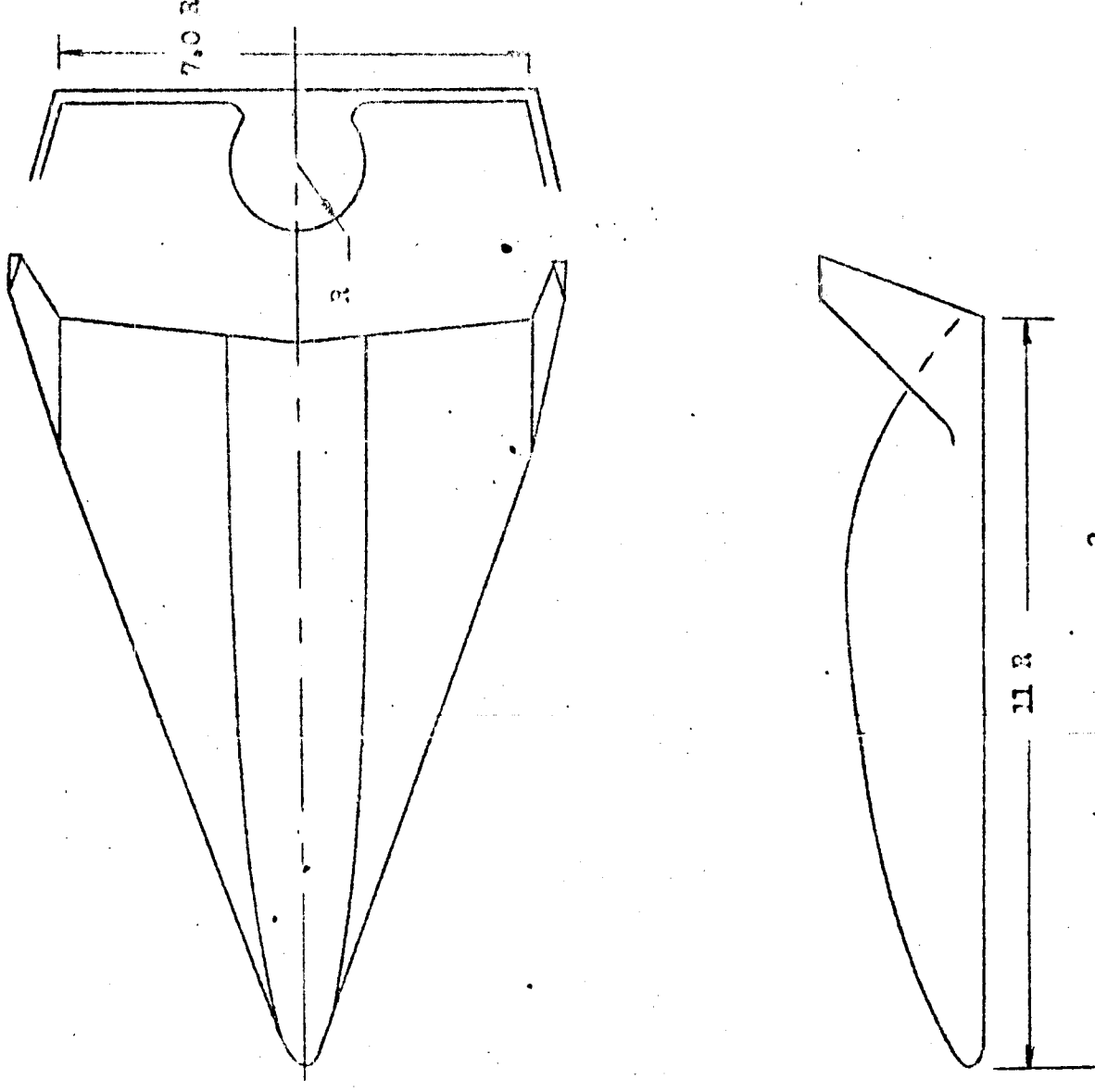
DELTA WINGED ($L/D = 3$)



Capsule Volume = $2.55 R^3$
 Surface A = $11.32 R^2$
 Heat Shield Area = $3.6 R^2$
 Payload Volume = $1.6 R^3$



Volume = $.9 R^3$
 Surface A = $6 R^2$
 Payload Volume = $.72 R^3$



$A_M = 44 R^2$
 $A_F = 8.8 R^2$
 Vol. Fuselage = $29.5 R^3$
 Area Fuselage = $44.5 R^2$

Fig. 9

Entry Vehicle Configurations

Payload Volume = $17.1 R^3$
 Total Area = $113 R^2$

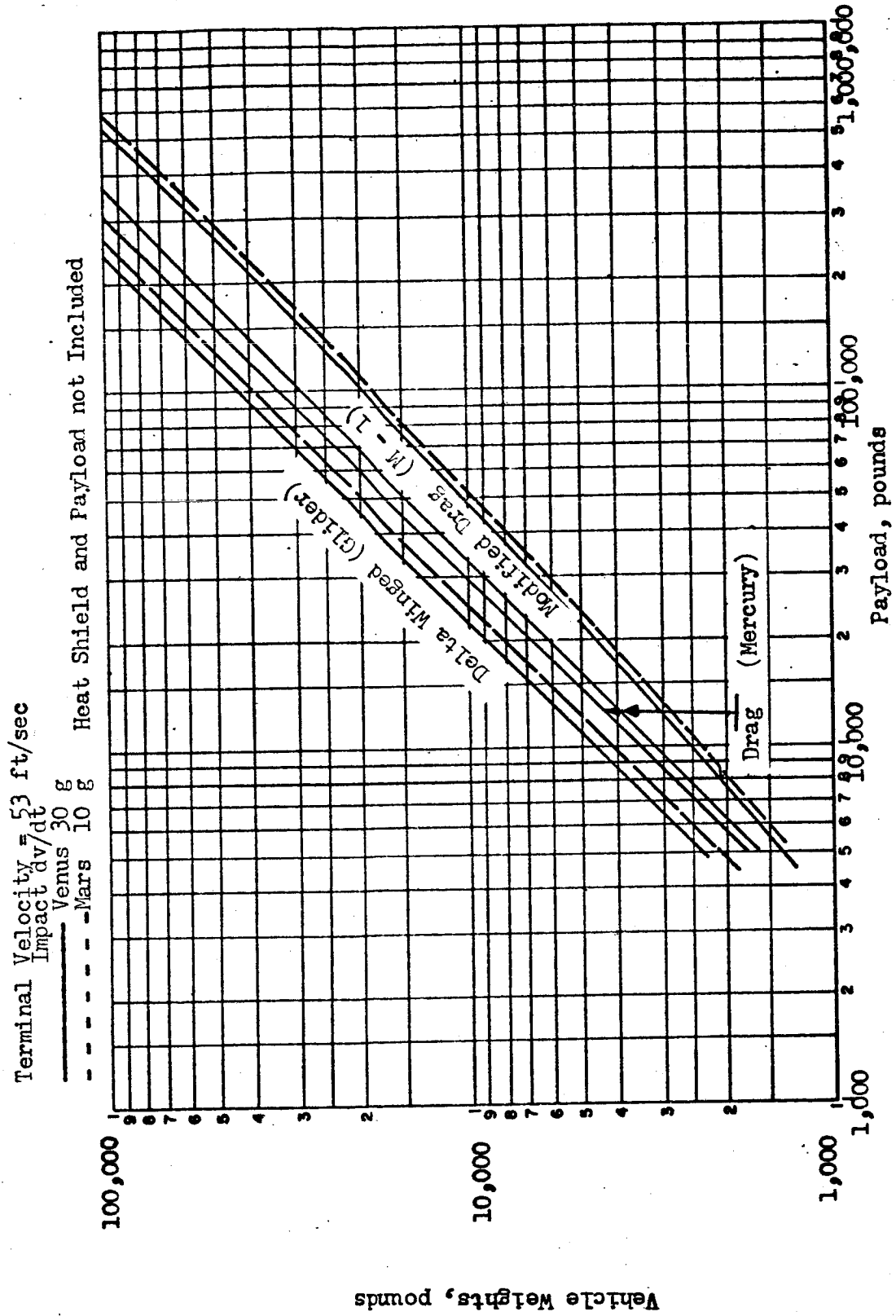


Figure 10 . Entry Vehicle Weight vs Payload

Overshoot boundaries and undershoot boundaries, for 6 g and 30 g maximum deceleration, were determined for the various vehicle designs. The entry conditions and resulting atmospheric deceleration trajectory profile for a modified drag vehicle having a high maximum deceleration are shown in Figure 11 .

Examination of entry trajectory analyses results indicates that the ballistic entry-vehicle design has the most stringent entry corridor requirements. Since this is a realistic system design, and entry vehicle design analysis has not progressed to the point of selection of optimum design concepts, the entry requirements for this vehicle were selected to determine terminal correction requirements.

Entry Corridor. The Earth Entry corridor requirements for a drag vehicle are described in Figure 12 . The upper (undershoot) boundary of entry angles represents tolerable deceleration loads, and the lower (undershoot) boundary is that which prevents the vehicle from skipping out of the atmosphere instead of performing a landing maneuver. The nominal entry angle, used in the terminal correction analysis, is also shown.

A vehicle can successfully achieve an atmospheric entry and deceleration for landing if, at the entry altitude, the velocity and entry angle correspond to a point within the confines of the corridor. The entry velocity and entry angle are determined by the approach trajectory to the planet.

Terminal Correction

Correction Requirements. The trajectory of a space vehicle must be exactly controlled for a successful transfer between celestial bodies; an incorrect trajectory causes the vehicle to miss rendezvous. The required trajectory accuracy may be achieved either at launch or by midcourse corrective maneuvers performed during the transfer. Present state-of-the-art accuracies of tracking, guidance, and propulsion prevent establishment of the correct transfer path at planetary departure. Therefore, midcourse corrective propulsion maneuvers are a requisite. However, the midcourse corrective maneuver is itself subject to inaccuracies in tracking, location and in maneuver execution. This necessitates multiple corrections during the transfer phase.

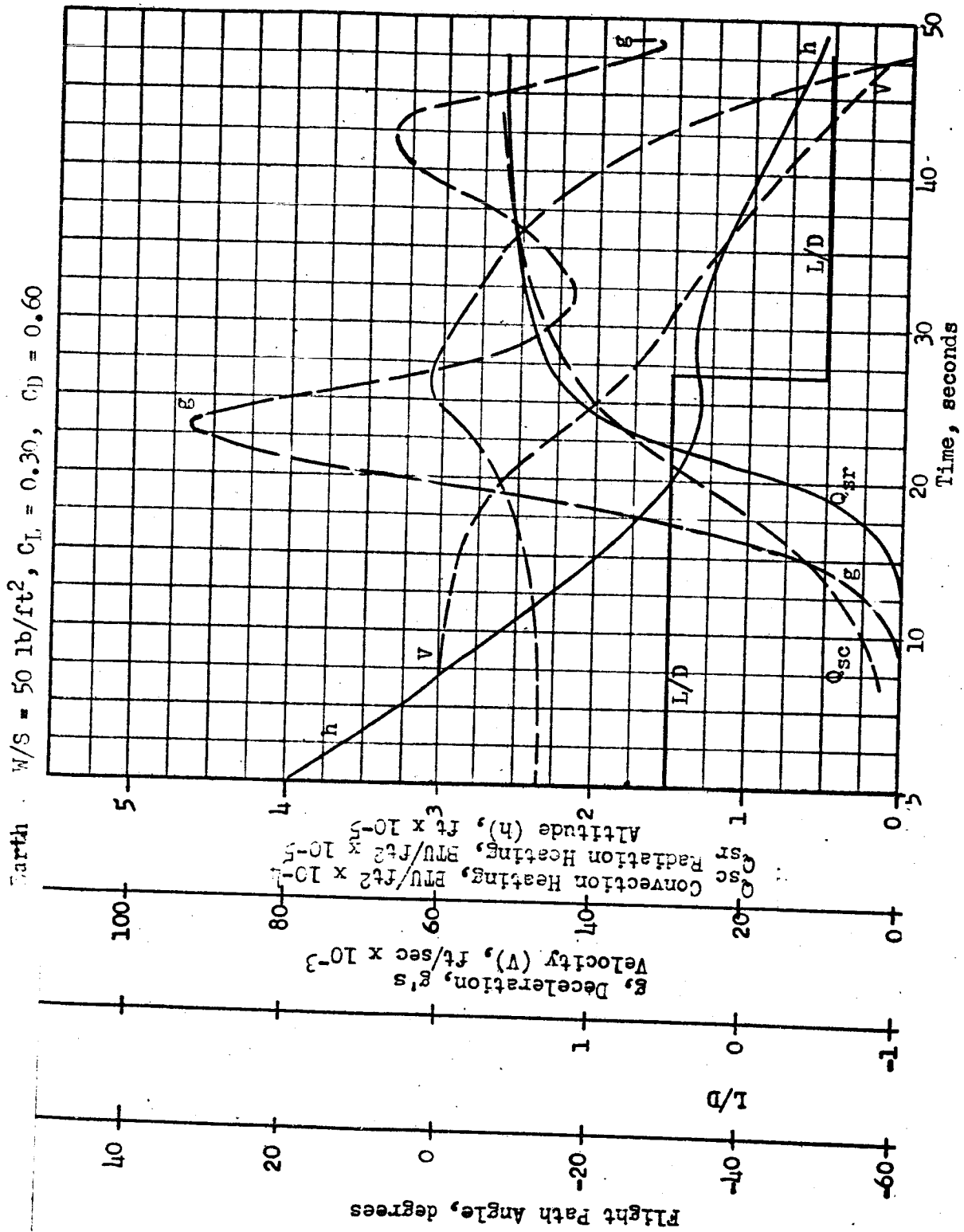


Figure 11. Typical Lift Vehicle Entry Trajectory Parameters. Modified Drag Vehicle.

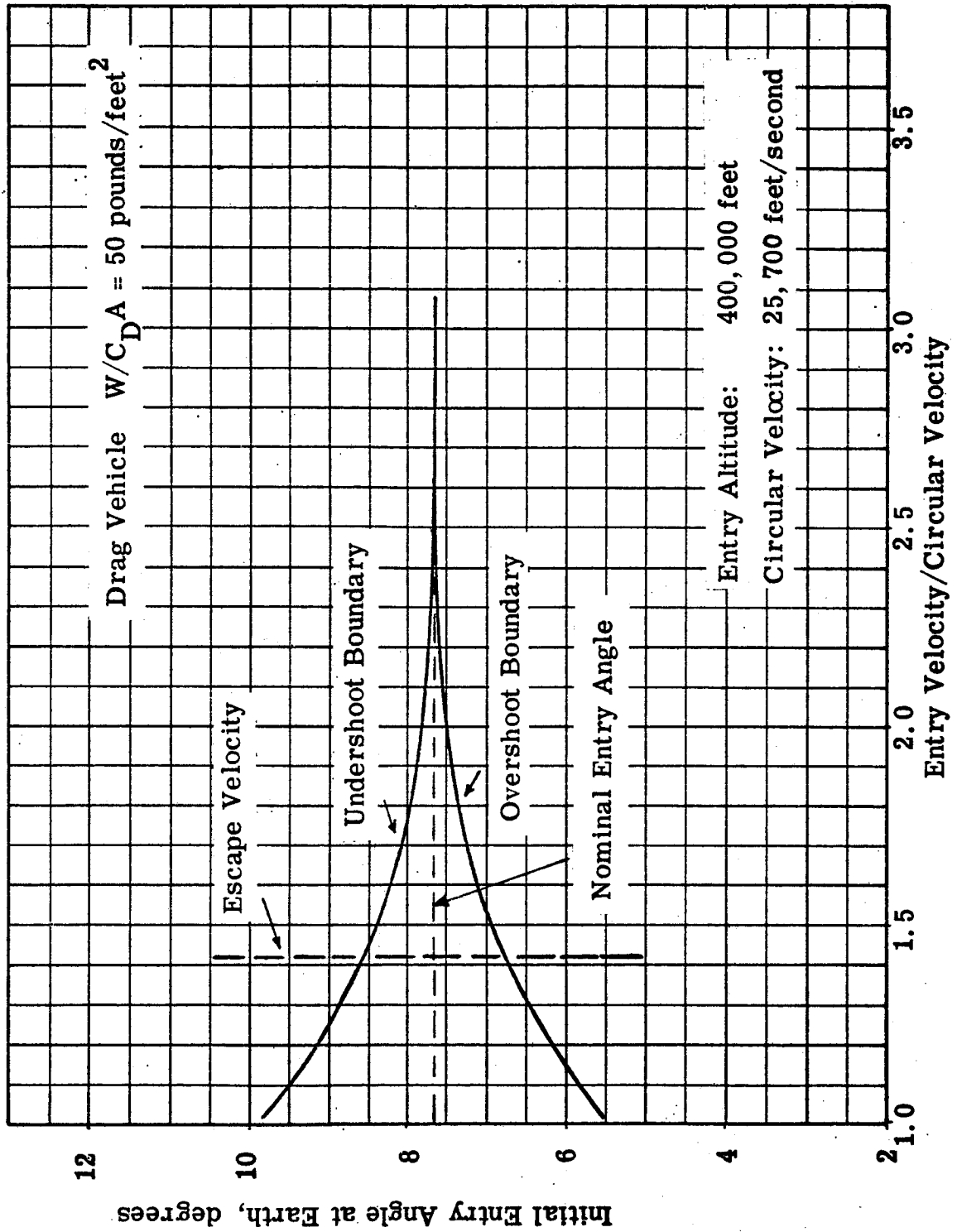


Fig. 12 Earth Entry Corridor

Midcourse corrections for the space missions presented in Table 4 were reviewed based on methods developed at Rocketdyne for NASA contract NAS 7-88 "Space Transfer Propulsion," described in Reference 2. Inaccuracies associated with planetary departure and midcourse corrective maneuvers, and the resulting accuracy of planetary rendezvous are also based on this reference.

After the final midcourse correction, the vehicle coasts to the region of space where the vehicle motion is governed primarily by the gravitational field of the planet. The vehicle approaches the planet along a planetocentric hyperbolic trajectory. In each mission, because of the various errors in the final midcourse corrective maneuver, the actual planetary approach hyperbola is not the desired one.

Deviations in the desired asymptotic approach distances existed at completion of the midcourse correction program (Table 5). In each mission, the deviation translated to an atmospheric entry condition outside the defined entry corridor. Thus, a necessity existed for additional corrective maneuvers (terminal maneuvers) to be applied in the proximity of the target planet to ensure a tolerable atmospheric entry.

TABLE 5

PLANETARY ARRIVAL CONDITIONS

Trajectory Number	Hyperbolic Arrival Velocity (V_{∞}), ft/sec	Nominal Asymptotic Approach Distance (D), n mi	Deviation in Asymptotic Approach Distance (D), n mi	Actual Asymptotic Approach Distance (D_a), n mi
2	43,500	4580	340	4920
4	29,000	5660	2700	8360
6	12,650	10,500	2420	12,920

Correction Objectives

Terminal correction maneuvers are specifically defined as those trajectory corrections occurring after the vehicle is in that region of space where the gravitational field of the destination body is predominant. Applied to planetary missions, this is the crossover point between the attraction

of the planet and the attraction by the sun (Figure 13). In so defining terminal corrections, it is assumed that measurements pertinent to the maneuvers are based on use of the target as a guidance reference.

In this study of terminal correction maneuvers, it was assumed that any trajectory plane of approach with respect to the planet was acceptable. No planetocentric plane changes were made in the terminal corrections. In making the terminal correction, the velocity changes were assumed to be impulsive; the impulsive velocity assumption is based on Reference 2 analysis which indicates it is valid for the correction distances from the planet and velocity magnitudes involved.

The hyperbolic excess velocity (V_{∞}) and the asymptotic approach distance (D) of an approach trajectory define the velocity of the vehicle and the entry angle at the specified 400,000 foot altitude for atmospheric entry. The definition of an entry corridor limits the combinations of acceptable V_{∞} and D. Those combinations that result in entry conditions outside the boundaries of the entry corridor are undesirable; the V_{∞} and the D_a values presented in Table 5 gave entry conditions outside these limitations.

To correct the trajectory for entry within the acceptable corridor, a terminal correction may be applied for one of two objectives:

1. to change both the energy and angular momentum of the vehicle by changing the vehicle velocity
2. to change the angular momentum of the vehicle by reorienting the vehicle velocity vector

The first method changes both the hyperbolic excess velocity and the asymptotic approach distance of the trajectory. The second method changes only the asymptotic approach distance.

The advantage of the first is to shift the entry toward lower ratios of entry velocity-to-circular orbit velocity (Figure 12) which broadens the applicable entry angle tolerance. However, the increase in the correction velocity increment to shift the entry condition in this manner is excessive. Thus, this technique was dropped in favor of the second concept, to establish nominal entry conditions (Table 6) by changing the angular momentum of the vehicle. In changing only the angular momentum the entry velocity of the vehicle and thus the entry corridor width remains unchanged.

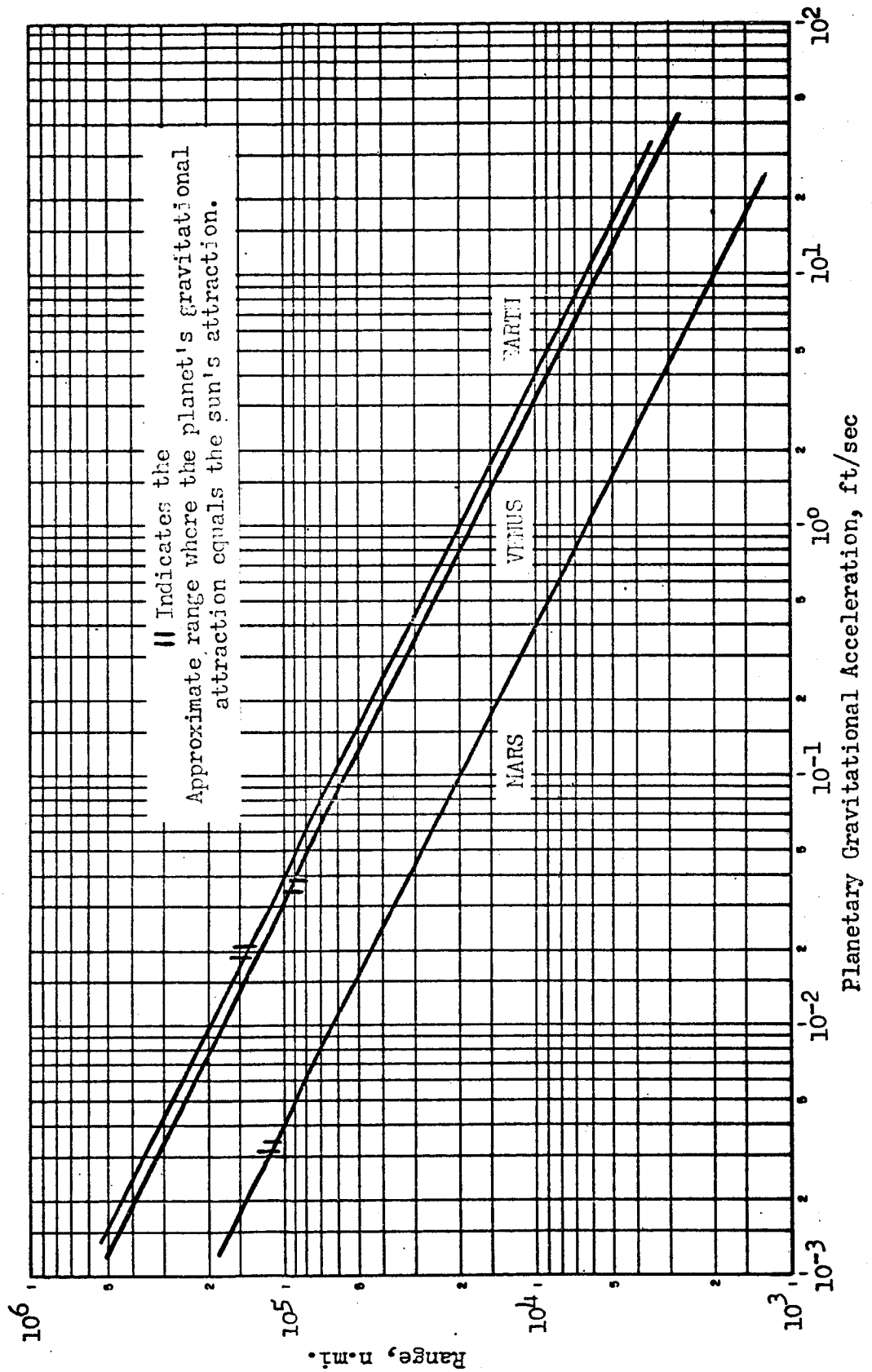


Figure 13 Gravitational Field of the Planets

TABLE 6
NOMINAL EARTH ATMOSPHERIC ENTRY CONDITIONS

Trajectory Number	Entry Altitude (h_E), feet	Entry Velocity (V_E) ft/sec	(V_E/V_{CO})	Entry Trajectory Elevation Angle (α_E) degrees
2	400,000	56,550	2.2	-7.68
4	400,000	46,260	1.8	-7.68
6	400,000	38,560	1.5	-7.68

Single Terminal Correction

The hyperbolic arrival velocities and actual asymptotic approach distances as shown in Table 5 are a result of the final midcourse correction maneuver. The deviation in the asymptotic approach distance is due to errors in performing the midcourse corrections; the errors vary with the assumed accuracies of midcourse correction equipment. Thus, an evaluation of the effect of deviations in asymptotic approach distance upon the magnitude of the terminal correction velocity increment was made.

In Figures 14, 15 and 16 the correction velocity increments of a single terminal correction are presented as functions of the range at correction and the deviations in asymptotic approach distance from the nominal for the mission hyperbolic approach velocities of Table 5. The deviations in asymptotic approach distance corresponding to the trajectories of Table 5 are shown in these figures for reference.

The effect of smaller deviations for these three trajectories is presented in Figures 17, 18 and 19. These curves clearly show the correction velocity magnitude decreasing to zero as the deviation in asymptotic approach distance vanishes.

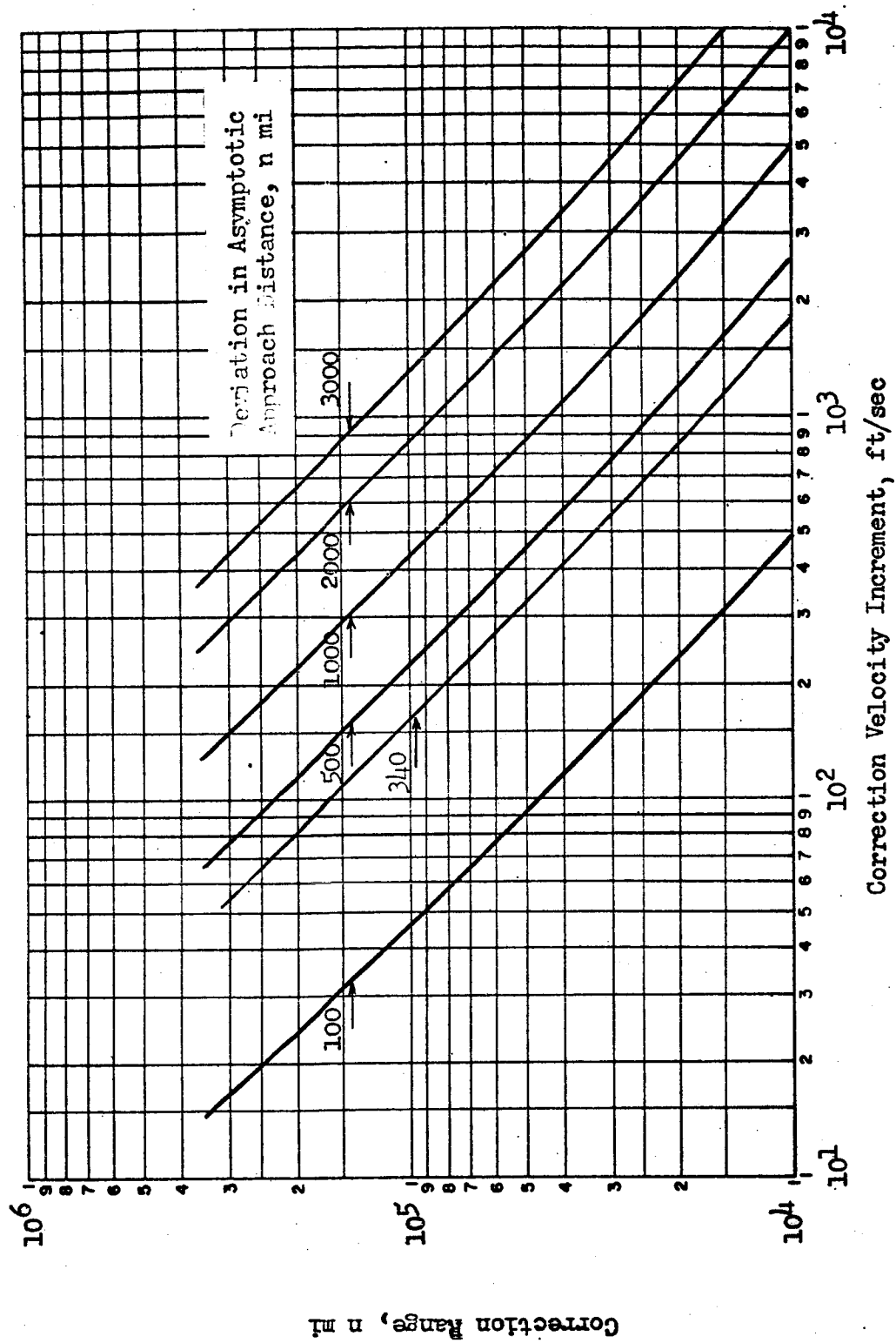


Fig. 14 The Effect of a Deviation in Asymptotic Approach Distance on the Terminal Correction Velocity Increment for Earth Atmospheric Re-entry. (Trajectory 2)

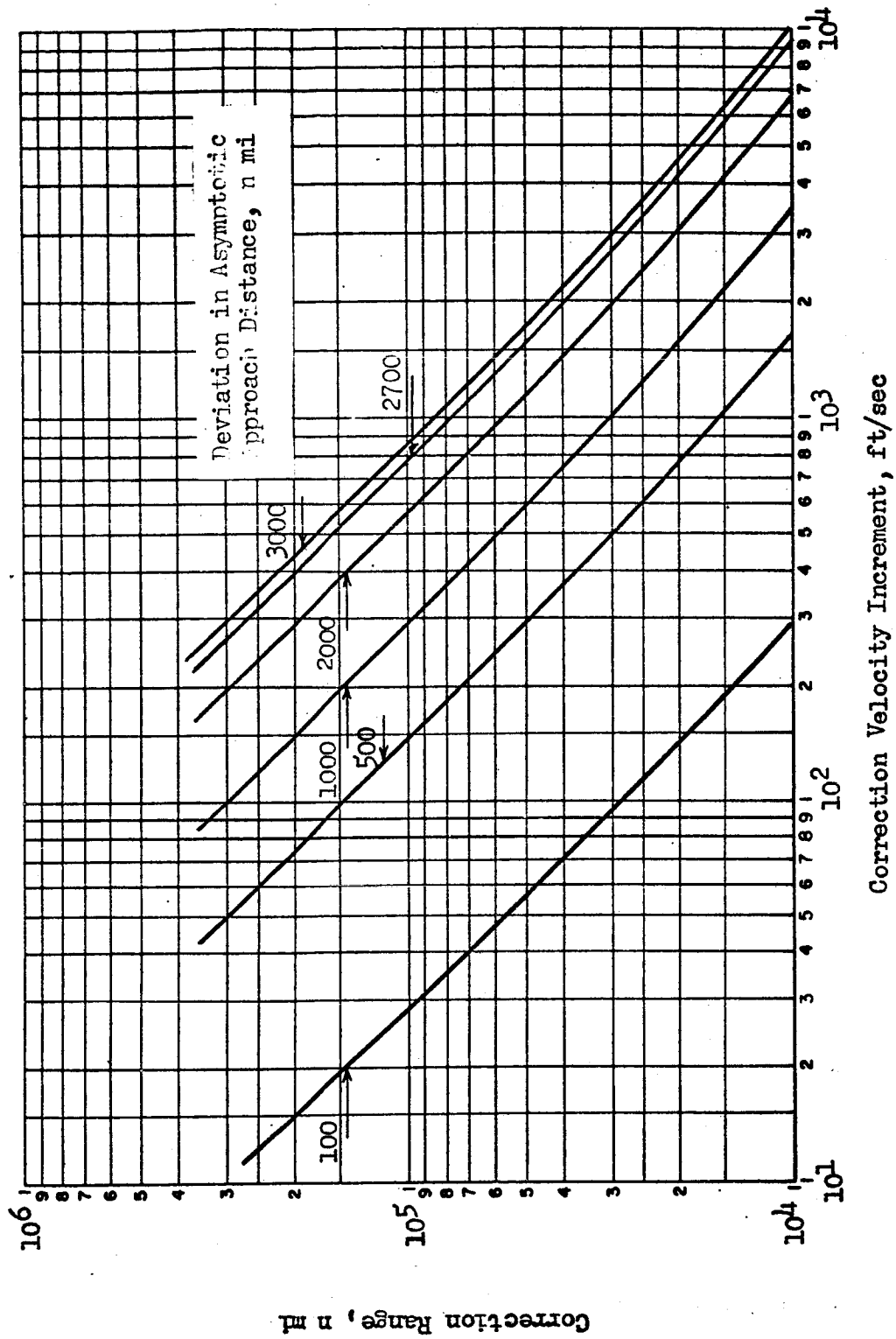


Fig. 15 The Effect of a Deviation in Asymptotic Approach Distance on the Terminal Correction Velocity Increment for Earth Atmospheric Re-entry. (Trajectory 4)

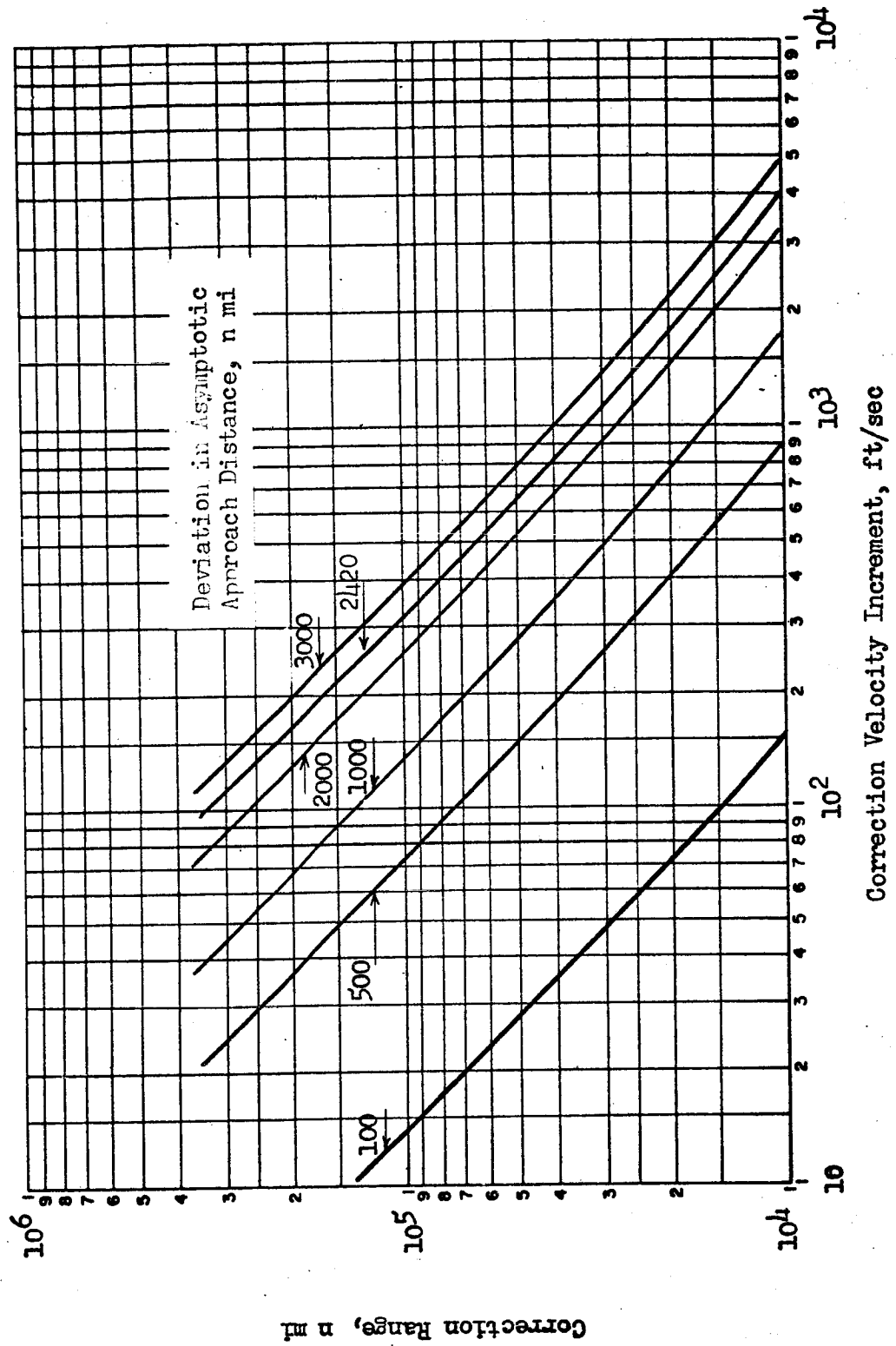


Fig. 16 The Effect of a Deviation in Asymptotic Approach Distance on the Terminal Correction Velocity Increment for Earth Atmospheric Re-entry (Trajectory 6)

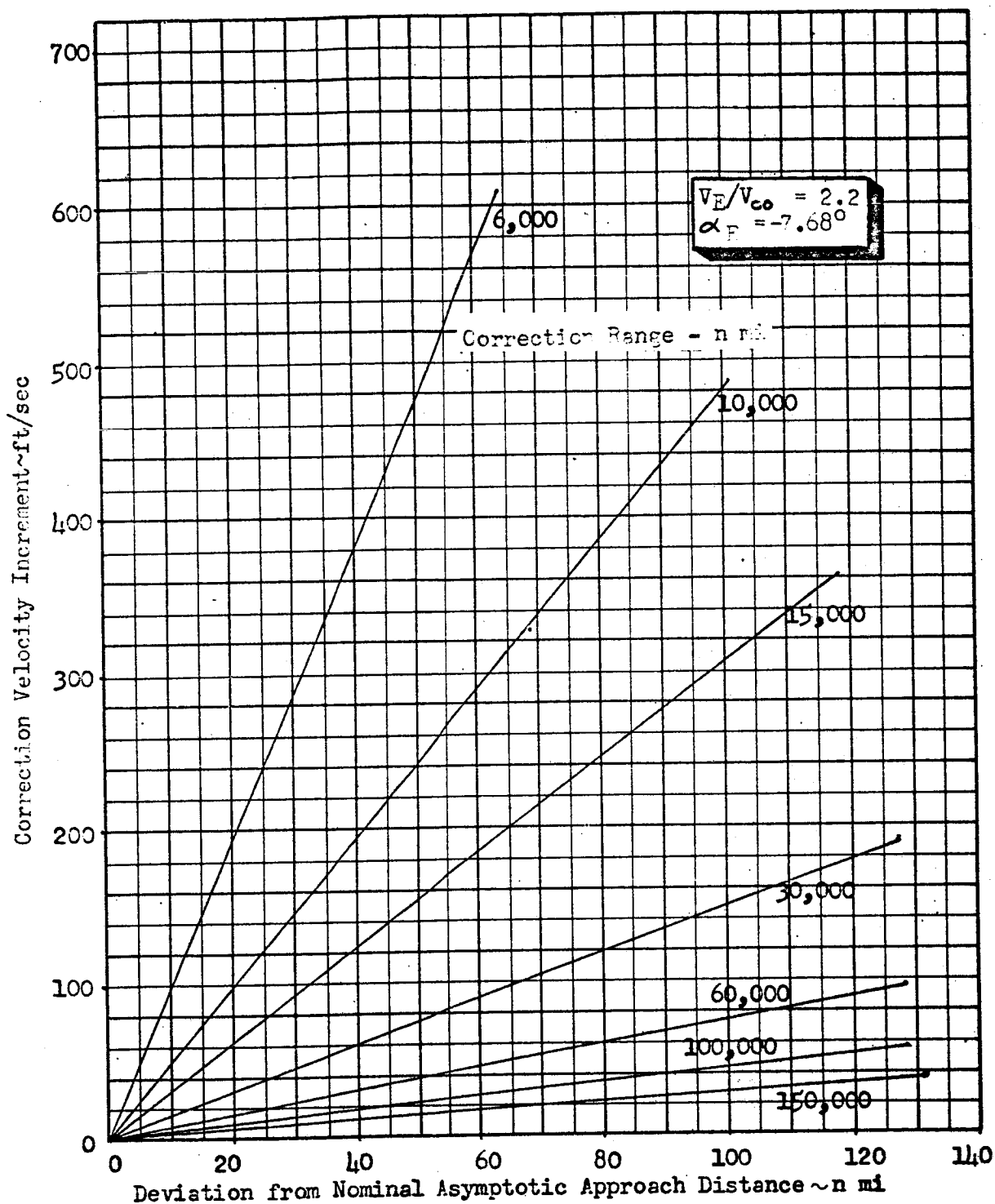


Fig. 17 The Effect of a Deviation in Asymptotic Approach Distance on the Terminal Correction Velocity Increment for Earth Atmospheric Re-Entry. (Trajectory 2)

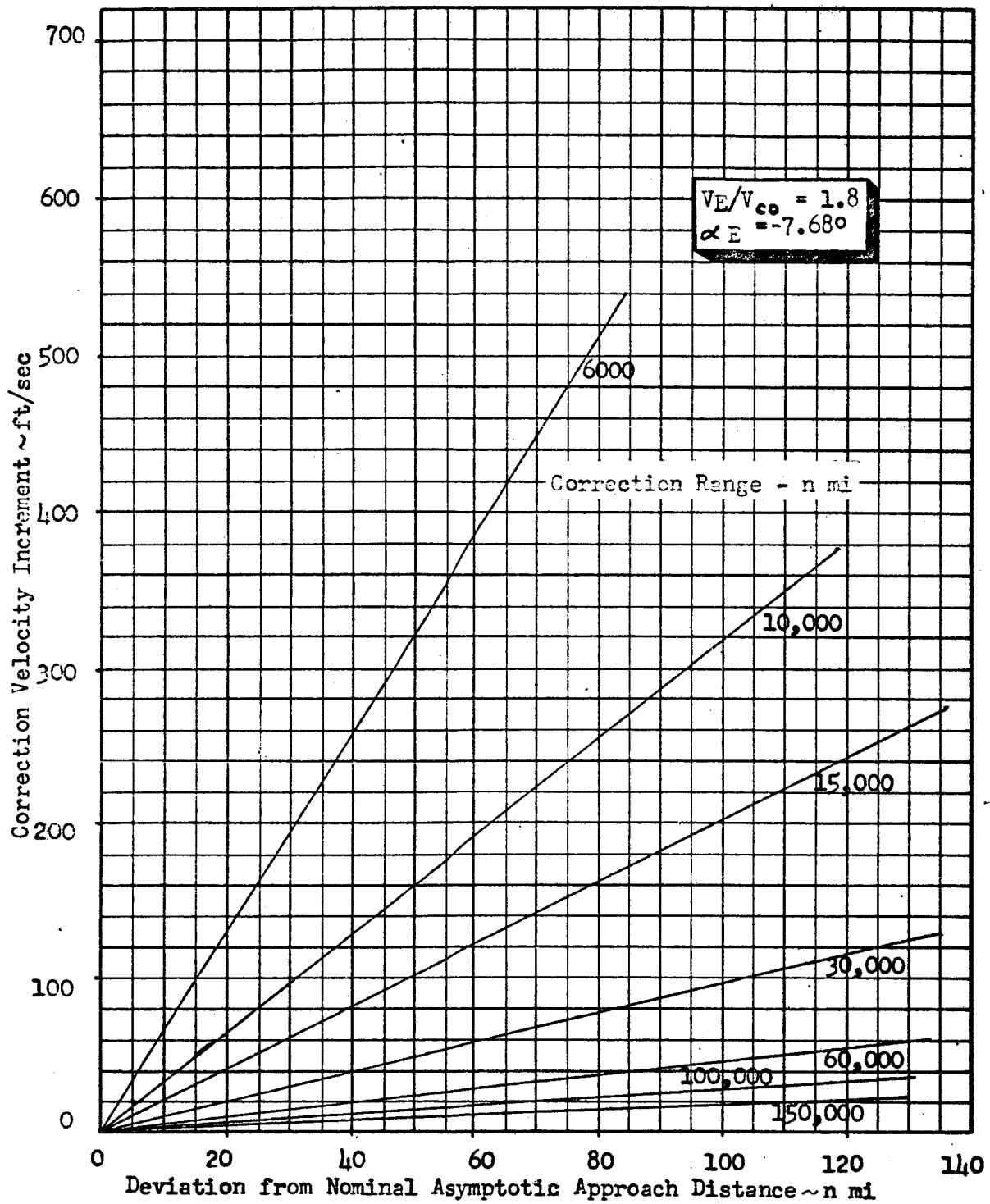


Fig. 18 The Effect of a Deviation in Asymptotic Approach Distance on the Terminal Correction Velocity Increment for Earth Atmospheric Re-Entry. (Trajectory 4)

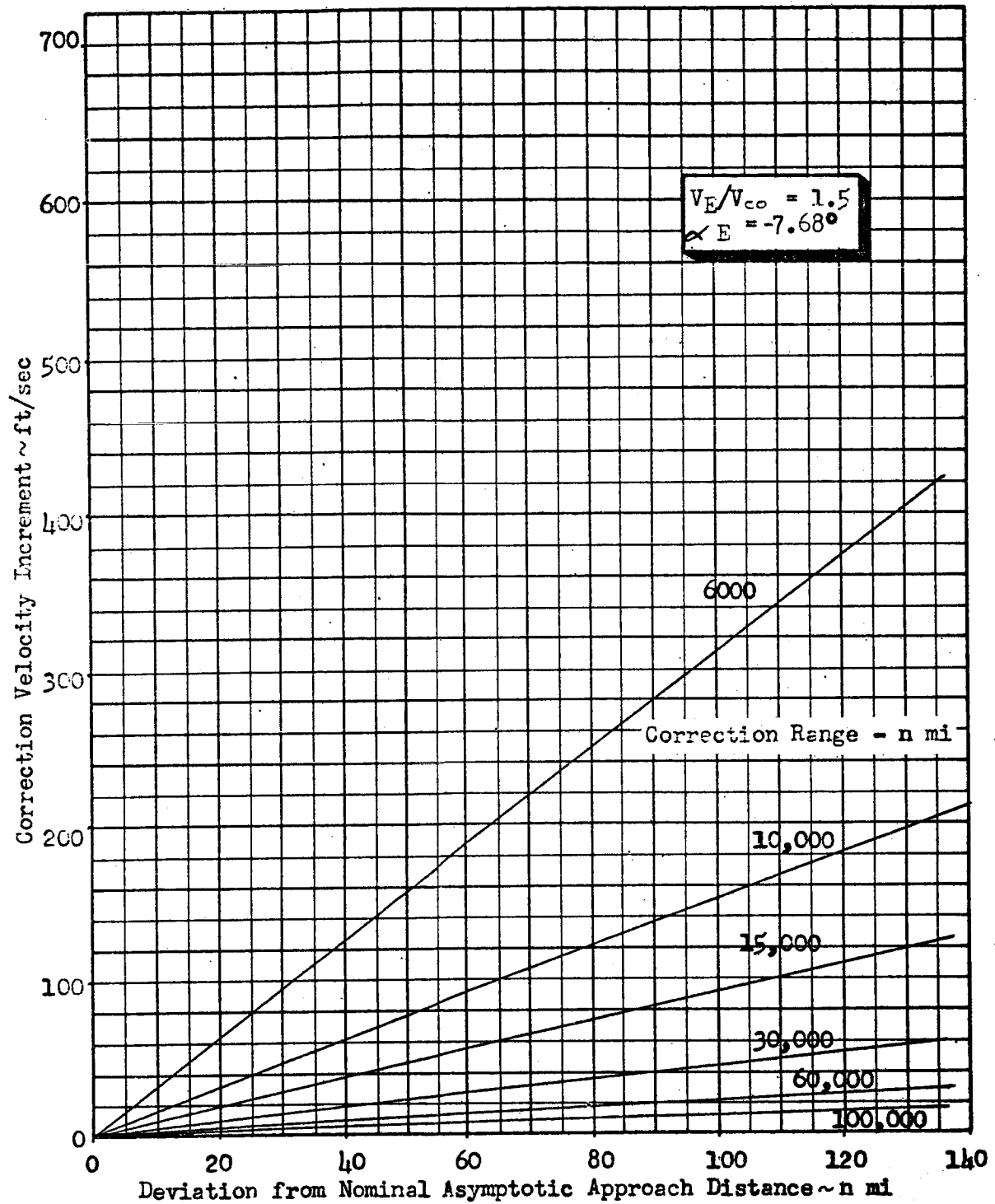


Fig. 19 The Effect of a Deviation in Asymptotic Approach Distance on the Terminal Correction Velocity Increment for Earth Atmospheric Re-Entry. (Trajectory 6)

The correction velocity increment is only one of two factors involved in terminal corrections. Errors in terminal corrections (position and velocity-measurement errors, tracking and propulsive-maneuver execution errors) are the second factor to be considered.

The errors in measurement are range-dependent whereas errors in correction mechanization are a function of the magnitude of the correction velocity increment and the thrust-to-weight ratio of the system. Range (r), range rate (\dot{r}) and range angle rate ($\dot{\theta}$) are the measured parameters subject to errors. Correction velocity increment magnitude (ΔV) and the elevation angle (α_c) of this increment are execution parameters which have associated errors. An error in any of the five parameters causes variations in the desired entry conditions.

First order partials were generated for each trajectory relating measurement and correction-mechanization errors to variations in the desired entry conditions. The partials were generated for ranges between 1×10^4 and 3×10^5 nautical miles, and were subsequently combined with representative error magnitudes for each parameter (based on analysis from Reference 2) to calculate rms deviations in entry conditions. Partial and error magnitudes for one correction range are presented in Table 7 for Earth terminal corrections.

TABLE 7

PARTIALS AND ERROR MAGNITUDES AT 60,000

NAUTICAL MILE RANGE

Entry Velocity Partial	Entry Angle Partial	Error Magnitude
$\partial v_e / \partial r = 0.98 \times 10^{-2}$	$\partial \alpha_e / \partial r = 0.35 \times 10^{-2}$	$\Delta r = 0.66 \times 10^2$
$\partial v_e / \partial \dot{r} = 0.65 \times 10^0$	$\partial \alpha_e / \partial \dot{r} = 0.60 \times 10^{-2}$	$\Delta \dot{r} = 0.18 \times 10^2$
$\partial v_e / \partial (r\dot{\theta}) = 0.67 \times 10^{-1}$	$\partial \alpha_e / \partial (r\dot{\theta}) = 0.16 \times 10^0$	$\Delta (r\dot{\theta}) = 0.62 \times 10^1$
$\partial v_e / \partial \Delta V = 0.12 \times 10^{-1}$	$\partial \alpha_e / \partial \Delta V = 0.16 \times 10^0$	$\delta (\Delta V) = 0.20 \times 10^0$
$\partial v_e / \partial \alpha_c = 0.15 \times 10^2$	$\partial \alpha_e / \partial \alpha_c = 0.31 \times 10^0$	$\Delta \alpha_c = 0.15 \times 10^0$

The execution errors listed in Table 7 correspond to a F/W of about 0.3. However, F/W ratios in the region between 0.1 to 0.5 have little effect on the execution errors and the analysis can therefore be considered valid for F/W ratios in this region.

The use of low values of F/W can reduce system weight, but long burning times result. For low thrust-to-weight ratios on the order of 0.01, the vehicle travels several thousand miles while the propulsive acceleration changes the vehicle velocity by the required value. Execution accuracy in applying a terminal correction over such a long duration and large translation distance restricts the use of low F/W ratios. A thrust-to-weight ratio of approximately 0.1 reduces the propulsive correction maneuver to a few minutes duration and to a few hundred miles of translation during execution of the correction.

At the other extreme, high thrust-to-weight ratios reduce operation time but tend to increase system weight. Thus, although any value within the quoted range of F/W could be used, a F/W of about 0.3 appears to be a reasonable compromise between the two factors attributed to thrust level selection.

The deviations (which result from the error magnitudes used in the study) in the vehicle velocity and trajectory elevation angle at atmospheric entry, for a single correction, are presented along with the correction velocity increment in Figures 20, 21 and 22 as a function of range. The figures indicate that the terminal correction errors have very little effect on changing the entry velocity. The parameter significantly affected by terminal correction errors is the entry angle.

Each trajectory had to be considered individually to determine the range for applying a correction to meet the entry corridor limitations. The entry corridor half-band width (for the nominal entry velocity), the range at correction and the ΔV for the correction are tabulated in Table 8 for the three trajectories.

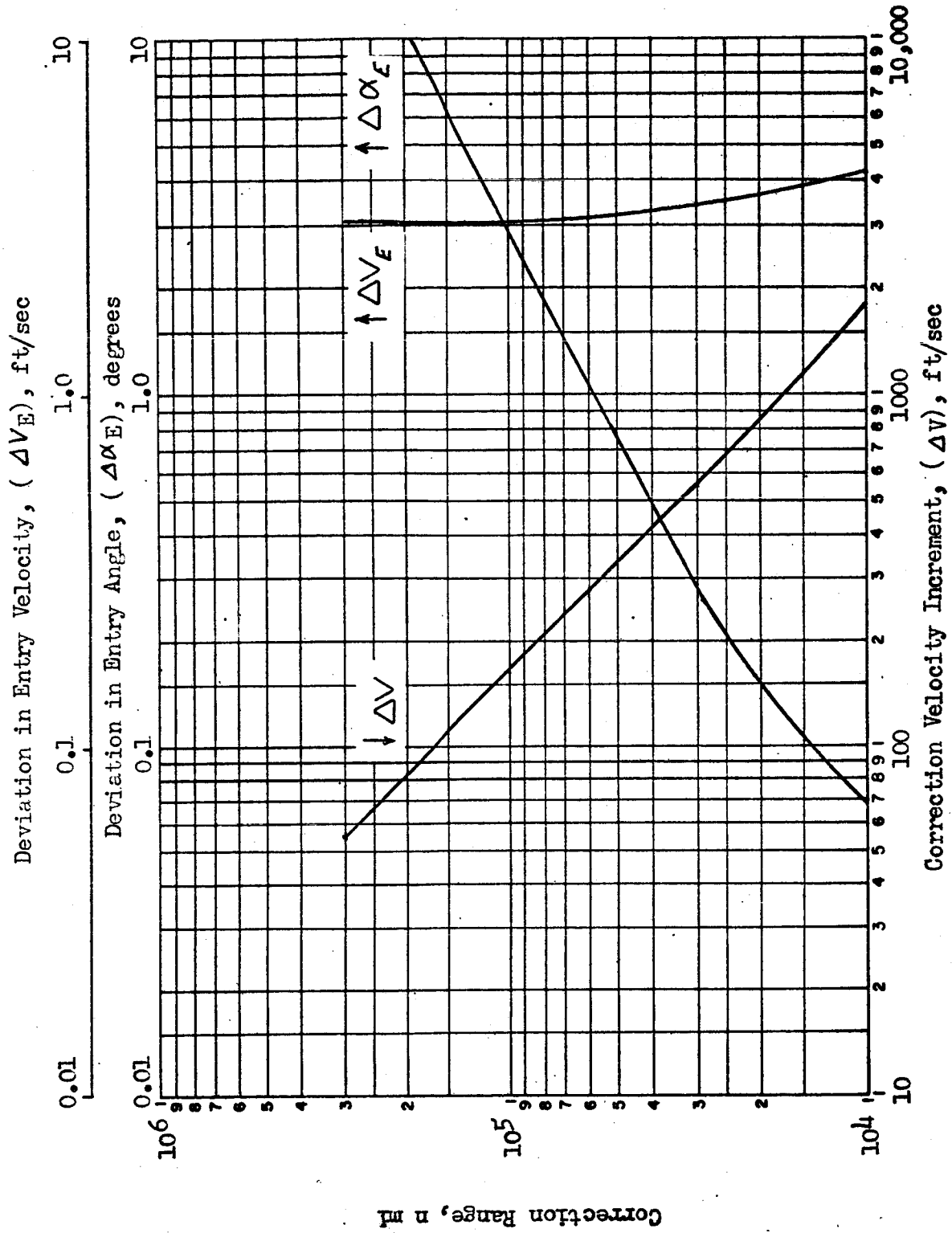


Fig. 20 Terminal Correction for Earth Atmospheric Re-Entry. (Trajectory 2)

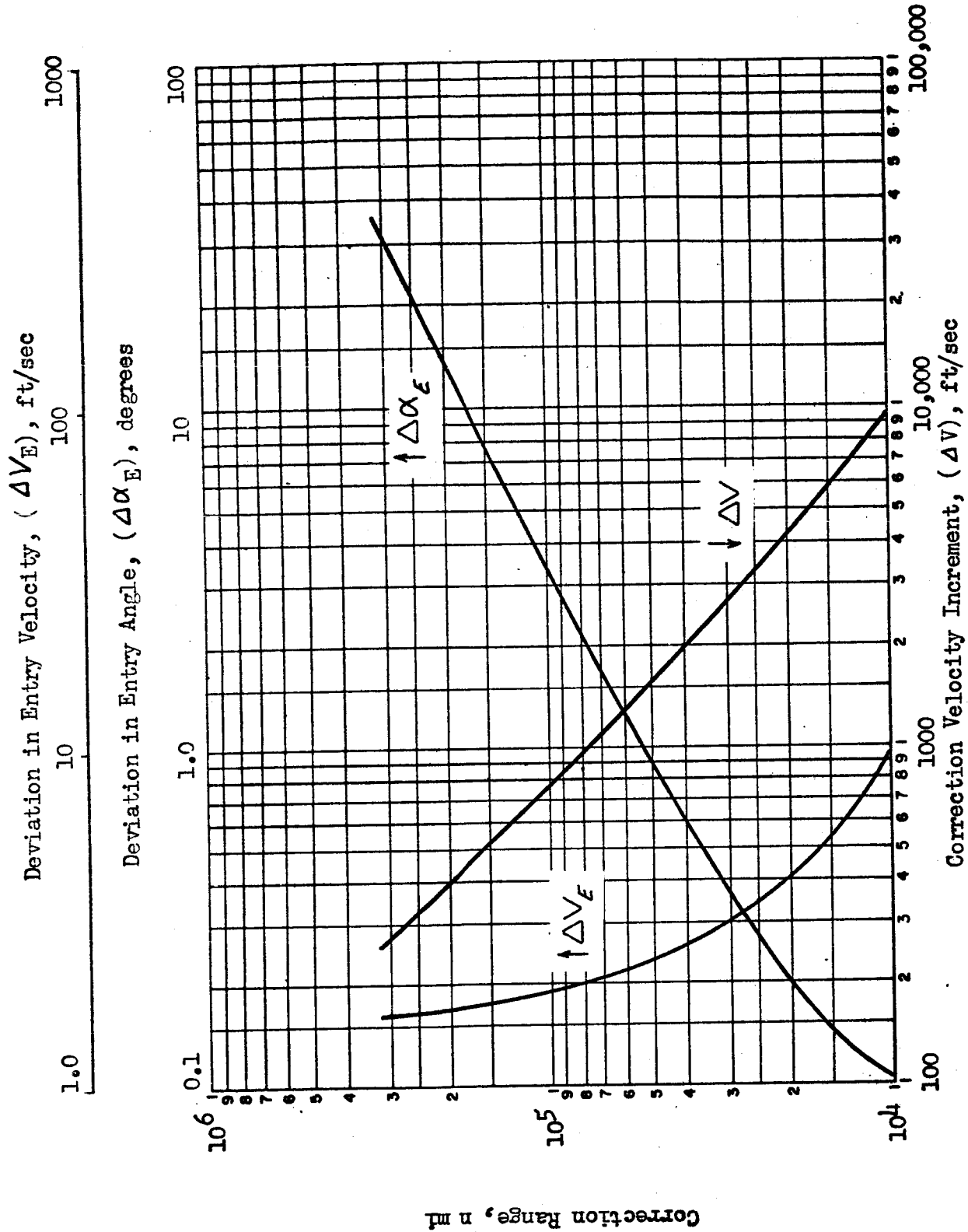


Fig. 21 First Terminal Correction For Earth Atmospheric Re-Entry. (Trajectory 4)

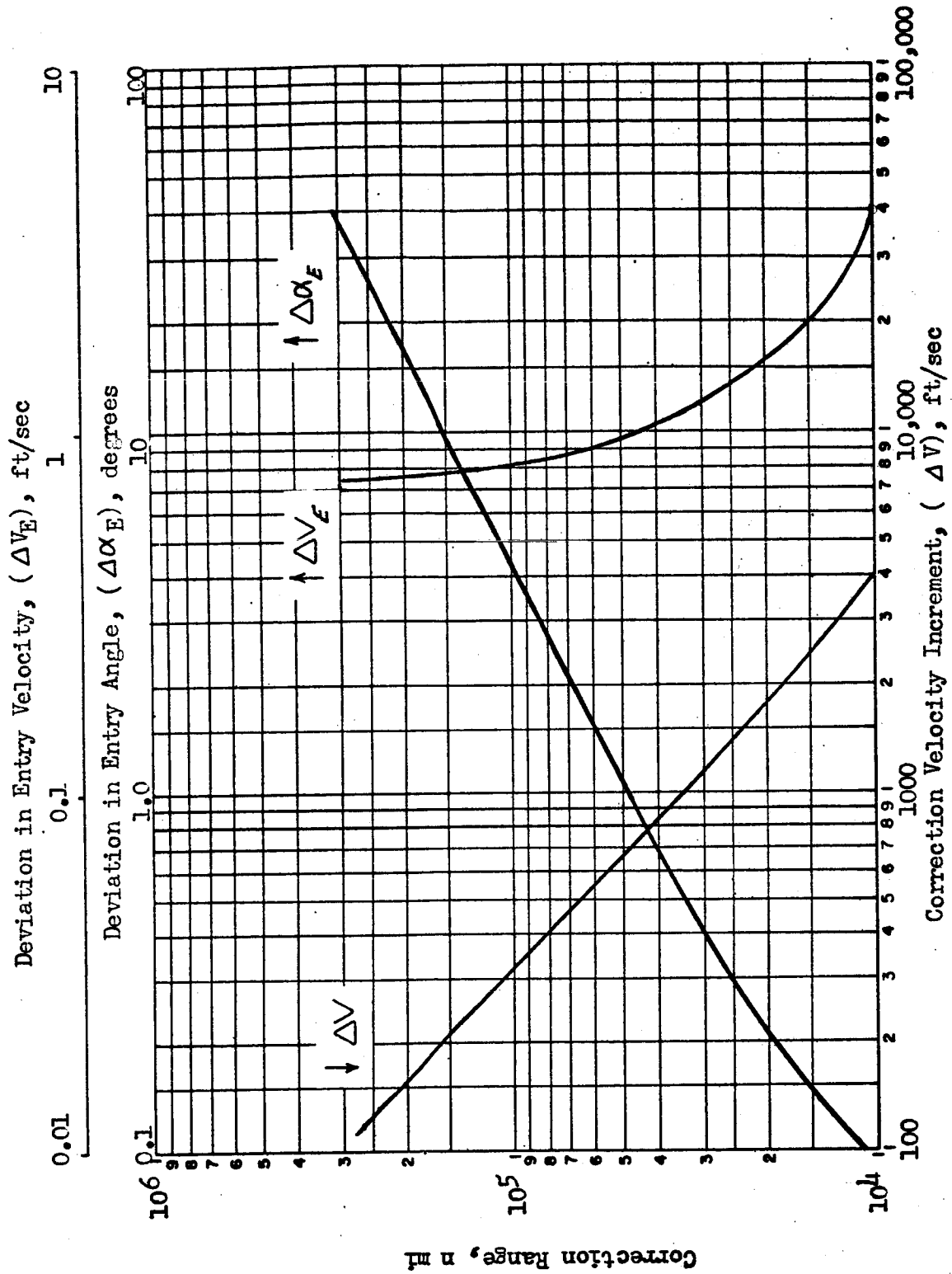


Fig. 22 Terminal Correction for Earth Atmospheric Re-Entry. (Trajectory 6)

TABLE 8
SINGLE TERMINAL CORRECTION FOR EARTH ATMOSPHERIC
REENTRY

Trajectory	Entry Corridor Half-band Width, degrees	Correction Range, n mi	Correction Velocity Increment, ft/sec
2	0.1	14,500	1,200
4	0.3	26,000	3,000
6	0.7	40,500	810

Dual Terminal Corrections. The velocity increments of trajectories 2 and 4 were considered to be excessive. As an alternative to providing such a large propulsion capability, the use of two terminal correction maneuvers was investigated for these trajectories. The first correction was made at 100,000-n mi range to reduce the velocity increment and yet stay within the realm of terminal corrections. The tabulation of these corrections are presented in Table 9 .

TABLE 9
A FIRST TERMINAL CORRECTION APPLIED AT 100,000-N MI RANGE

Trajectory	Entry Angle Deviation, degrees	Correction Range, n mi	First Correction Velocity Increment, ft/sec
2	+ 2.9	100,000	160
4	+ 3.3	100,000	760

Entry angle deviations for the corrected trajectories of Table 9 are larger than the half-band width of the entry corridor; therefore, a second correction is required. For the corrected trajectory, first order partials were generated, as previously described, relating measurement and

second correction-mechanization errors to variations in desired entry conditions. The partials were used with the representative error magnitudes to obtain actual entry condition deviations.

The characteristics of the second correction maneuver are presented in Figures 23 and 24. As a result of the substantial improvement in trajectory accuracy (i.e., reduction in deviation from nominal asymptotic approach distance) achieved by the first correction, the velocity requirements for the second correction are relatively low. Note that, as in previous cases, executing a terminal correction has a negligible effect on entry velocity.

The essential factors of the second terminal corrections are given in Table 10.

TABLE 10
SECOND TERMINAL CORRECTIONS

Trajectory	Entry Corridor Half-band Width, degrees	Deviation in Entry Angle, degrees	Correction Range, n mi	Second Correction Velocity Increment, ft/sec
2	0.1	+ 0.1	14,000	125
4	0.3	+ 0.3	28,000	60

Velocity requirement data from Tables 8, 9 and 10 are presented in Table 11 to illustrate the substantial benefit derived by the use of a two-correction technique instead of a single-correction method.

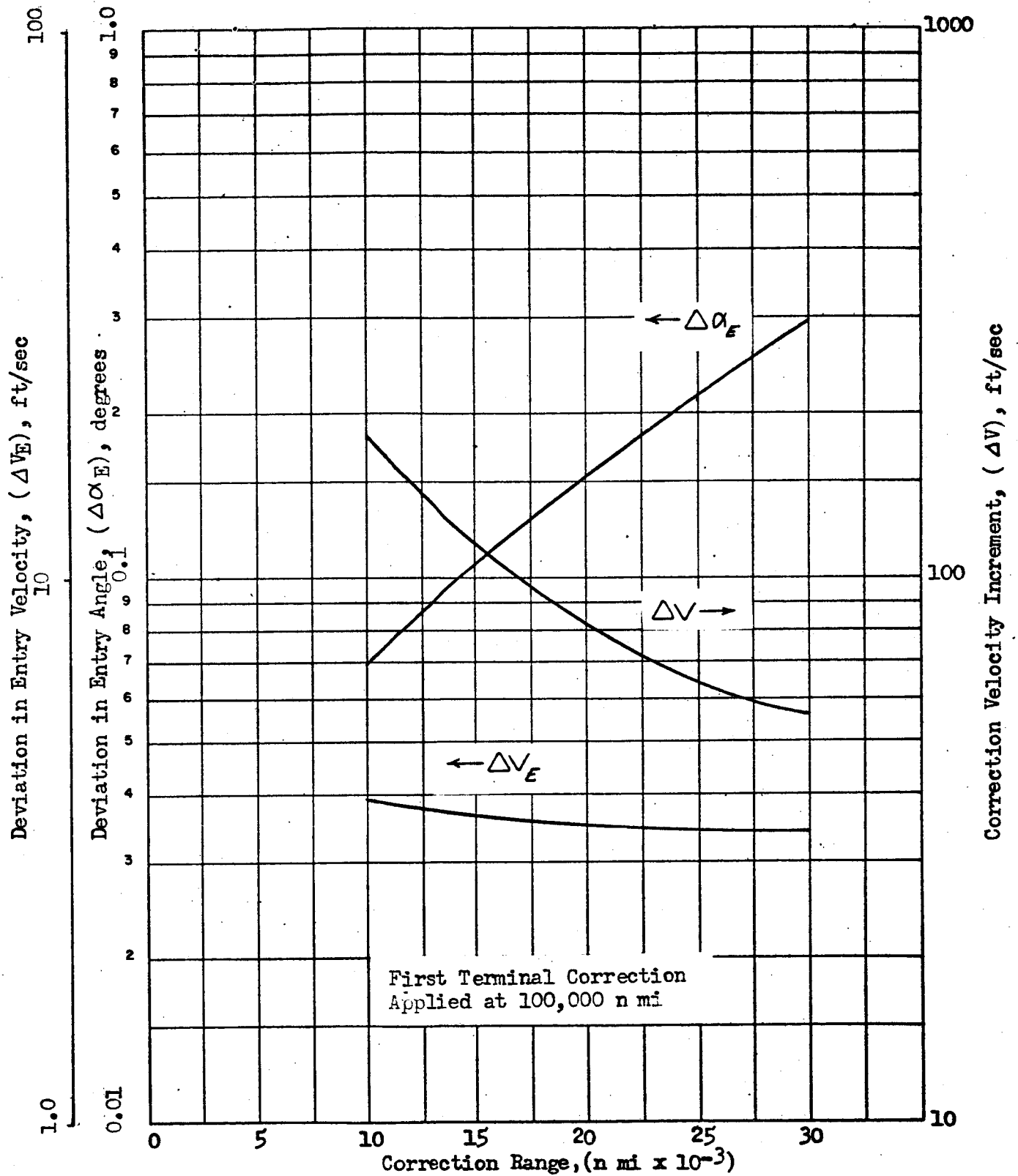


Fig. 23 Second Terminal Correction for Earth Atmospheric Re-Entry.
(Trajectory 2)

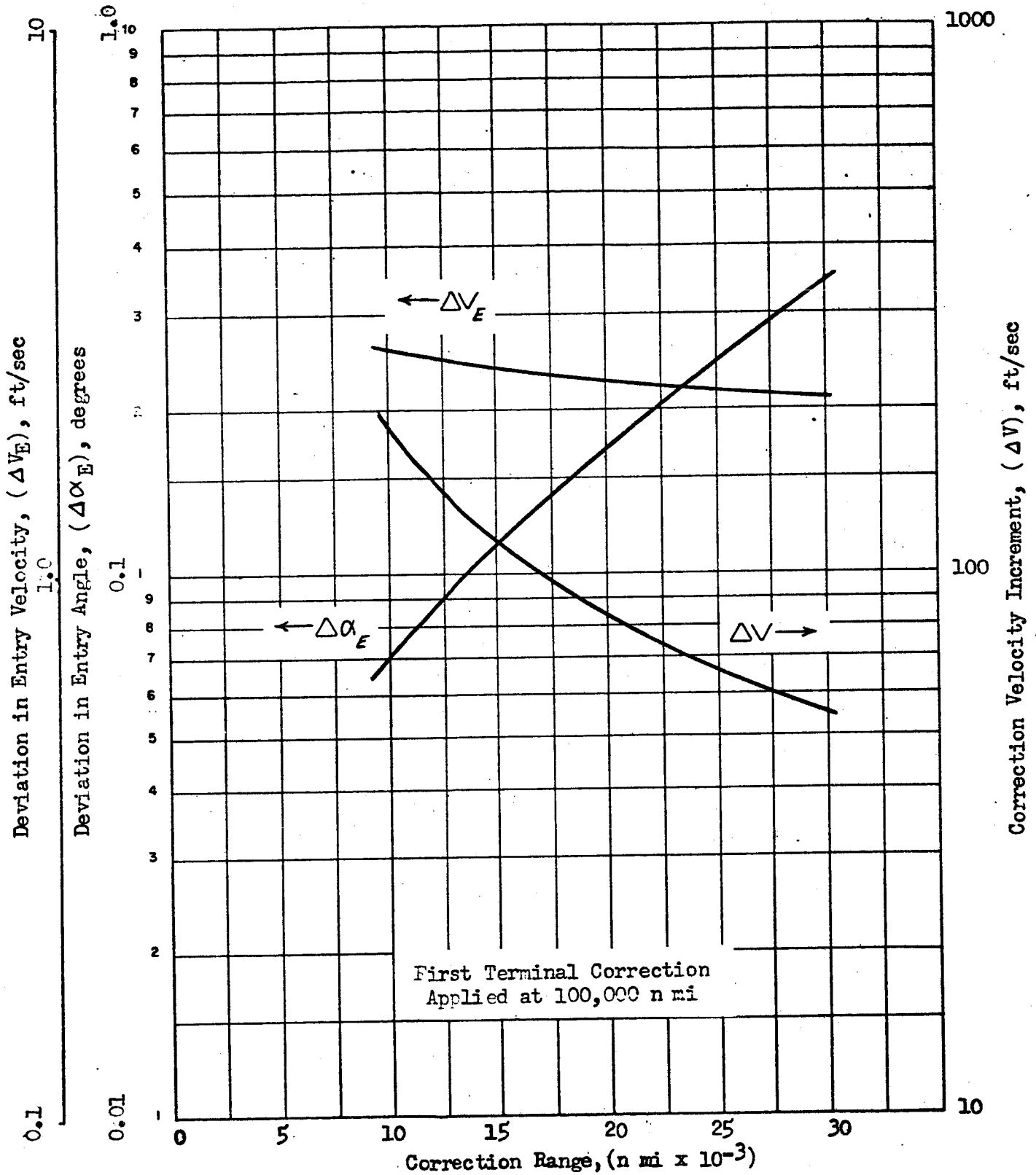


Fig. 24 Second Terminal Correction for Earth Atmospheric Re-Entry.
(Trajectory 4)

TABLE 11

COMPARISON OF TERMINAL CORRECTION VELOCITY REQUIREMENTS

Trajectory	Single Correction Method		
	Velocity Increment, ft/sec		
2	1200		
4	3000		
	Dual Correction Method		
	1st Correction	2nd Correction	Total Correction, ft/sec
2	160	125	285
4	760	60	820

A similar reduction in velocity requirement could be obtained by the use of a 2-correction scheme for trajectory (6); in that case, however the velocity requirement for a single correction is reasonably small (810 ft/sec), and the possible propellant saving probably does not warrant the addition of need for engine restart capability imposed by utilization of a 2-correction technique.

Terminal Correction Results. The analysis of the accuracy of midcourse corrections for the trajectories has shown the necessity of terminal corrections if the selected entry corridor requirements are to be satisfied. The study results show the propulsive requirements that should be included in evaluation of missions employing atmospheric entry.

Although use of dual terminal corrections involves restarting an engine, the sizable reduction in correction velocity increment obtained justifies employment of the technique. Use of the two-correction schemes for trajectory Number 6 was not considered to be warranted since the single-correction velocity increment for that trajectory was about the same magnitude as the velocity requirements for the two corrections of Trajectory 4.

The terminal correction analysis results for atmospheric entry of drag vehicles are summarized in Table 12. The range for applying a single correction or the second correction of dual corrections was specifically selected to restrict the deviations about the nominal entry angle to values equalling entry corridor half-band widths. The results are valid for F/W in the range of 0.1 to 0.5.

TABLE 12

**SUMMARY OF TERMINAL CORRECTIONS FOR EARTH
ATMOSPHERIC REENTRY**

Trajectory	Entry Corridor Half-band Width, degrees	Number of Terminal Corrections	Deviation in Entry Angle, degrees	Range at Correction, n mi	Total Terminal Correction ΔV , ft/sec
2	0.1	2	+ 0.1 -	100,000 14,000	285
4	0.3	2	+ 0.3 -	100,000 28,000	820
6	0.7	1	\pm 0.7	40,500	810

Based on these results, the use of terminal-correction maneuvers (single or dual as required) will provide the entry corridor required without a major deceleration propulsion phase (which would increase corridor width) prior to atmospheric entry.

PROPULSIVE EARTH-ORBIT ESTABLISHMENT AND DEPARTURE MANEUVERS

Single Stage Systems

The establishment of planetocentric orbits following an interplanetary transit represents a principal objective in early exploratory missions and an important intermediate step in many later extraterrestrial landing missions. Analyses were conducted to determine maneuver propulsion requirements, optimum thrust-to-weight ratios (F/W) for maximum payload and relative payload-to-weight ratios for orbit establishment (and departure) maneuvers. The effect of specific impulse (I_s), hyperbolic excess velocity (V_h), thrust-dependent weight factor (K_F) and propellant-dependent weight factor (K_T) on these parameters was evaluated.

The investigation of propulsion requirements for an establishment or departure maneuver is described in Ref. 3, and includes an analysis of the effect of thrust-to-weight ratio and specific impulse. The appropriate nomographs and correction curves from Ref. 3 are presented in Figures 25, 26 and 27. These data represent a graphical presentation of an extensive body of results obtained from numerous simulated trajectory computations. The use of total impulse, rather than the more commonly used ideal-velocity increment, as an intermediate parameter to relate thrust-to-weight ratio to payload was based on the convenience of presentation permitted by utilizing the total impulse parameter. Transformation from one to the other can be accomplished readily by the relationship,

$$V = I_s g \ln \left[\frac{1}{1 - \frac{N}{I_s}} \right] \quad \text{where } N = \text{total impulse-per} \\ \text{lb of gross weight, } \frac{\text{lb-sec}}{\text{lb}}$$

The optimization of thrust level was based on a tradeoff between the increased engine weight but decreased gravitational losses of high thrust-to-weight systems, and the decreased engine weight but increased gravitational losses of low thrust-to-weight systems. The optimization was achieved by determining the thrust-to-weight ratio for which engine weight plus propellant and tank weight was a minimum.

The parameters selected for analysis of Earth-orbit establishment and departure maneuvers were varied over a sufficiently wide range to include many types of systems. K_F varied from a value representative of a pump-fed system to a high value indicative of a redundant pump- or pressure-fed system. K_T and I_s had values typical of Earth-storable and cryogenic propellants. V_h ranged from zero (appropriate for a lunar mission) to velocities required for interplanetary missions.

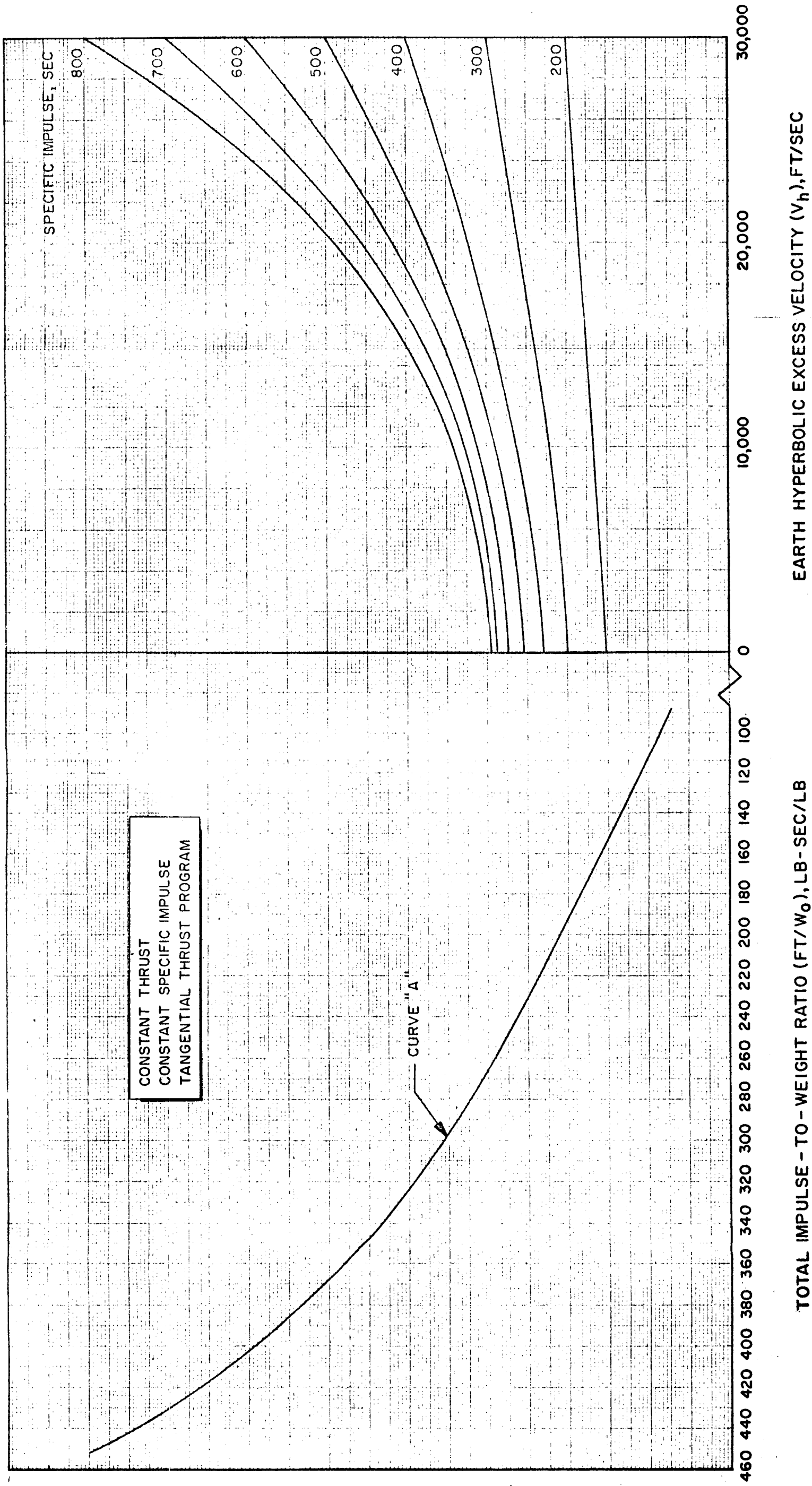


Figure 25 Earth Nomograph

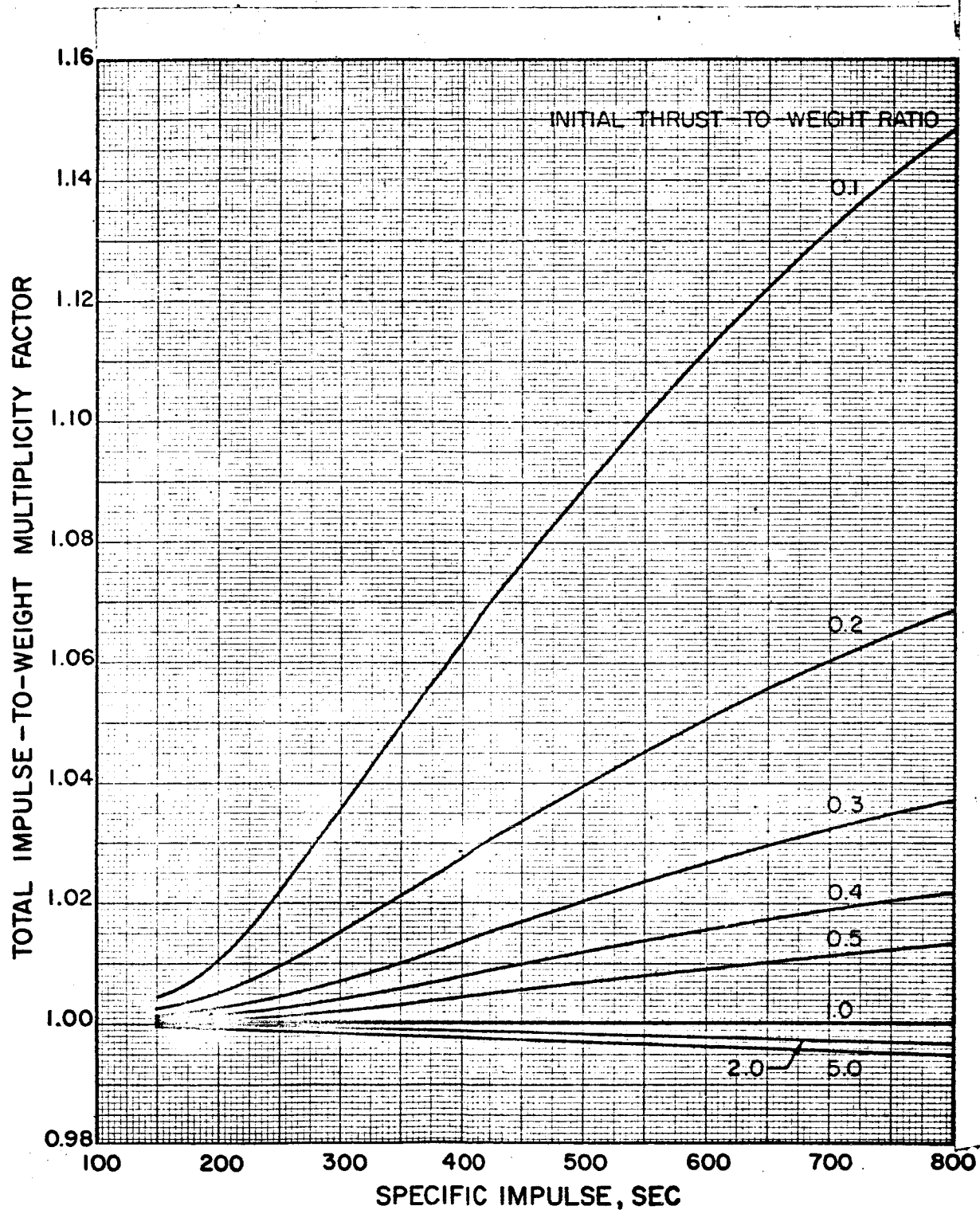


Figure 26 Total Impulse-to-Weight Correction Factor

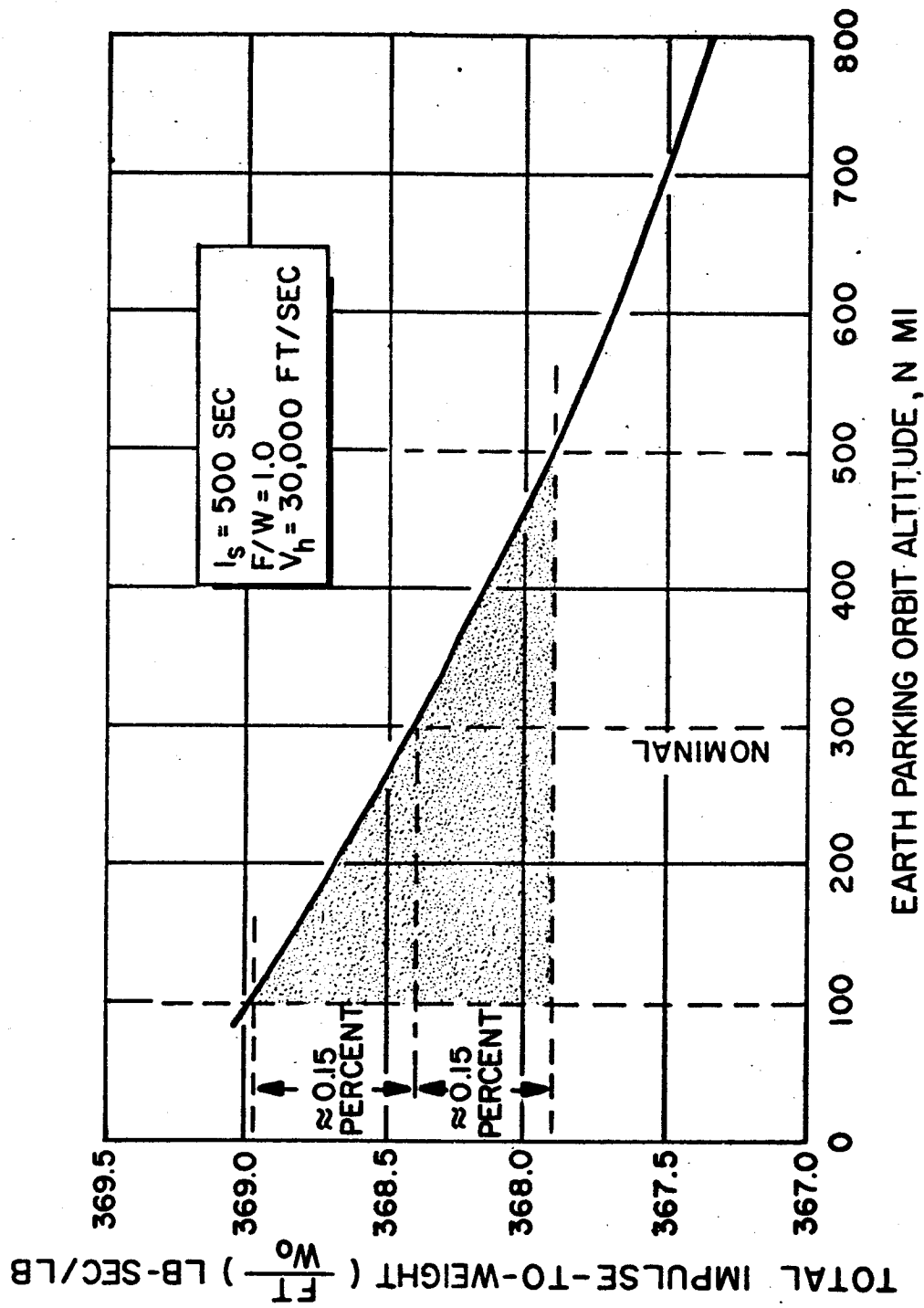


Figure 27 The Variation of Total Impulse-to-Weight Ratio With Parking Orbit Altitude

The results presented are applicable to both injection into, and departure from, planetocentric orbit. The propulsion requirements are, in fact, not totally independent of whether the maneuver is a departure or an arrival, but computation of a series of Mars trajectories indicated that they are sufficiently similar in the significant F/W range to neglect the small difference that exists. Figure 28 presents the ratio of total impulse-to-initial weight ($F.T/W_0$) for orbit establishment and departure for a 300-n mi circular Martian orbit. For F/W greater than 0.2, the total impulse difference is less than 0.6 percent.

Parametric Analysis. Values of the parameters selected for analysis of Earth-vicinity maneuvers were:

1. Hyperbolic excess velocity = V_h : 0; 15,000; 30,000 ft/sec
2. Propellant dependent weight factor = K_T : 0.08, 0.16 lb/lb
3. Thrust dependent weight factor = K_E : 0.025, 0.05, 0.075 lb/lb
4. Specific impulse = I_s : 320 seconds, 420 seconds

Hyperbolic excess velocities were chosen in accordance with Reference 4. A V_h of 15,000 ft/sec is a reasonable value for Earth-orbit departure to Mars or Venus. A 30,000-ft/sec hyperbolic excess velocity is representative of a trip to Mercury or a fast trip to Mars or Venus. These numbers are not intended to be exact but rather to encompass a wide range of missions.

For this analysis, the weight factors are defined as follows. K_E is defined such that $F.K_E$ equals engine weight plus all thrust associated structure weight. K_T is defined such that $W_p.K_T$ (where W_p equals propellant weight) equals tank weight, shielding, insulation, and all propellant dependent structure weight. The guidance package and other fixed weights are considered to be zero since they are usually a small part of gross weight. The equation for weight is then

$$W_G = W_p + K_T W_p + K_E F + PL \quad (1)$$

Rearranging equation (1) gives

$$\frac{PL}{W_G} = 1 - K_E \frac{F}{W} - \frac{W_p}{W_G} (1 + K_T)$$

$V_{\infty} = 36,000$ ft/sec, Mars 300 n mi Circular Orbit, Specific Impulse = 420 seconds.

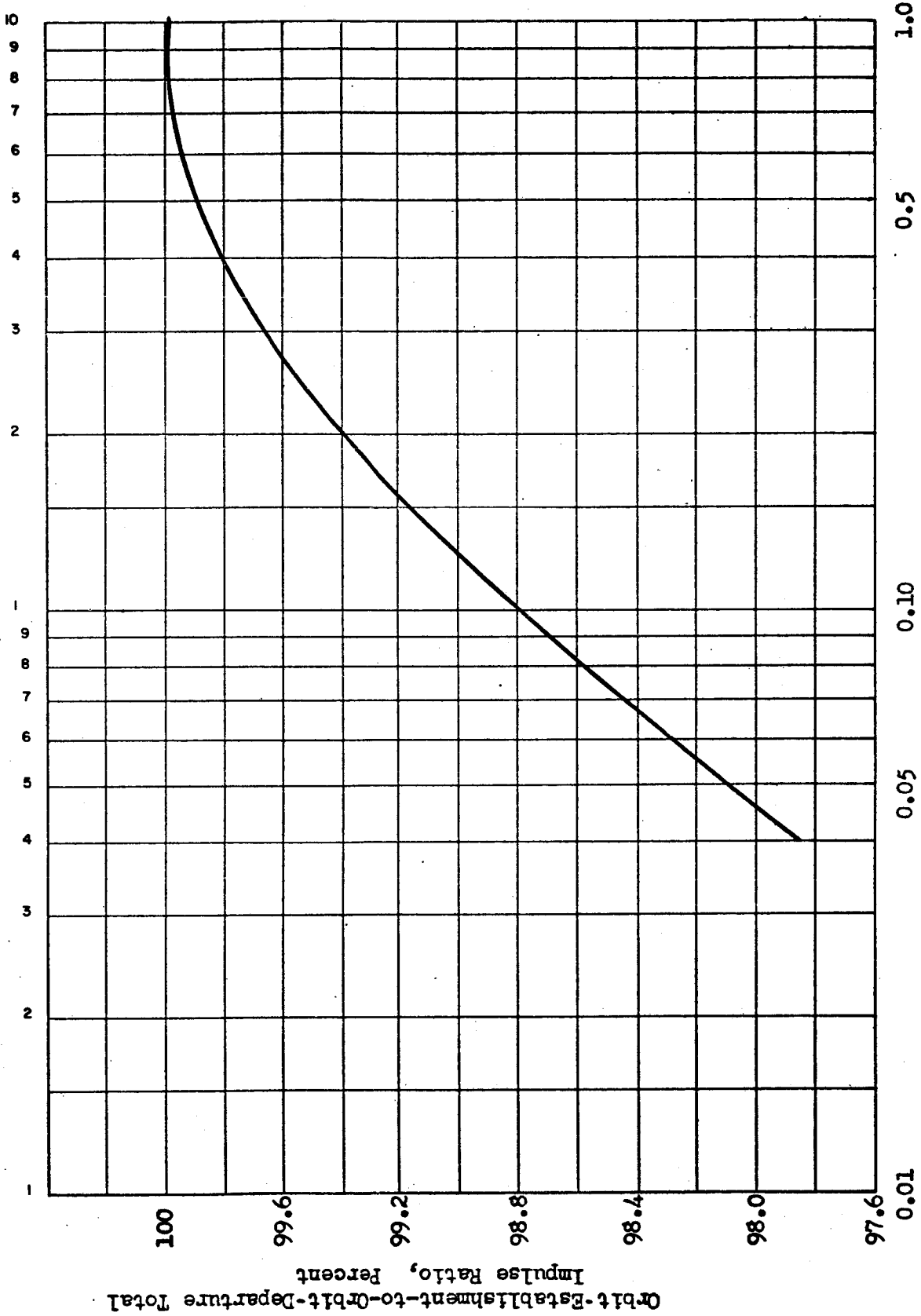


Figure 28 • Ratio of Orbit-Establishment to Orbit-Departure Propulsion Requirements as a Function of Initial Thrust-to-(Earth) Weight Ratio.

K_E , F/W , and K_T can be chosen arbitrarily and $F \cdot T / W_G$ is determined from the nomographs. $F \cdot T / I_s \cdot W_G$ can be computed and equals W_p / W_G as can be shown:

$$I_s = F / \dot{W}$$

$$\frac{F \cdot T}{I_s \cdot W_G} = \frac{F \cdot T}{\frac{F}{\dot{W}} \cdot W_G} = \frac{\dot{W} \cdot T}{W_G} = \frac{W_p}{W_G} \quad (2)$$

The parameters were varied independently although in fact, they would not do so. If I_s , for example, were 320 seconds, corresponding to Earth-storable propellants, K_T would be about 0.08 due to the higher mass density and less stringent insulating requirements as compared to a liquid oxygen-hydrogen system. The parameters were varied separately, however, to determine their individual effects on F/W_G and payload.

The principal results of the thrust level investigation are presented in Figure 29 to Figure 39. Typical effects of K_T , K_E , I_s and V_h on optimum thrust level are summarized in Figure 40. The nominal values represent a typical liquid oxygen-hydrogen system. The effect of variation in hyperbolic excess velocity on payload-to-gross weight capability of a propulsion stage is shown in Figure 41.

The results shown in Table 13 indicate that K_E has a small effect on payload, whereas K_T , I_s , and V_h all affect payload considerably. K_E has the most pronounced effect on optimum F/W , with increasing K_E resulting in decreased optimum F/W . The flatness of the payload curves over a wide range of F/W values in the vicinity of the optimum F/W , particularly for nonredundant systems ($K_E = 0.025$ or less), indicates that the selected system thrust can vary over a range of values without penalizing payload significantly. Secondary considerations (i.e., other than maximizing payload) such as vehicle packaging or utilization of available engines can be permitted to influence the choice of thrust level for orbit establishment and departure propulsion systems.

Staging Considerations for Orbit Departure Vehicles

As the mission hyperbolic excess velocity increases, the ideal velocity requirement for the orbit departure maneuver becomes sufficiently high that a two-stage vehicle or a vehicle with tank staging provides a significantly larger payload than a single stage vehicle. An analysis was conducted to

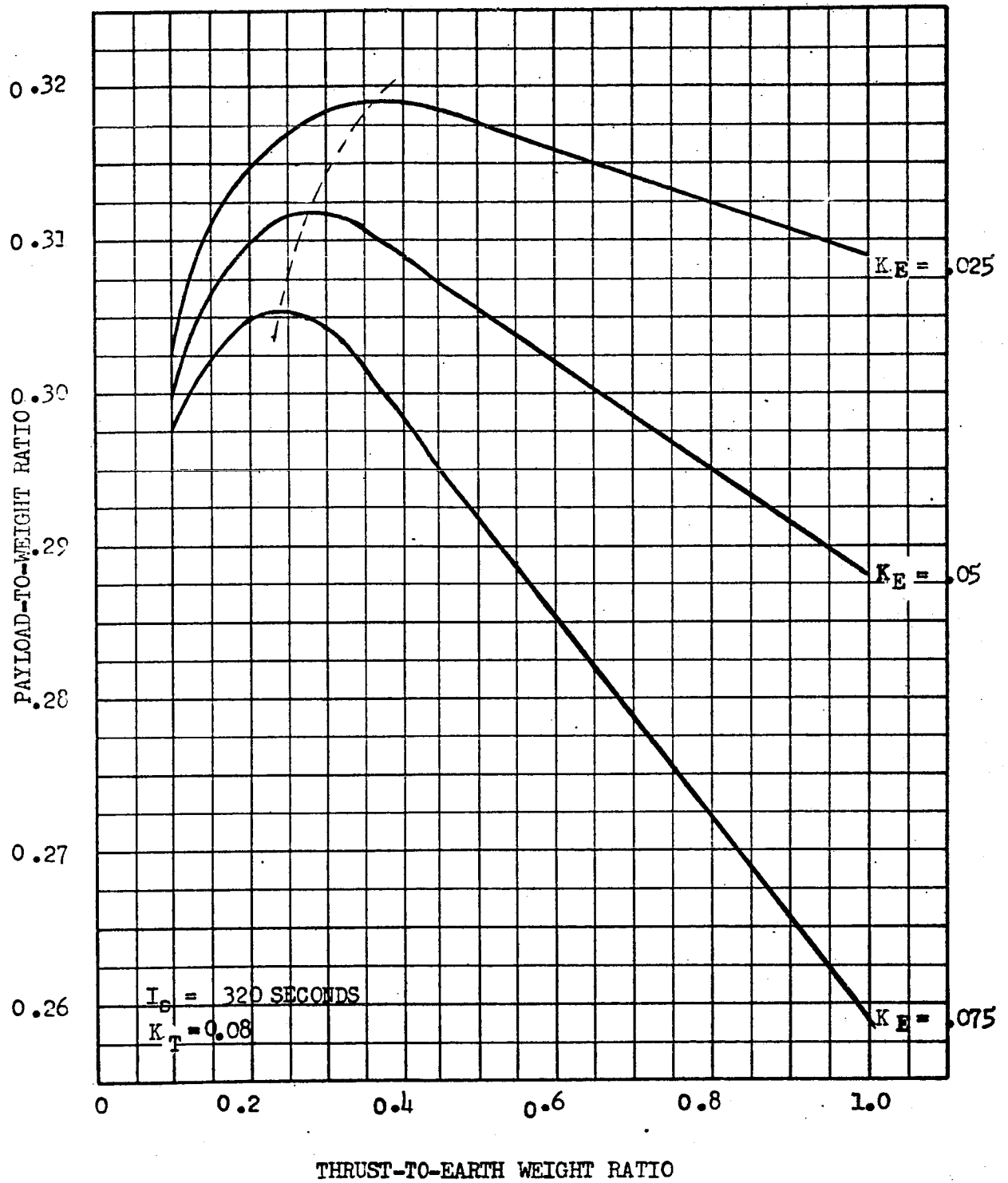


Figure 29
EARTH - HYPERBOLIC EXCESS = 0 ft/sec

ROCKETDYNE
A DIVISION OF NORTH AMERICAN AVIATION, INC.

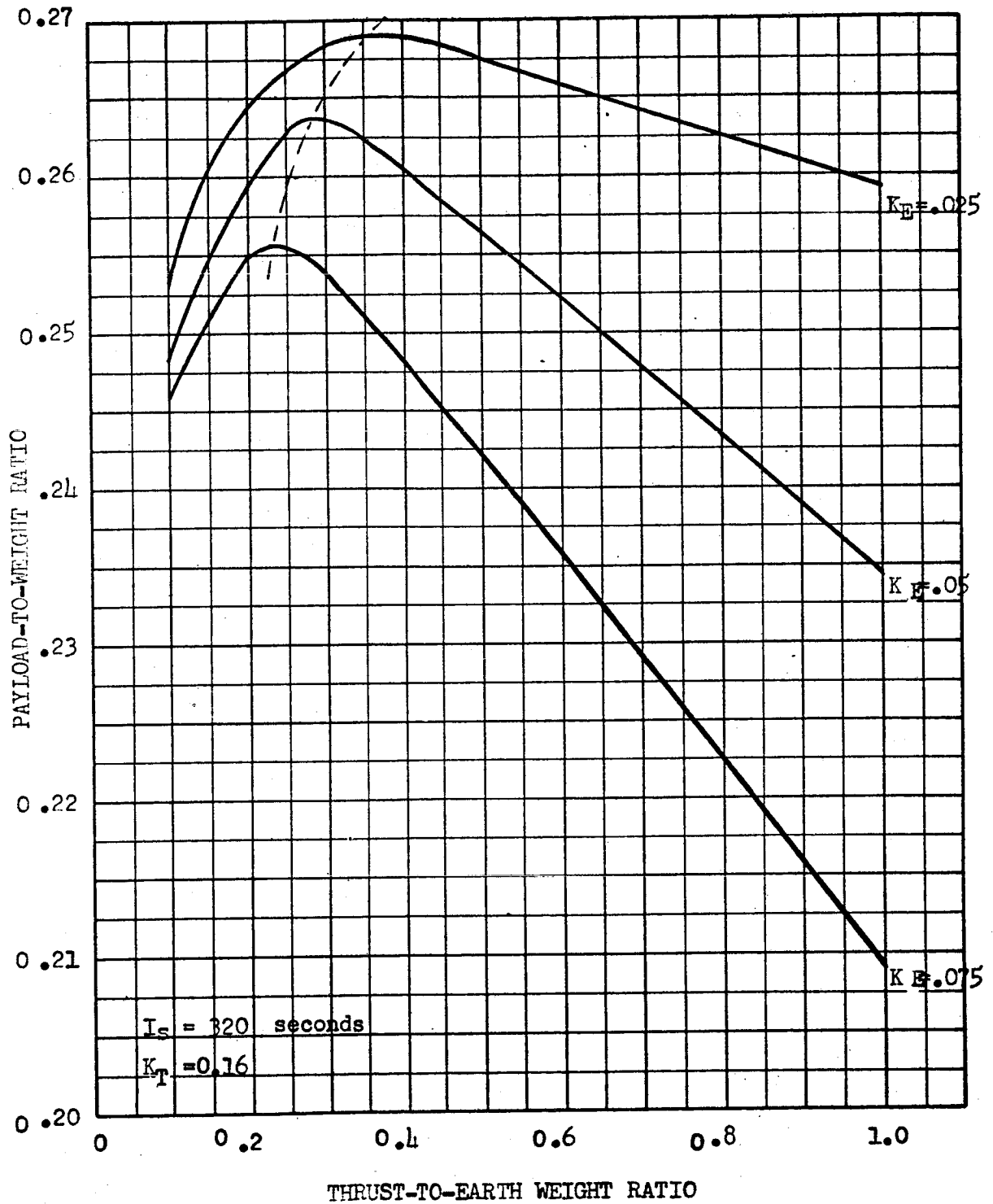


Figure 30

EARTH - HYPERPOLIC EXCESS = 0 ft/sec

ROCKETDYNE
A DIVISION OF NORTH AMERICAN AVIATION, INC.

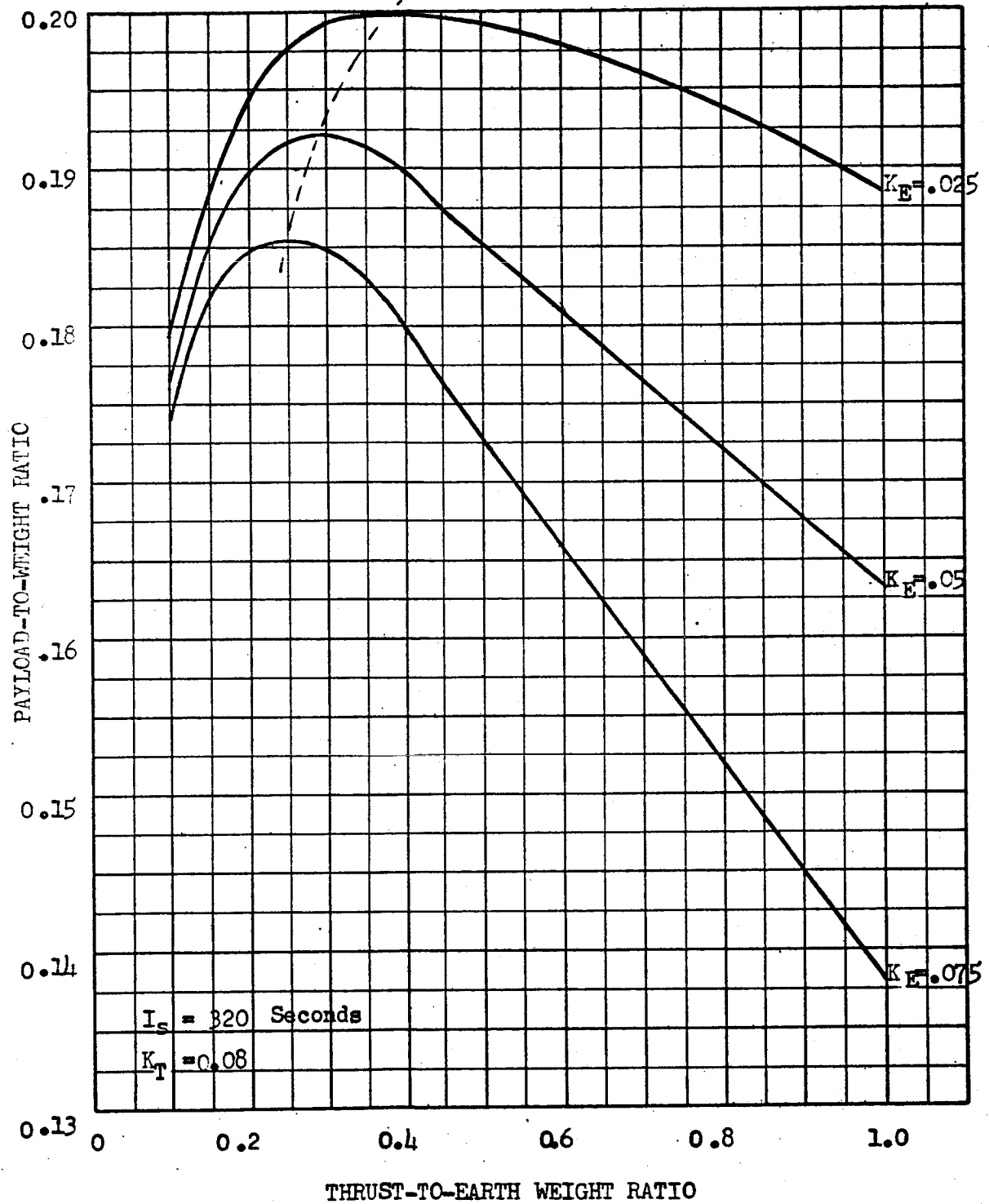


Figure 31
EARTH - HYPERBOLIC EXCESS = 15,000 ft/sec

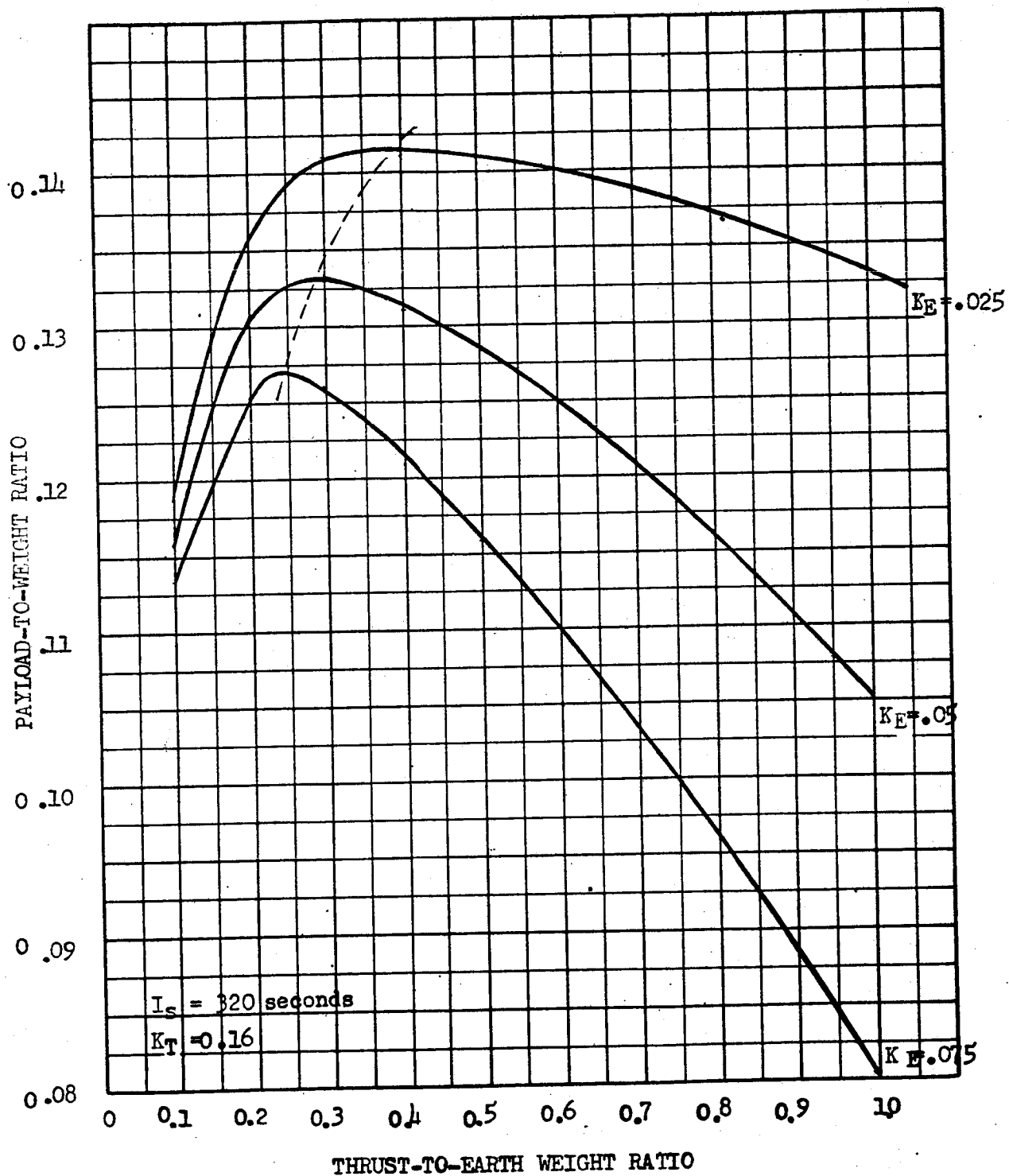


Figure 32
EARTH - HYPERBOLIC EXCESS = 15,000 ft/sec

ROCKETDYNE
A DIVISION OF NORTH AMERICAN AVIATION, INC.

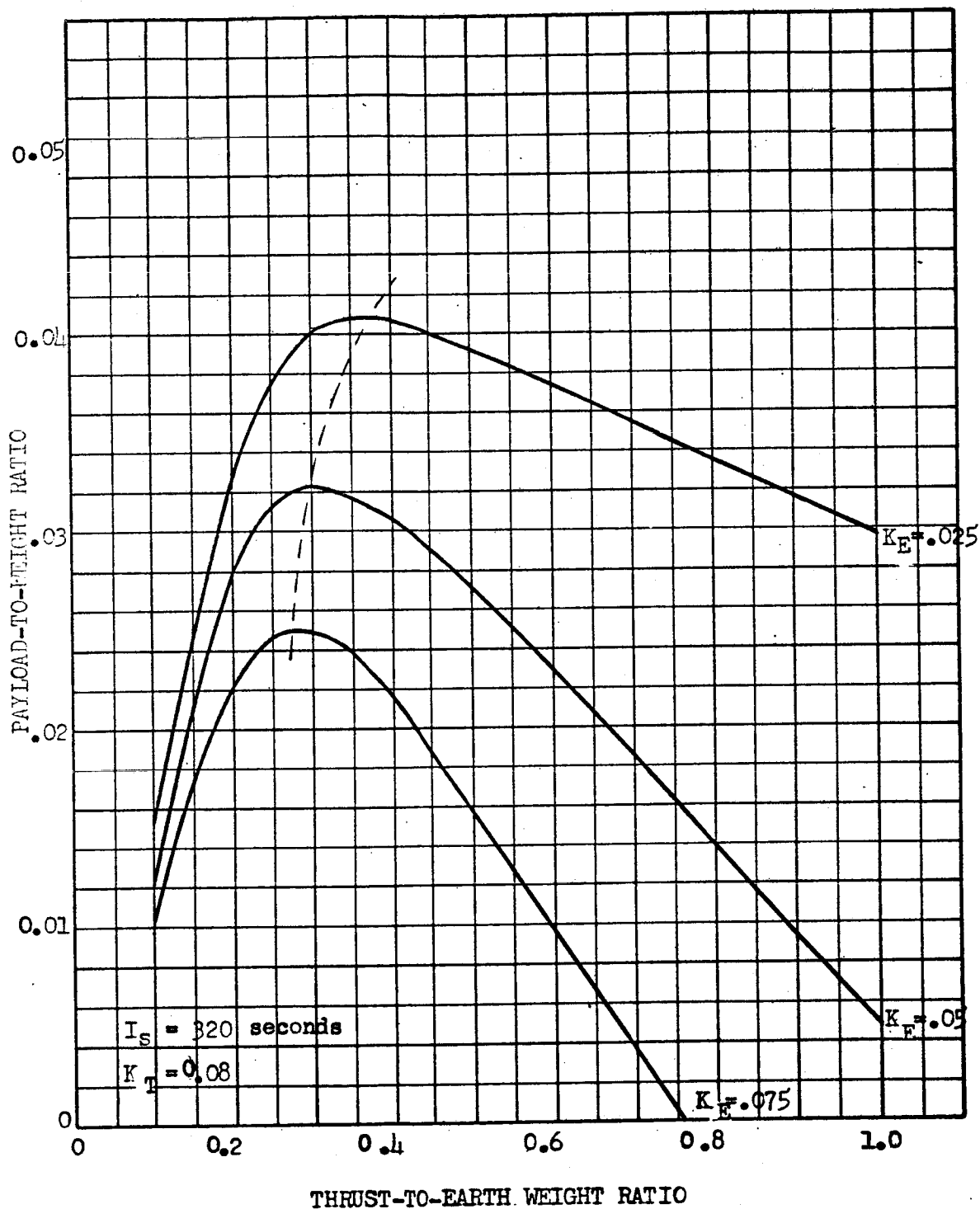


Figure 33
EARTH - HYPERBOLIC EXCESS = 30,000 ft/sec

ROCKETDYNE
A DIVISION OF NORTH AMERICAN AVIATION, INC.

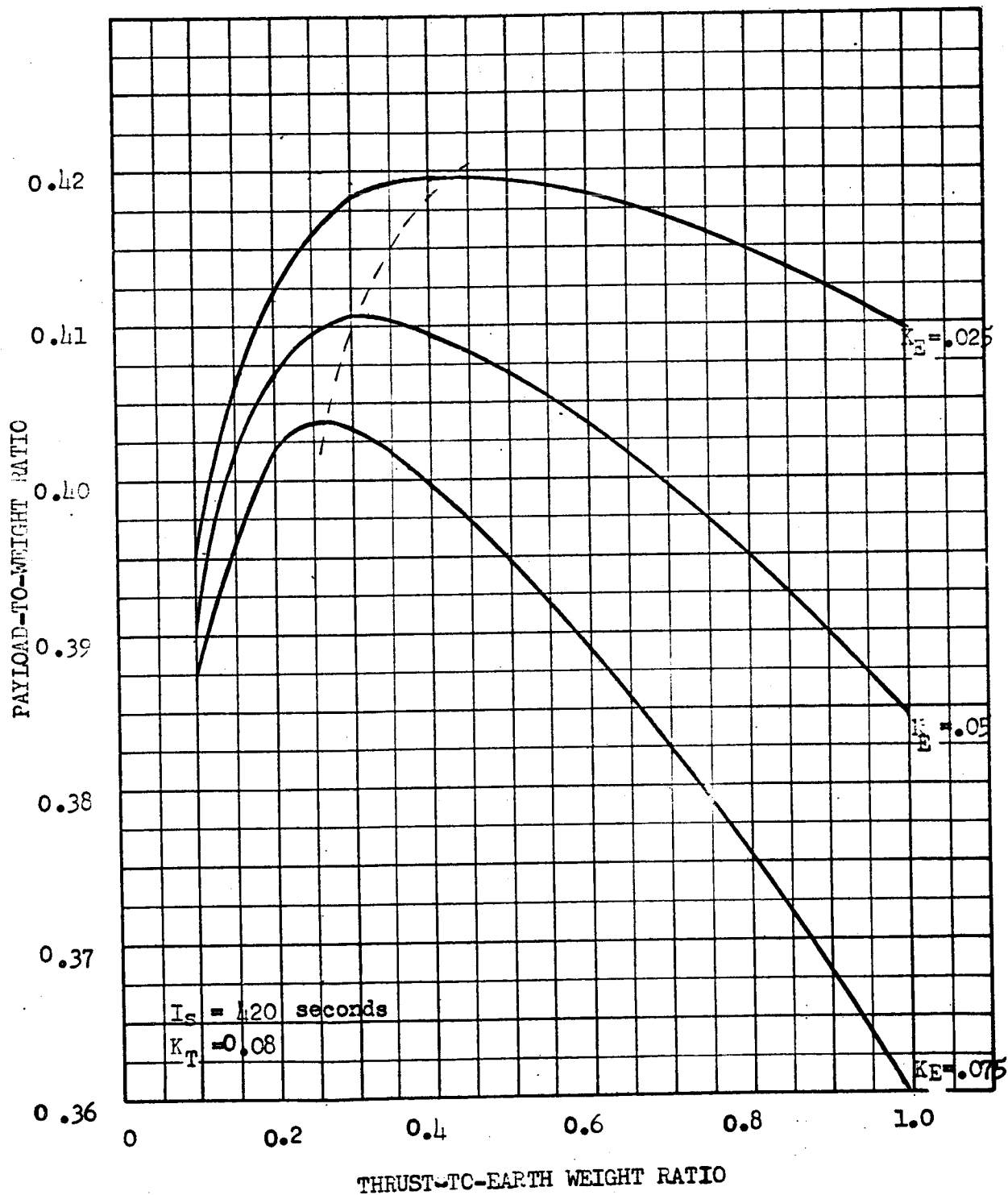


Figure 34
EARTH- HYPERBOLIC EXCESS = 0 ft/sec

ROCKETDYNE
A DIVISION OF NORTH AMERICAN AVIATION, INC.

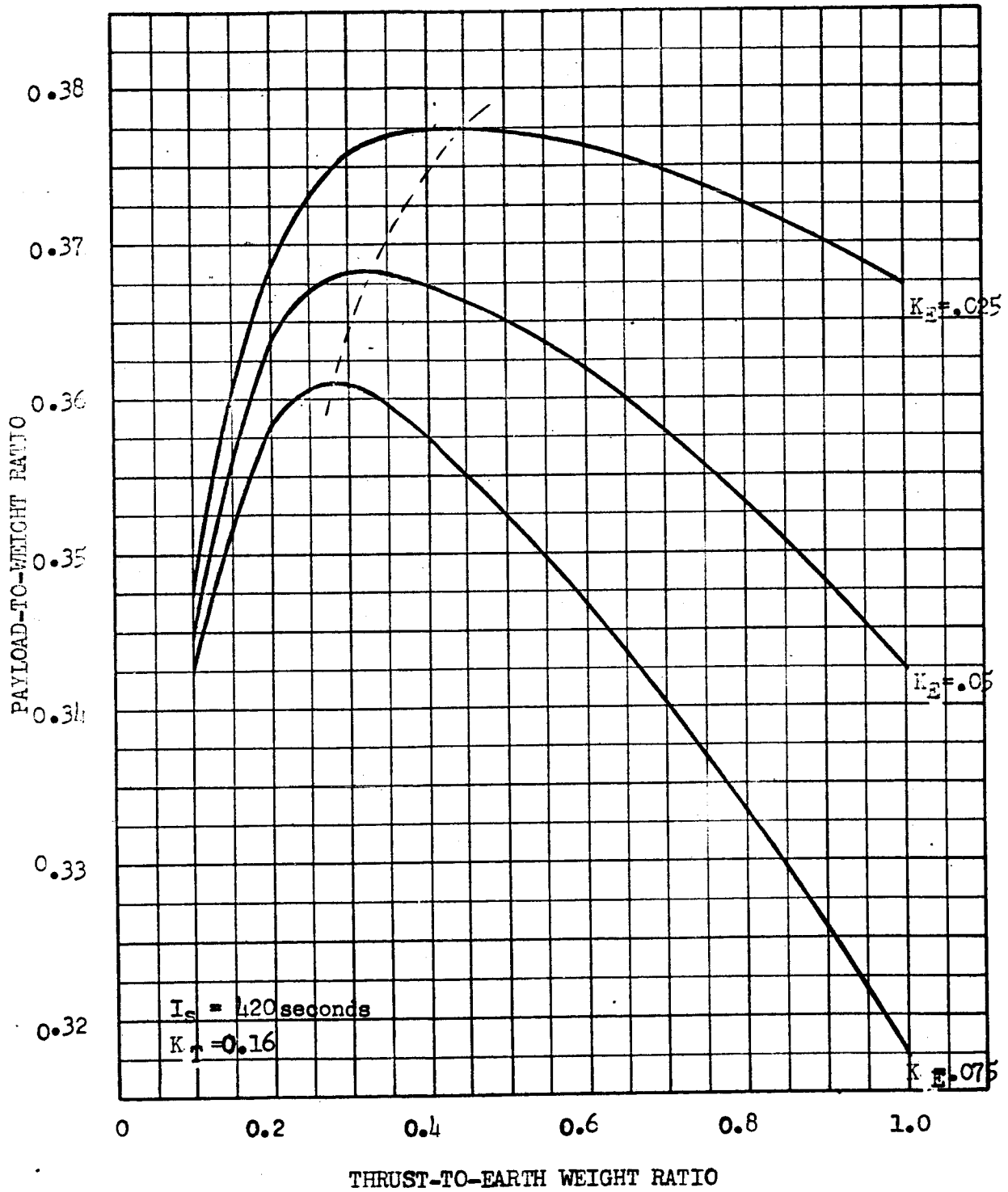


Figure 35
EARTH - HYPERBOLIC EXCESS = 0 ft/sec

ROCKETDYNE
A DIVISION OF NORTH AMERICAN AVIATION, INC.

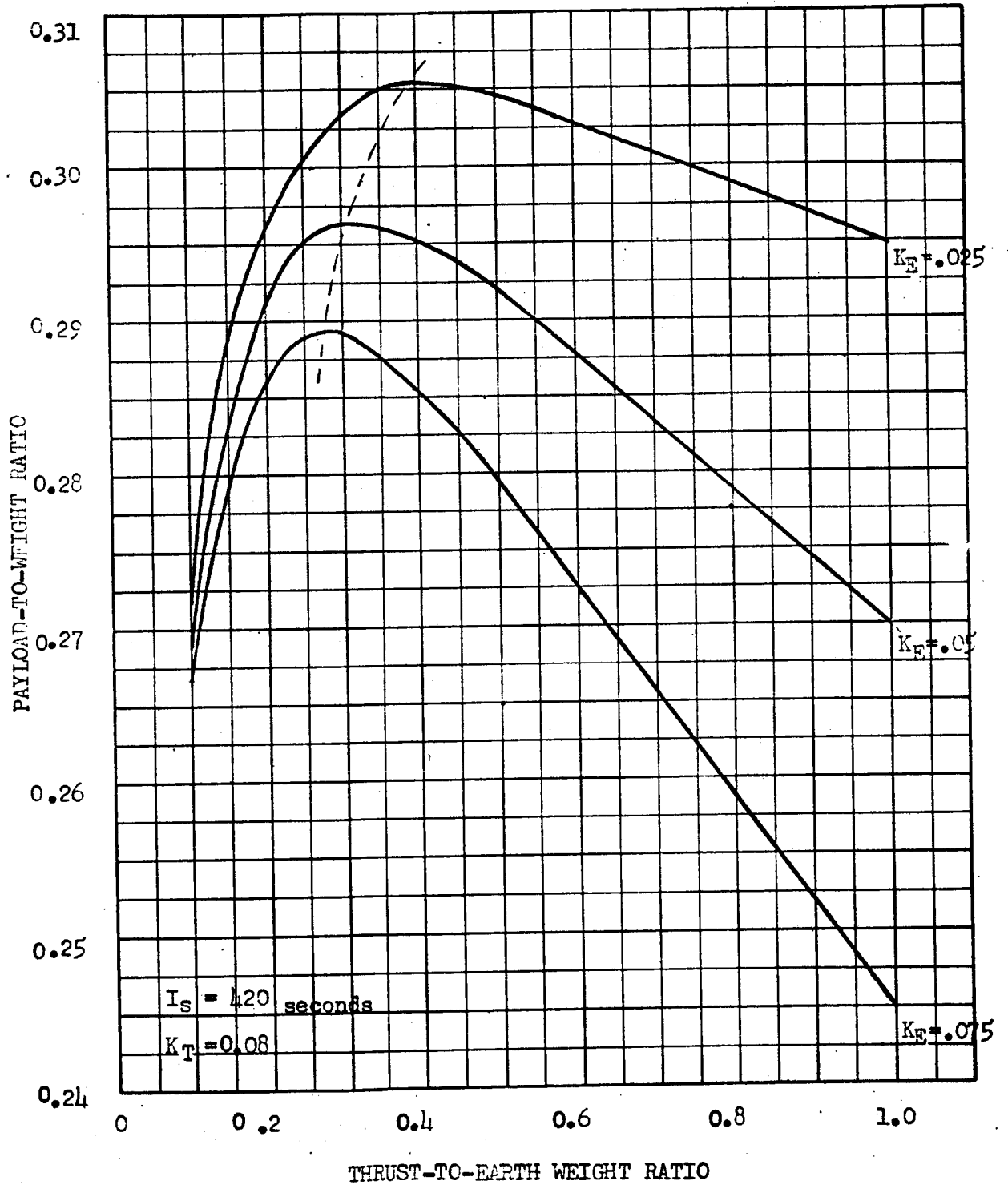


Figure 36
EARTH - HYPERBOLIC EXCESS = 15,000 ft/sec

ROCKETDYNE
A DIVISION OF NORTH AMERICAN AVIATION, INC.

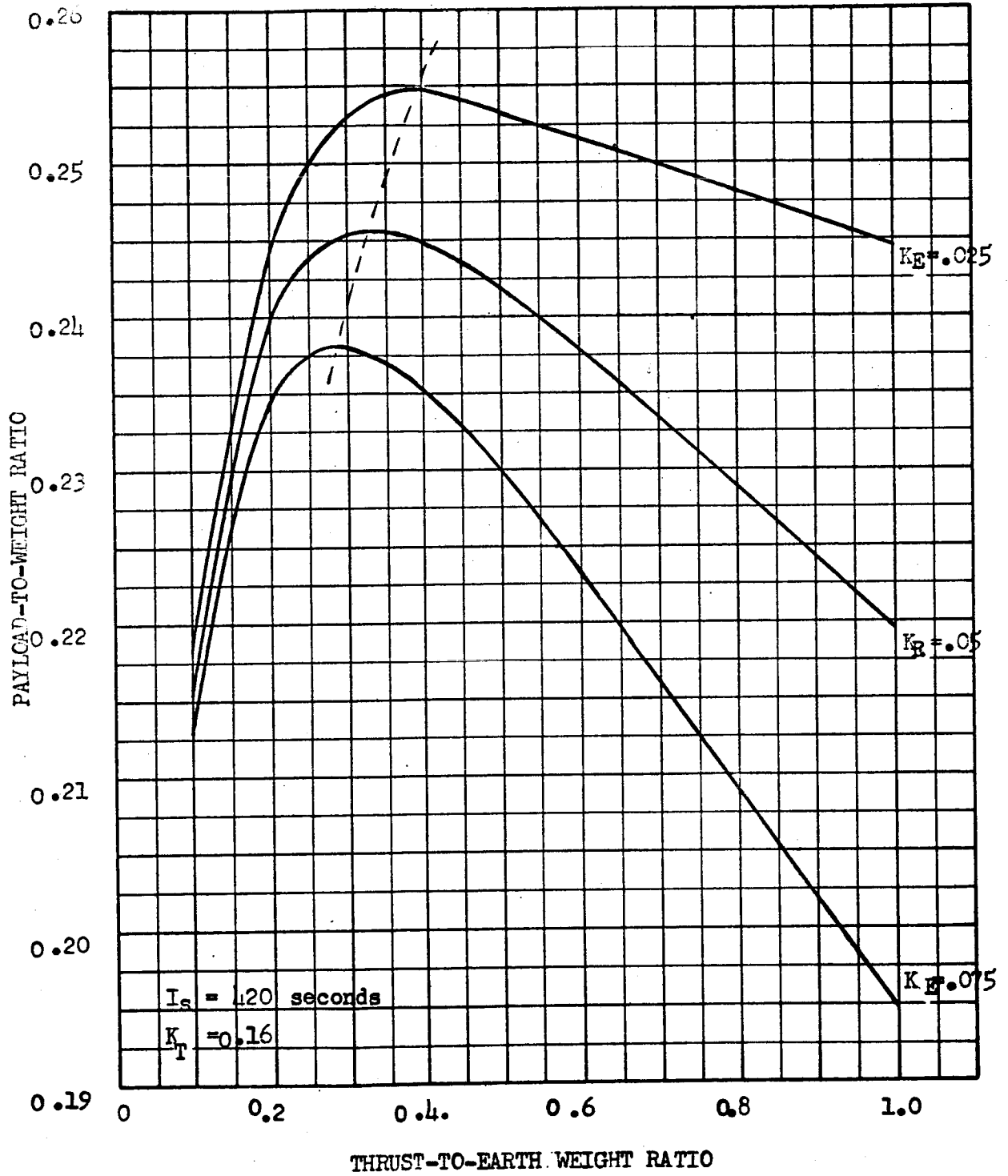


Figure 37
EARTH - HYPERBOLIC EXCESS = 15,000 ft/sec

ROCKETDYNE
A DIVISION OF NORTH AMERICAN AVIATION, INC.

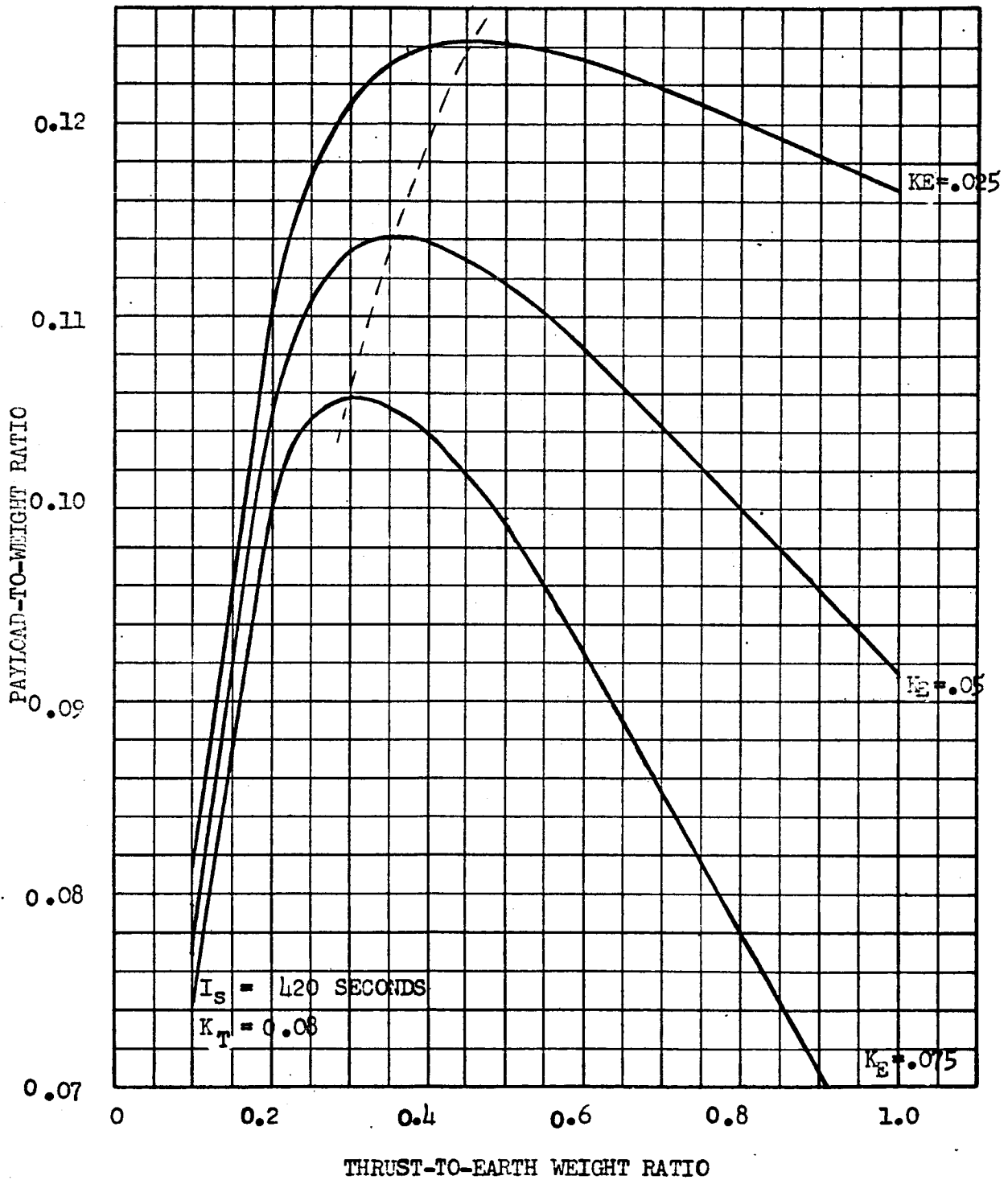


Figure 38

EARTH - HYPERBOLIC EXCESS = 30,000 ft/sec

ROCKETDYNE
A DIVISION OF NORTH AMERICAN AVIATION, INC.

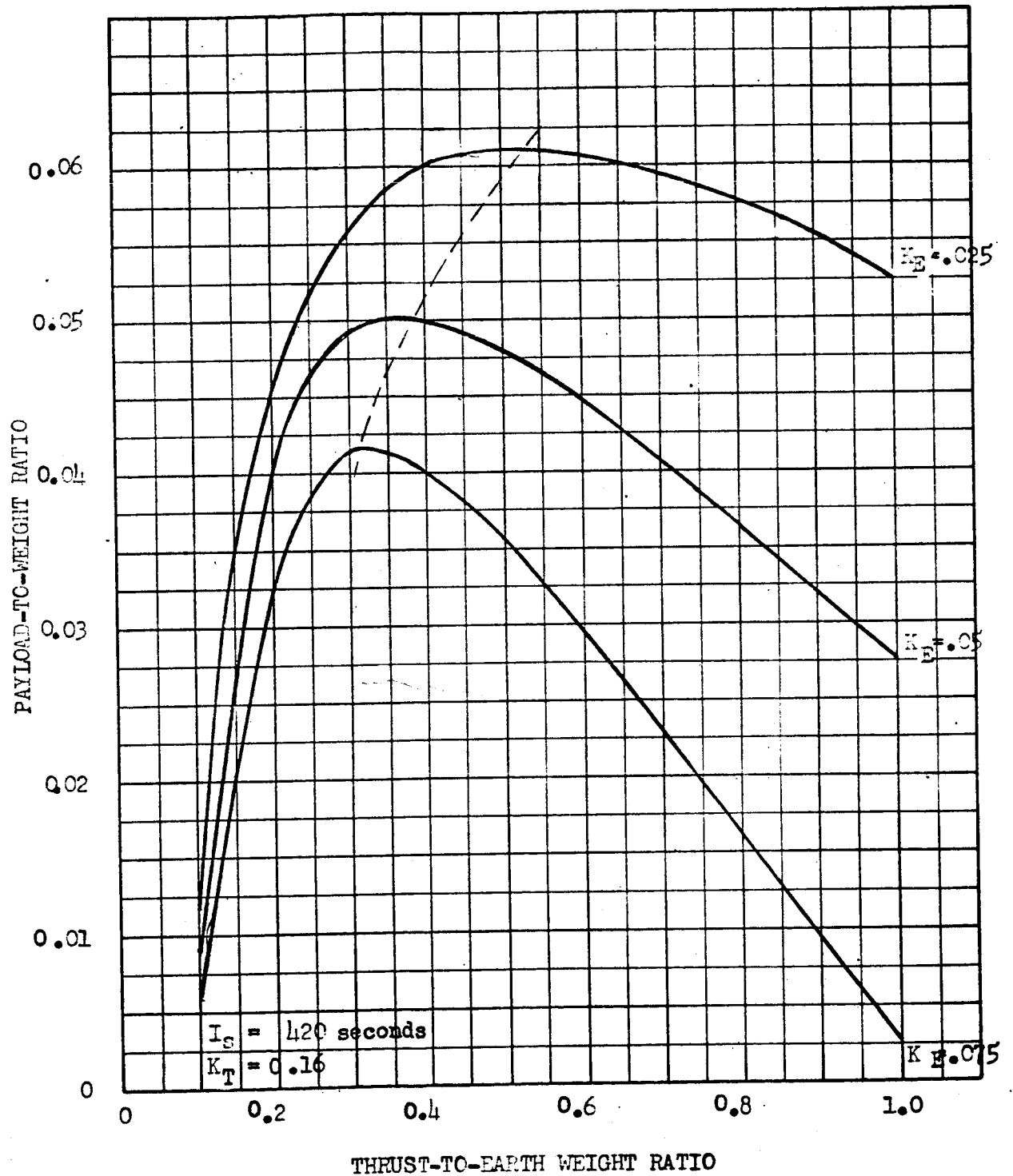


Figure 39

EARTH - HYPERBOLIC EXCESS = 30,000 ft/sec

Nominal Vehicle: $I_s = 420 \text{ sec}$, $K_P = 0.16$, $K_T = 0.05$, $V_h = 15,000 \text{ ft/sec}$

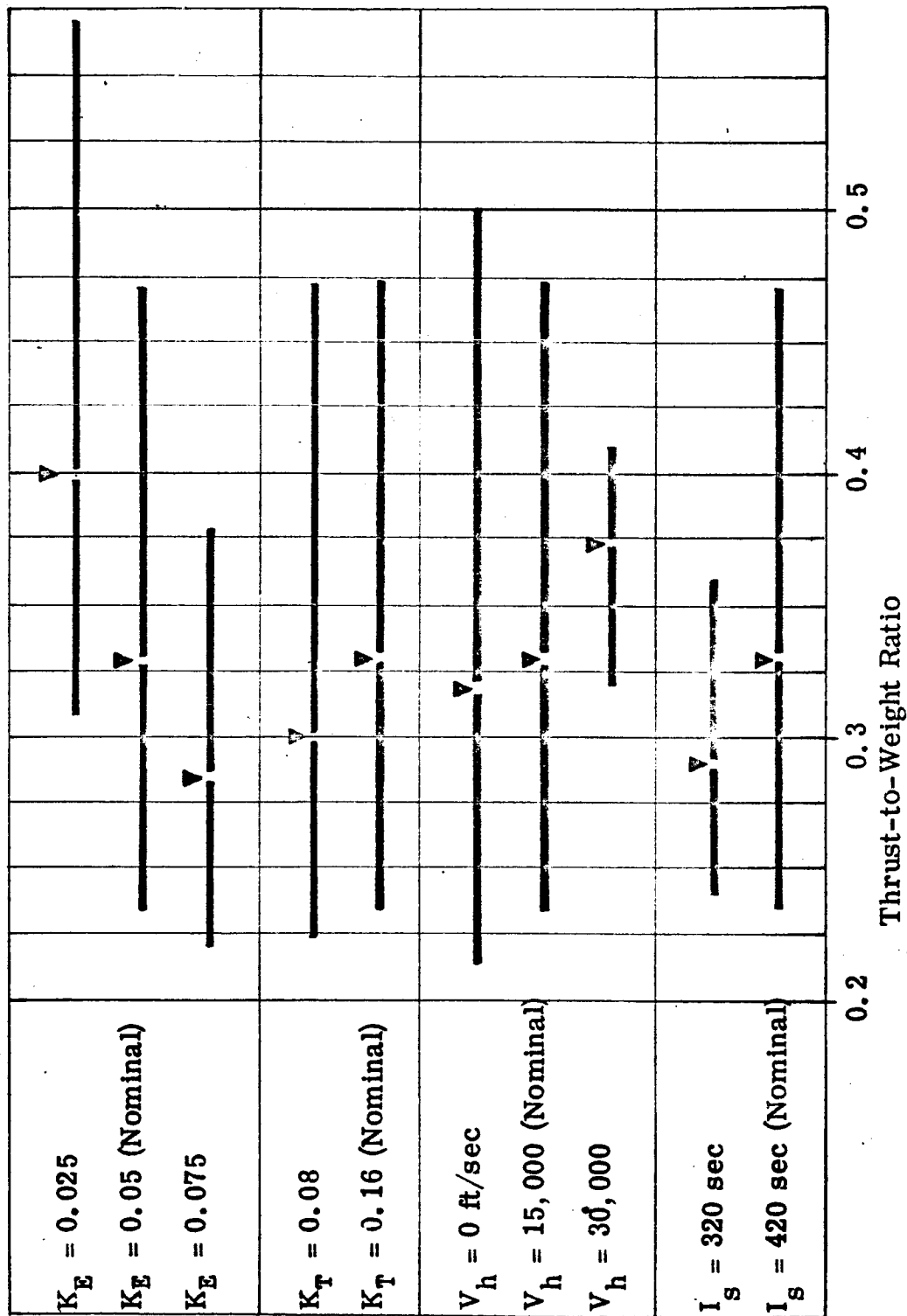


Fig. 40 Thrust-to-Weight Ratio Variation for 1 Percent Change in Payload for Earth Orbit

ROCKETDYNE
A DIVISION OF NORTH AMERICAN AVIATION, INC.

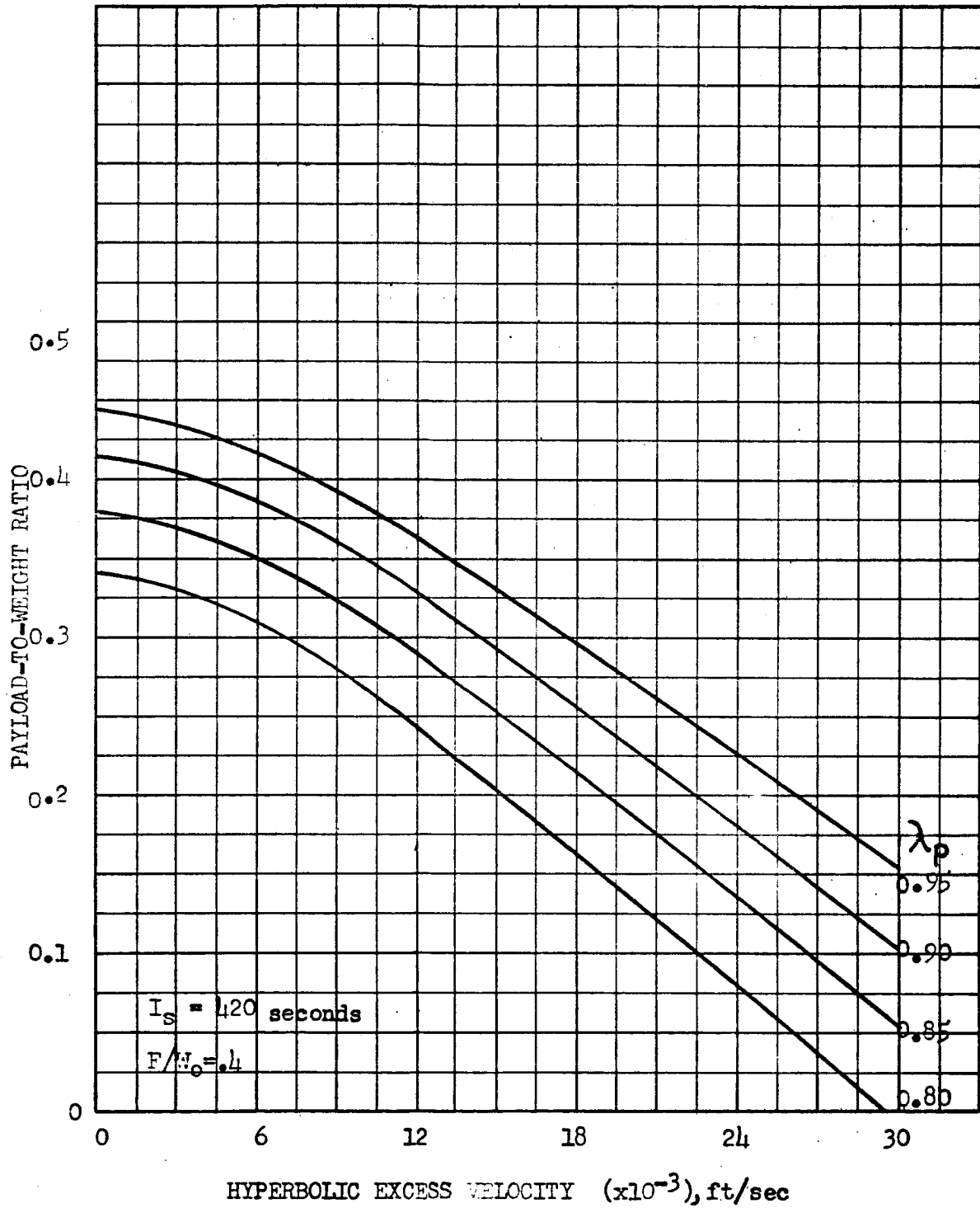


Figure 41
EARTH PAYLOAD VS. HYPERBOLIC EXCESS

TABLE 13
SUMMARY OF THRUST OPTIMIZATION RESULTS FOR EARTH ORBIT-ESTABLISHMENT
AND DEPARTURE MANEUVERS

Thrust-Dependent Weight Factor (K_E) = 0.025			Thrust-Dependent Weight Factor (K_E) = 0.050							
Specific Impulse, Seconds	Hyperbolic Excess Velocity, ft/sec (V_h)	Propellant-Dependent Weight Factor (K_T)	Optimum Payload-to-Gross Weight Ratio (PL/WG _{max})	Lower Thrust-to-Weight Ratio for 1-percent Payload Loss (F/W) _L	Optimum Thrust-to-Weight Ratio	Higher Thrust-to-Weight Ratio for 1-percent Payload Loss (F/W) _H	Optimum Payload-to-Gross Weight Ratio (PL/WG _{max})	Lower Thrust-to-Weight Ratio for 1-percent Payload Loss (F/W) _L	Optimum Thrust-to-Weight Ratio	Higher Thrust-to-Weight Ratio for 1-percent Payload Loss (F/W) _H
320	0	0.08	0.319	0.24	0.36	0.56	0.312	0.18	0.27	0.39
320	0	0.16	0.268	0.25	0.35	0.53	0.263	0.22	0.27	0.38
320	15,000	0.08	0.200	0.25	0.38	0.61	0.192	0.20	0.29	0.40
320	15,000	0.16	0.142	0.27	0.39	0.60	0.133	0.24	0.29	0.36
320	30,000	0.08	0.041	0.31	0.37	0.43	0.032	0.28	0.30	0.33
420	0	0.08	0.420	0.26	0.43	0.72	0.411	0.22	0.31	0.46
420	0	0.16	0.378	0.28	0.45	0.70	0.368	0.22	0.33	0.48
420	15,000	0.08	0.305	0.30	0.39	0.57	0.296	0.22	0.30	0.47
420	15,000	0.16	0.255	0.28	0.40	0.45	0.245	0.24	0.33	0.57
420	30,000	0.08	0.124	0.36	0.45	0.60	0.114	0.29	0.36	0.45
420	30,000	0.16	0.061	0.42	0.53	0.60	0.050	0.32	0.37	0.41

Thrust-Dependent Weight Factor (Kg) = 0.075						
Specific Impulse, Seconds	Hyperbolic Excess Velocity, ft/sec (V _H)	Propellant-Dependent Weight Factor (K _T)	Optimum Payload-to-Gross Weight Ratio (PL/WG _{max})	Lower Thrust-to-Weight Ratio for 1-percent Payload Loss (F/W) _L	Optimum Thrust-to-Weight Ratio	Higher Thrust-to-Weight Ratio for 1-percent Payload Loss (F/W) _H
320	0	0.08	0.305	0.15	0.24	0.34
320	0	0.16	0.255	0.18	0.23	0.31
320	15,000	0.08	0.185	0.16	0.25	0.35
320	15,000	0.16	0.128	0.21	0.25	0.29
320	30,000	0.08	0.025	0.25	0.27	0.32
420	0	0.08	0.404	0.19	0.27	0.36
420	0	0.16	0.361	0.20	0.28	0.38
420	15,000	0.08	0.289	0.21	0.28	0.37
420	15,000	0.16	0.238	0.22	0.28	0.38
420	30,000	0.08	0.106	0.25	0.30	0.37
420	30,000	0.16	0.042	0.29	0.32	0.36

investigate, for an Earth orbit departure maneuver, the optimum characteristics and relative payload capability of a single stage vehicle, a two-stage vehicle, and a single stage vehicle which jettisons emptied propellant tanks during flight (staging tanks). The velocity requirements for the different systems were determined on the basis of an orbit departure performed with a thrust parallel-to-velocity maneuver.

The vehicle comparison was based on a system with 400 seconds specific impulse, representative of a high-energy cryogenic propulsion system. For the single-stage vehicles with tank staging, the propellant was assumed to be divided between two or more tank units with all tank units of equal volume. The weight of the tank units was determined using the propellant-dependent weight factor. Vehicle weights were assumed equal to the sum of a propellant-dependent weight and a thrust-dependent weight, where propellant-dependent weight = $0.08 \times$ stage propellant weight and thrust-dependent weight = $0.02 \times$ stage thrust level. No additional inert weight was included for the added fixtures which a jettisonable tank unit would require. The thrust-dependent weight was added to the final tank unit which remained at the end of the propulsive phase for a final vehicle burn-out weight.

Single Stage Vehicle. The ideal velocity requirements for an Earth orbit-departure maneuver leaving from a 300 n mi Earth orbit are presented in Figure 42, 43 and 44 for a single-stage vehicle. Indicated are ideal velocity requirement versus initial thrust-to-weight ratio for departure maneuvers of 0, 15,000, and 30,000 ft/sec hyperbolic excess velocity. In Figure 45 is presented ideal velocity requirement versus hyperbolic excess velocity for three F/W values: 2.0, 0.5, and 0.2.

The variation of payload-to-gross weight ratio as a function of initial thrust-to-weight ratio for a single stage orbit departure vehicle for three hyperbolic excess velocities is illustrated in Figure 46. The optimum thrust-to-weight ratio for the departure stage is 0.4 to 0.5. The hyperbolic excess velocity does not have a large effect on the optimum thrust-to-weight, although the results in Figure 46 indicate that optimum thrust-to-weight increases slightly as the hyperbolic excess velocity increases.

Two Stage Vehicle. For a two-stage Earth orbit departure vehicle, the ideal velocity requirement depends upon the thrust-to-weight ratios of both stages. An evaluation of the effect of thrust-to-weight was conducted based on a hyperbolic excess velocity of 30,000 ft/sec. This value was selected as typical of an orbit departure mission with a high ideal velocity requirement, where a two-stage vehicle would provide a significant improvement in payload compared to a single stage vehicle.

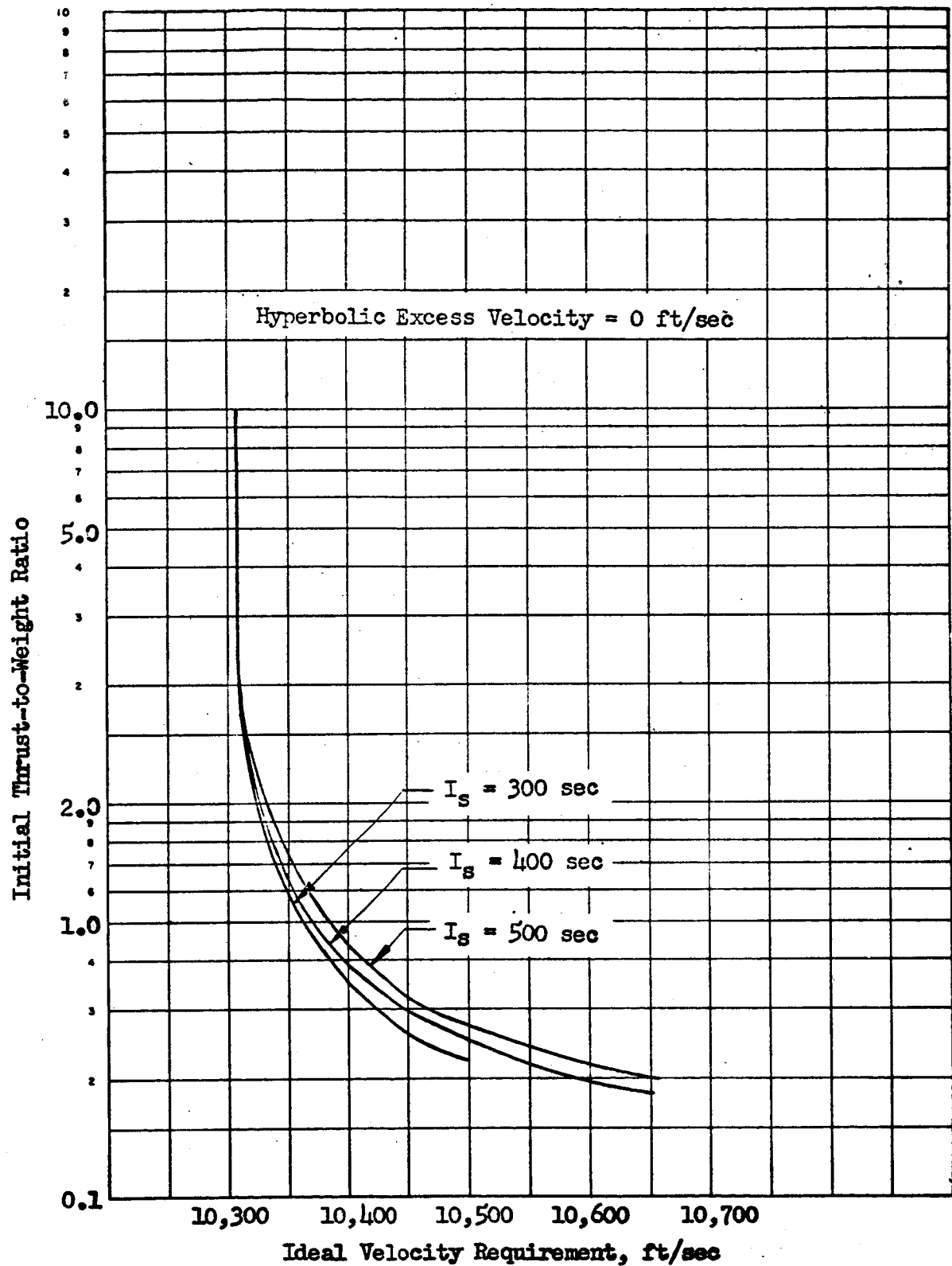


Figure 42 . Ideal Velocity Requirement; Single Stage Orbit
Departure from 300 n.mi. Earth Orbit

ROCKETDYNE
A DIVISION OF NORTH AMERICAN AVIATION, INC

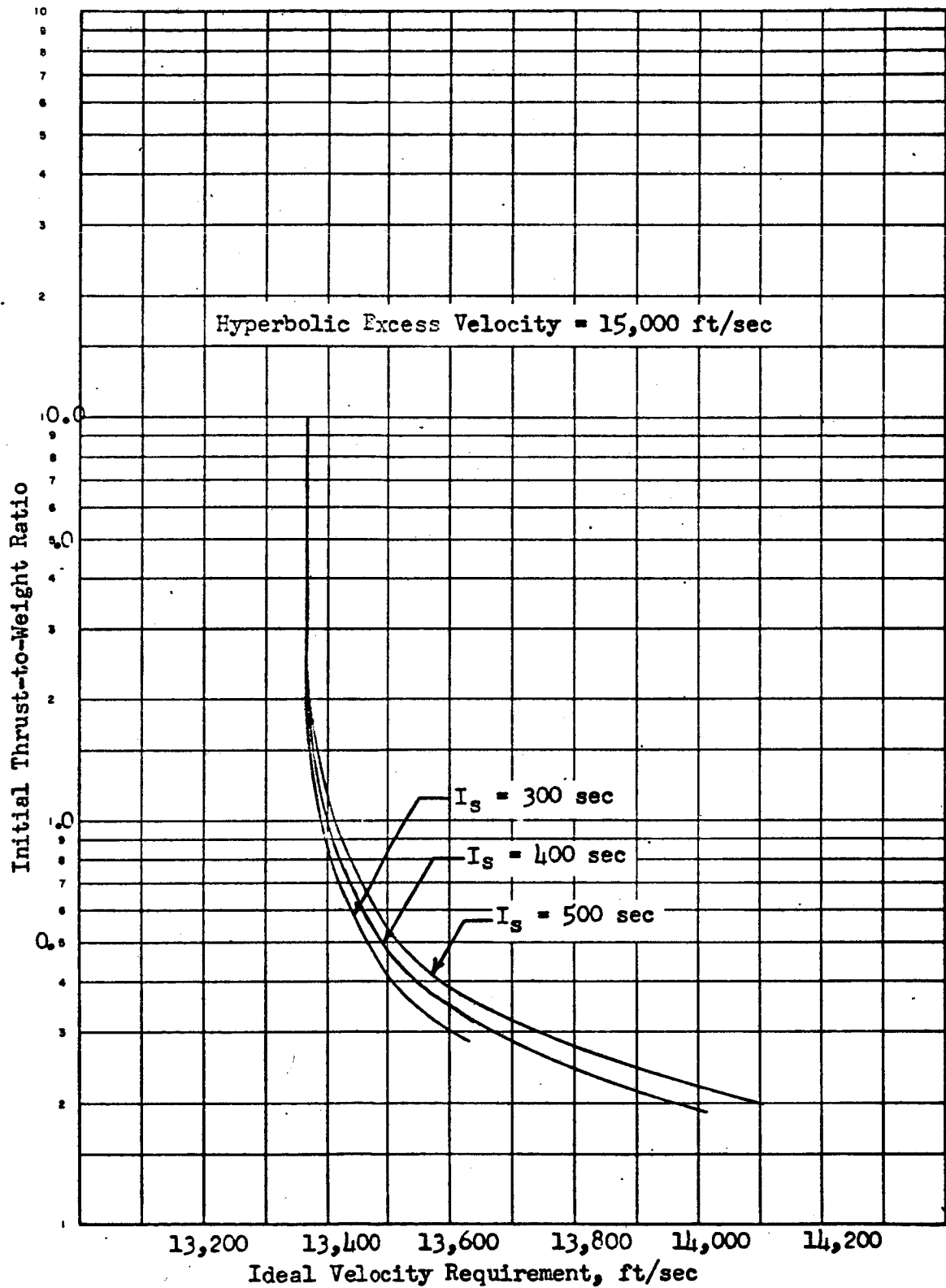


Figure 43 Ideal Velocity Requirement; Single Stage Orbit Departure from 300 n mi Earth Orbit

ROCKETDYNE

A DIVISION OF NORTH AMERICAN AVIATION, INC

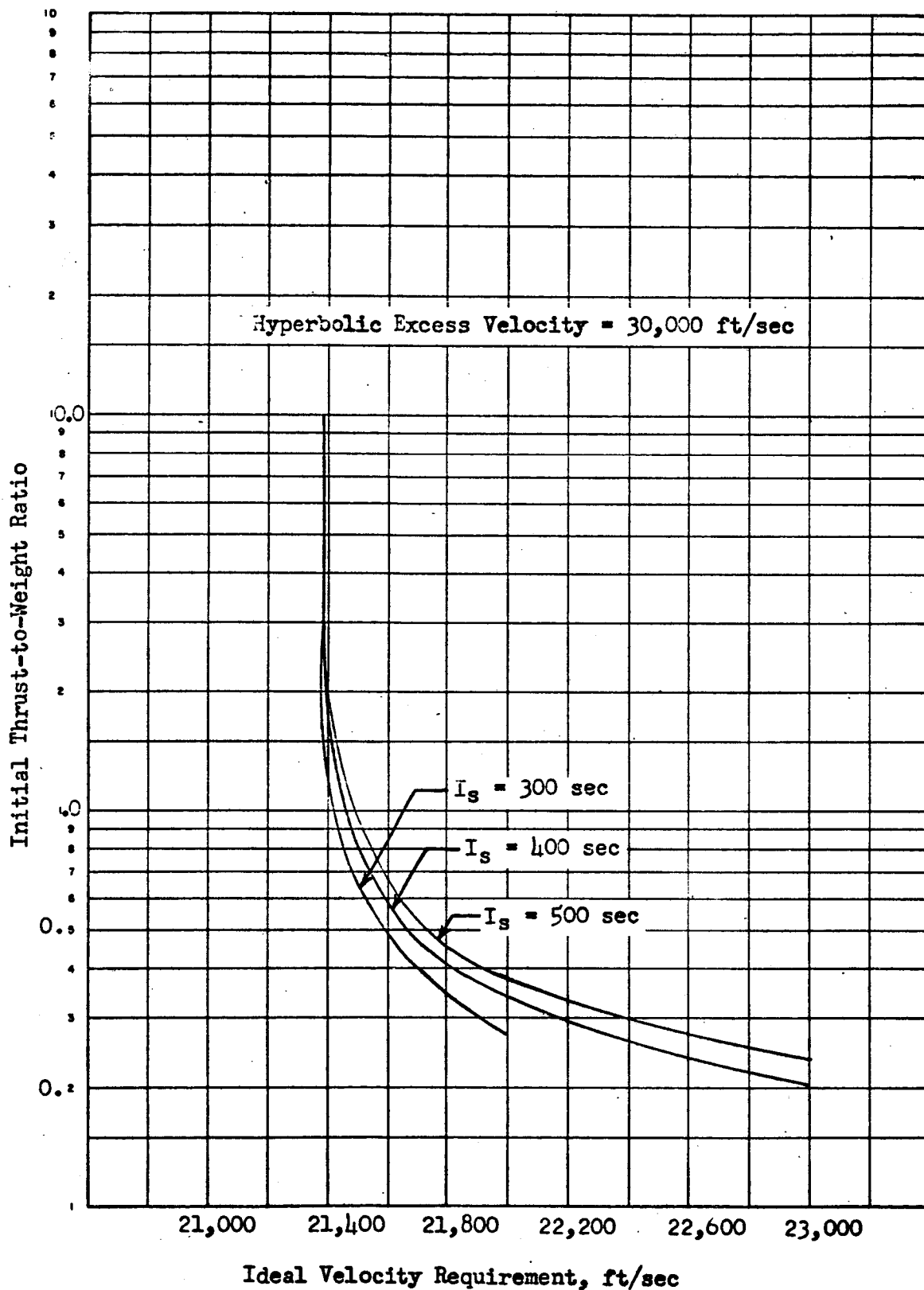
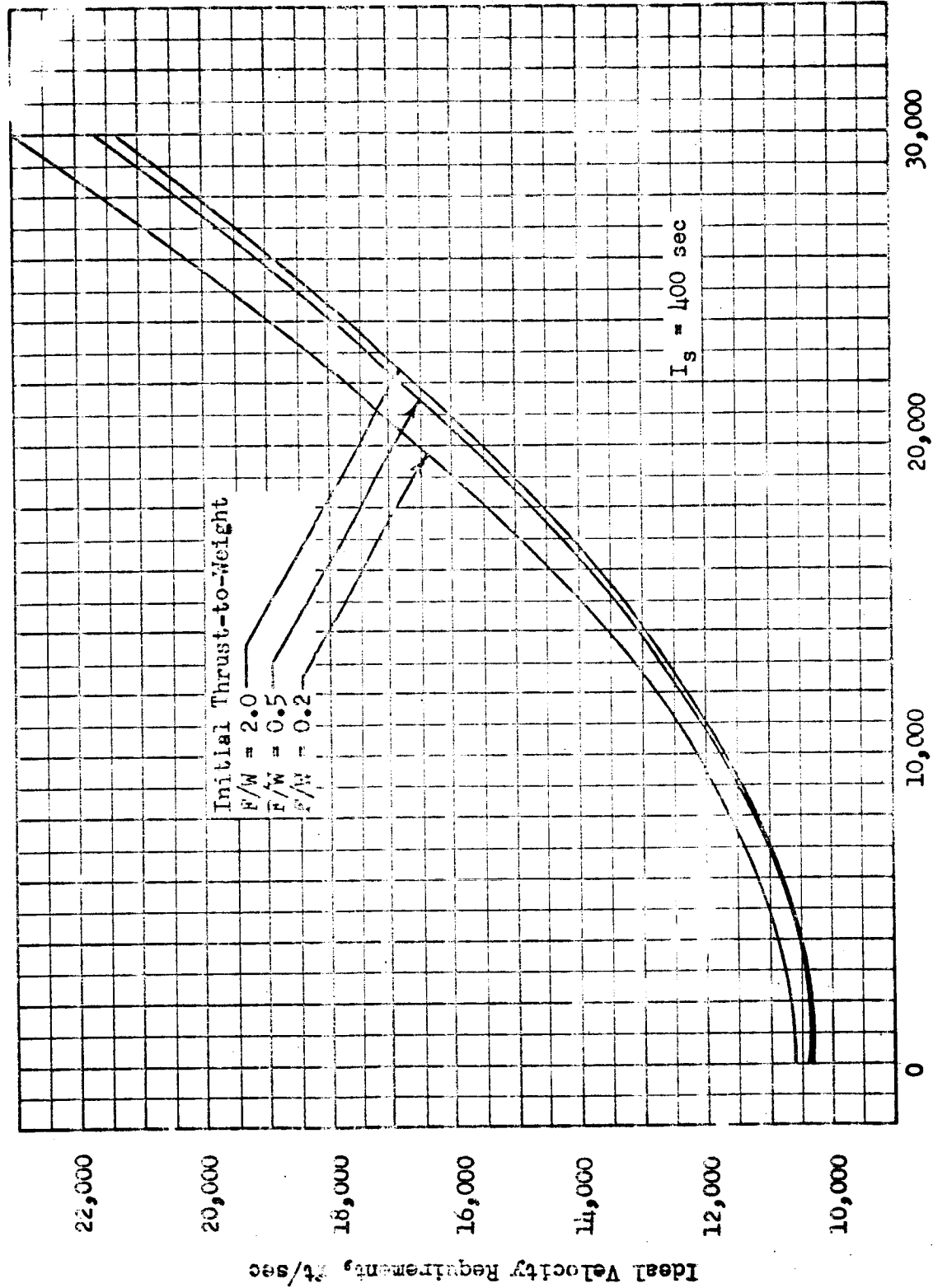


Figure 44 Ideal Velocity Requirement; Single Stage Orbit Departure from 300 n mi Earth Orbit



Hyperbolic Excess Velocity, ft/sec

Fig. 45 Ideal Velocity Requirement and Single Stage Orbit Departure from 300 n mi Earth Orbit.

ROCKETDYNE

A DIVISION OF NORTH AMERICAN AVIATION, INC.

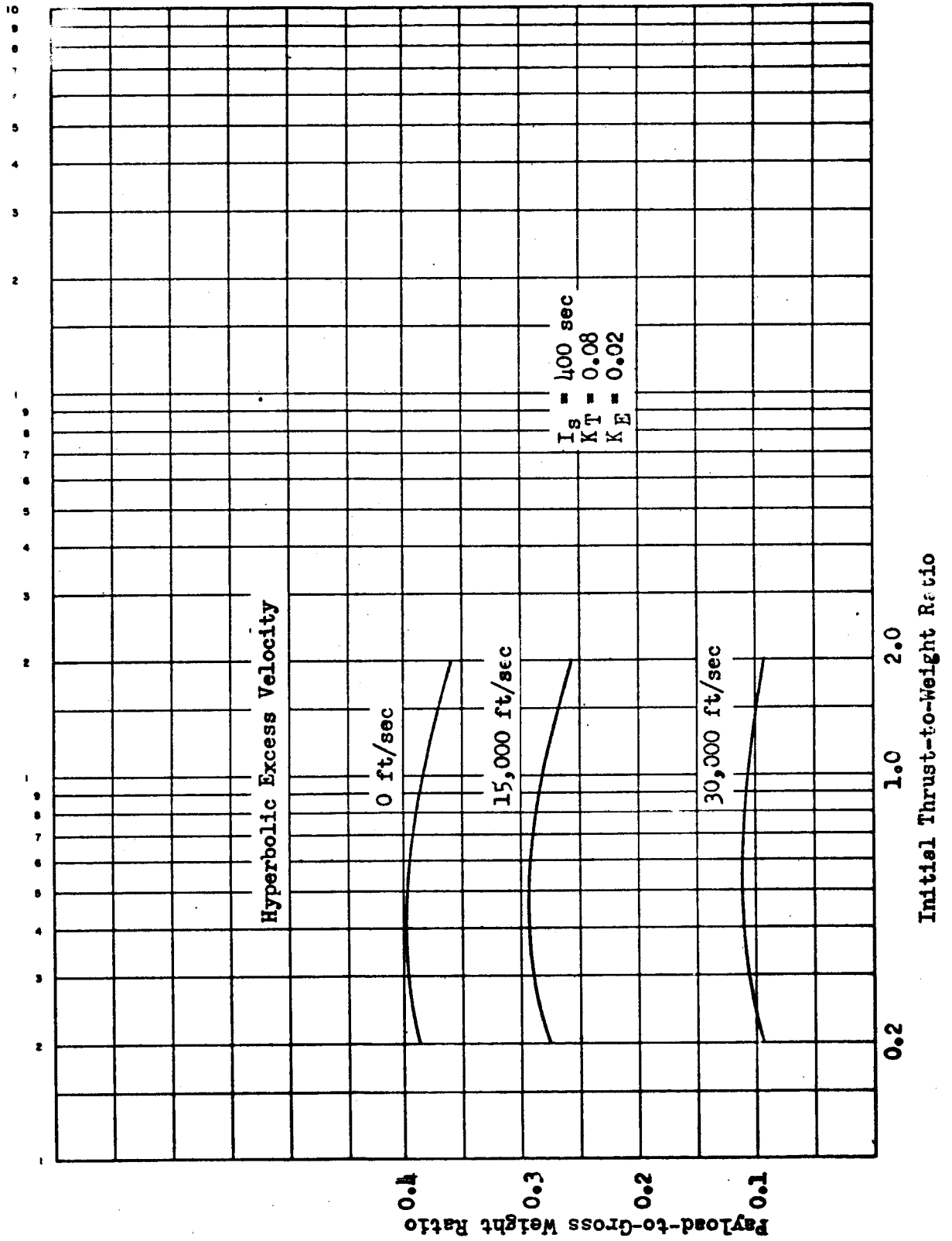


Figure 46. Deliverable Payload; Single Stage Orbit Departure from 300 n mi Earth Orbit.

In Figure 47, ideal velocity requirements versus initial thrust-to-weight ratios for the first stage are illustrated. Curves for four different ratios of second stage to first stage thrust-to-weight ratios are presented. The results are for two-stage vehicles where the total mission ideal velocity requirement is evenly divided between the two stages.

In Figure 48, payload-to-gross weight ratios versus first stage thrust-to-weight ratios for a two-stage orbit departure vehicle are illustrated. Curves are presented for four different ratios of first stage to second stage thrust-to-weight ratios. A vehicle with a first stage thrust-to-weight ratio of approximately 0.65 and with equal thrust-to-weight ratios in both stages will result in the highest payload for a two-stage vehicle.

Payload versus hyperbolic excess velocity for a two-stage vehicle is presented in Figure 49. A two-stage vehicle where both stages have a thrust-to-weight ratio of 0.65, and with stage sizes selected so that the mission ideal velocity requirement is divided evenly between the two stages was considered.

Staging Tanks. An alternative to the use of a two-stage vehicle for orbit departure is the use of a vehicle with propellant tank staging only. Payload-to-gross-weight ratio versus initial thrust-to-weight ratio for a single stage vehicle and a vehicle with continuous tank staging is presented in Figure 50 (emptied tanks are jettisoned an infinite number of times). This figure is for an orbit departure stage which accelerates the vehicle to 30,000 ft/sec hyperbolic excess velocity. The optimum thrust-to-weight ratios for the single stage vehicle ($F/W = 0.5$) and for the vehicle with continuous tank staging ($F/W = 0.45$) are very similar. From this result, it was assumed that a thrust-to-weight ratio of 0.5 would result in nearly optimum payload for a vehicle with tank staging no matter how many times tanks are jettisoned. The effect on payload-to-gross weight ratio of the number of times emptied tanks are jettisoned is presented in Figure 51, also for the 30,000 ft/sec hyperbolic excess velocity mission.

The simulated trajectories determined for the single stage vehicles and tank staging vehicles indicate that the ideal velocity requirements are similar. The payload-to-gross weight for the 30,000 ft/sec hyperbolic excess velocity mission for a single stage vehicle with a thrust-to-weight ratio of 0.5 is 0.11, and for a vehicle which jettisons tanks an infinite number of times at the same thrust-to-weight ratio, the payload to gross weight is 0.15. If the vehicle with tank staging was assumed to have the same ideal velocity requirement as the single stage vehicle, it would have a payload-to-gross weight smaller by 0.0005. This difference, caused by the ideal velocity-requirement difference, is small and consequently in most studies could be neglected. As the number of times tanks are jettisoned is decreased (in actuality it obviously will always be lower than the infinite number used in the comparison), the difference in ideal velocity requirement between a single stage vehicle and a vehicle with tank staging will decrease.

ROCKETDYNE

A DIVISION OF NORTH AMERICAN AVIATION, INC.

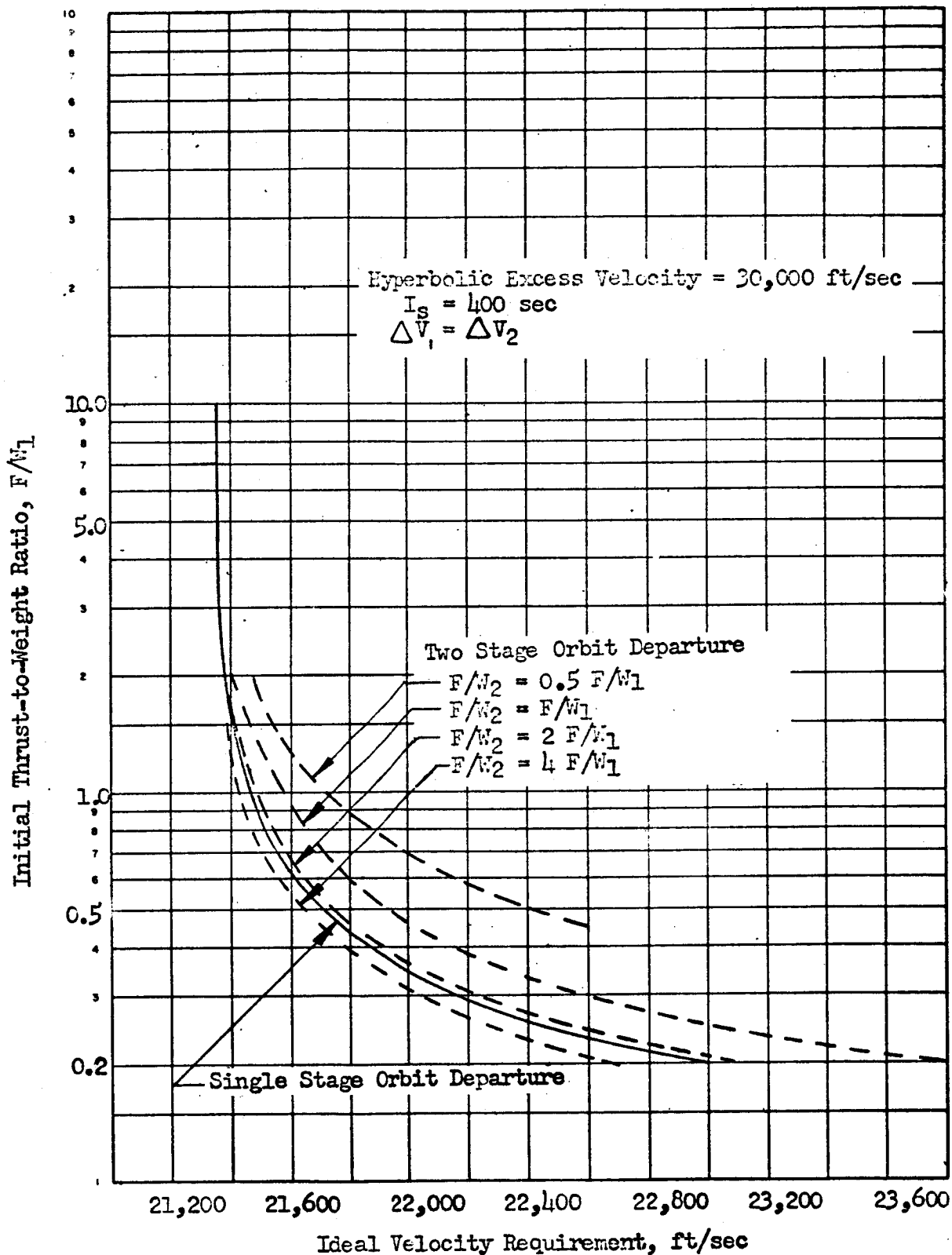


Figure 47. Ideal Velocity Requirement; Two Stage Orbit Departure from 300 n. mi. Earth Orbit

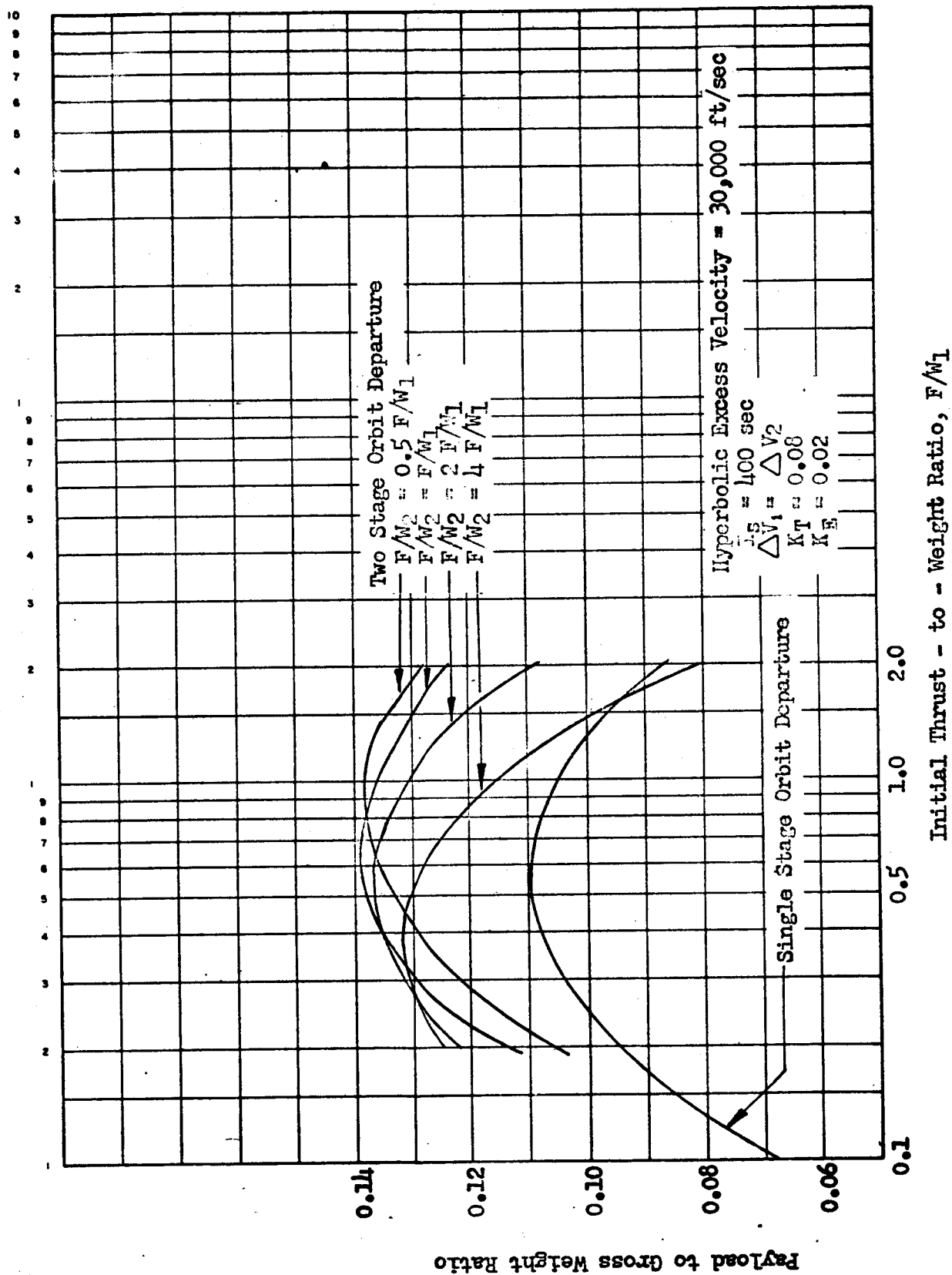


Figure 48 . Deliverable Payload; Two Stage Orbit Departure from 300 n. mi. Earth Orbit

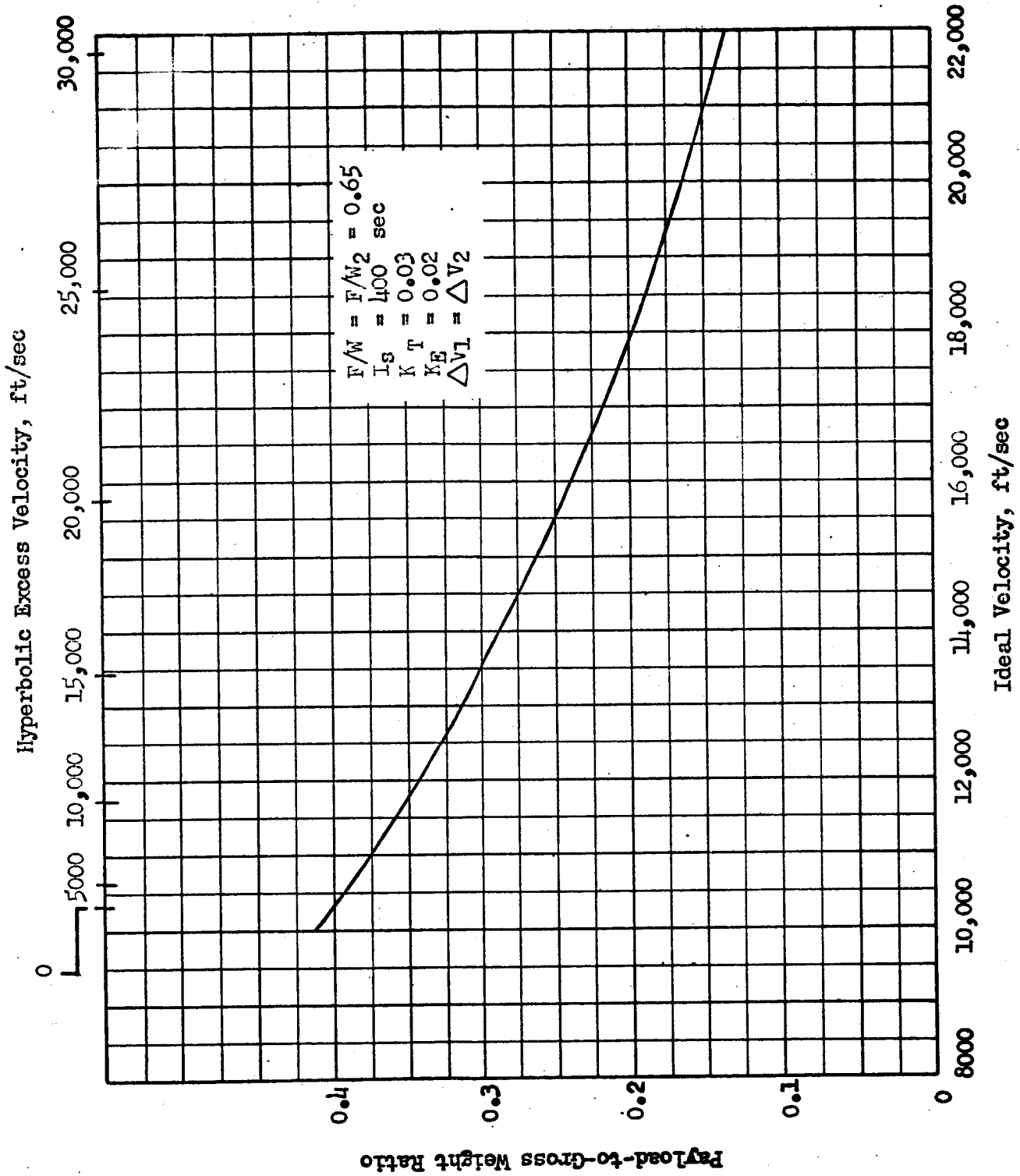


Figure 49. Deliverable Payload; Two Stage Vehicle Orbit Departure
from 300 n. mi. Orbit

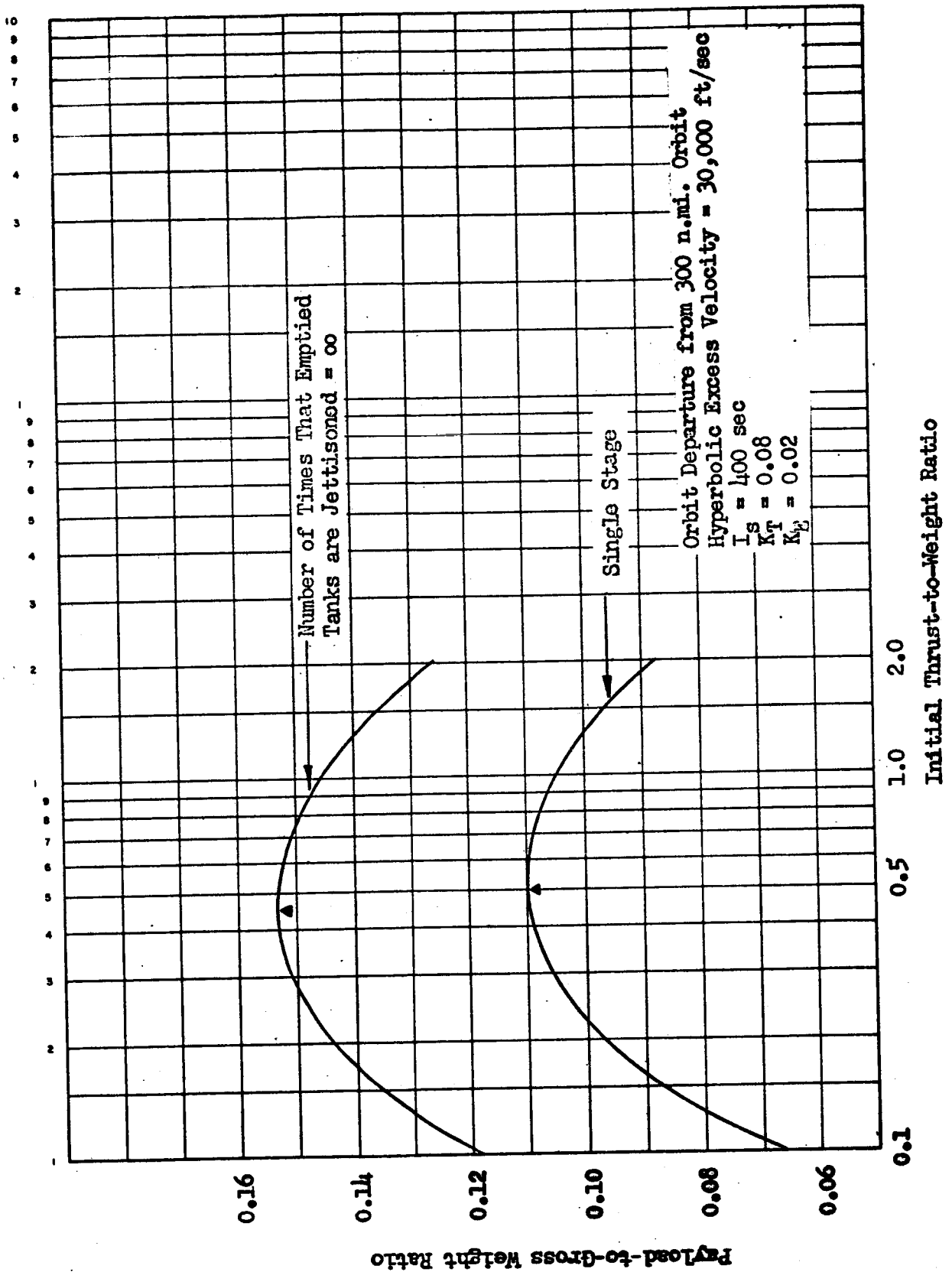


Figure 50 . Effect of Tank Staging on Optimum Thrust-to-Weight

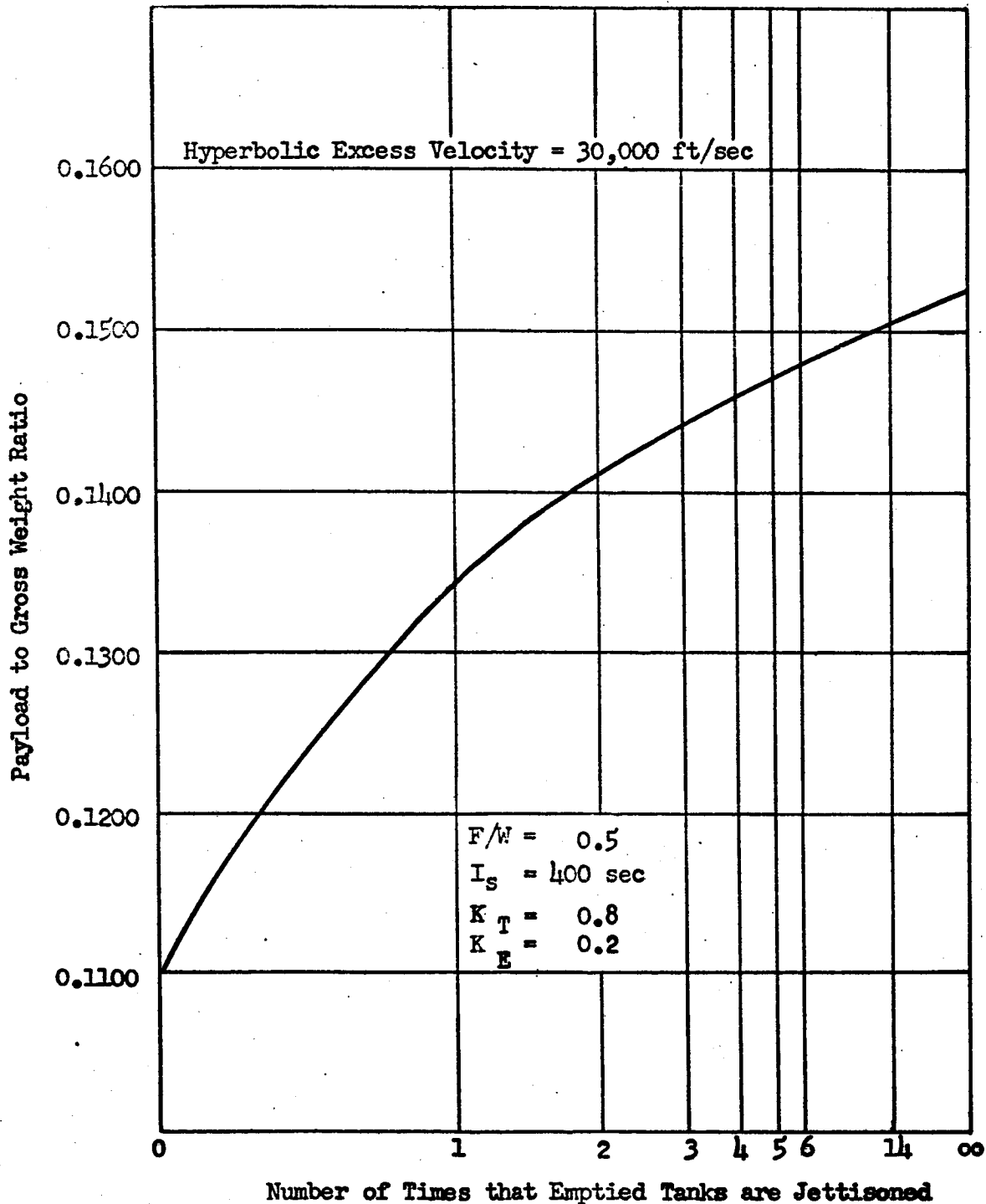


Figure 51 . Deliverable Payload; Tank Staging Vehicle: Orbit Departure from 300 n. mi. Orbit

Payload-to-gross weight ratio versus hyperbolic excess velocity (or ideal velocity) for an orbit departure vehicle with tank staging is shown in Figure 52. This figure is for a vehicle with an initial thrust-to-weight ratio of 0.5. Since ideal velocity requirements for a single stage vehicle and a vehicle with tank staging are similar, Figure 52 was prepared using single stage vehicle ideal velocity requirements.

In this study, no weight penalty was added to the propellant dependent weight of the tank staging vehicles to account for a more complicated tank design required by tank staging. The tank staging vehicle payloads therefore may be somewhat optimistic.

Orbit Departure Vehicle Comparison. A comparison between a single stage, a two-stage, and a tank staging vehicle is presented in Figure 53 to indicate the approximate percent of single stage vehicle payload that a two-stage vehicle or a vehicle with tank staging will deliver as a function of hyperbolic excess velocity. At a hyperbolic excess velocity of approximately 20,000 ft/sec; the two-stage vehicle and the vehicle with tank staging have a payload advantage of 10 percent over a single stage vehicle. This advantage increases significantly as hyperbolic excess velocity increases.

A single stage vehicle, a two-stage vehicle, and a tank staging vehicle are compared in Tables 14 and 15 for a 30,000 ft/sec hyperbolic excess velocity Earth orbit departure mission. An optimum thrust-to-weight ratio and the range of thrust-to-weight ratios which could be used and still deliver a payload which is within 2 percent of the optimum payload value are presented in Table 14. The mission ideal velocity requirement and payload-to-gross weight ratio are presented in Table 15.

The results of this study indicate that single-stage orbit departure ideal velocity requirement is not significantly different from that for a vehicle which stages tanks. The ideal velocity requirement for a two-stage vehicle can vary significantly from that for a one-stage vehicle with the same initial thrust-to-weight. The magnitude of this difference depends upon the thrust-to-weight ratio of the second stage.

For low hyperbolic excess velocity missions, a single stage vehicle would probably be selected. At higher excess velocities, however, the two-stage vehicle and the vehicle with tank staging deliver significantly higher payloads. At approximately 20,000 ft/sec hyperbolic excess velocity, the advantage of these two vehicles in payload over the single-stage vehicle is 10 percent.

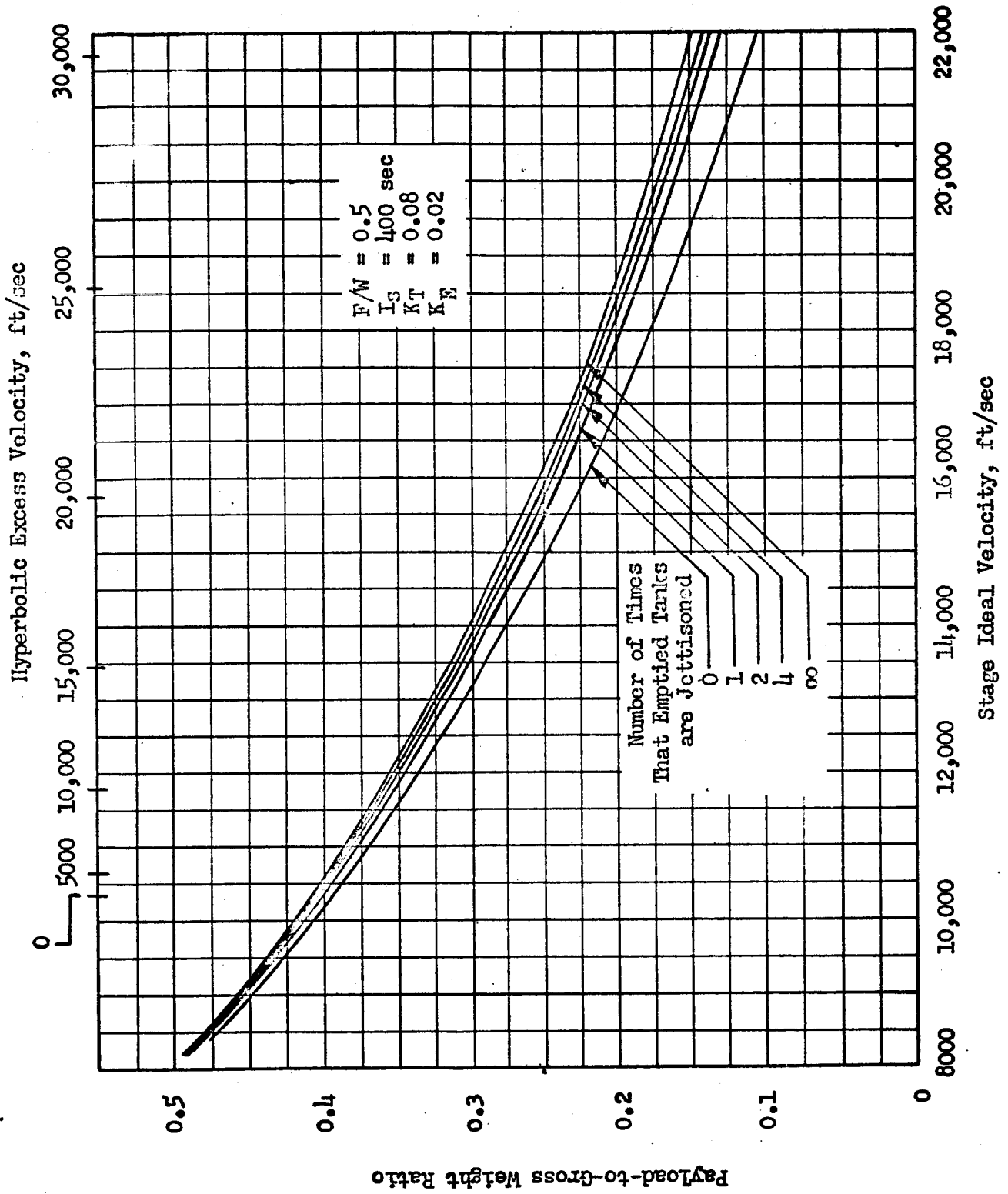


Figure 52. Deliverable Payload; Tank Staging Vehicle: Departure from 300 n. mi. Orbit

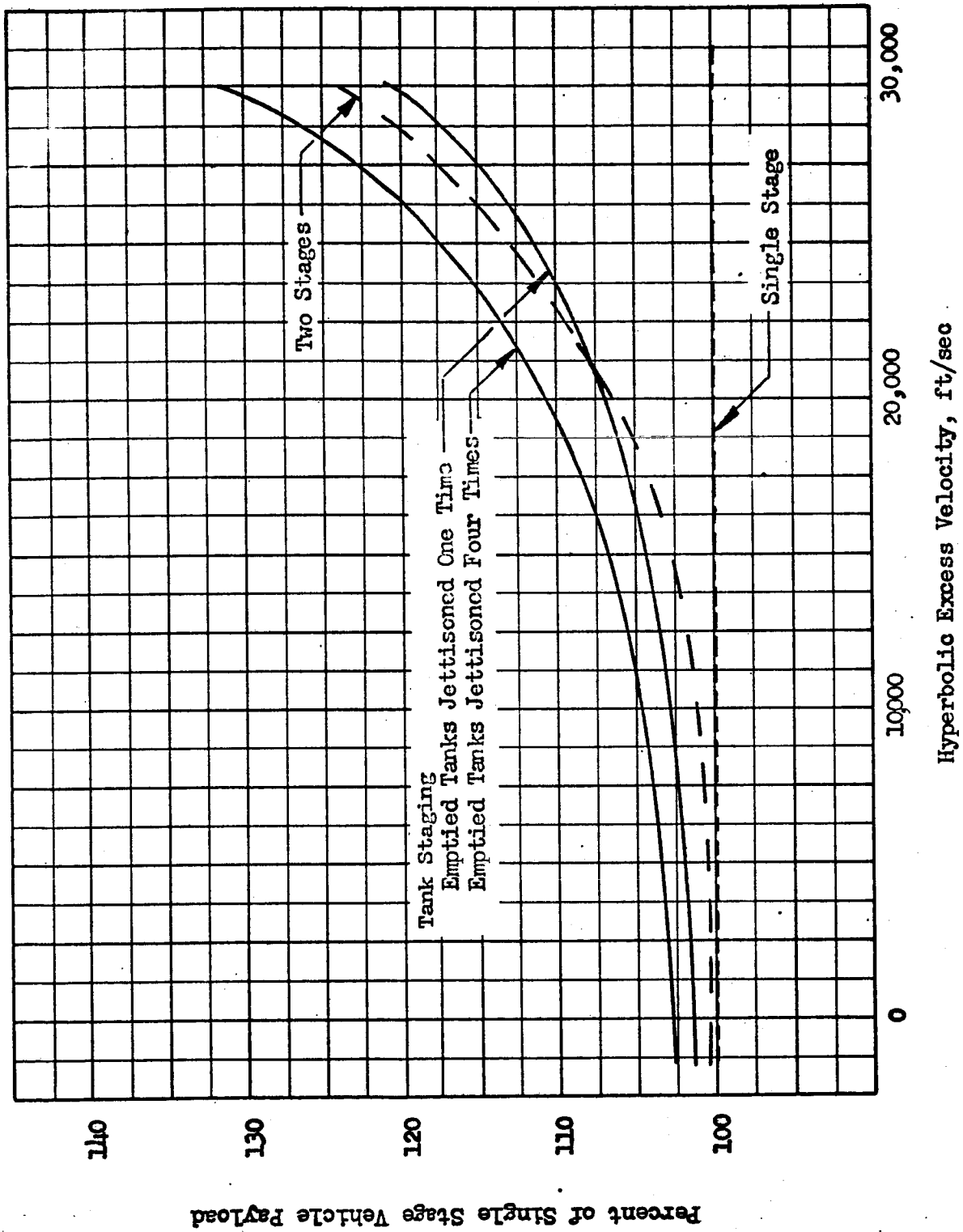


Figure 53 . Orbit Departure Vehicle Comparison; 30,000 ft/sec Hyperbolic Excess Velocity Mission

TABLE 14

ORBIT DEPARTURE VEHICLE OPTIMUM THRUST-TO-WEIGHT RATIOS

MISSION: 30,000 ft/sec HYPERBOLIC EXCESS VELOCITY ORBIT DEPARTURE

Vehicle	Optimum Initial Thrust-to-Weight Ratio	Initial Thrust-to-Weight Ratio Range for a Minus 2-Percent Payload
Single Stage	0.5	0.34 → 0.78
Two-Stage $F/W_2 = 0.5 F/W_1$	0.65	0.64 → 1.22
$F/W_2 = F/W_1$		0.44 → 1.04
$F/W_2 = 2 F/W_1$		0.36 → 0.64
∞ Tank Staging	0.46	0.28 → 0.79

TABLE 15

ORBIT DEPARTURE VEHICLE IDEAL VELOCITY INCREMENT AND PAYLOAD

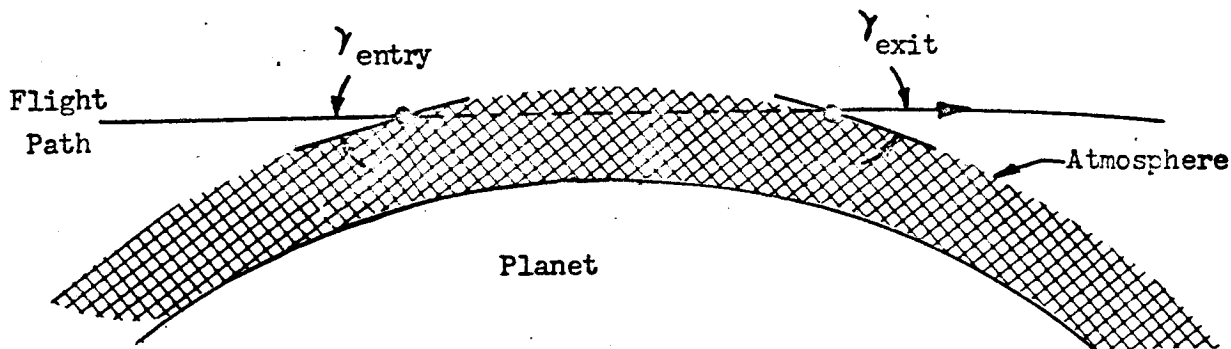
MISSION: 30,000 ft/sec HYPERBOLIC EXCESS VELOCITY ORBIT DEPARTURE

Vehicle	Ideal Velocity Requirement, ft/sec	Relative Payload-to-Gross Weight Ratio	Percent of Single Stage Payload
Single Stage ($F/W = 0.5$)	21,700	0.110	100
Two-Stage ($F/W_1 = 0.65$) ($F/W_2 = 0.65$)	21,720	0.138	125
Single Stage (Tanks Jettisoned One Time ($F/W = 0.5$))	21,680	0.134	122
Single Stage (Tanks Jettisoned 4 Times ($F/W = 0.5$))	21,670	0.146	133

A single stage orbit departure vehicle to place a payload on a trajectory with 30,000 ft/sec hyperbolic excess velocity will have a payload-to-gross weight ratio of 0.110. Use of a two-stage vehicle increases the payload-to-gross weight ratio to 0.138 (a 25-percent increase) and jettisoning emptied tanks twice during the flight increases it to 0.141 (a 28-percent increase). At 30,000 ft/sec hyperbolic excess velocity the optimum thrust-to-weight for a single stage vehicle or a vehicle with tank staging is approximately 0.5. For a two-stage vehicle with the total ideal velocity requirement divided evenly between the two stages, the optimum thrust-to-weight ratio for both stages is approximately 0.65.

EARTH ATMOSPHERIC GRAZE MANEUVERS

A major portion of the velocity reduction required to decelerate a returning space vehicle into an Earth orbit can be accomplished by means of the aerodynamic drag experienced during an atmospheric graze maneuver. The atmospheric graze maneuver, as defined in the study performed, consists of the vehicle "skimming" the upper atmosphere of the Earth for the purpose of decelerating the vehicle prior to subsequent propulsive orbit-establishment maneuvers. The vehicle flight path is described pictorially in the following sketch.



Entry conditions to the atmosphere of the Earth are defined by the magnitude and direction of velocity existing at the entry altitude. The entry altitude for Earth is taken to be 400,000 feet. The exit conditions following the graze maneuver are defined in a similar manner at the same altitude.

The relationship between entry and exit conditions depends on many parameters. Among these are the ballistic coefficient ($W/C_D A$), ablation weight loss rate, and the nature of the atmosphere. For a ballistic vehicle, the relationship between entry and exit is unique. For lifting vehicles this relationship is not single-valued, since the flight path can be controlled by the lift vector.

The purpose of the study was to obtain and present parametric data on propulsion maneuvers and requirements following the graze maneuver; the study was not concerned therefore with the grazing maneuver per se, but merely with the pertinent range of exit conditions; consequently, an analysis of the aerodynamic graze maneuver was not performed. To gain insight into the nature

of the exit conditions, data were obtained from General Dynamics/Astronautics for aerodynamic entry trajectories. Several general characteristics of atmosphere graze exit conditions were noted for the ballistic and the low L/D vehicles analyzed: 1) the exit velocity is usually greater than the local circular velocity; 2) for high entry velocities (on the order of twice the local escape velocity), the exit velocity may be as much as 30 percent less than the entry velocity; 3) the exit and entry elevation angles are of the same magnitude, that is 5 to 10 degrees.

Impulsive Analysis

Impulsive Orbit Establishment Techniques. The three impulsive orbit establishment schemes investigated are illustrated in Figure 54. For all schemes, the velocity increments are applied parallel to the local velocity vector. Scheme 1 is a two-impulse technique. The first velocity increment (ΔV) is applied at the exit point, resulting in a transfer ellipse whose apoapsis coincides with the desired circular orbit altitude; the second ΔV is applied to achieve circular velocity. Scheme 2 applies only to exit velocities (V_{ex}) less than the local escape velocity (V_p). Upon leaving the atmosphere, the vehicle coasts to apoapsis whereupon a ΔV is applied resulting in a transfer ellipse whose periapsis (or apoapsis) coincides with the desired circular orbit altitude. A second increment is then applied to attain circular velocity. Scheme 3 (for $V_{ex} > V_p$) is the same as Scheme 2 with the addition of a ΔV at the exit point, reducing the velocity of the vehicle to some value less than V_p .

The equations of motion applicable to determining the above velocity increments are the familiar vis-viva law,

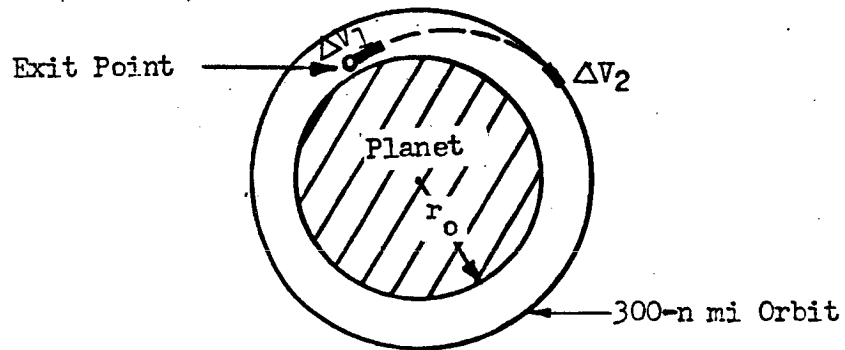
$$v^2 = \epsilon_0 R_o^2 \left(\frac{2}{R} - \frac{1}{a} \right)$$

and Kepler's second law,

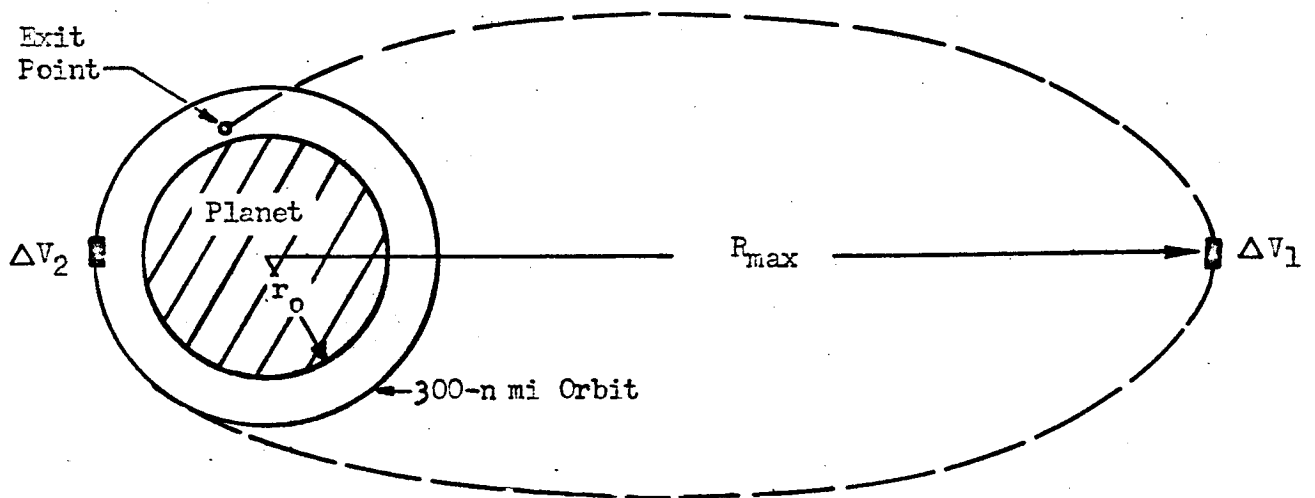
$$\sqrt{p} = \left| \vec{R} \times \vec{V} \right| = R V \cos \gamma$$

Applying these equations at two points along a conic (a and p are constant) and solving for velocity yields

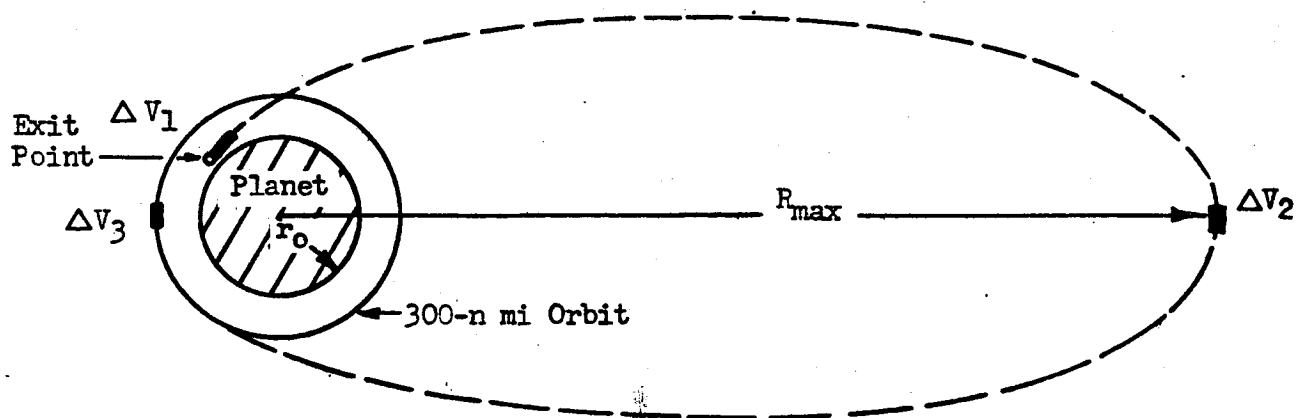
$$v_1^2 = 2\epsilon_0 R_o^2 \left(\frac{1}{R_1} - \frac{1}{R_2} \right) / \left(1 - \frac{R_1^2 \cos^2 \gamma_1}{R_2^2 \cos^2 \gamma_2} \right)$$



Scheme 1



Scheme 2



Scheme 3

Figure 54 Impulsive Orbit Establishment Techniques

This equation gives the velocity magnitude (with elevation angle, γ_1) required at radius R_1 to achieve R_2 and γ_2 . For instance, if R_2 corresponds to the circular orbit altitude and γ_2 is set equal to zero, this equation gives the required velocity magnitude (at γ_1) following the first velocity increment of Scheme 1. The velocity increment can then be determined.

$$\Delta V_1 = |V_{ex} - V_1|$$

Similar relationships can be developed from two basic laws to obtain the remaining velocity increments.

Results of Impulsive Analysis. A 300-n mi circular orbit altitude was selected for use in the analysis of the velocity increments for the range of exit conditions mentioned previously. The velocity increments for Scheme 1 (two-impulse, direct-to-orbit) as a function of exit velocity and angle are illustrated in Figure 55. Also shown is the sum of the two increments, or the total impulsive velocity requirements (ΔV_T) for orbit establishment. The velocity increments and the total velocity requirements for Scheme 2 ($V_{ex}\sqrt{V_p}$) are given in Figures 56 and 57. For both schemes the total velocity requirements reach minima when the exit velocity is near the local circular velocity ($V_p/\sqrt{2}$). This fact indicates that the graze maneuver should not necessarily be designed to reduce the velocity of the vehicle by the maximum amount possible, since the velocity requirements for orbit-establishment increase significantly when the exit velocity is reduced below the value where the minimum velocity requirement occurs.

Scheme 3 is for exit velocities greater than escape velocity. (It also is applicable to exit velocities less than escape velocity, but has no advantage over Scheme 2.) The function of the first velocity increment is to reduce the velocity of the vehicle to some value below the escape velocity. The velocity increments for this scheme depend on that value of velocity attained following the first increment; however, rather than prescribing this velocity, the apoapsis of the transfer ellipse was specified instead. Calculations were performed for apoapsides (R_{max}) of 2, 5 and 10 times the radius of the Earth. The velocity increments and the total velocity requirements for exit velocities equal to the escape velocity of the Earth ($V_{ex} = V_p$) are presented in Figures 58 and 59. This presentation (in comparison to a presentation of ΔV vs V_{ex}) affords better insight into the effects of exit angle (γ_{ex}) and R_{max} . For other exit velocities only the first velocity increment is different; in fact, it is increased by the difference between the exit velocity and escape velocity.

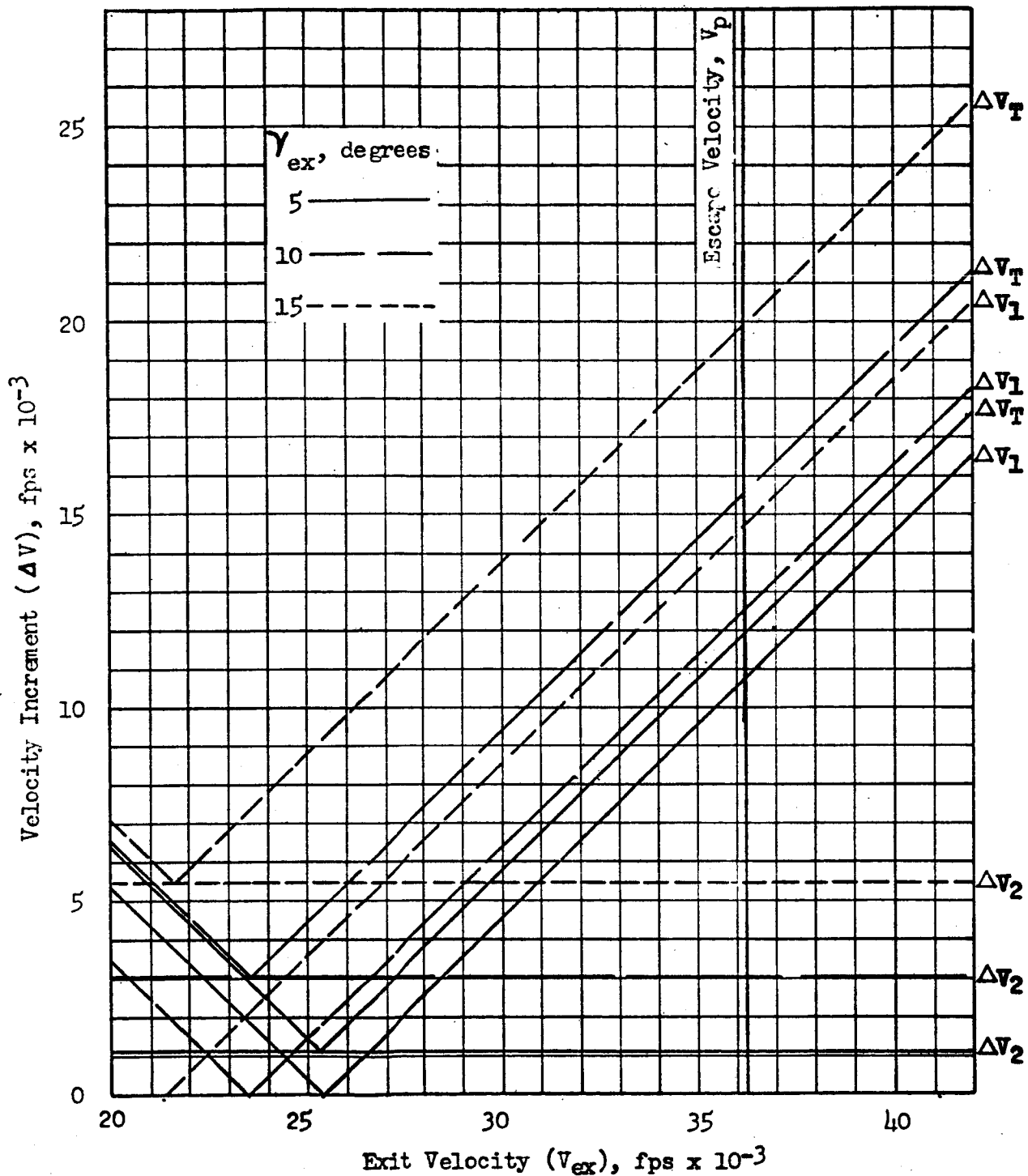


Fig. 55 Velocity Requirements for Establishing a 300 n mi Orbit at Earth, Scheme 1

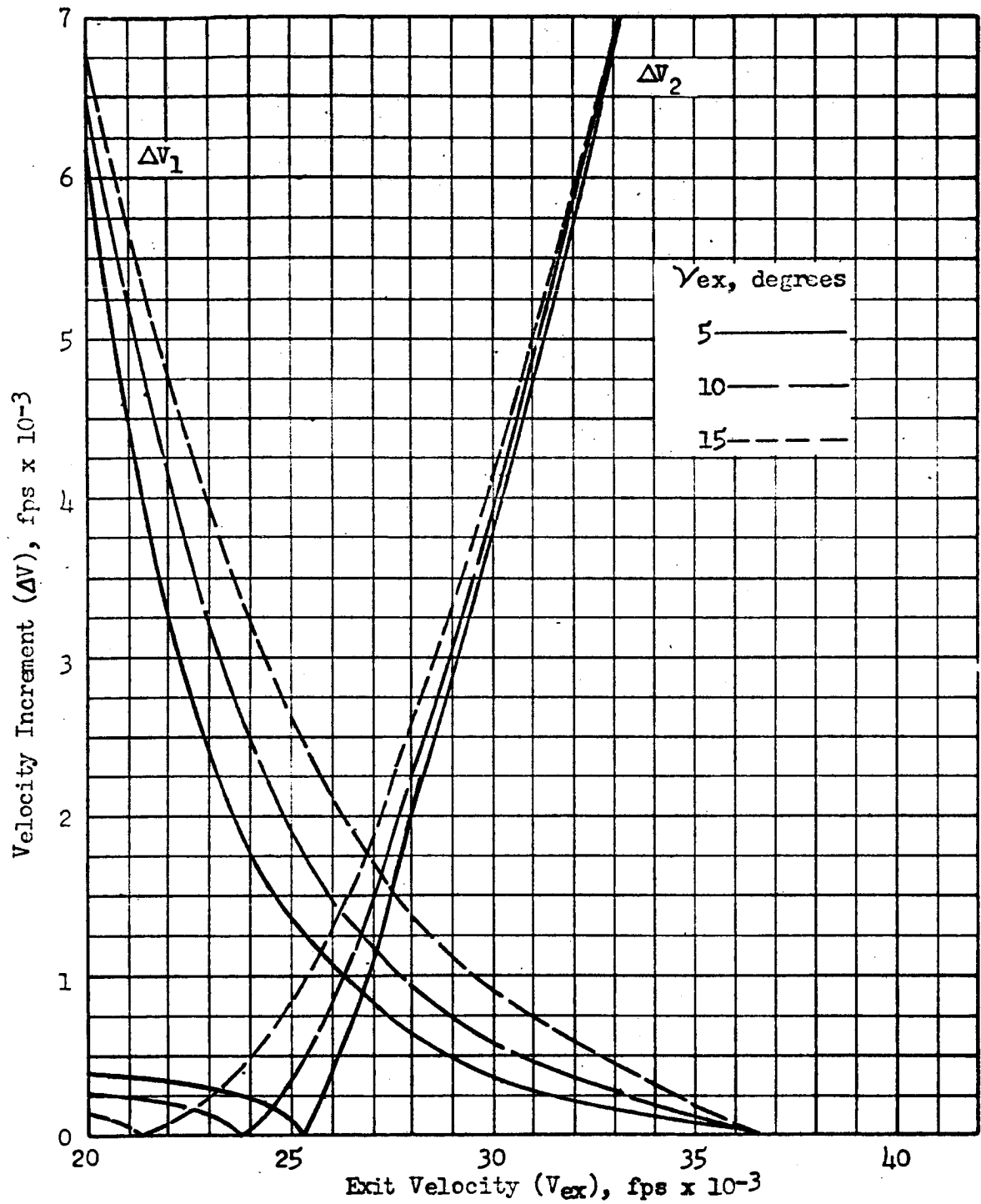


Fig. 56 Velocity Increments for Establishing a 300 n mi Orbit at Earth, Scheme 2

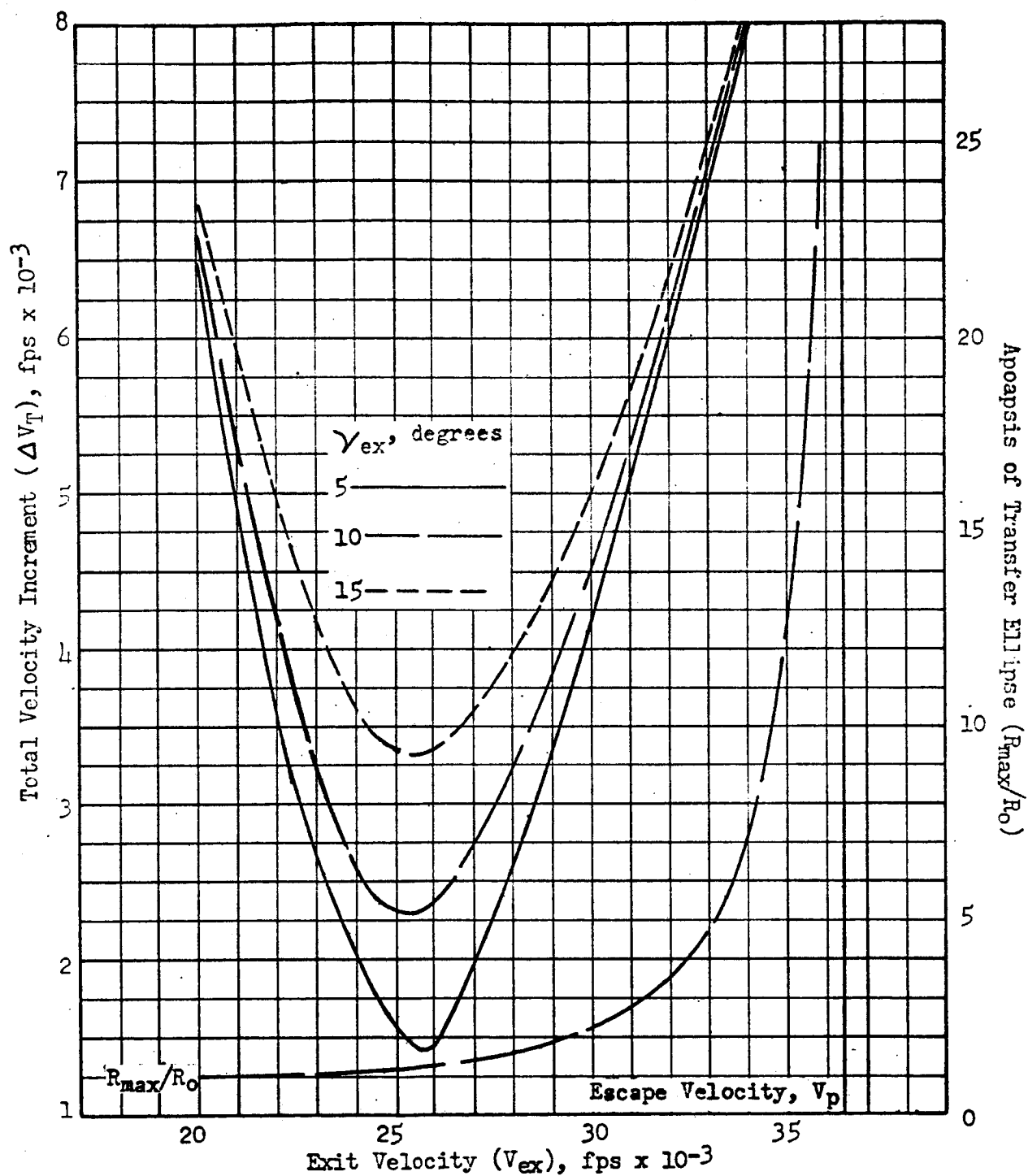


Fig. 57 Total Velocity Requirements for Establishing a 300 n mi Orbit at Earth, Scheme 2

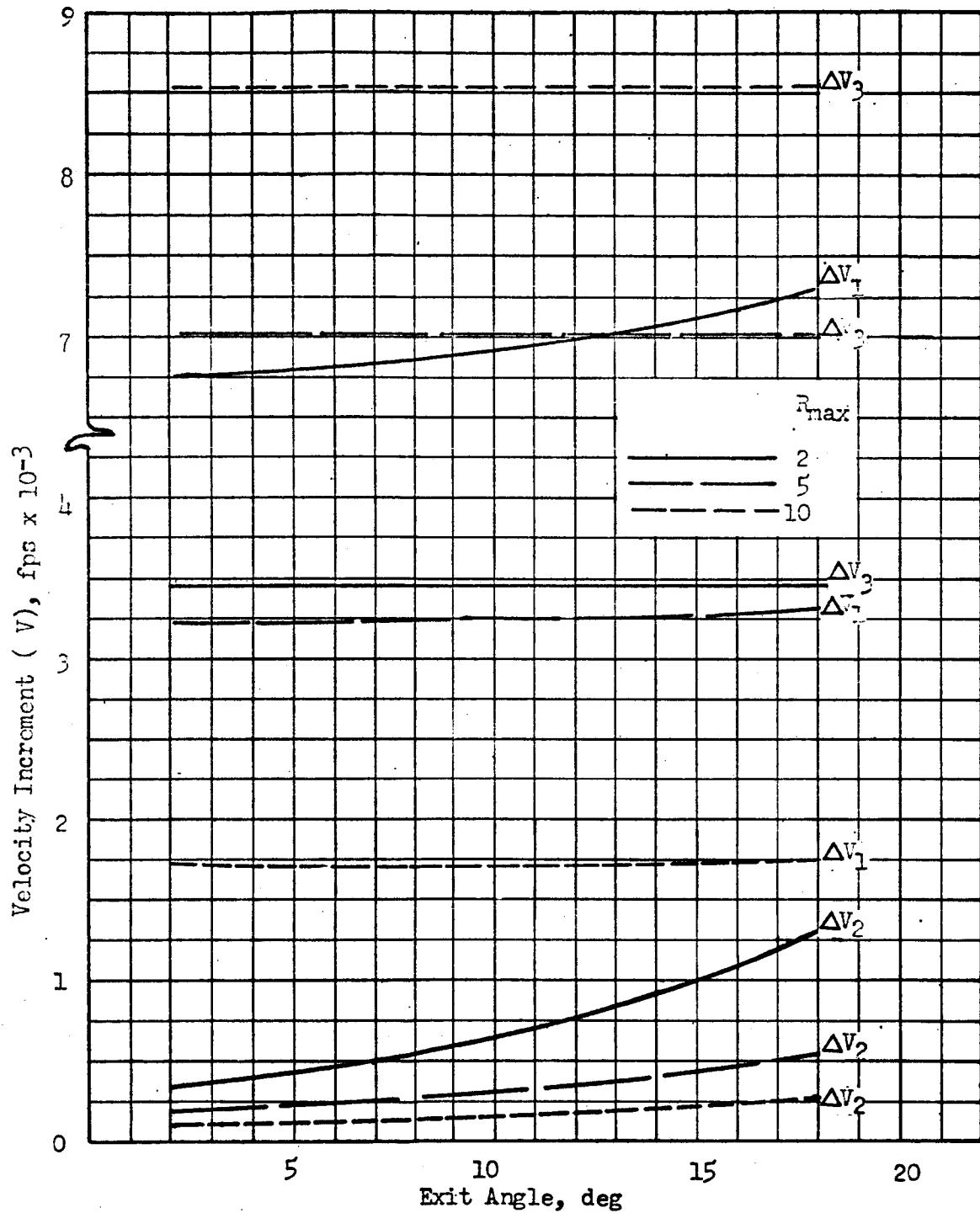


Figure 58 Velocity Increments for Establishing a 300 n mi Orbit at Earth, $V_{ex} = V_p = 36,334$ fps, Scheme 3

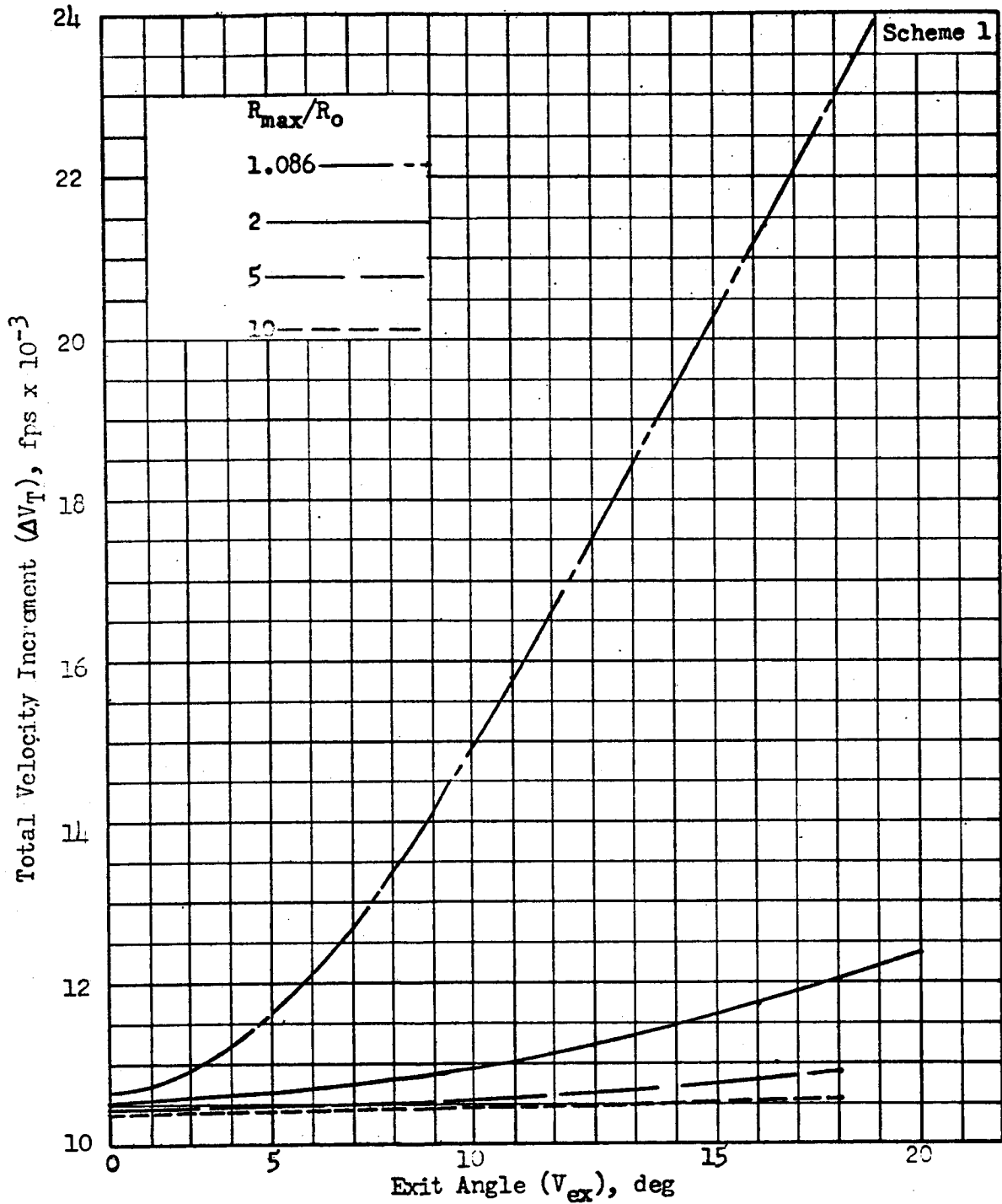


Fig. 59 Total Velocity Requirements for Establishing a 300 n mi Orbit at Earth, $V_{ex} = V_p = 36,334$ fps, Scheme 3

$$\Delta V_1 = \Delta V_{1,P} + (V_{ex} - V_P)$$

and

$$\Delta V_T = \Delta V_{T,P} + (V_{ex} - V_P)$$

Since Scheme 1 is just a special case of Scheme 3 ($R_{max} = R_0 + 300$ n mi), the total impulsive velocity requirement for this scheme is also illustrated in Figure 59. As R_{max} is increased, the velocity requirements decrease; this effect is particularly pronounced at the large values of exit angles. However, as R_{max} increases, the time required for orbit establishment also increases. Approximate values of the time for orbit establishment for various values of R_{max}/R_0 are given; equivalent data for Mars and Venus are also presented.

R_{max}/R_0	Time to Orbit, Hours		
	Earth	Mars	Venus
5	7.5	9	8
10	18	22	19.5
50	182	220	194

Long time periods for orbit establishment may not be compatible with mission objectives; consequently the maximum apoapsis allowable, and in turn the minimum ΔV possible, may be restricted for some missions.

The problem of long time periods for orbit establishment also exists in Scheme 2 when the exit velocity approaches escape velocity (see Figure 57). Consequently it may be desirable to use Scheme 3 and control the time to orbit if the exit velocity is near escape velocity.

Evaluation of Impulsive Schemes. To facilitate an evaluation of the merits and advantages of the different orbit establishment schemes, a typical value of the exit angle (γ_{ex}) was selected; the value chosen to represent a typical grazing trajectory was 5 degrees. The apoapsis of the transfer ellipse of Scheme 3 was restricted to a value of 5 times the planetary radius. This value was believed to be a reasonable compromise between time-to-orbit and velocity requirements.

The relative merits of the three impulsive schemes are indicated in Figure 60. For the lower range of exit velocities ($V_{ex} < V_p$), Scheme 2 yields the lowest velocity requirements over most of the range. Lower velocity requirements at some exit velocities are given in Scheme 1, this occurs mostly at exit velocities less than circular which are unlikely occurrences from the graze maneuver. Schemes 2 and 3 intersect at the point where the apoapsis of Scheme 2 is 5 times the planetary radius. For exit velocities greater than this intersection ($V_{ex} = 33,000$ ft/sec), the apoapsis of Scheme 2 is larger than $5 R_0$; consequently the time required to establish orbit becomes excessive. To keep the time-to-orbit within a reasonable limit, a switch to Scheme 3 at this intersection point is warranted. For exit velocities greater than escape velocity, Scheme 3 appears best. In summary, Schemes 2 and 3 are most favorable of the impulsive orbit establishment maneuvers.

Nonimpulsive Orbit Establishment

The impulsive velocity requirements presented are useful for indicating trends and relative merits of the various maneuvering techniques. However, impulsive analyses are not necessarily indicative of the actual propulsive energy required, particularly if long burning times are involved. The energy change of the trajectory of the vehicle resulting from an impulse depends on the instantaneous potential energy of the vehicle. Finite thrust can be thought of as a series of impulses over which the potential energy is changing. Consequently, the trajectory energy change caused by an impulsive velocity increment will differ, if the same impulse is applied over a non-zero time interval, unless the average potential energy over the time period is effectively the same as the potential energy at which the impulsive increment is applied.

Another effect is the relation between burning time and the time required to perform the maneuver. The burning time may be of such magnitude that it is not possible for the vehicle to attain the desired position and velocity at

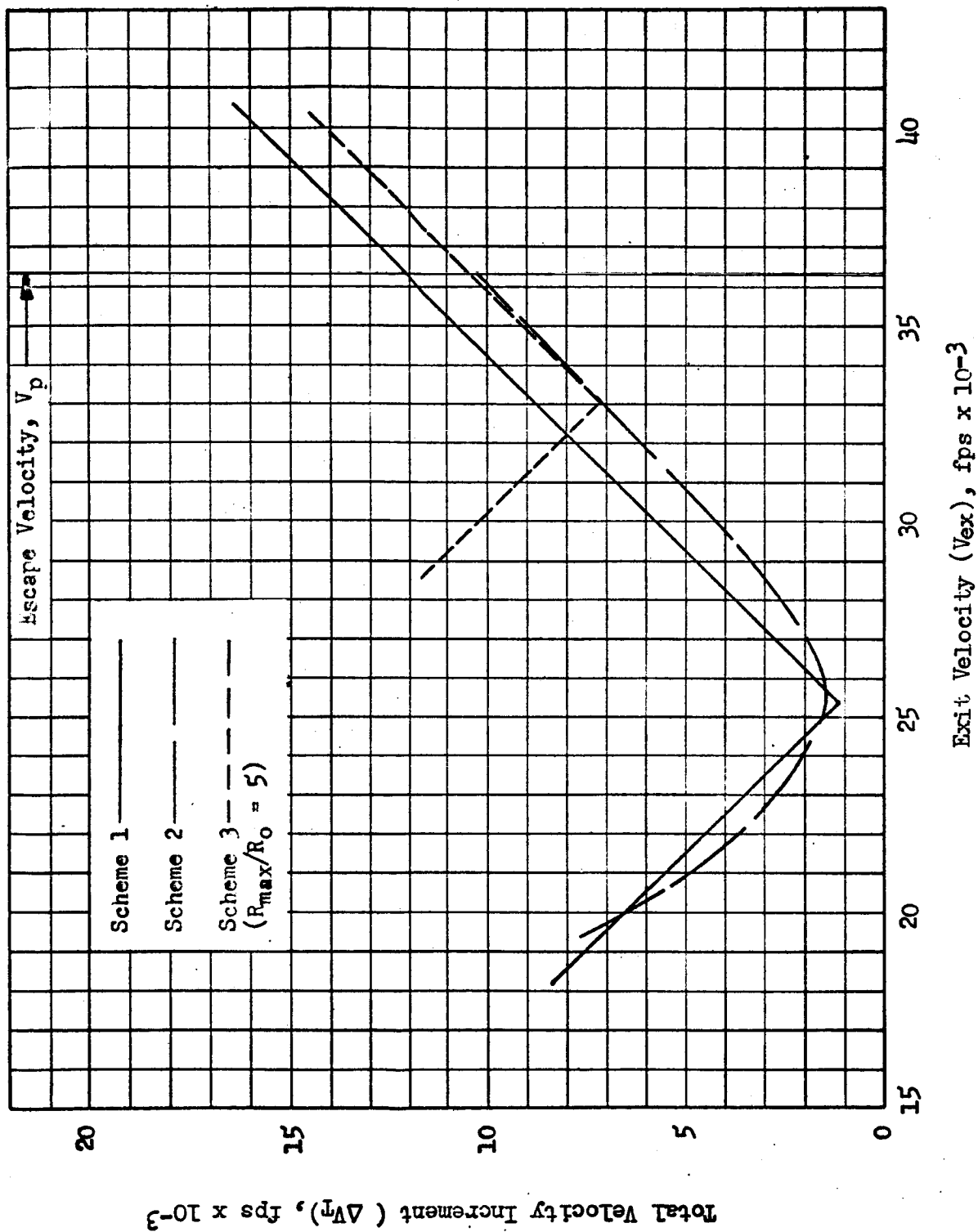


Fig. 60 Summary of Impulsive Velocity Requirements for Establishing a 300 n mi Orbit at Earth, $\gamma_{ex} = 5$ degrees

all. For instance, for the two-impulse direct-to-orbit maneuver (Scheme 1), the vehicle may have already passed the desired circular orbit altitude before burning is completed. Therefore for Scheme 1, the impulsive velocity requirements are not necessarily indicative of the actual requirements, particularly if long burning times are required (large V 's). For Schemes 2 and 3 the maneuver time is an order of magnitude greater than the burning time (for chemical propulsion systems) and the above effect is not prevalent; however, the actual velocity requirements are slightly different from the impulsive caused by the changing potential energy over the burning time.

The existence of the Van Allen radiation belts surrounding the Earth makes it desirable to employ direct-to-orbit maneuvering techniques similar to Scheme 1. The other impulsive schemes pass through the Van Allen Belts twice. To determine the requirements of a direct-to-orbit maneuver, an orbit-establishment analysis for finite thrust systems was performed utilizing a computer trajectory simulation program. To assure a flight path that would not pass through the Van Allen Belts, thrust was applied so as to minimize the altitude rate during the maneuver. For the maneuver selected, the thrust vector is aligned at a constant attitude (with respect to local vertical) in essentially a downward direction. The flight path for this maneuver is illustrated in Figure 61. After departing the atmosphere, the vehicle coasts for a time interval whereupon thrust is applied at the exact pitch angle (ψ) that will result in the simultaneous attainment of the 300-n mi altitude and its corresponding circular velocity. (To simulate this maneuver on the trajectory program, the vehicle was flown backwards from the 300-n mi orbit until the exit altitude was intercepted.)

The velocity requirements for the nonimpulsive orbit establishment maneuver at vehicle thrust-to-weight ratios of 0.5 and 1.0 are illustrated in Figures 62 and 63. The range of exit conditions that can be accepted by this maneuver is bounded by the "limiting exit conditions" line. Values of exit conditions beyond this line are too large for the accomplishment of this maneuver with the specified F/W ; i.e., the vertical component of velocity cannot be cancelled before the 300-n mi altitude is reached. Consequently, the range of exit conditions to be expected will be a criterion for thrust level selection.

Evaluation of Orbit-Establishment Techniques

A comparison of the velocity requirements for the nonimpulsive orbit-establishment maneuver and the corresponding impulsive maneuver (Scheme 1) is illustrated in Figure 64. Over the range of exit velocities considered,

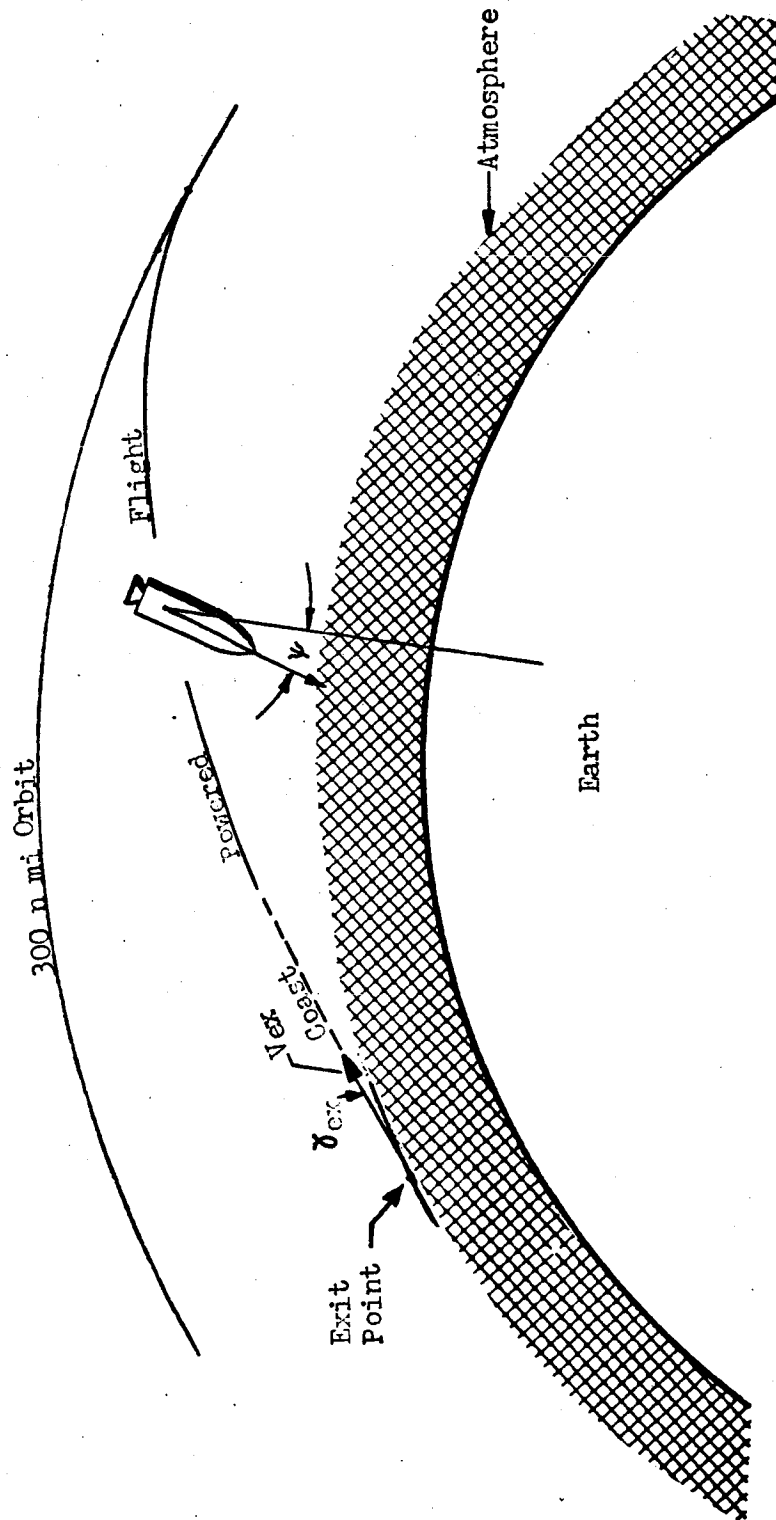


Figure 61 Nonimpulsive Orbit Establishment Maneuver

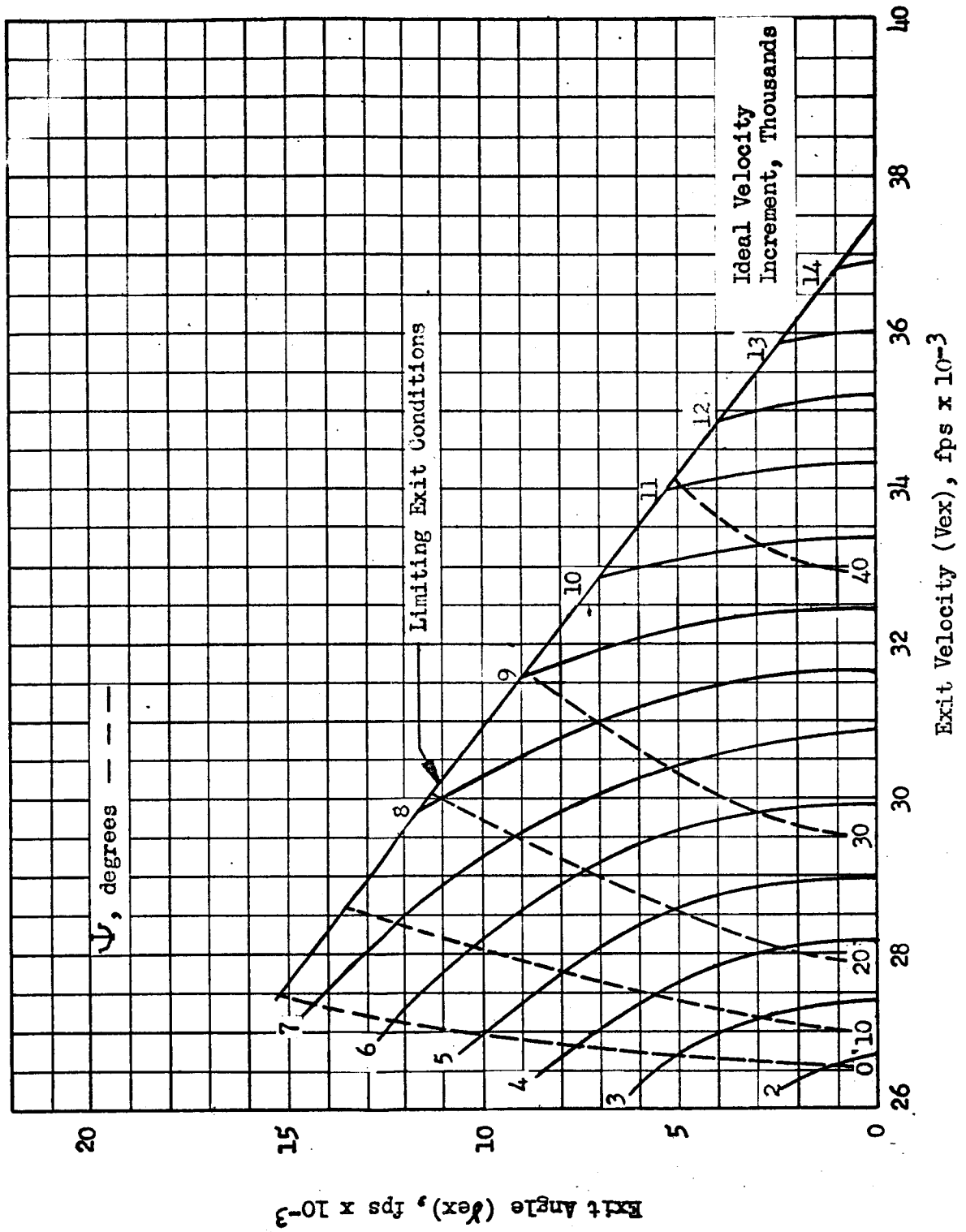


Fig. 62 Ideal Velocity Contours for Establishing a 300 n mi Orbit at Earth, Nonimpulsive Maneuver, $F/W = 0.5$

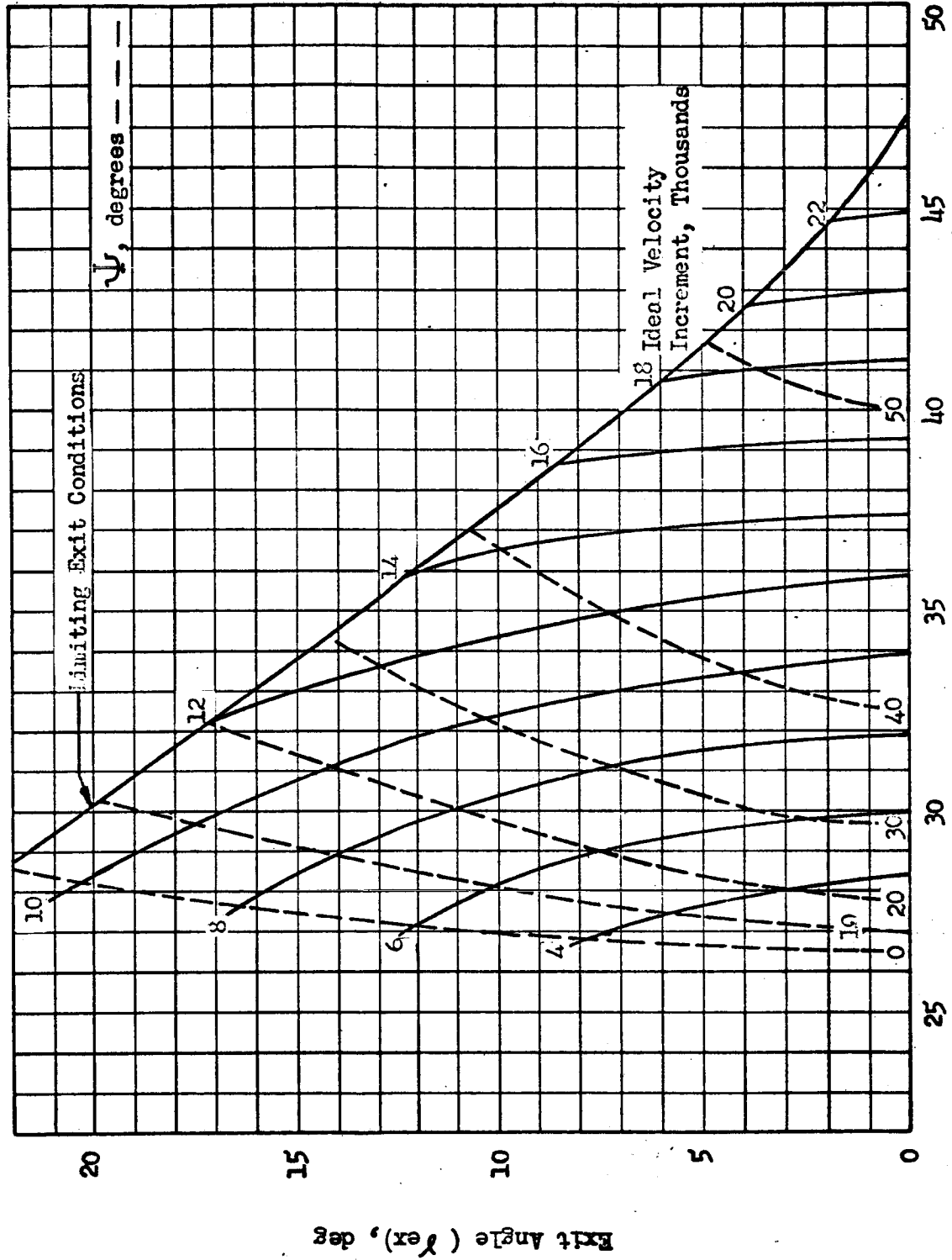


Fig. 63 Ideal Velocity Contours for Establishing a 300 n mi Orbit at Earth, Nonimpulsive Maneuver, $F/W = 1.0$

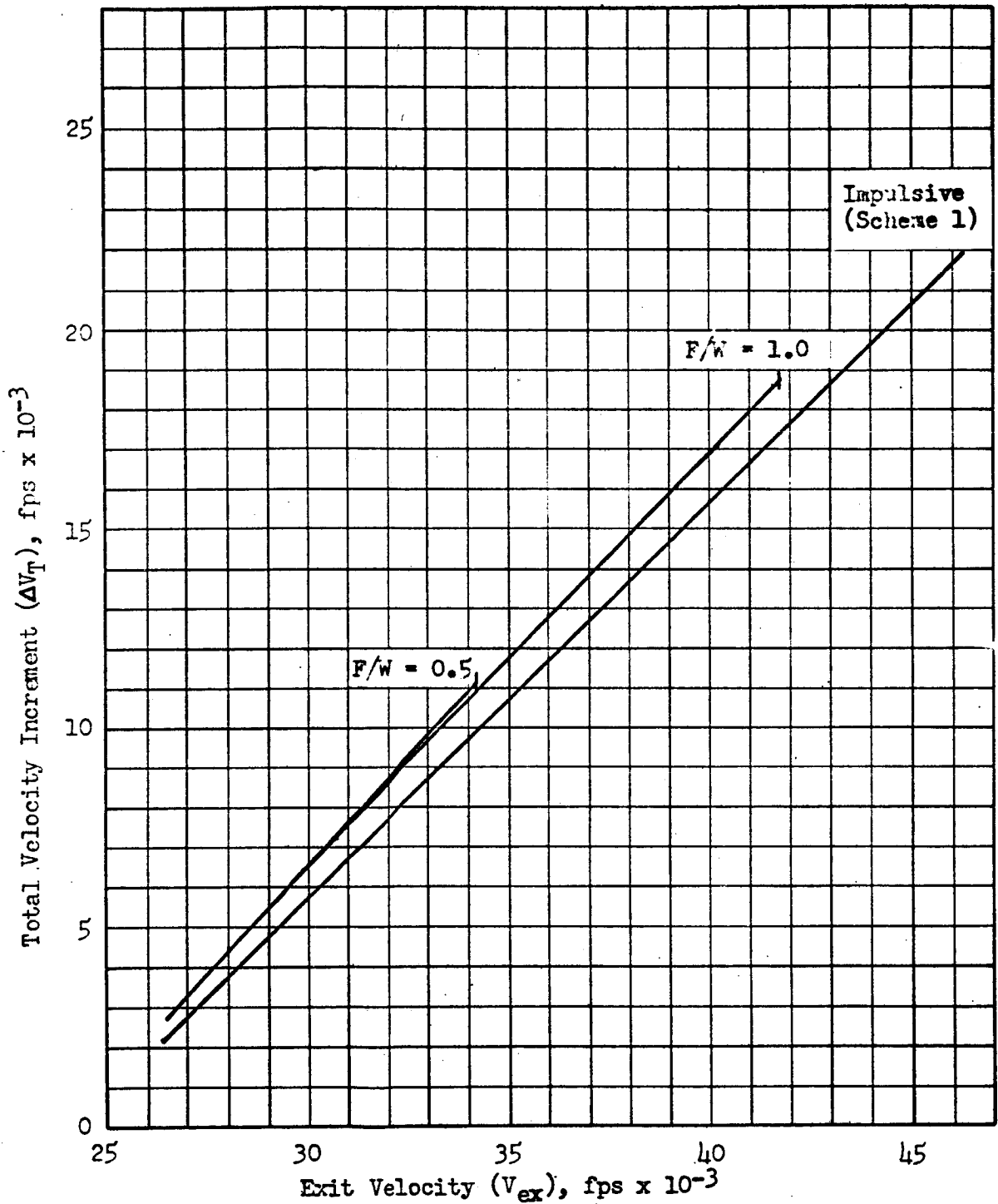


Fig. 64 Comparison of Impulsive and Nonimpulsive Velocity Requirements for Establishing a 300 n. mi. Orbit at Earth.

the velocity requirements are greater for the nonimpulsive maneuver (roughly 10 percent greater) than the impulsive requirements; however, the trend in velocity requirement is similar. The losses are partially explained by the fact that the nonimpulsive scheme applies its deceleration at a lower kinetic-energy level, in contrast to the impulsive scheme which applies a large portion (ΔV_1) of its total impulse at a low potential energy (high kinetic energy). In addition, the nonimpulsive scheme does not use thrust-parallel-to-velocity to achieve the 300-n mi circular orbit, thereby reducing the effectiveness of the deceleration maneuver from the standpoint of velocity requirements.

The selection of a particular orbit-establishment technique depends on two factors: 1) the magnitude of the atmosphere graze exit velocity and 2) the ability of the vehicle to traverse the radiation belts. For vehicles that can pass through the radiation belts, Schemes 2 and 3 yield the lowest velocity requirements, Scheme 2 for exit velocities less than 33,000 ft/sec and Scheme 3 for exit velocities greater than 33,000 ft/sec. The velocity requirements determined for the impulsive analyses are adequate for systems with thrust-to-weight ratios above approximately 0.5. For lower thrust-to-weight ratios, the impulsive analysis tends to be optimistic.

For vehicles which do not possess sufficient shielding for repeated penetration of the radiation belts, a direct-to-orbit maneuver should be used. For this maneuver, the finite thrust analysis indicates velocity requirements and thrust-to-weight ratio limits. In general, the results indicate that the propulsion velocity requirement for orbit establishment after graze is approximately equal to the difference in graze exit velocity and orbital velocity.

The applicability of the atmospheric graze maneuver to a vehicle and mission depends upon the vehicle design configuration and upon possible mission constraints. If it is feasible to utilize a ballistic or lifting vehicle, the graze maneuver can be used to reduce the propulsion required for orbit establishment in comparison to that required for an entirely propulsive orbit-establishment maneuver.

PROPULSIVE/AERODYNAMIC DECELERATION FOR DIRECT EARTH LANDING

In addition to providing the deceleration and direction necessary to assist a space vehicle to acquire a specified entry corridor, a retropropulsion phase prior to atmospheric entry can, by reducing the ablative heat shield requirement, reduce the weight of the overall landing vehicle system. This possibility is not obvious when considered for the contemporary large rockets required to accelerate small payloads to orbital velocity compared to the modest heat shields required to cancel orbital velocity by aerodynamic deceleration. The important difference when considering more ambitious space missions in comparison to a satellite mission is that the pertinent velocity is not orbital, but 2 to 3 times orbital; at velocities of this magnitude, propulsion systems to cancel the entire amount are undeniably large, but heat shields to perform the same task are by no means modest, and may equal or exceed the equivalent propulsion system weight. Because of the different rates at which propulsive and aerodynamic braking devices increase in weight as velocity increases, a combination system may be best.

An evaluation of propulsion/ablation systems for space vehicles with extremely high velocities, based on weight tradeoff considerations, was made to determine the desirability of adding the propulsion system to the vehicle design. The initial study, conducted to indicate preliminary trends in system requirements, was predicated on an impulsive velocity change for the propulsion phase. The optimum division between propulsive and aerodynamic braking for a planetary entry body was determined, and the influence of several vehicle and trajectory parameters on the optimization results was evaluated.

The basic retropropulsion and aerodynamic landing system phases are illustrated in Figure 65. The system velocity increases as it enters the planet gravitational field (1 to 2); retropropulsion initiates the deceleration phase (2 to 3); aerodynamic deceleration to position (4) follows; and the final parachute (etc.) phase decelerates the vehicle to touchdown (4 to 0). The impulsive retropropulsion assumption yields the constant altitude braking phase shown as 2' to 3'; as propulsive thrust-to-weight ratio is decreased, the altitude decrease during the retropropulsion phase becomes greater.

The implied assumption that suitable entry corridors for all payloads exist for all the entry velocities considered is obviously invalid in some instances, as was demonstrated in the previous section. For a sufficiently low -g deceleration requirement, there is no acceptable corridor no matter how low the entry velocity, and for a permissible high -g deceleration level, there is a corridor no matter how high the entry velocity.

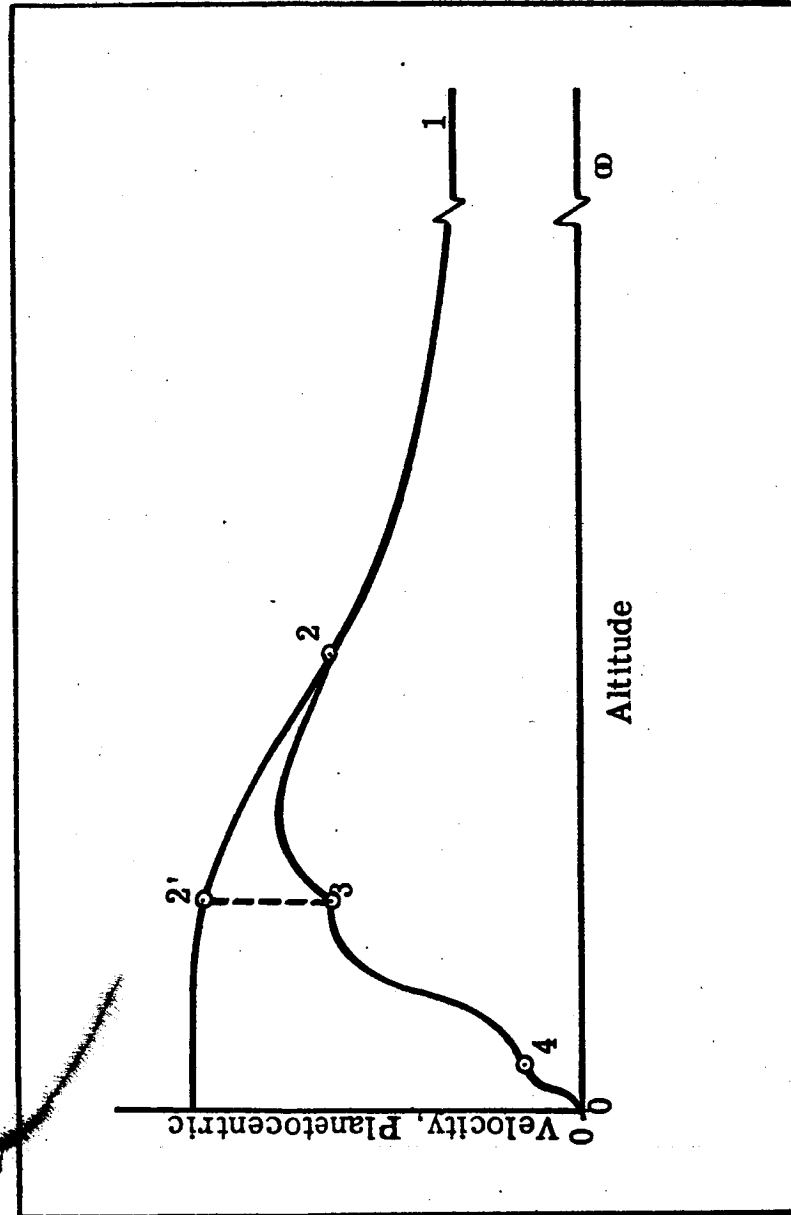


Figure 65 . Entry Velocity Conditions

Thus, while the optimum indicated design may have no propulsive braking for many missions, constraints such as maximum allowable g level can be stipulated such that propulsive braking of some specific magnitude must be applied prior to entry into the atmosphere so that the g-level limit is not exceeded. The questions of the existence of appropriate entry corridors at extremely high velocities and the ability to guide a vehicle to these corridors are included in analyses of terminal correction requirements, but are not considered in the present investigation.

Entry Conditions

The initial conditions of the entry phase, i.e., the magnitude and direction of the arrival velocity vector (at a specified altitude), are dependent on the characteristics of the interplanetary transfer. The boundary conditions for the landing phase are generally expressed as a velocity and elevation angle at a defined entry altitude. This terminology can be translated readily from the hyperbolic excess velocity and asymptotic approach distance used for the transfer analysis.

The relation between V_h and V_a can be expressed as:

$$V_a = \left[\frac{2g_0 R_0^2}{R_0 + h} + V_h^2 \right]^{\frac{1}{2}}$$

where V_h = Hyperbolic excess velocity
 V_a = Arrival velocity at altitude h
 g_0 = Surface gravity
 R_0 = Planet radius

The entry altitude values used were: Earth, 400,000 ft; Mars, 1,400,000 ft; Venus, 435,000 ft. Above these altitudes, aerodynamic effects are negligible. For Earth and planetary entry, Figure 66 presents arrival velocity (i.e., vehicle velocity at the entry altitudes and before any retropropulsion is applied) as a function of hyperbolic excess velocity.

For an impulsive (and constant altitude) retropropulsion phase, both the arrival and entry velocities (defined as: velocity at the entry altitude after the retropropulsion phase) are at the same altitude. Thus, the entry velocity (V_e) is:

$$V_e = V_a - \Delta V$$

ROCKETDYNE
A DIVISION OF NORTH AMERICAN AVIATION, INC.

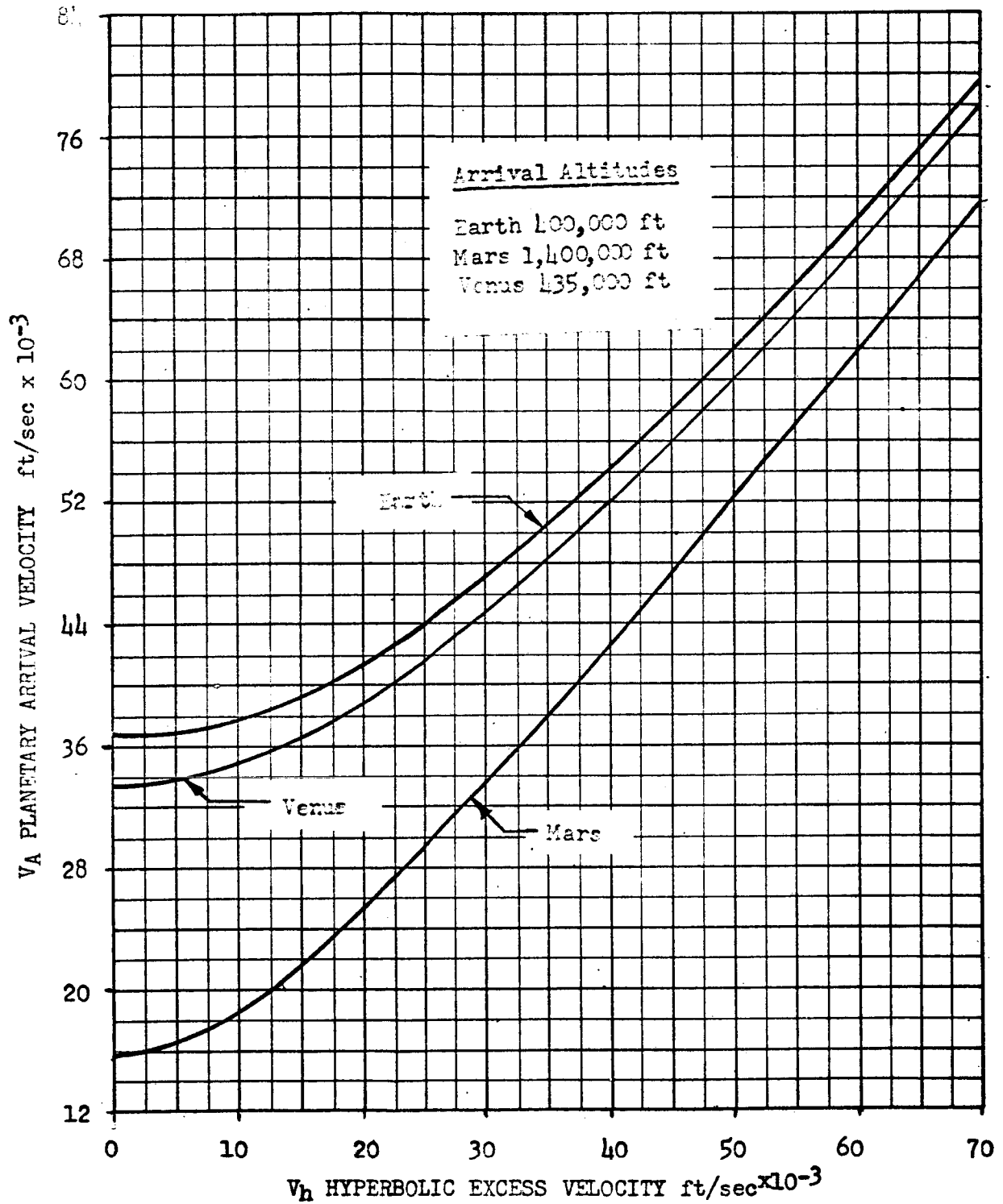


Fig. 66 Planetary Arrival Velocity and Hyperbolic Excess Velocity

where ΔV is the propulsion velocity change. For a nonimpulsive retropropulsion phase, ΔV must be increased due to the gravity loss associated with a finite thrusting period.

Equivalent Specific Impulse of Ablative Shields

In comparing the effectiveness of aerodynamic and propulsive braking systems, one might consider the ablation material as the equivalent of the propellant of a retrorocket system and define its effectiveness in terms of an equivalent specific impulse. Basically, if a velocity, ΔV , is cancelled completely while ablation of a fraction, L , of the vehicle takes place, the mass ratio is $1/1-L$, and the equivalent specific impulse is

$$I_s = \frac{-\Delta V}{g \ln(1-L)}$$

Unlike propellant, however, I_s in this instance is not constant and independent of ΔV , but is instead dependent on ΔV . Thus, each increment of ΔV is represented by a different I_s . The I_s value obtained by the use of the expression above represents an average value over the interval from zero to ΔV , and although the value might be quite high in an illustrative case, the effectiveness of the ablative material in cancelling a small increment of velocity at the high velocity end of the interval might actually be quite poor.

To derive an expression for the instantaneous equivalent specific impulse of ablative materials, the ablative material loss during atmospheric entry can, at high velocities, be approximated by an expression of the form

$$L = e^{\alpha V + \beta}$$

where L = Fraction of gross weight devoted to heat shield

V = Entry velocity

α, β = Constants

The mass ratio, R , during the braking phase is

$$R = \frac{1}{1-L} = \frac{1}{1 - e^{\alpha V + \beta}}$$

which yields

$$e^{\alpha V + \beta} = \frac{R-1}{R}$$

then

$$\alpha V + \beta = \ln(R-1) - \ln R$$

and

$$V = \frac{1}{\alpha} [\ln(R-1) - \ln R - \beta] \quad (1)$$

Since, in the expression, $\Delta V = I_s g \ln R$, $I_s g$ represents the proportionality constant relating ΔV to $\ln R$, the instantaneous slope of a V vs $\ln R$ characteristic for an aerodynamic entry vehicle represents g times the equivalent specific impulse of the heat shield material. Thus, the derivative, $dV/d(\ln R)$, obtained from Eq. (1), is the required solution.

To obtain the first term of the derivative, $d\ln(R-1)/d\ln R$, substitute $y = \ln R$

then

$$\begin{aligned} e^y &= R, \text{ and } e^y - 1 = R - 1 \\ \ln(e^y - 1) &= \ln(R - 1) \\ \frac{d\ln(e^y - 1)}{dy} &= \frac{d\ln(R - 1)}{d\ln R} \\ \frac{d\ln(R - 1)}{d\ln R} &= \frac{e^y}{e^y - 1} = \frac{R}{R - 1} \end{aligned}$$

Thus

$$\frac{dV}{d\ln R} = \frac{1}{\alpha} \left[\frac{R}{R-1} - 1 \right] = \frac{1}{\alpha} \left[\frac{1}{R-1} \right] = \frac{1}{\alpha} \left[\frac{1-L}{L} \right]$$

and

$$I_s \text{ EQ} = \frac{1}{\alpha g} \left[\frac{1 - e^{\alpha V + \beta}}{e^{\alpha V + \beta}} \right]$$

The variation with velocity of average and instantaneous equivalent specific impulse for a selected ablative material is presented in Figure 67. It should be noted that Figure 67 cannot be employed directly to compare propulsive and aerodynamic systems, since in addition to equivalent specific impulse, nonpayload inert weights must be compared; i.e., an equivalent propellant fraction is also needed.

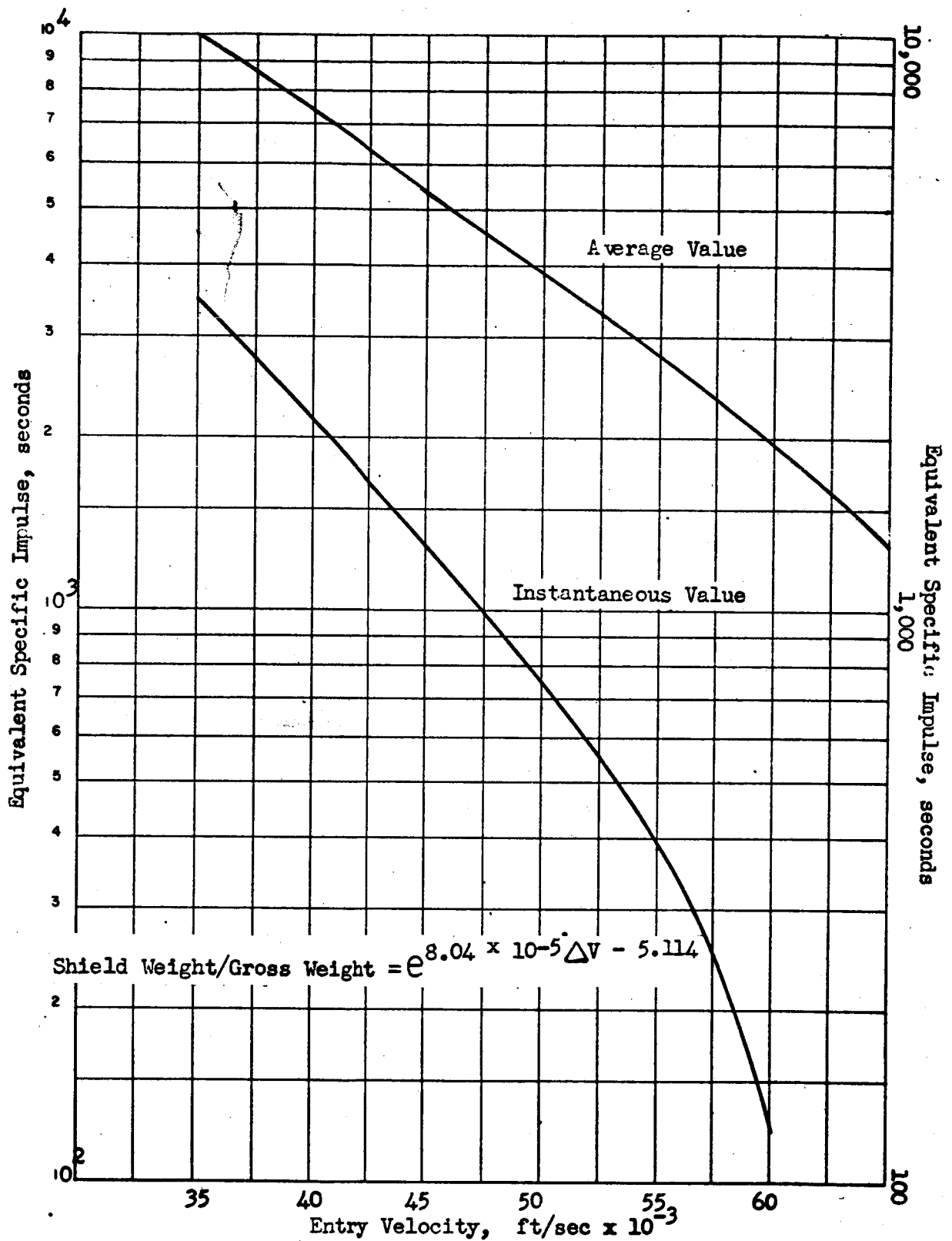


Figure 67 . Equivalent Specific Impulse of Ablative Heat Shield Material.

Impulsive Thrust Analysis

The trade-off analyses were based on the assumption of a simple exponential relationship between ablative shield weight and atmosphere entry velocity. Though this assumption circumvents detailed investigation of the more esoteric aspects of hypersonic entry into, and flight within, planetary atmospheres, it is nevertheless reasonably accurate at very high velocities*.

Ablative Material Selection. An optimization analysis, based on impulsive velocity changes (ΔV) for the retropropulsive phase, was conducted to evaluate the effects of the ablation weight characteristic, propulsion system performance and arrival velocity on the optimum value of propulsive ΔV . A conservative ablation characteristic, presented in Figure 68, was utilized for the impulsive thrust analysis. A band of ± 10 percent is indicated; this perturbation of ablation characteristics was used to evaluate the effect of the ablation curve on the optimum propulsion system velocity increment and the payload.

The equation fitting these data expresses weight loss (L) as a function of entry velocity.

$$L = e^{\beta V - \gamma}$$

where L = Ablative weight
 $\beta = 1.388 \times 10^{-4}$
 $\gamma = 6.467$
 V_e = Entry velocity

Analysis Method. The difference between the arrival velocity and the entry velocity is the ΔV which must be cancelled by impulsive retropropulsion. By manipulation of the ideal velocity equation for the retrothrust propulsion stage, its payload weight can be expressed as a function of gross weight (W_G), propellant fraction (λ_p), specific impulse (I_s), and ΔV . The factor (1-L) is then applied to reduce the vehicle weight by an amount equal to the ablative material loss, where L equals the ablative weight loss expressed as a percentage of initial vehicle weight. A factor, (1 - α), is then applied to

* Although the exponential form of the ablation characteristic is a good assumption, the constants which govern its precise character are particularly difficult to ascertain; as a result, the studies presented utilize an extremely conservative ablation characteristic in the present analysis, a "best guess" characteristic in the following section, and finally a broadly parametric presentation.

ROCKETDYNE

A DIVISION OF NORTH AMERICAN AVIATION, INC

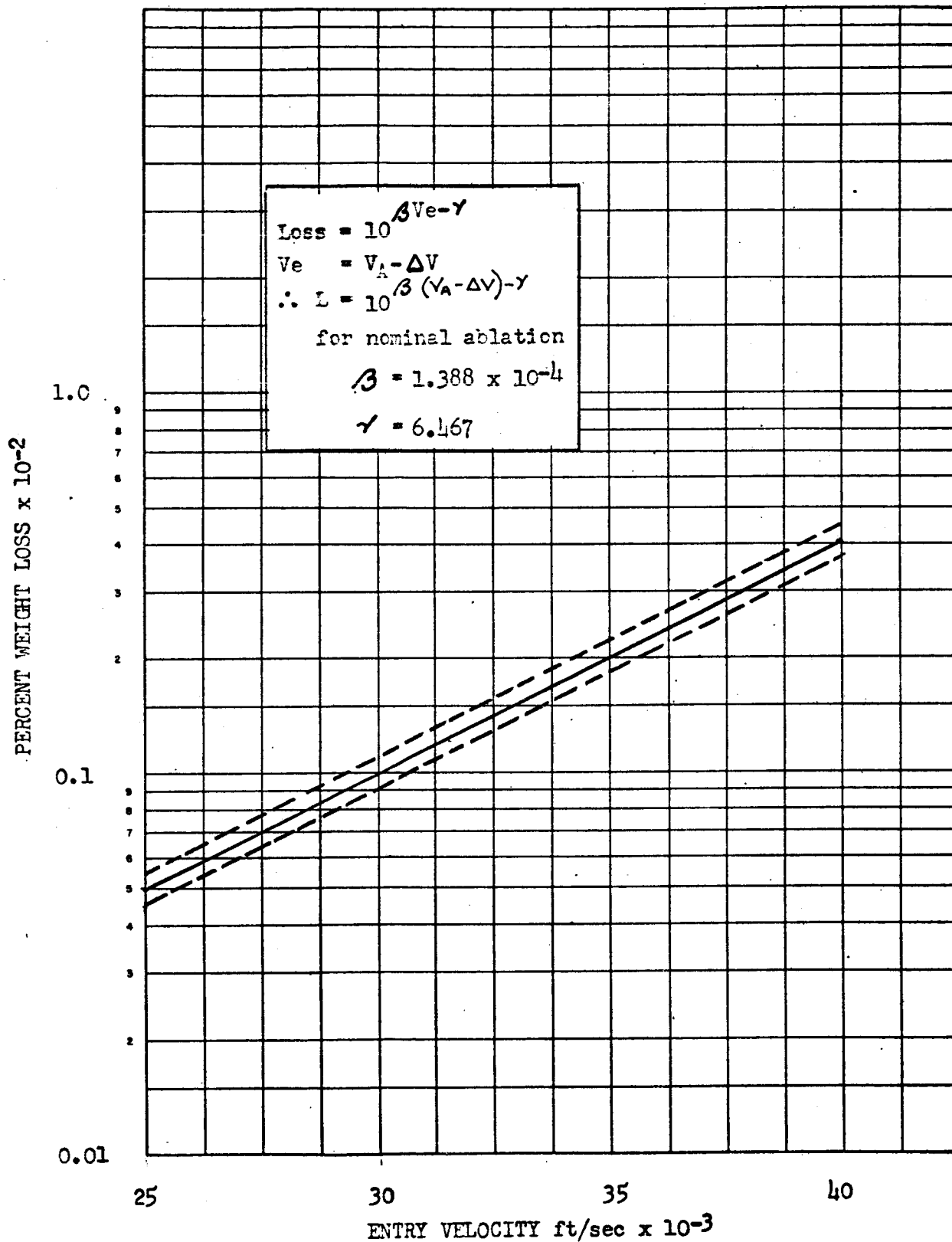


Fig. 68 Percentage of Vehicle Weight Loss for Ablative Entry vs. Entry Velocity

account for the weight necessary for the final descent device, where α is the percentage of vehicle weight after entry losses that is required for the final descent device. The resulting combined equation is:

$$\left(\frac{PL}{W_G}\right)_\Sigma = (1-L)(1-\alpha)\left(\frac{PL}{W_G}\right)_P$$

where:

$$\left(\frac{PL}{W_G}\right)_P = \text{Retropropulsion stage payload-to-gross weight ratio}$$

$$\left(\frac{PL}{W_G}\right)_\Sigma = \text{Overall landing system payload-to-gross weight ratio}$$

or

$$\frac{P.L.}{W_G} = \frac{1}{\lambda_p} \left[\lambda_p - 1 + e^{\Delta V / I_{SGO}} \right] \left[1 - e^{\beta(V_A - \Delta V) - \gamma} \right] (1 - \alpha)$$

In the analysis, propulsion system design was based on a λ_p of 0.85; specific impulse values of 420 seconds (nominal) and ± 100 were used.

The percentage of vehicle weight (α) for the final descent device was considered as 0.08, which was suggested by the limited data available; the particular value affects payload, but has no effect on optimization of ΔV .

Results. The effects of arrival velocities, specific impulse, and ablation characteristics on the optimum propulsive ΔV are presented in Figures 69 to 72. The effect of planetary arrival velocity and specific impulse on propulsion system selection is shown in Figure 69. The optimum propulsive ΔV and payload-to-gross weight ratios from Figure 69 are presented as a function of arrival velocity in Figure 70. The resulting curves show that, based on the ablation weight curve used in the analysis, for planetary arrival velocities of 40,000 ft/sec or less, no propulsion system is required.

Entry velocities can be found by subtracting the propulsive ΔV from the arrival velocity; therefore, it can be seen that the optimum entry velocity is approximately 40,000 ft/sec for all arrival velocities in excess of this value. These figures also show that for a 100-second change in specific impulse, the optimum propulsive ΔV changes approximately 1000 ft/sec. For smaller variations in specific impulse, the change in optimum propulsive ΔV and payload would be insignificant.

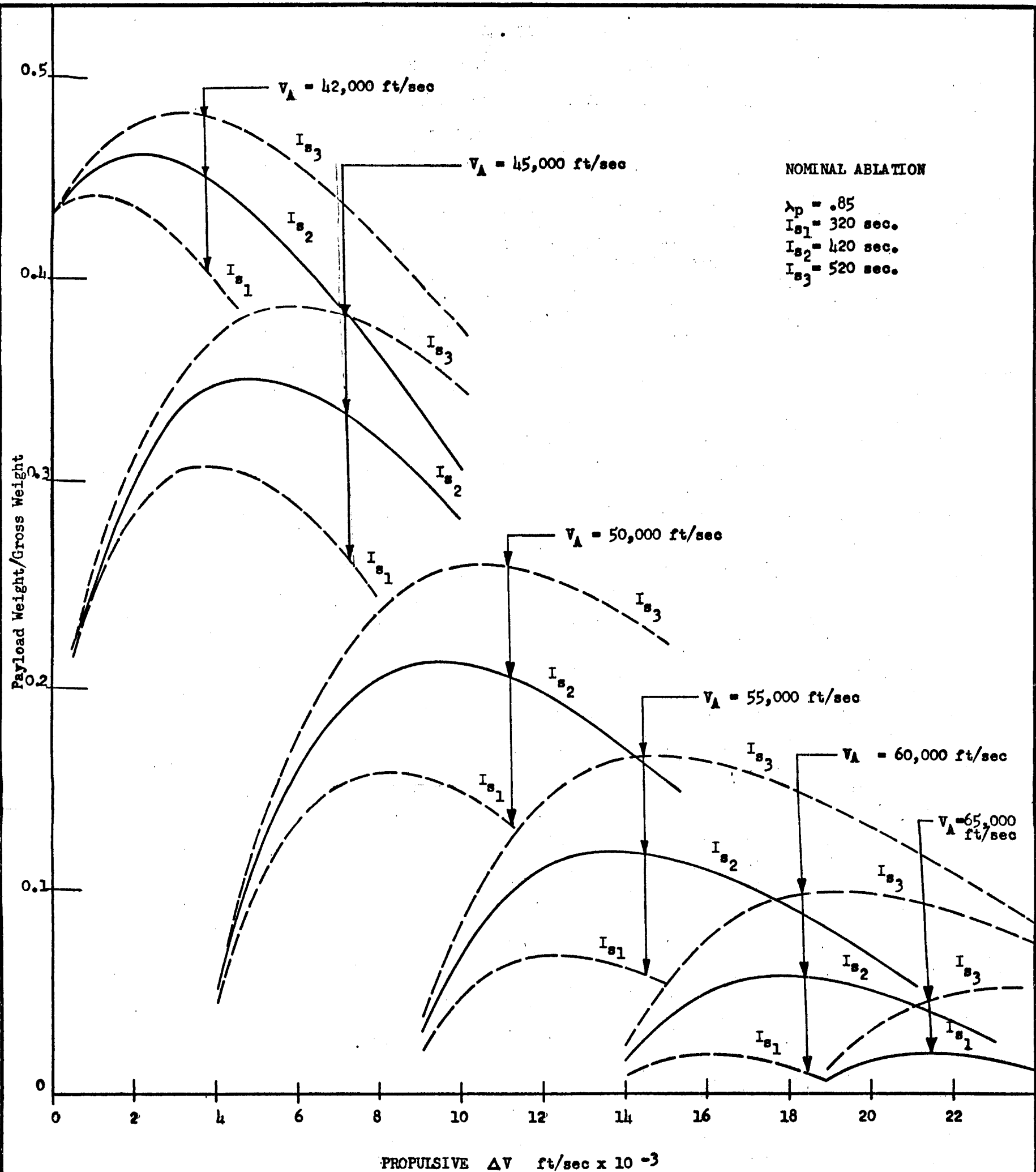


Fig. 69

EFFECT OF PLANETARY ARRIVAL VELOCITY
AND SPECIFIC IMPULSE ON PROPULSION
SYSTEM SELECTION

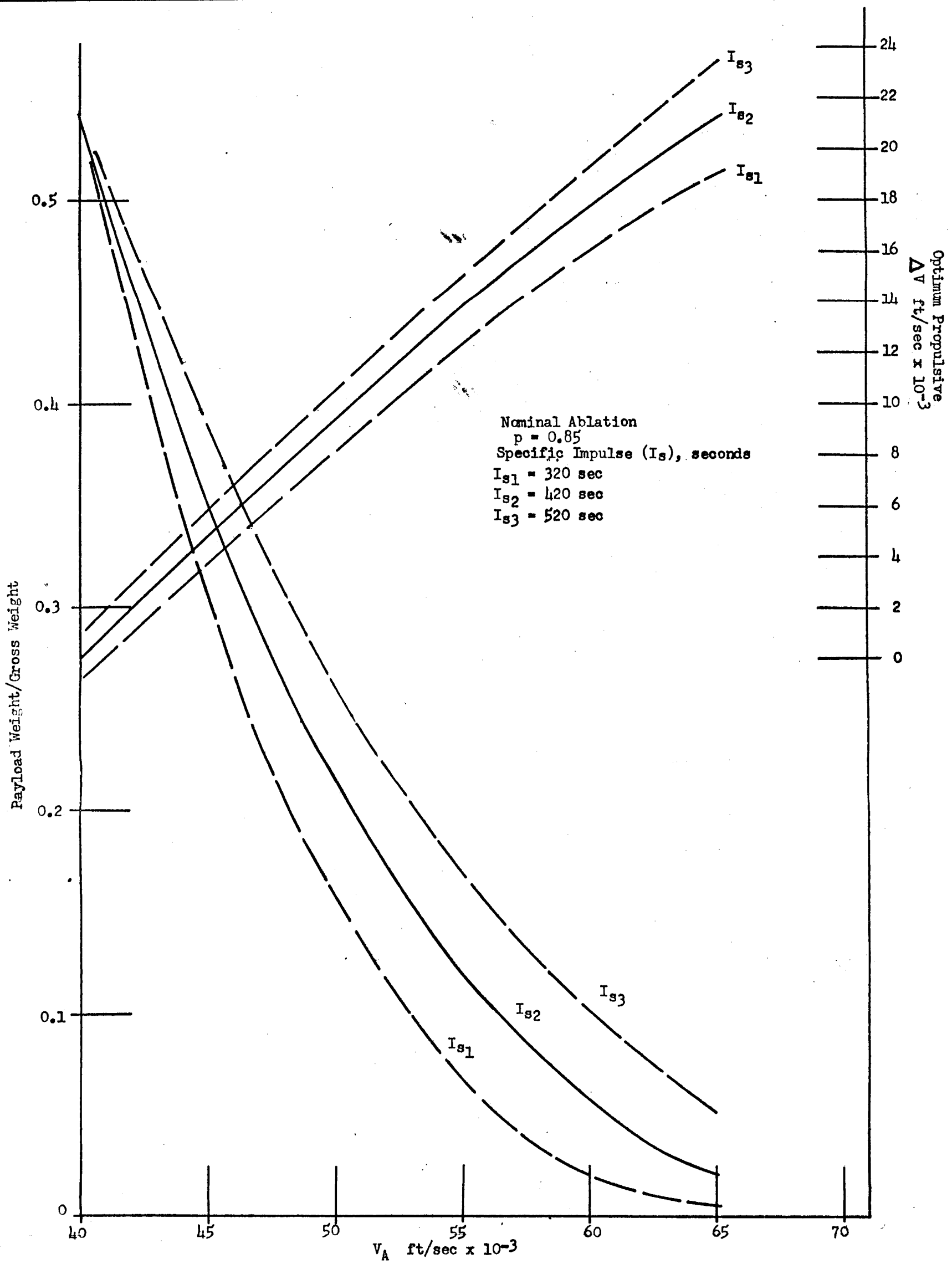


Figure 70. Optimum Propulsive ΔV and Payload Weight/Gross Weight
 vs
 Planetary Arrival Velocity

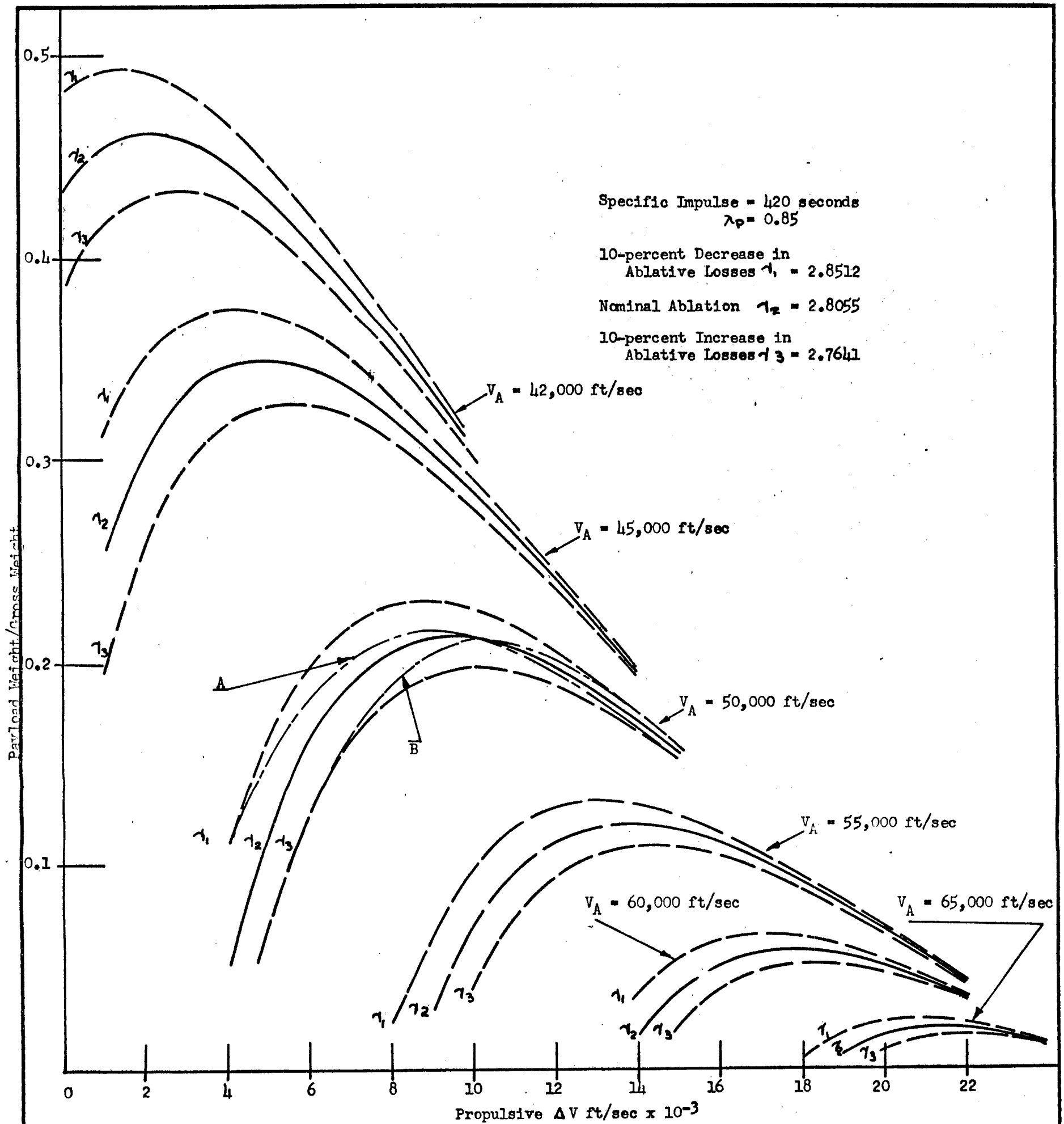


Figure 71. Effect of Planetary Arrival Velocity and Ablation Characteristics on Propulsion System Selection

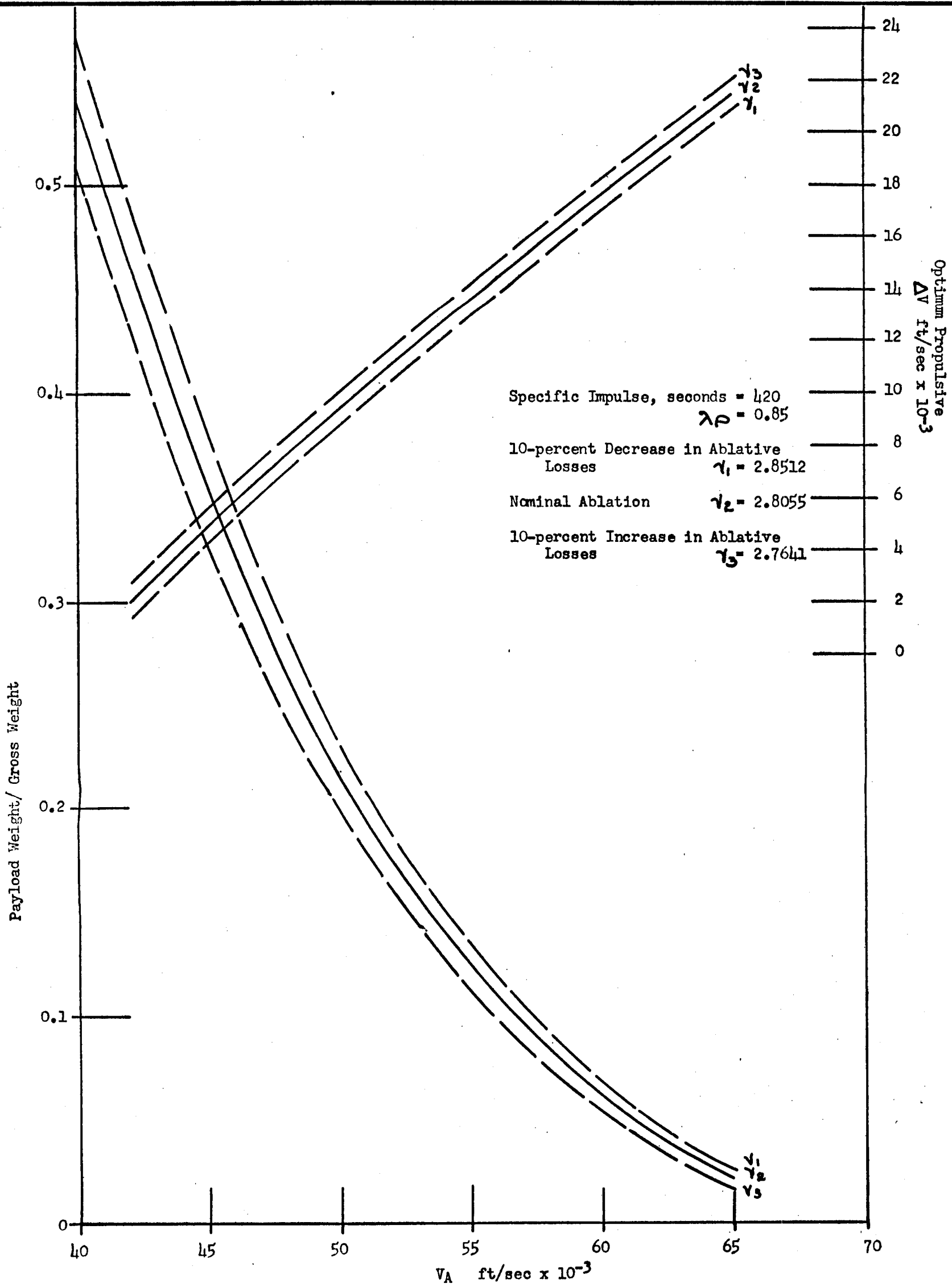


Figure 72. Optimum Propulsive V and Payload Weight/Gross Weight vs Planetary Arrival Velocity

The effect of ablation characteristics on propulsion system requirements is shown in Figure 71. In addition to the nominal ablation case, results are shown for a 10-percent increase and a 10-percent decrease in the nominal ablation losses. With a decrease in ablation loss, the optimum propulsive ΔV shifts to a lower value resulting in a slightly higher optimum aerodynamic entry velocity. In Figure 72 are presented the optimum propulsive ΔV and payloads for Figure 71.

To illustrate the effect of a change in slope of the nominal ablation curve, the nominal ablative weight loss curve was rotated about the point for an entry velocity of 40,000 ft/sec and passed through the 10-percent decrease characteristic at an entry velocity of 45,000 ft/sec. The effect of decreasing the slope is shown in Figure 71 for an arrival velocity of 50,000 ft/sec (Curve A). The effect of a similar increase in the Figure 68 slope is shown in Curve B of Figure 71.

When the slope of the weight loss curve of Figure 68 is increased, there is a slight increase in the optimum ΔV ; and when the slope is decreased, the optimum ΔV shifts to a lower value. In these cases, since the ablation characteristics were rotated about a point near the optimum entry velocity, there was a very small change in the optimum payload; but if the curve had been rotated about some velocity point other than the optimum, there would have been a greater effect on the optimum payload and propulsive ΔV . If the nominal ablative weight loss curve of Figure 68 is rotated about a velocity point below 40,000 ft/sec, a decrease in the slope produces an increase in the optimum payload and a reduction in optimum propulsive ΔV ; an increase causes a decrease in the optimum payload and an increase in the optimum propulsive ΔV . If the rotation point is above a velocity of 40,000 ft/sec, the reverse occurs.

Finite Thrust Analysis

Analysis was conducted to indicate optimum thrust for the propulsion phase, and to determine the effect on velocity requirements of employment of a finite thrust phase. The vehicle considered had an Earth hyperbolic excess velocity of 48,000 ft/sec which is indicative of a fast (100-day) return trip from Mars. In comparison to the lesser hyperbolic velocities associated with other trips (e.g., 30,000 ft/sec for 240-day Mars-Earth, 10,000 ft/sec for 120-day Venus-Earth and 0 ft/sec for 3-day Moon-Earth), the subject journey represents close to an extreme condition of magnitude of Earth-approach velocity. In the absence of propulsive braking, the vehicle would enter the Earth's atmosphere (400,000 ft altitude) at 60,200 ft/sec.

Propulsive Braking Phase. The first phase of the analysis was selection of optimum propulsion system characteristics over a wide range of possible required propulsive capabilities. The propulsive phase was terminated in all cases at the selected Earth entry altitude, 400,000 ft (representing an effective outer fringe of the atmosphere) at velocities ranging from 38,000 ft/sec to 60,200 ft/sec (the latter corresponding to no propulsive application).

The propulsion system ideal velocity requirement was computed based on digital computer simulated trajectories for various initial thrust-to-weight values. The results are presented in Figures 73 to 78. Vehicle characteristics representative of a pump-fed Liquid oxygen/Hydrogen propulsion system were assumed, and thrust-dependent weight factors, K_E , ranging from 0.015 lb/lb thrust to 0.035 were selected, with 0.025 utilized as a typical nominal value.

Results of the thrust-to-weight optimization for the retro-propulsion phase are presented in Figure 79. The data were normalized in each instance to the gross weight-to-payload ratio obtained at F/W equal to 0.15, and the locus of optimum F/W values for K_E of 0.025 was superimposed on the data presented. It is evident from Figure 79 that as atmospheric entry velocity increases above 46,000 ft/sec, corresponding to propulsive ideal ΔV values below 16,000 ft/sec, the optimum F/W decreases due to the penalty that thrust-dependent weight imposes on propulsion system propellant fraction. However, the influence of F/W on gross weight becomes quite small. The decrease in optimum F/W as entry velocity decreases below 46,000 ft/sec reflects the lessening significance of gravity effects as the propulsive maneuver is initiated progressively further out in space. In Table 16, propulsion system data are summarized for vehicles (all initially at a hyperbolic excess velocity of 48,000 ft/sec) with entry velocities ranging from 38,000 ft/sec to 60,200 ft/sec. The results show that the ΔV -loss associated with the optimum F/W indicated is small. Thus, for most preliminary analyses, the difference between the arrival velocity and desired entry velocity can be used for propulsion studies. The payload for the propulsion phase is the entry vehicle weight. This payload, indicated as a fraction of the initial gross weight, is partly useful landed payload and partly heat shield for protection of the vehicle during the aerodynamic phase of the landing.

Those vehicles which employ large propulsion systems prior to atmospheric entry require small heat shields for the aerodynamic braking phase, and vice versa. The lightest overall vehicle is obtained by selecting an integrated landing system which optimally trades off propulsion system and heat shield weights. The analytical process involved is described below.

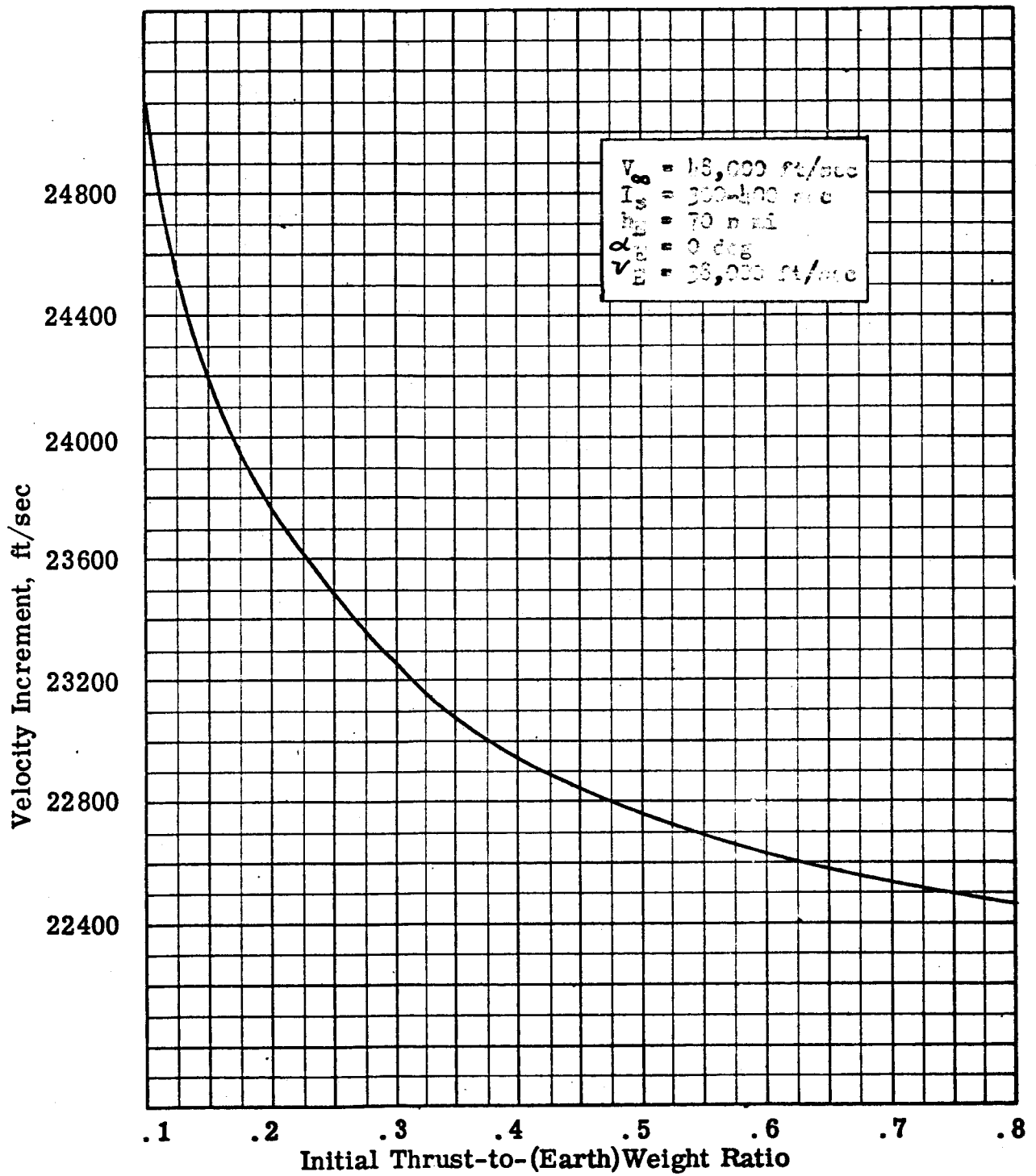


Fig.73 Earth Terminal Maneuver

ROCKETDYNE

A DIVISION OF NORTH AMERICAN AVIATION, INC.

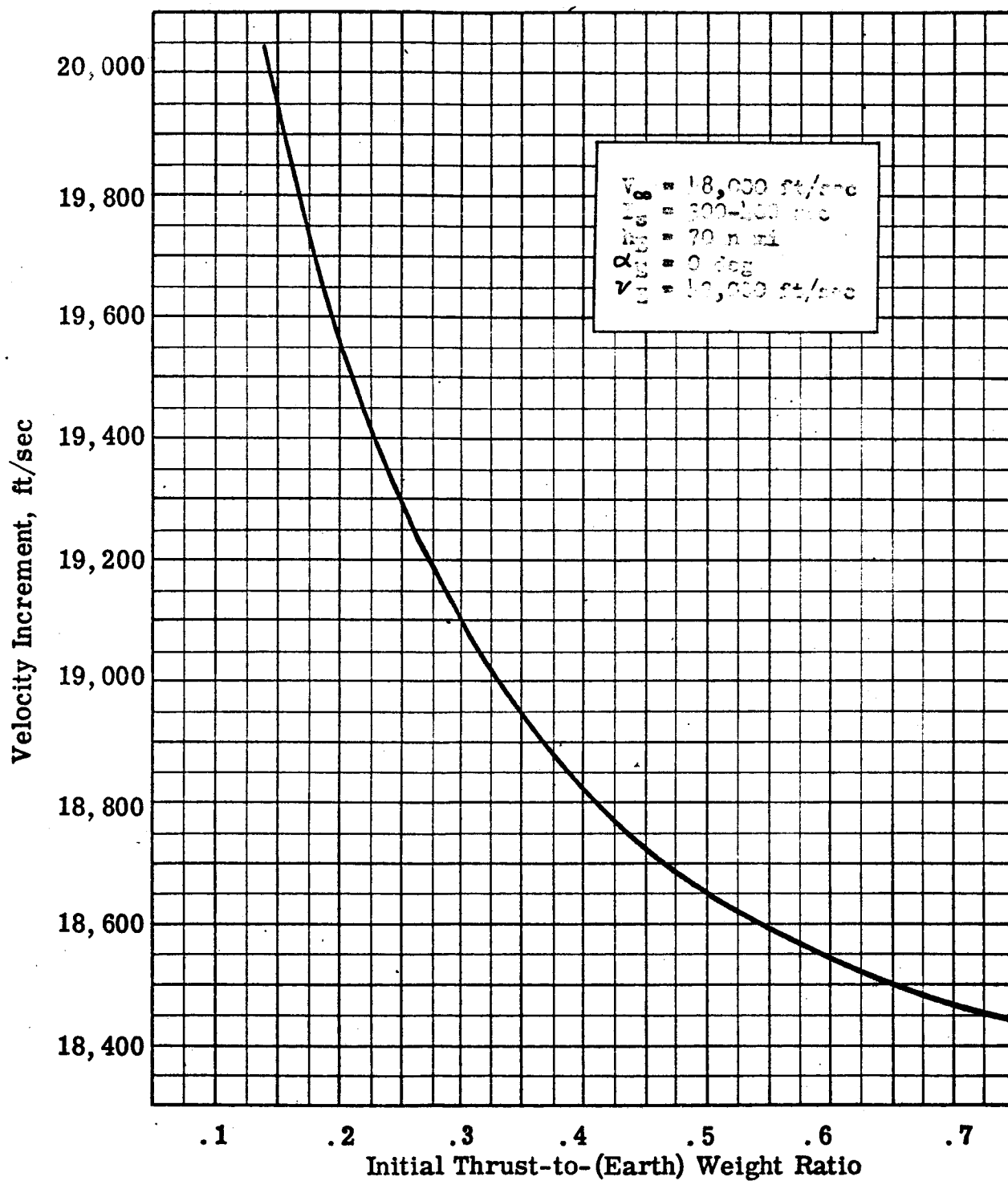


Fig.74 Earth Terminal Maneuver

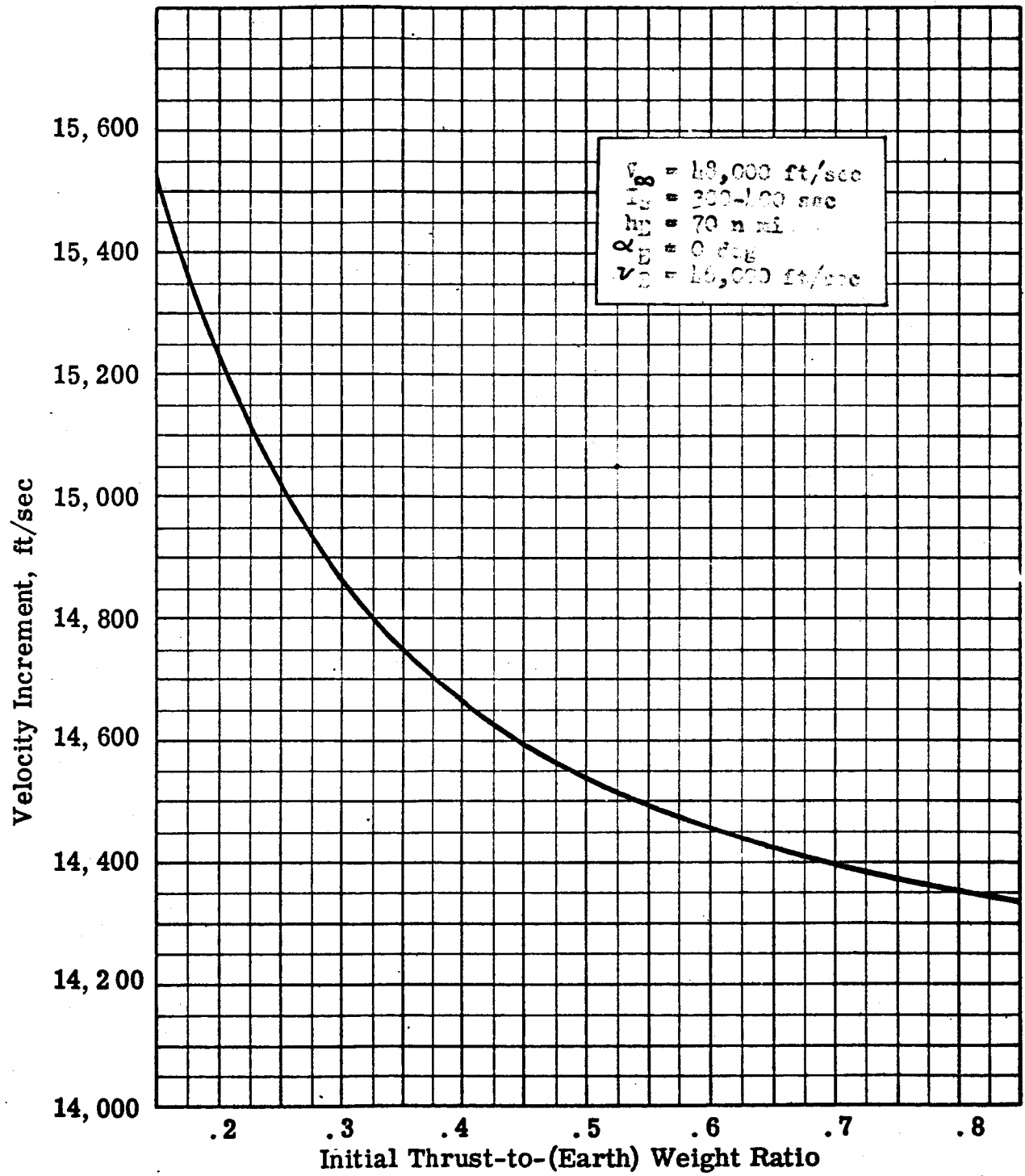


Fig. 75 Earth Terminal Maneuver

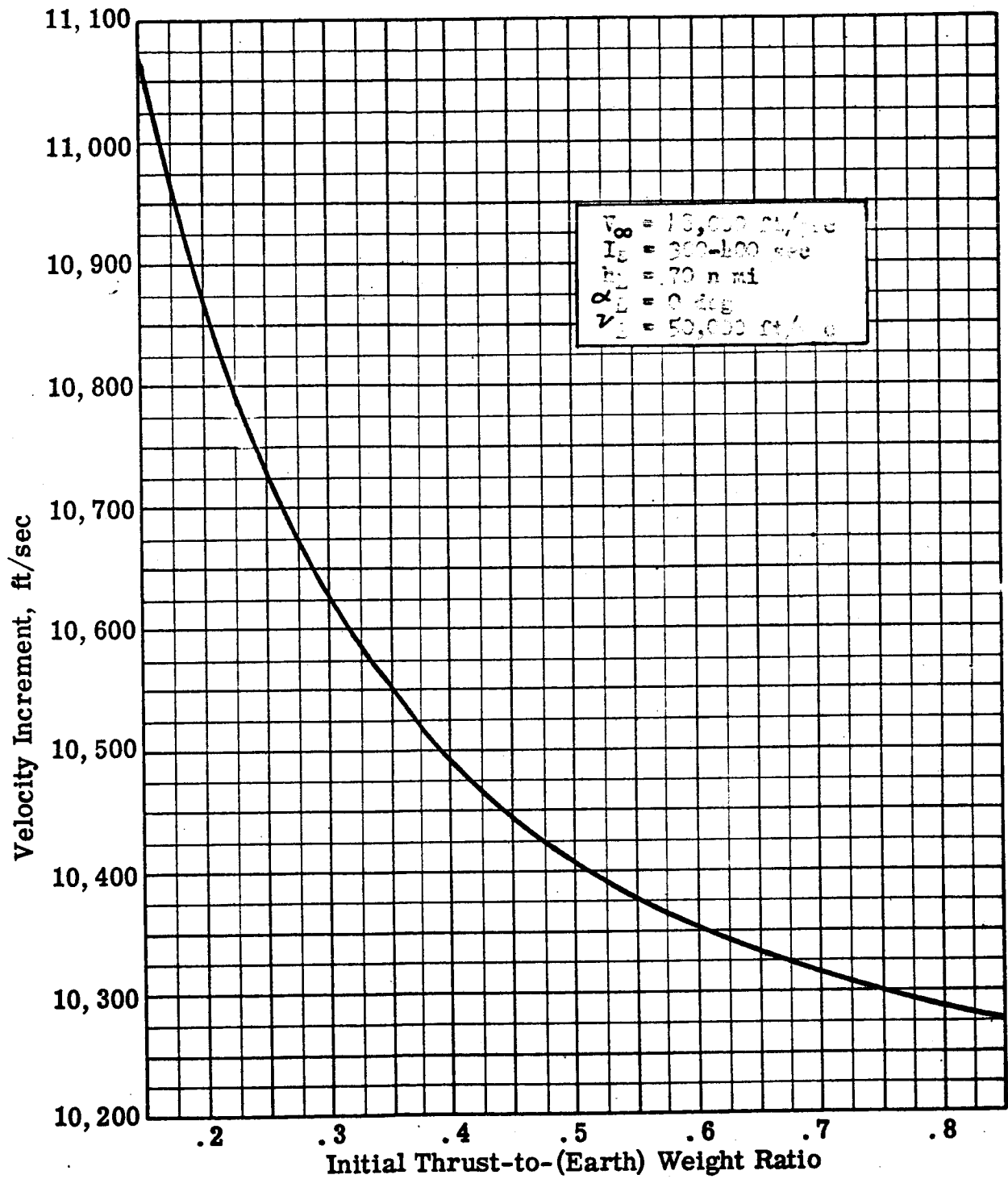


Fig.76 Earth Terminal Maneuver

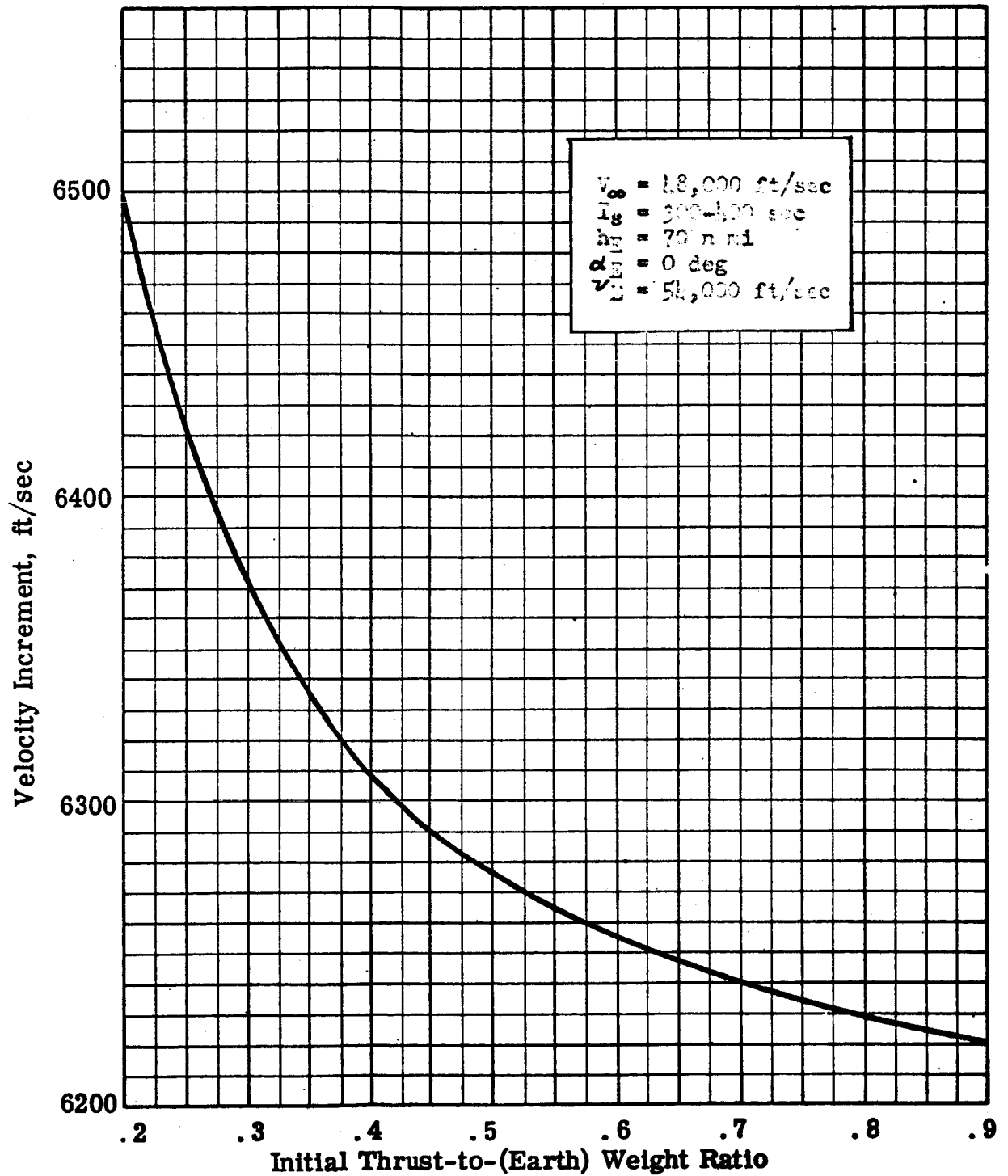


Fig. 77 Earth Terminal Maneuver

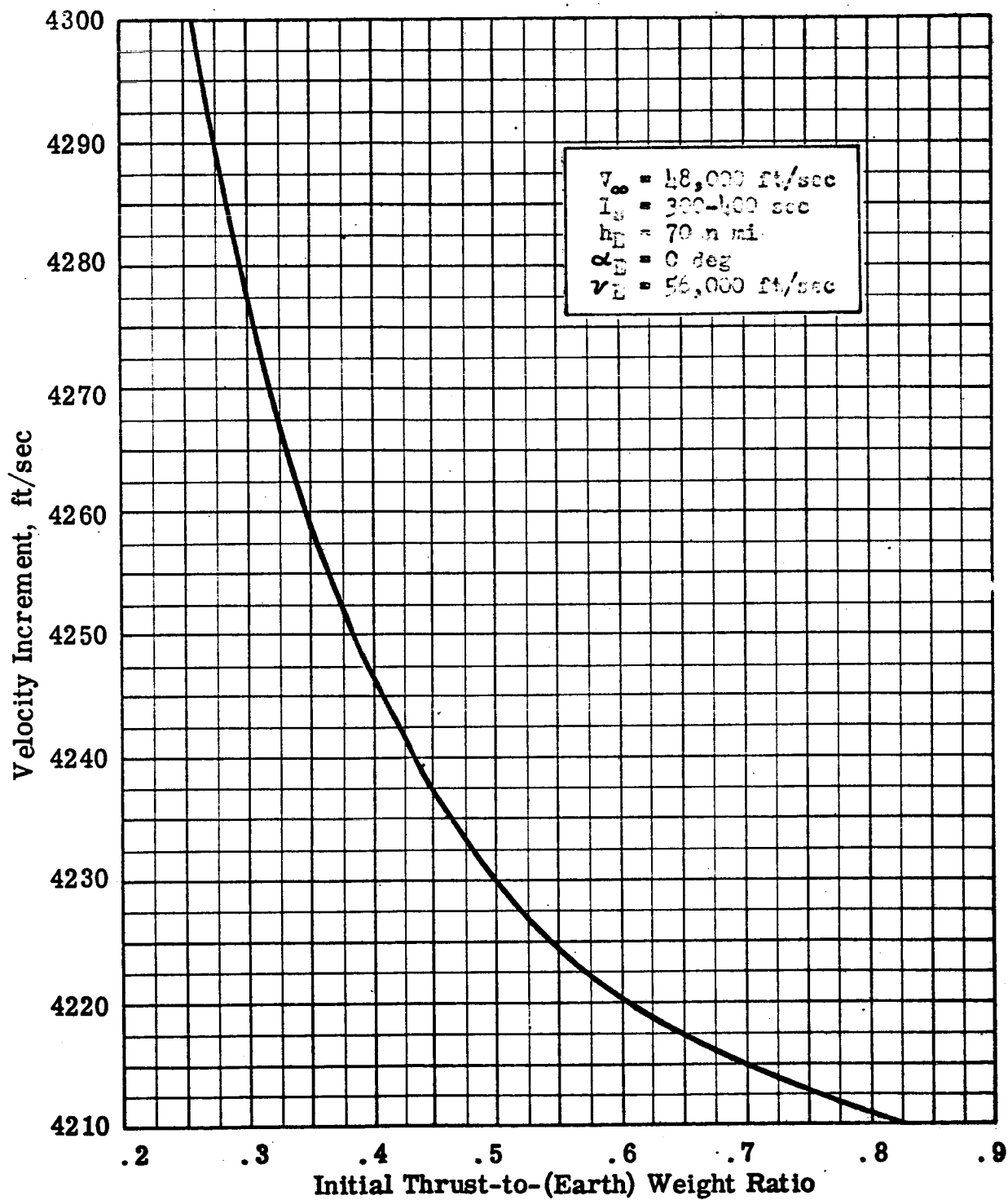


Fig. 78 Earth Terminal Maneuver

ROCKETDYNE
A DIVISION OF NORTH AMERICAN AVIATION, INC.

Hyperbolic Excess Velocity = 48,000 ft/sec

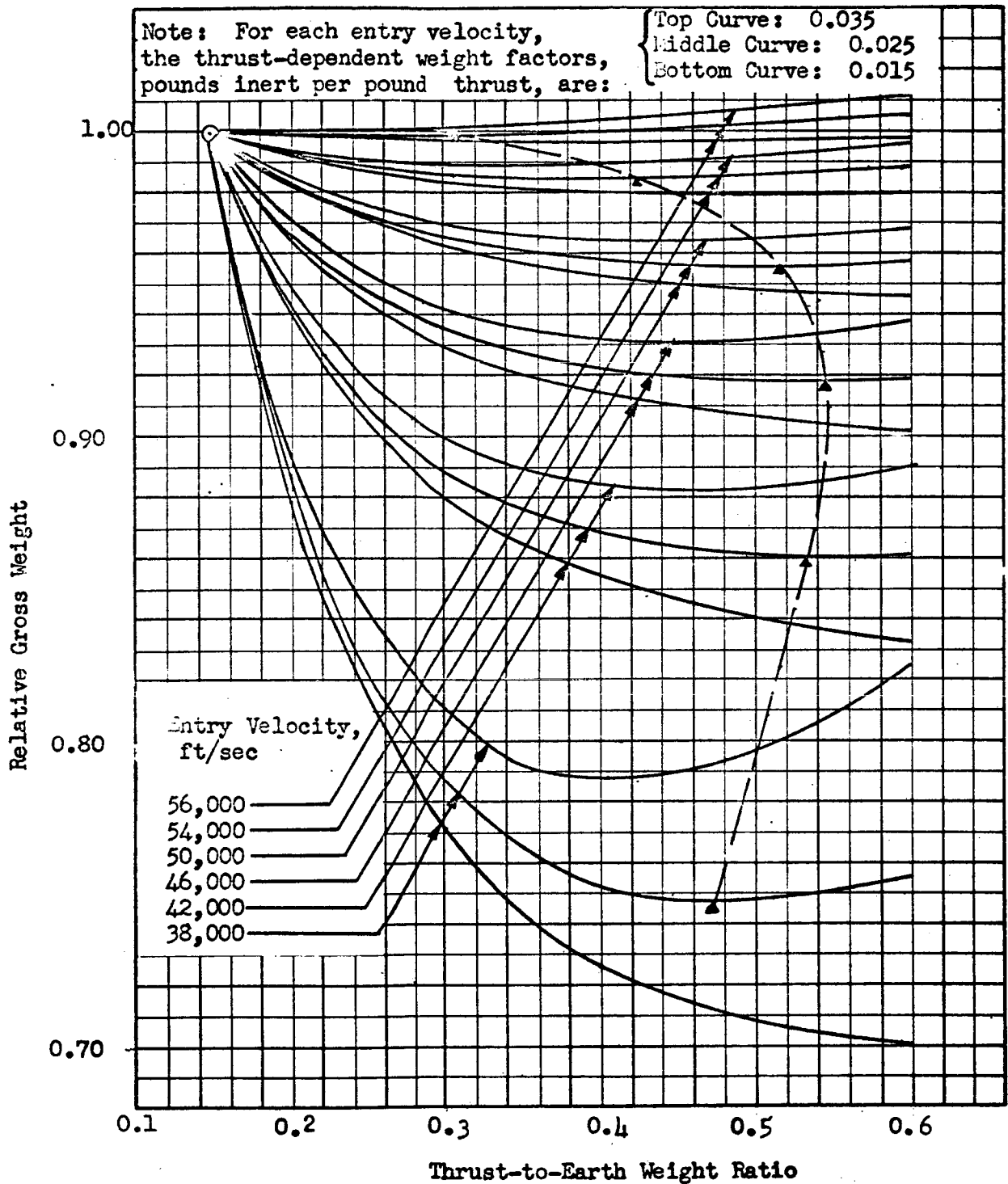


Figure 79 . Thrust-to-Weight Ratio Selection for Earth Reentry Vehicle

TABLE 16

EARTH ENTRY VEHICLE PROPULSION SYSTEM DATA

Arrival Velocity (V_A), ft/sec	Entry Velocity (V_E), ft/sec	$V_A - V_E$, ft/sec	Optimum Propulsion Thrust-to- Weight Ratio	Propulsion Ideal Velocity Increment, ft/sec	Propulsion Payload-to- Gross Weight Ratio
60,200	38,000	22,200	0.47	22,810	0.0509
	42,000	18,200	0.53	18,610	0.1267
	46,000	14,200	0.55	14,490	0.2298
	50,000	10,200	0.52	10,390	0.3694
	54,000	6,200	0.43	6,300	0.5610
	56,000	4,200	0.32	4,270	0.6805
60,200	60,200	0	0.00	0	1.0000

System Integration. An approximate expression relating heat shield fraction to atmosphere entry velocity was presented earlier. In Figure 80, three ablation characteristics are presented: (1) represents a highly conservative estimate, (2) is a current "best guess" gleaned from available data, (3) is an arbitrary characteristic deliberately chosen to indicate a borderline condition beyond which propulsive braking offers no weight advantage.

The entry vehicle weight shown in Table 16, multiplied by the factor, 1-L, yields the useful payload of the overall landing vehicle. The results of this operation are presented in Figure 81 for the Table 16 data used in conjunction with each of the heat shields represented in Figure 80. The use of heat shield curve (1) yielded an optimum entry velocity of 42,000 ft/sec, thus requiring a retropropulsive ΔV of 18,610 ft/sec. (This result is in close agreement with the results of the impulsive study and substantiates the validity of assuming impulsive velocity additions for vehicle optimization analyses.) From the nominal heat shield data, Curve (2) of Figure 81, it is indicated that the optimum configuration has 4270 ft/sec of propulsive braking capability and an entry velocity of 56,000 ft/sec. The payload, representing approximately 31 percent of the original space vehicle weight, includes all weight that survives atmospheric entry. Further distinction between structure and purely useful payload (men, scientific equipment) is beyond the scope of the present analysis.

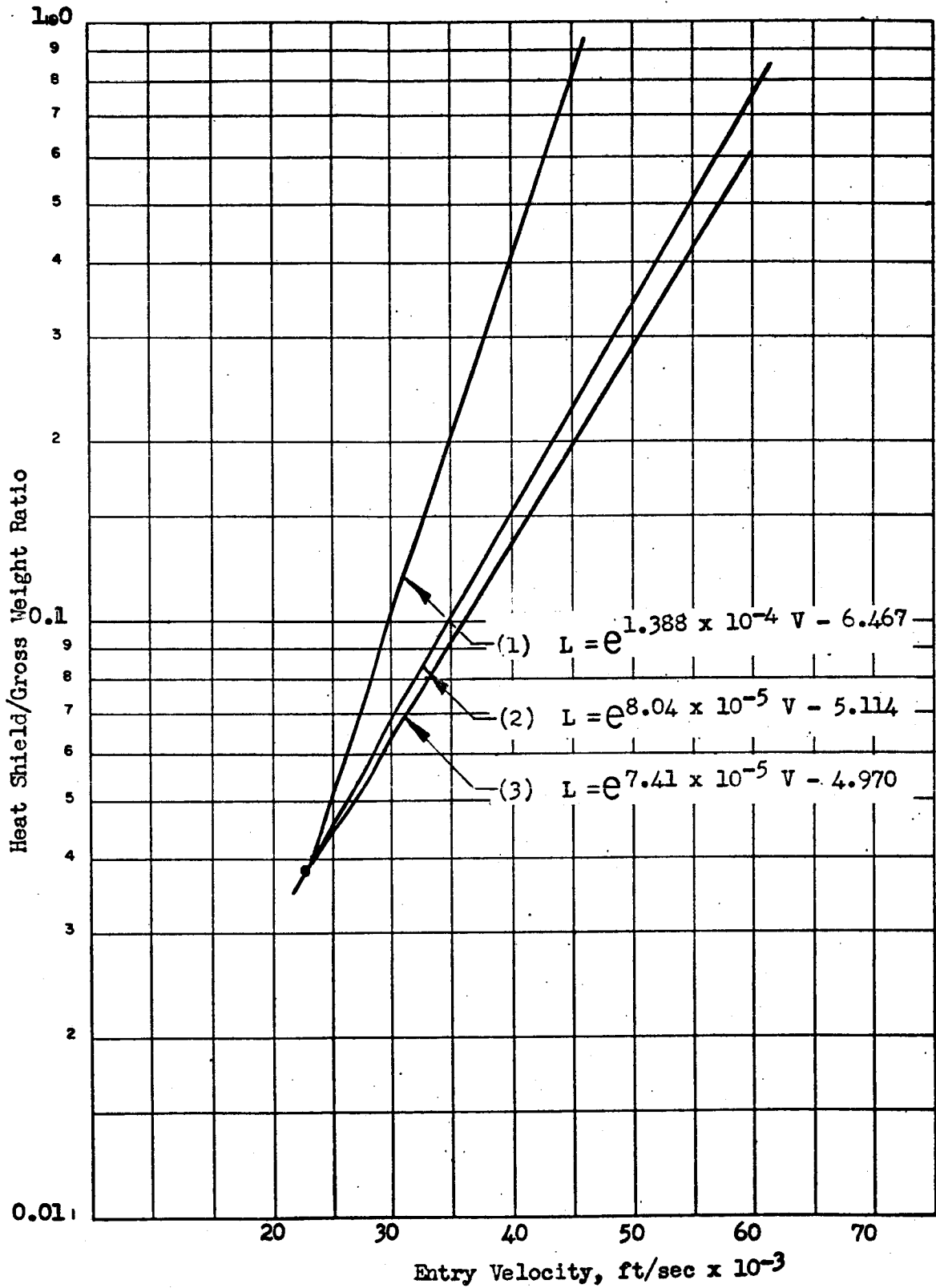


Figure 80 . Heat Shield Characteristics for Earth Entry Vehicles.

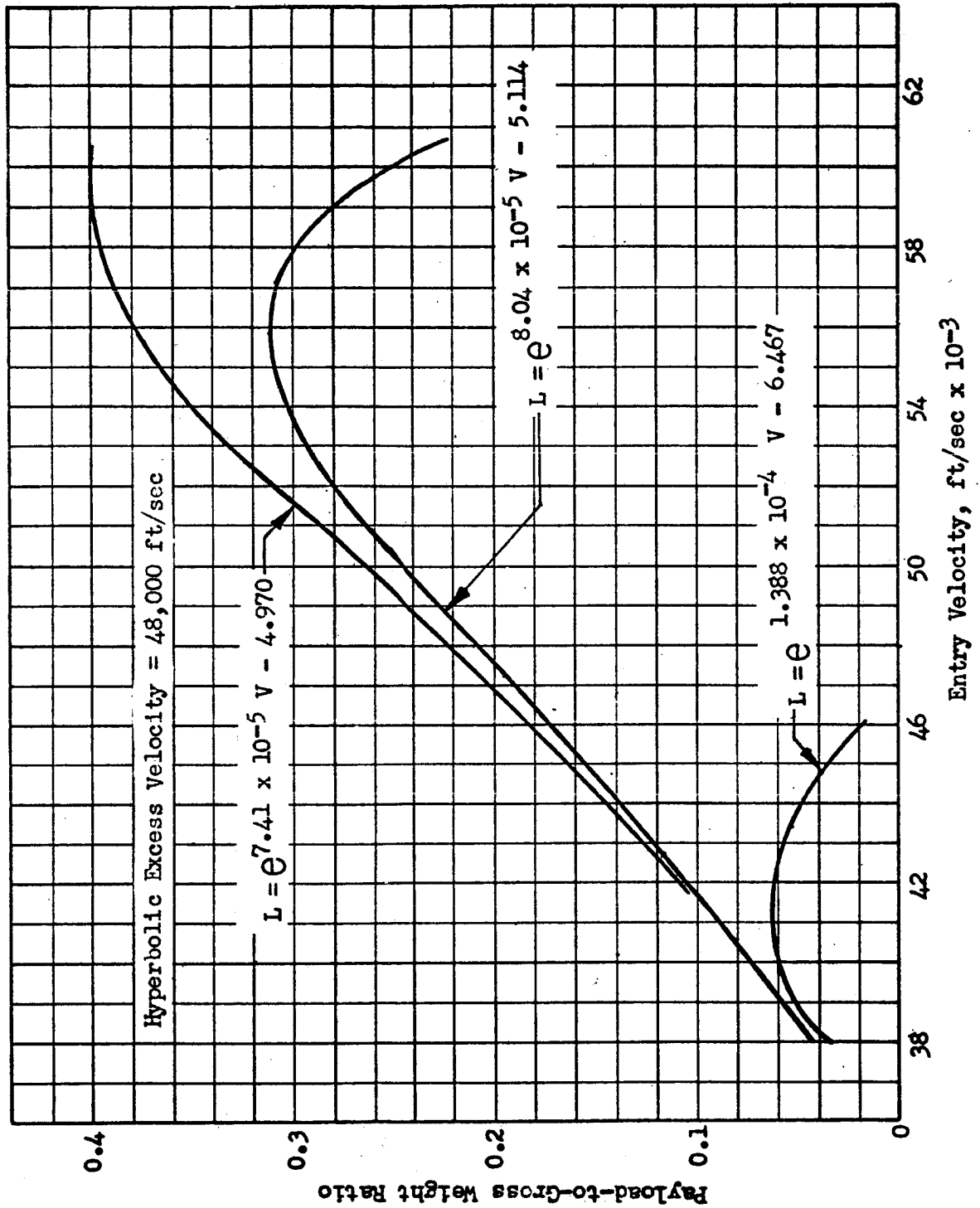


Figure 81 • Propulsion/Ablation Systems for Earth Reentry

Curve (3) results in a limiting condition; the optimum propulsive velocity increment is zero. For lower shield weights, the propulsion requirement obviously continues to be zero.

For the mission conditions and ablation characteristics used in this analysis, a propulsion system, albeit a relatively small one, was desirable. The mission conditions used are probably more severe than are actually likely to be encountered at either terminus of any presently envisioned interplanetary mission. Practical missions, at least in the next decade, are unlikely to be so ambitious as to attempt a 100-day Mars return; trip times closer to 200 days are more feasible. From a performance standpoint, propulsive braking is not required for the direct landing trajectory considered for nominal heat shield weights and hyperbolic excess velocities less than 42,000 ft/sec; propulsive braking, as a means of reducing overall vehicle weight, therefore does not appear necessary.

Parametric Ablation Shield Analysis

Six ablation characteristics, shown in Figure 82, were selected to cover the broad range of available heat shield weight data. The ablation weight curves are shown radiating from the point, a 3-percent heat shield weight at 20,000 ft/sec entry velocity. Because convective heat transfer is the dominant mode at this low velocity, the analytical difficulties of radiative heat transfer, and the related wide diversity of predicted ablation shield weight, are not manifested; there is, as a result, relatively good agreement among available data sources on the selected common point.

Further experimental and design data on heating conditions, and optimum ablation shield configurations, are required to verify a particular ablation characteristic. Thus, a parametric approach was employed in this analysis.

Techniques described previously were employed to determine optimum retropropulsive velocity additions for the selected ablation characteristics and planetary entry conditions. Impulsive velocity increments were utilized, and a nominal propulsion system with a specific impulse of 420 seconds and a propellant fraction of 0.85 was assumed.

Results of the analysis are presented in Figures 83 to 88, each figure corresponding to one of the selected ablation characteristics. Note that a particular arrival velocity implies different hyperbolic excess velocities at Earth, Mars and Venus. Values of hyperbolic excess velocity are stated along with each arrival velocity to relate the data presented to specific interplanetary trips.

Curve (3) results in a limiting condition; the optimum propulsive velocity increment is zero. For lower shield weights, the propulsion requirement obviously continues to be zero.

For the mission conditions and ablation characteristics used in this analysis, a propulsion system, albeit a relatively small one, was desirable. The mission conditions used are probably more severe than are actually likely to be encountered at either terminus of any presently envisioned interplanetary mission. Practical missions, at least in the next decade, are unlikely to be so ambitious as to attempt a 100-day Mars return; trip times closer to 200 days are more feasible. From a performance standpoint, propulsive braking is not required for the direct landing trajectory considered for nominal heat shield weights and hyperbolic excess velocities less than 42,000 ft/sec; propulsive braking, as a means of reducing overall vehicle weight, therefore does not appear necessary.

Parametric Ablation Shield Analysis

Six ablation characteristics, shown in Figure 82, were selected to cover the broad range of available heat shield weight data. The ablation weight curves are shown radiating from the point, a 3-percent heat shield weight at 20,000 ft/sec entry velocity. Because convective heat transfer is the dominant mode at this low velocity, the analytical difficulties of radiative heat transfer, and the related wide diversity of predicted ablation shield weight, are not manifested; there is, as a result, relatively good agreement among available data sources on the selected common point.

Further experimental and design data on heating conditions, and optimum ablation shield configurations, are required to verify a particular ablation characteristic. Thus, a parametric approach was employed in this analysis.

Techniques described previously were employed to determine optimum retropropulsive velocity additions for the selected ablation characteristics and planetary entry conditions. Impulsive velocity increments were utilized, and a nominal propulsion system with a specific impulse of 420 seconds and a propellant fraction of 0.85 was assumed.

Results of the analysis are presented in Figures 83 to 88, each figure corresponding to one of the selected ablation characteristics. Note that a particular arrival velocity implies different hyperbolic excess velocities at Earth, Mars and Venus. Values of hyperbolic excess velocity are stated along with each arrival velocity to relate the data presented to specific interplanetary trips.

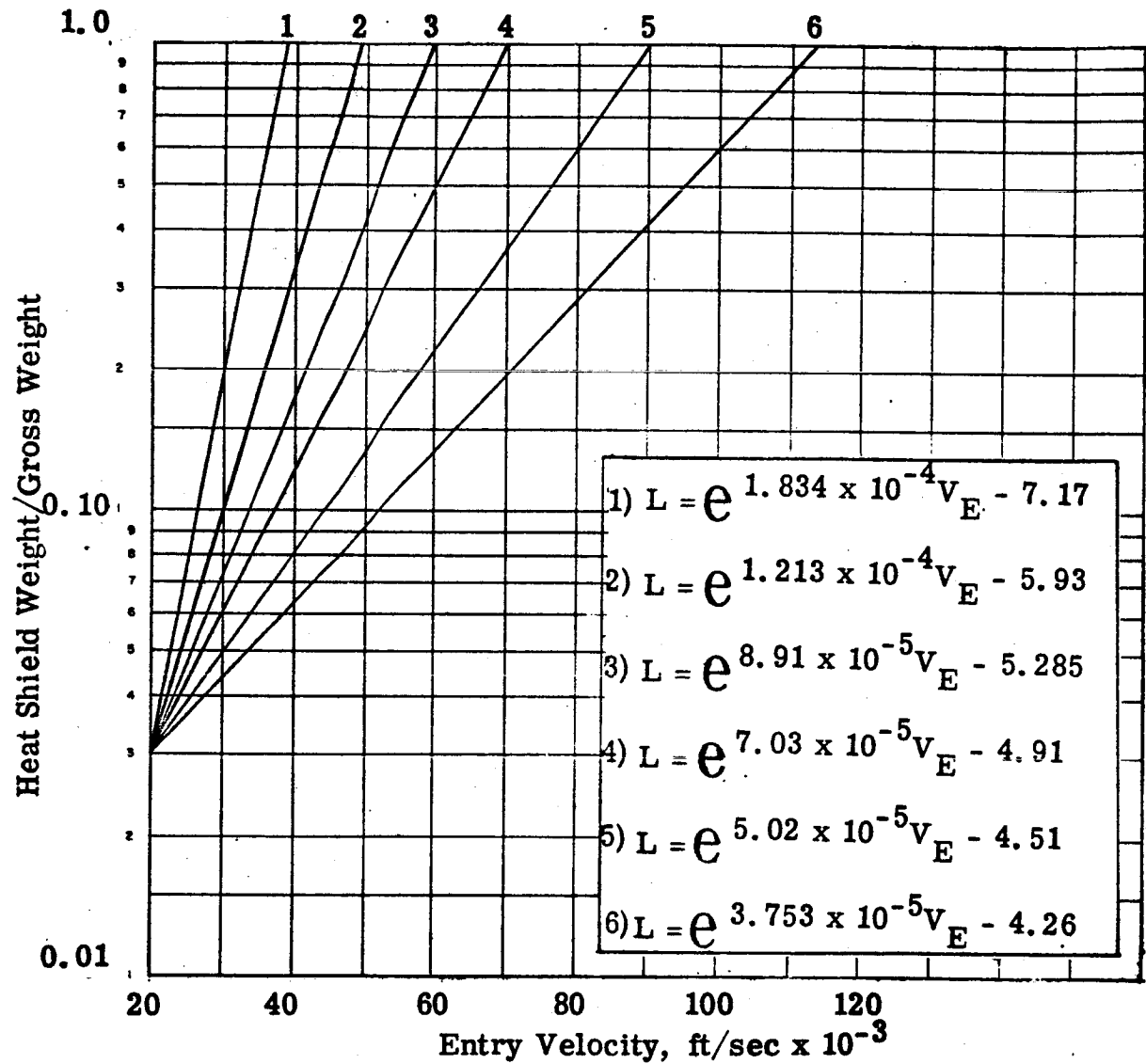


**Fig. 82 Selected Ablation Characteristics for Propulsive/
Aerodynamic Landing System Analysis**

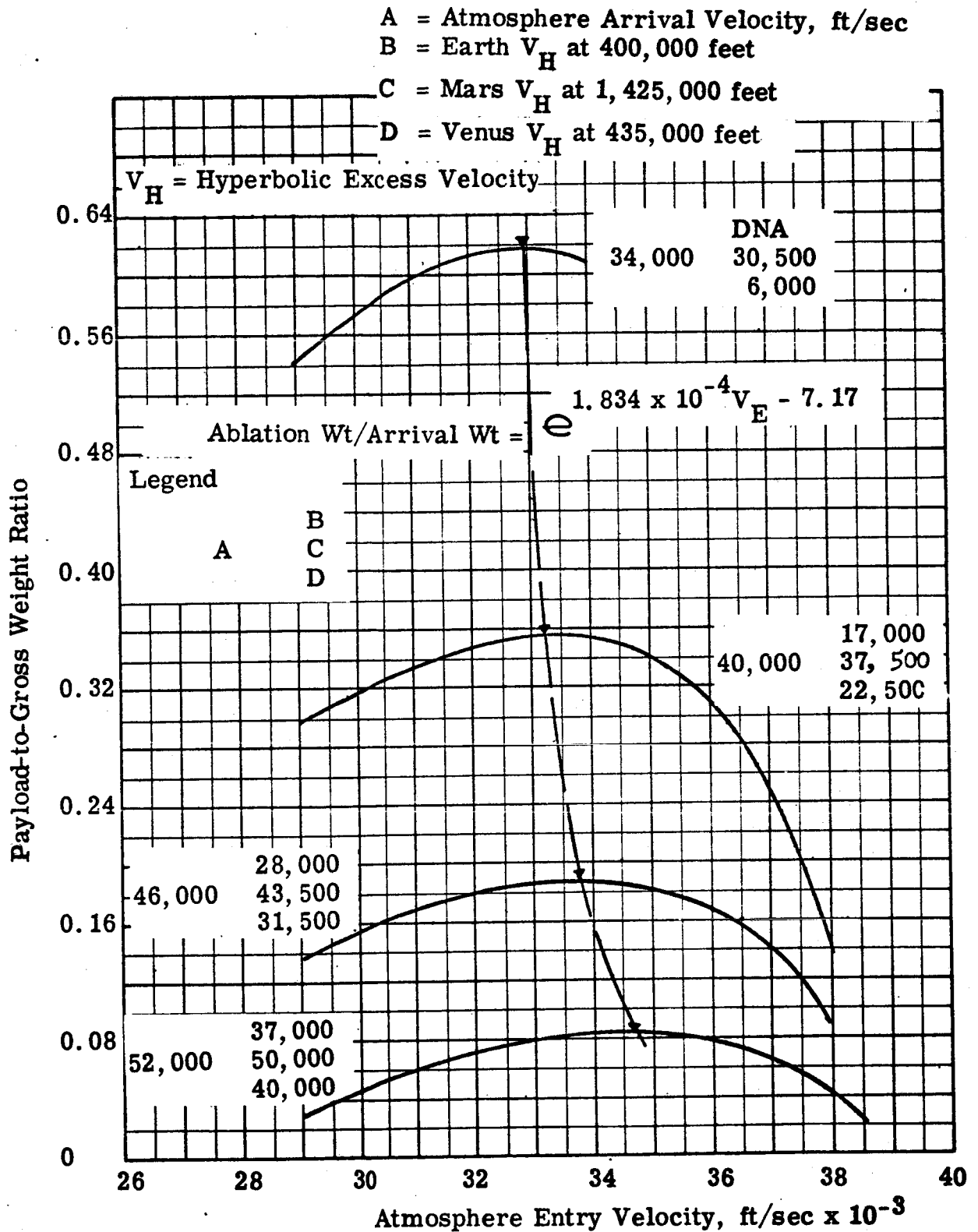


Figure 83 . Optimization of Atmospheric Entry Velocity for Propulsive/Aerodynamic Systems

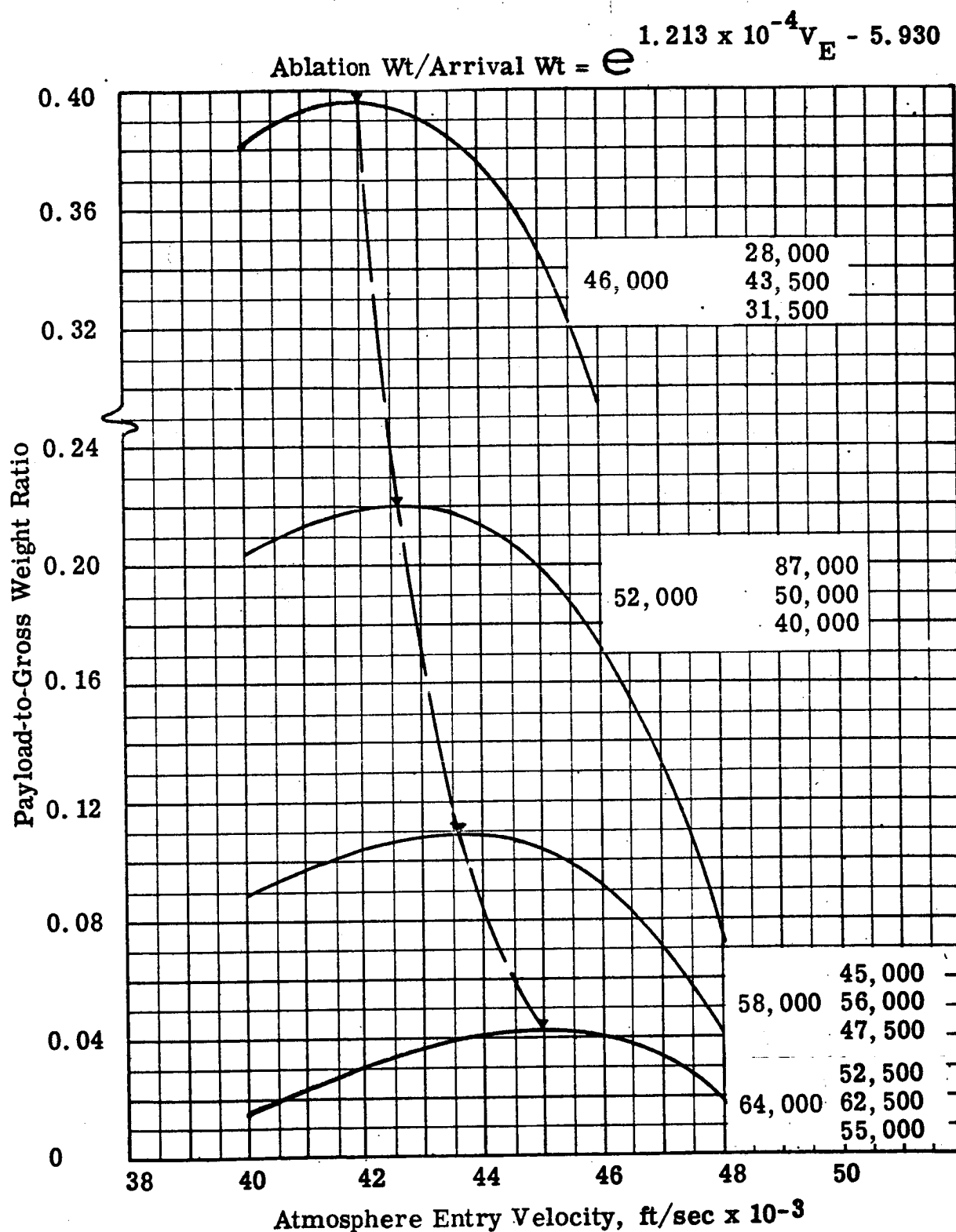


Figure 84. Optimization of Atmospheric Entry Velocity for Propulsive/Aerodynamic Systems

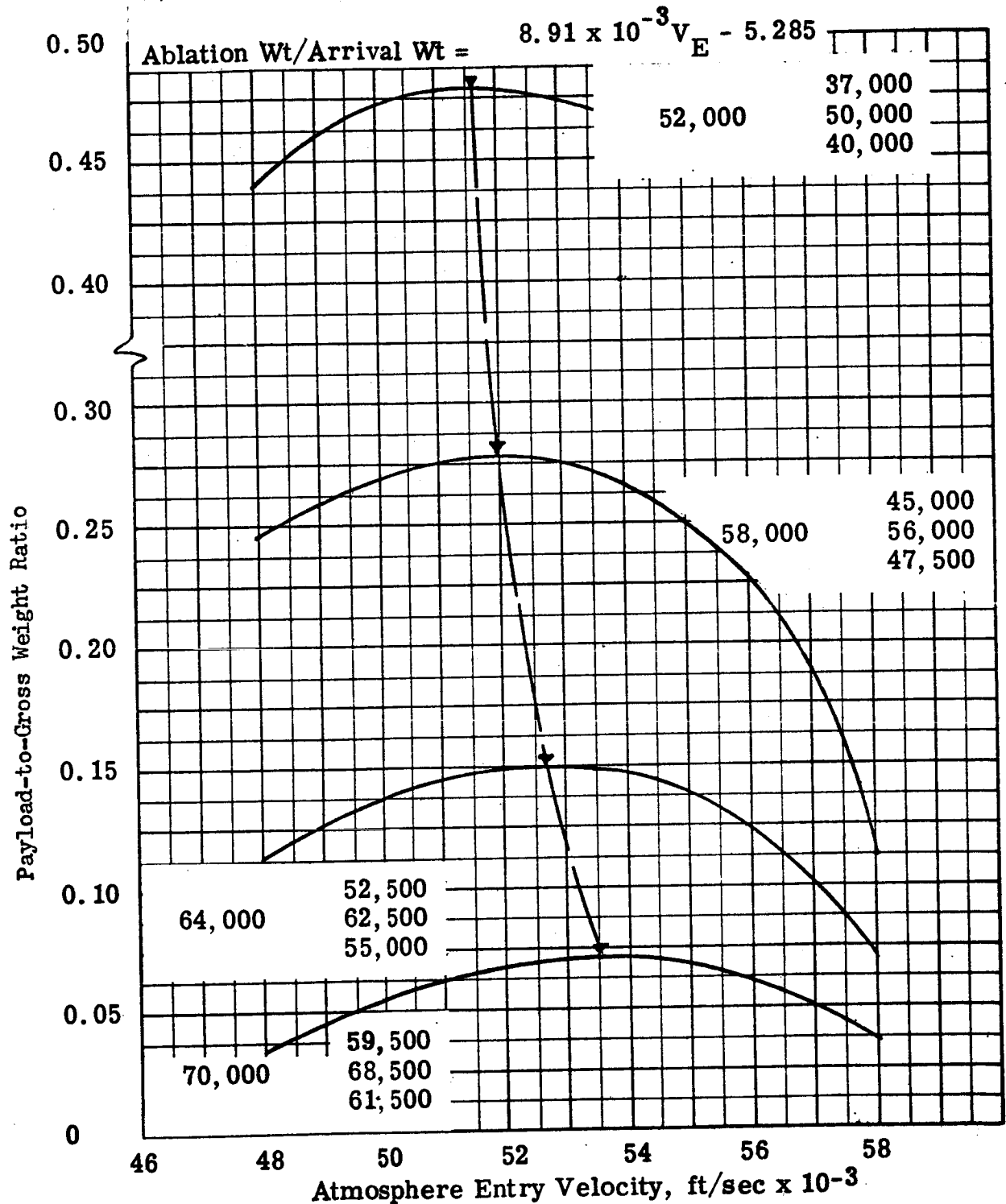


Figure 85. Optimization of Atmospheric Entry Velocity for Propulsive/Aerodynamic Systems

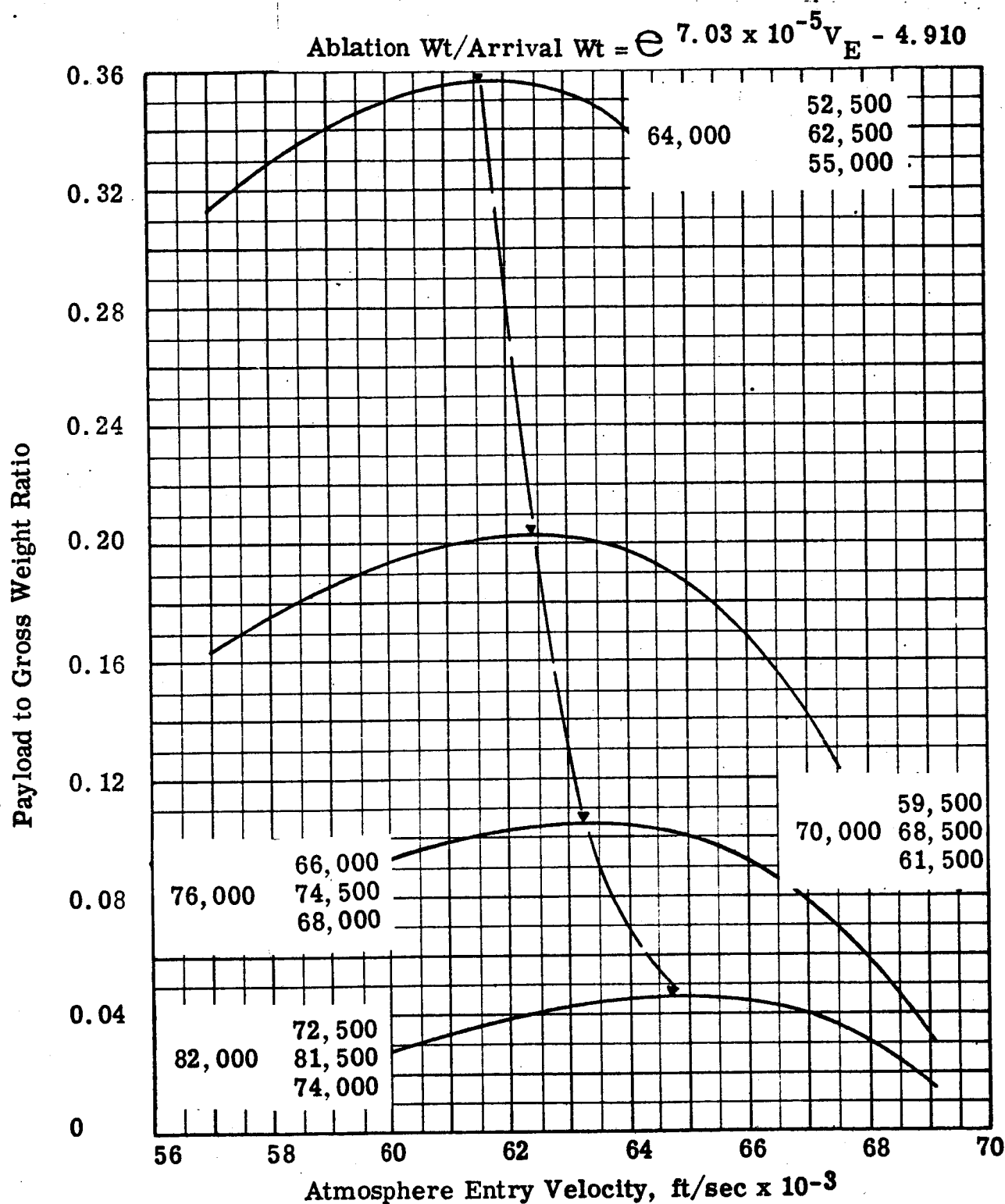


Figure 86 . Optimization of Atmospheric Entry Velocity for Propulsive/Aerodynamic Systems

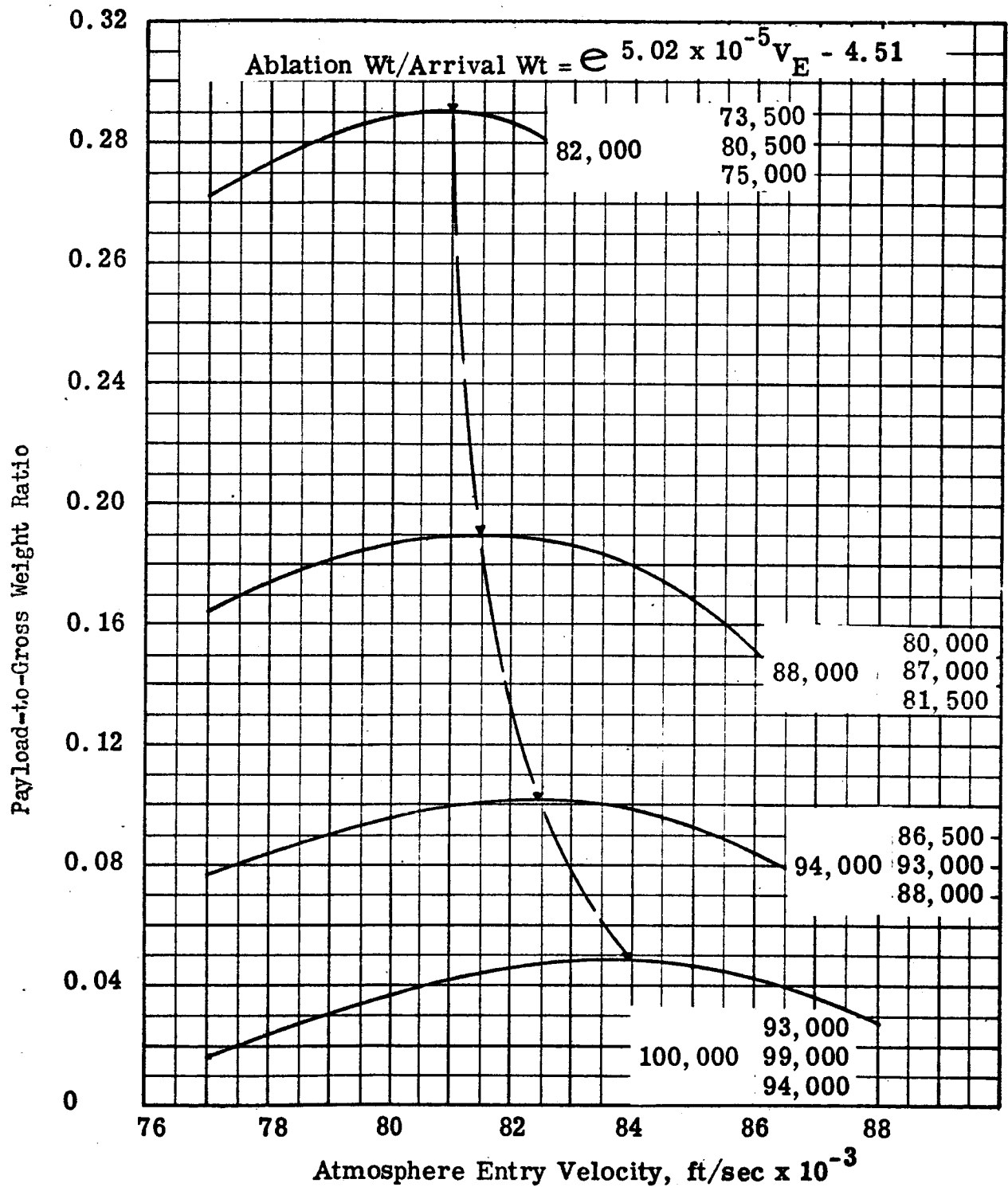


Figure 87. Optimization of Atmosphere Entry Velocity for Propulsive/Aerodynamic Systems

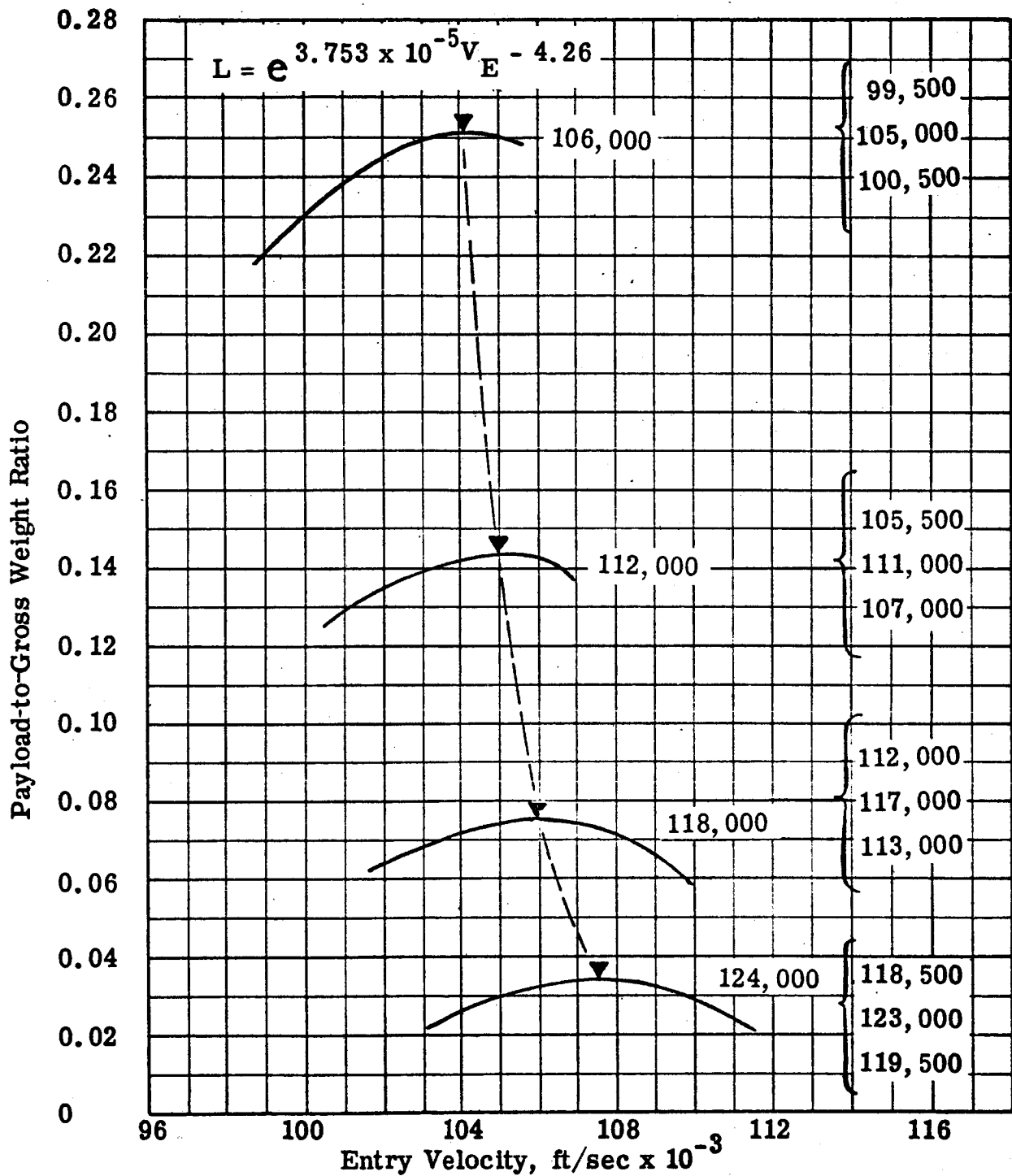


Fig. 88 Optimization of Atmospheric Entry Velocity for Propulsive/Aerodynamic Systems

The importance of knowing the ablation characteristic is clearly illustrated by the fact that for a minimum weight system, a conservative ablation weight estimate, Curve (1) of Figure 82, dictates the use of a retrorocket for arrivals above 33,000 ft/sec, while an optimistic estimate, Curve (6) of Figure 82, yields the result that no propulsion system is needed for arrivals below 104,000 ft/sec.

The payload expression derived earlier, which combined the separate effects of the propulsion system, the ablative heat shield and the terminal deceleration device, was differentiated with respect to the propulsive velocity change, ΔV , to obtain the expression

$$\frac{\partial (PL/WG)}{\partial \Delta V} = I_s g_0 \left[\lambda_p - 1 + e^{-\Delta V/I_s g_0} \right] \left[\gamma e^{\gamma(V_A - \Delta V)} + \beta \right] + e^{-\Delta V/I_s g_0} \left[e^{\gamma(V_A - \Delta V)} + \beta - 1 \right]$$

This was set equal to zero, and optimum ΔV was then computed directly as a function of arrival velocity.

The results are shown in Figure 89 for Earth landings. For a given mission hyperbolic excess velocity, the optimum ΔV is the vertical distance between the arrival velocity curve and the optimum entry velocity curve corresponding to the appropriate ablation characteristic. Thus for any ablation characteristic, the desirability of using a propulsion system, and the corresponding optimum ΔV , can be determined. The resultant payload can be determined from Figure 83 to 88, or by the use of the payload-to-gross weight ratio equation presented previously.

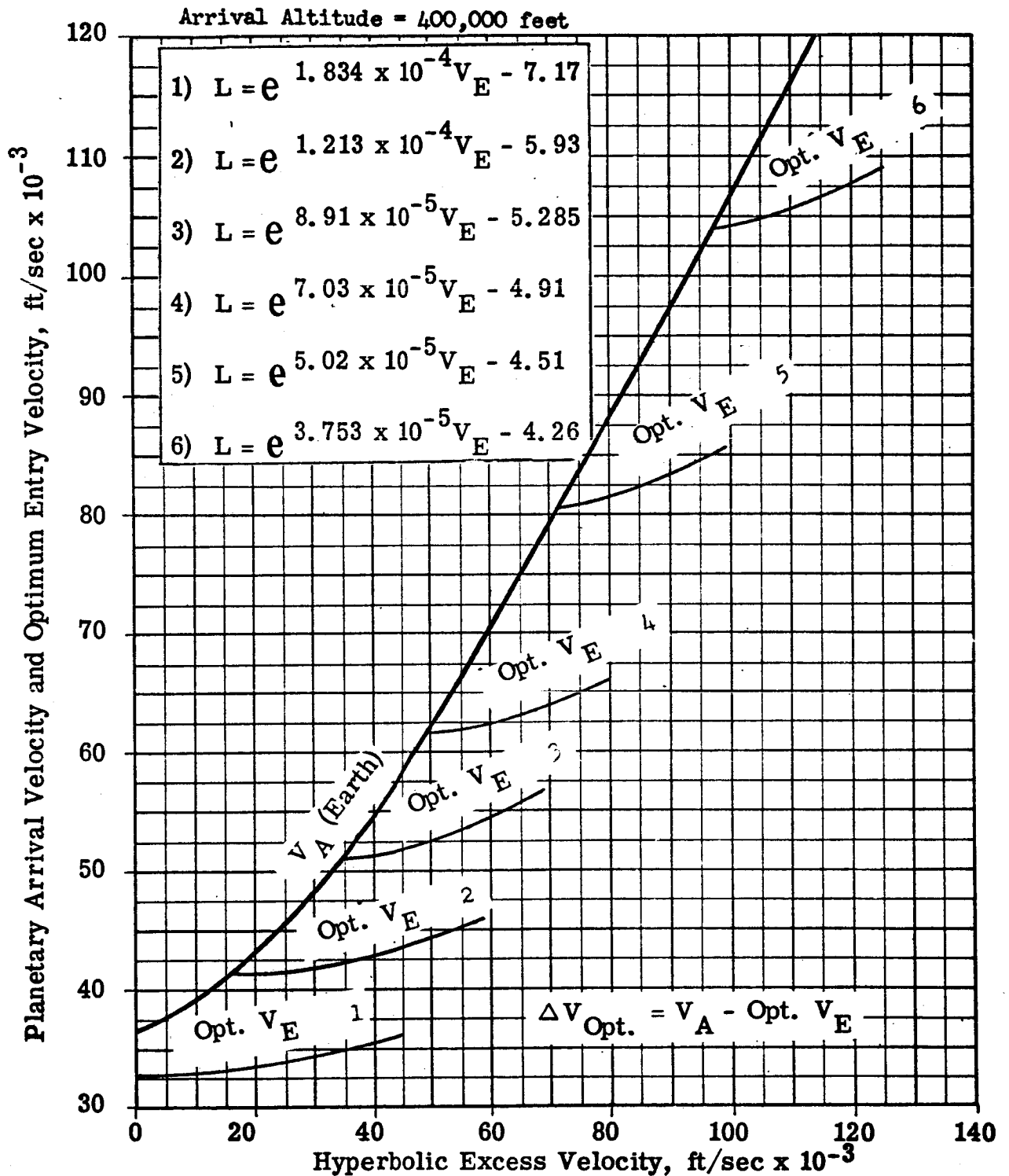


Fig.89 Optimum Propulsive ΔV (Impulsive) for Earth Re-Entry of Propulsive/Aerodynamic Systems.

EARTH TERMINAL DECELERATION PHASE SYSTEMS

The inability of a parachute to decelerate a mass efficiently to very low velocity and the independence of a rocket device from any such constraint on operating regime suggests that a combined system for final deceleration of a landing vehicle might be more efficient than either device employed singly for the same task. An investigation was therefore conducted to evaluate parachute/rocket systems for the terminal-descent phase of Earth landings.

The parachute is first deployed to slow the vehicle to parachute terminal velocity, V_T . The vehicle then continues to descend at terminal velocity to an altitude determined by the thrust-to-weight ratio (F/W) of the rocket. (The higher the F/W , the lower the ignition altitude.) The rocket then slows the vehicle to impact velocity (V_F).

A complete terminal descent system includes not only a parachute and retrorocket, but an impact absorption device as well. For the initial analysis, impact velocity, and therefore impact-absorber weight, was fixed at one of two discrete values (10 and 25 ft/sec). As a result, the weight of the impact device was constant and did not affect the optimization of the parachute/retrorocket combination. Subsequently, the variation of impact absorber weight with impact velocity was considered, and optimization of parachute/rocket/impact device systems was performed. It should be noted that inclusion of impact velocity as a permissible variable implies that no restrictions are imposed by touchdown stability considerations. From a practical standpoint, it is unlikely that design impact velocity for a landing vehicle will exceed 25 ft/sec; however, if lateral velocity at impact can be closely controlled and reliable operation of long-stroke impact absorption devices can be assured, there need be no limit on impact velocity.

Pararocket System

Parachute System. The forces acting on the vehicle during a parachute descent are the vehicle local weight (W_L) and the parachute drag force which is dependent on the descent velocity (V). At equilibrium conditions $V = V_T$ (parachute terminal velocity), and the drag force is equal to the local weight of the vehicle.

$$W_L = \frac{1}{2} \rho_p C_D \left(\frac{\pi D^2}{4} \right) V_T^2$$

D = Vehicle diameter

ρ_p = Atmospheric density near surface of planet

C_D = Parachute drag coefficient

The vehicle local weight may be written in terms of vehicle Earth weight, W_E

$$W_L = W_E \frac{g_p}{g_e}$$

where g_p/g_e is the ratio of planetary gravity to Earth gravity.

The parachute weight may be considered directly proportional to its cross sectional area. (Reference). Therefore, by applying some proportionality constant (γ), the parachute weight (W_p) is:

$$W_p = \gamma \left(\frac{\pi D^2}{4} \right)$$

Dividing W_p by W_L and reducing constant values into one constant K (assuming C_D a constant)

$$\frac{W_p}{W_E} = \frac{g_p}{g_e} \frac{K}{\rho_p V_T^2}$$

Based on representative data provided by the Ames Research Laboratory for an Earth landing parachute system,

$$\frac{W_p}{W_E} = 42.7/V_T^2$$

Therefore,

$$\frac{K}{\rho} = 42.7, \text{ since } g_p/g_e = 1 \text{ for Earth.}$$

The resulting equation for parachute system weight for extra-terrestrial landing is:

$$\frac{W_p}{W_E} = \frac{g_p}{g_e} \frac{\text{Earth}}{p} \left(\frac{42.7}{V_T^2} \right)$$

Retrorocket System. A rocket engine having a specific impulse of 240 seconds was used. The propulsion system weight, including propellants used was:

$$W_R/W_G = (F/W) (0.0097 + 0.00457 t_b)$$

where t_b is the burning time.

The expression for t_b was derived on the basis of constant F/W during burning (there is actually about a 3-percent variation if constant thrust is employed) with drag assistance provided by the parachute during rocket operation.

The forces acting on the vehicle during rocket operation are thrust (F) weight (W) (both assumed constant) and parachute drag which is equal to $k V^2$. The proportionality constant may be evaluated at equilibrium conditions of parachute-only operation where $V = V_T$ and the drag force is equal to the weight of the vehicle; i.e.,

$$k = W/V_T^2$$

The equation of motion for combined rocket and parachute retardation is, therefore,

$$\frac{dV}{dt} = \frac{\sum F}{M} = \frac{F + (W/V_T^2) V^2 - W}{W/g} = g \left[(F/W - 1) + V^2/V_T^2 \right]$$

Separating variables and integrating:

$$\frac{1}{g} \int_{V_T}^{V_F} \frac{dV}{(F/W-1) + V^2/V_T^2} = \int_0^{t_b} dt$$

$$\text{which yields } t_b = \frac{1}{g} \left[\frac{V_T}{\sqrt{F/W-1}} \arctan \left(\frac{V}{V_T \sqrt{F/W-1}} \right) \right]_{V_T}^{V_F}$$

Expanding and letting $(F/W - 1)^{-1/2} = c$

$$t_b = \frac{c V_T}{g} \left[\arctan (c V_F/V_T) - \arctan c \right]$$

Systems Analysis. Initially, an impact velocity (V_F) of 10 ft/sec was assumed and values of V_T and F/W were varied to obtain the minimum pararocket system weight (W_{system}) - to - gross vehicle weight (W_G) ratio.

$$\frac{W_{\text{system}}}{W_G} = \frac{W_{\text{rocket}}}{W_G} + \frac{W_{\text{parachute}}}{W_G}$$

The optimization was repeated using 50 percent greater parachute weights with nominal rocket weights, and again using 50 percent rocket weights with nominal parachute weights.

As a parachute terminal velocity is increased at constant rocket F/W and vehicle-impact velocity, a greater part of the velocity must be cancelled by the rocket. Thus, the rocket weight increases and the parachute weight decreases as shown in Figure 90. Equal terminal and impact velocities imply that the parachute performs the entire retro task and the rocket weight is zero. The parachute weight curve of Figure 90 may also be used to show the weight of a parachute-only system for an Earth landing, with impact velocities corresponding to the indicated parachute terminal velocities.

Total system weights versus F/W for a range of parachute terminal velocities, V_T , and an impact velocity, V_I , of 10 ft/sec are presented in Figure 91. In Figure 91 it is indicated that for a 10 ft/sec impact velocity, the optimum system employs the parachute to slow the vehicle to between 60 and 80 ft/sec, and then applies rocket thrust at an F/W of approximately 1.6 to supply an ideal ΔV of approximately 65 to 85 ft/sec. The system weight is approximately 4 percent of the vehicle weight.

The effect of increasing the parachute weight and the rocket system weight by 50 percent is shown in Figure 92 and 93. The system optimizes at a terminal velocity close to 80 fps if the parachute weight constant is increased by 50 percent. The slight increase in system weight as compared to the nominal case reflects the fact that the parachute accounts for only a small part of the system weight. For a 50-percent larger rocket weight factor, the optimum parachute terminal velocity is 80 ft/sec, the optimum F/W is approximately 1.5 and the system weighs approximately 5.3 percent of the vehicle gross weight.

Reducing the design impact velocity, V_I , does not significantly change the F/W optimization as indicated in Figure 94. Increasing the design value to 25 ft/sec, however, results in a reduction of optimum F/W to 1.15. A complete F/W and V_T optimization was made for a V_I of 25 ft/sec and is presented in Figure 95.

In Figure 96, the optimum total system weights are shown as a function of parachute terminal velocity. The optimum F/W values versus parachute terminal velocities are presented in Figure 97. If the parachute weight constant is increased by 50 percent, the optimum F/W for a particular parachute terminal velocity does not change;

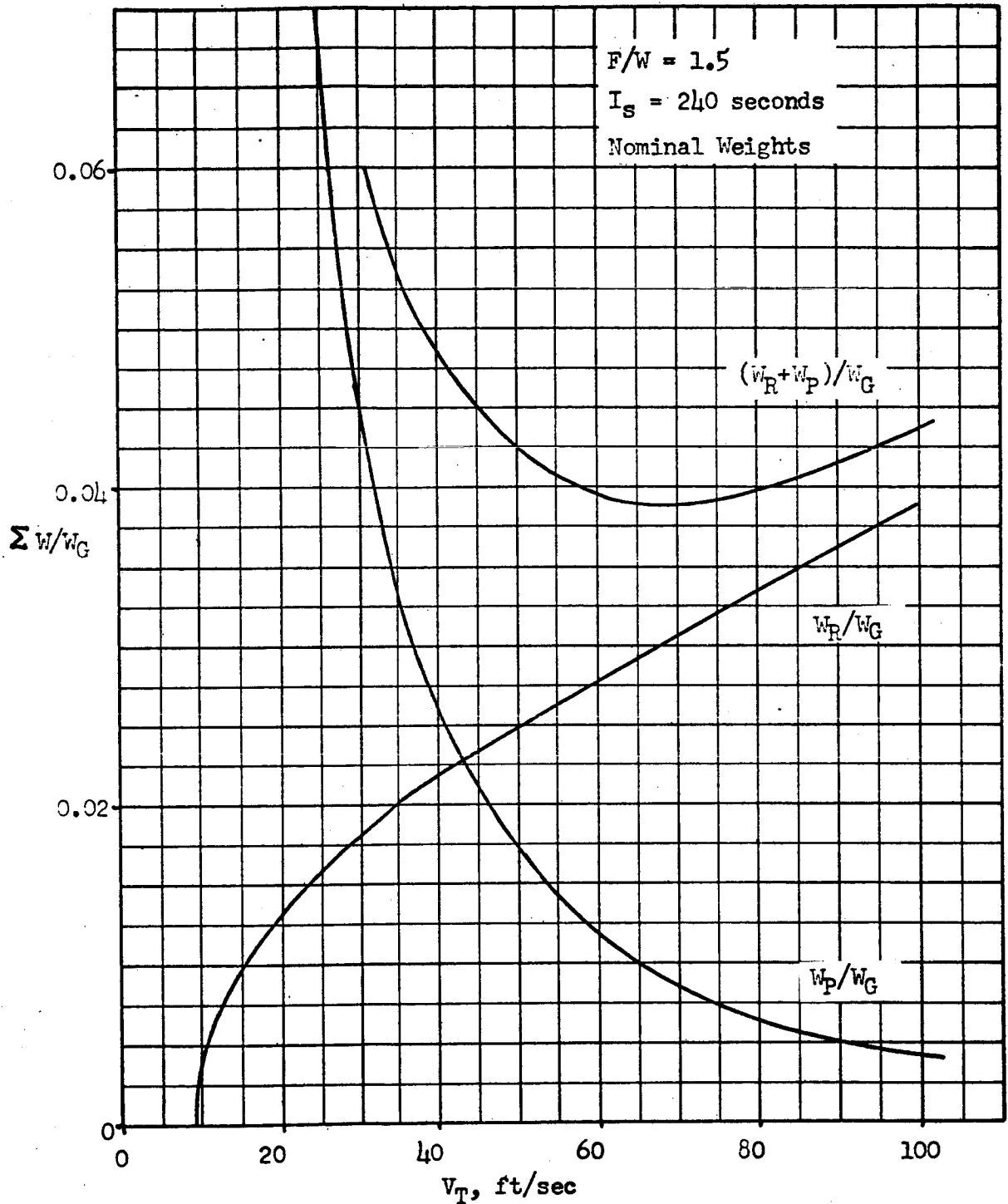


Figure 90 Required Weights of Rocket and Parachute vs Parachute Terminal Velocity for Impact Velocity (V_f) of 10 ft/sec for an Earth Landing

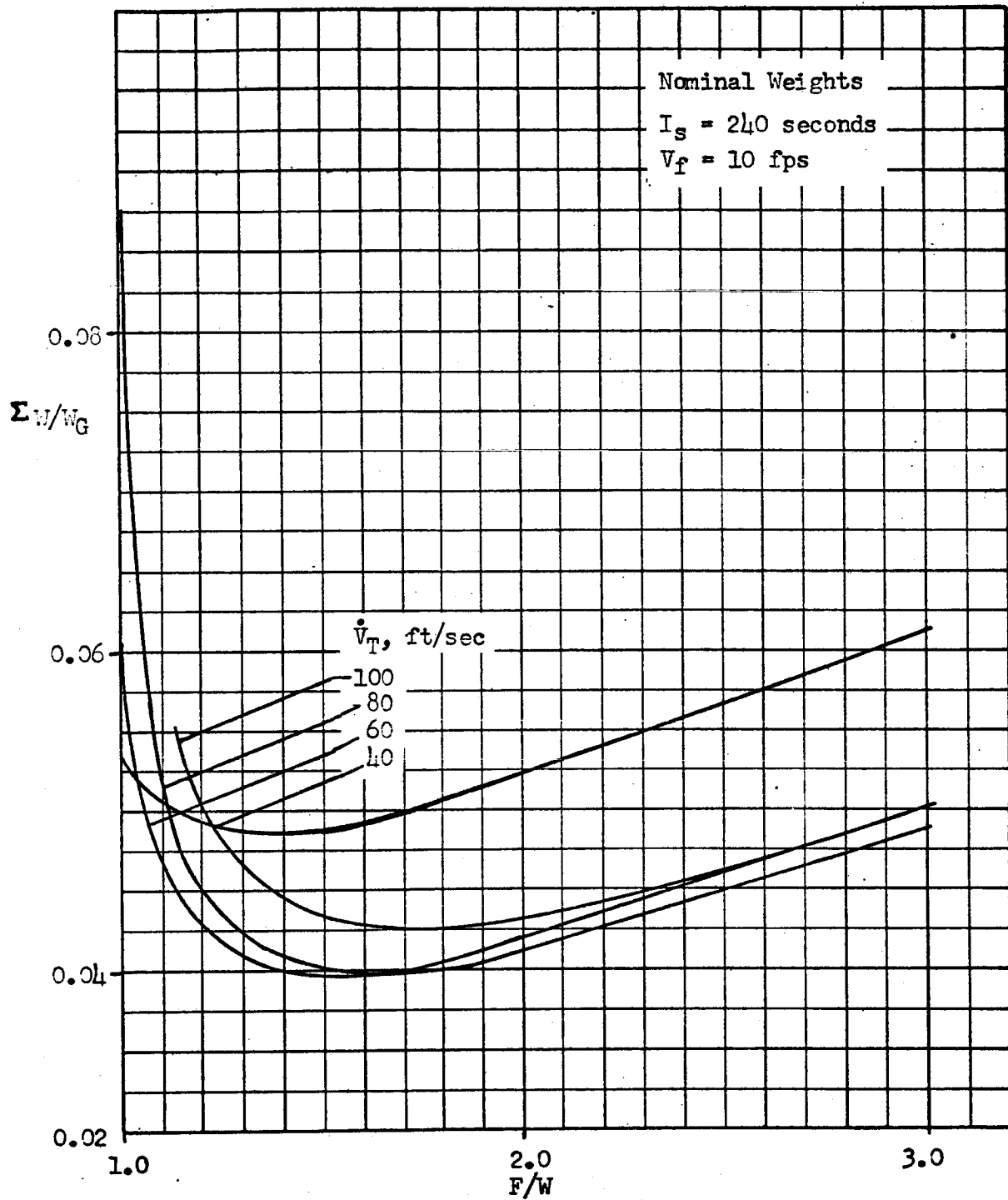


Figure 91 Variation of System Weight with Parachute Terminal Velocity and Rocket Thrust-to-Weight Ratio

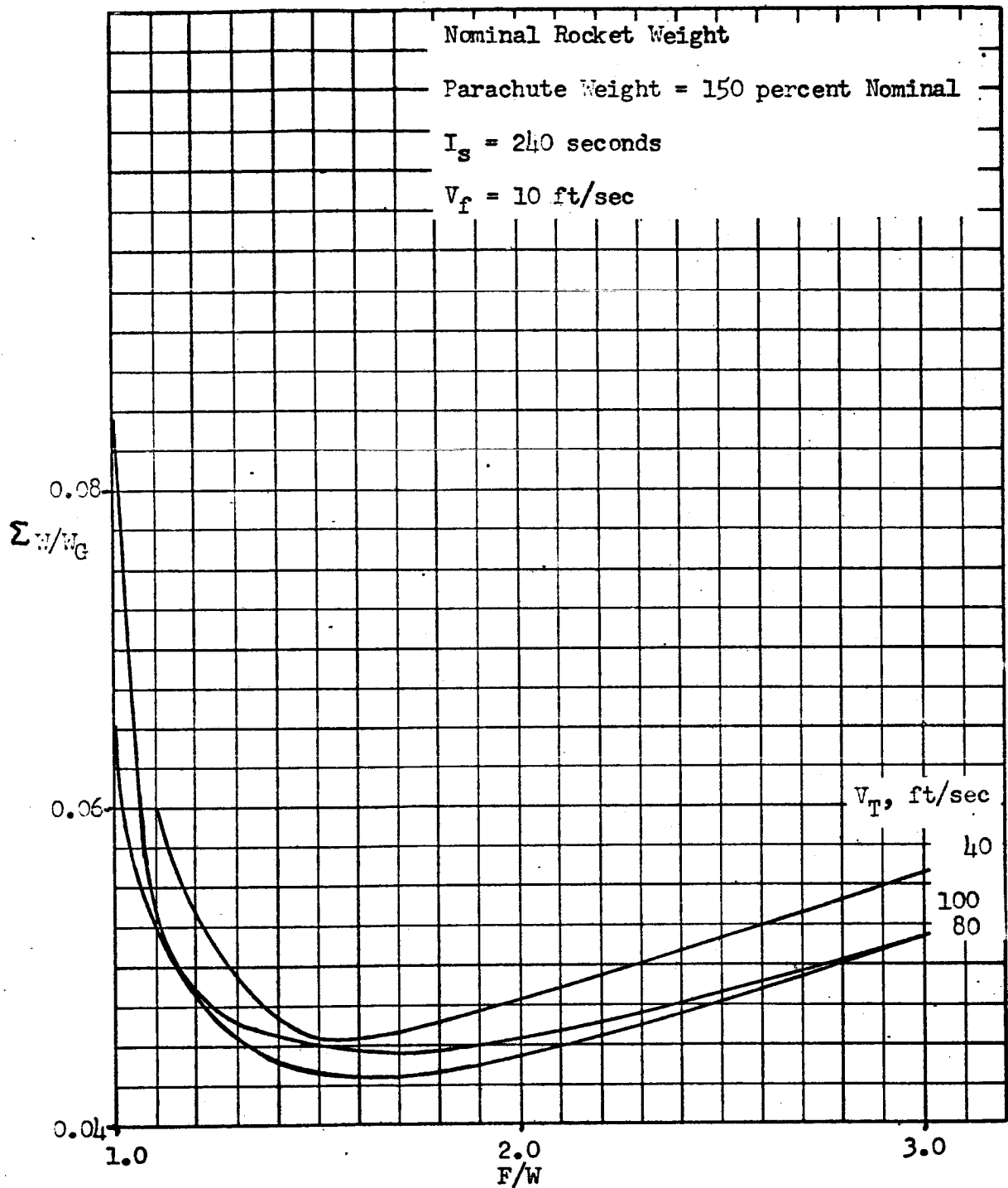


Figure 92 Variation of System Weight with Parachute Terminal Velocity and Rocket Thrust-to-Weight Ratio

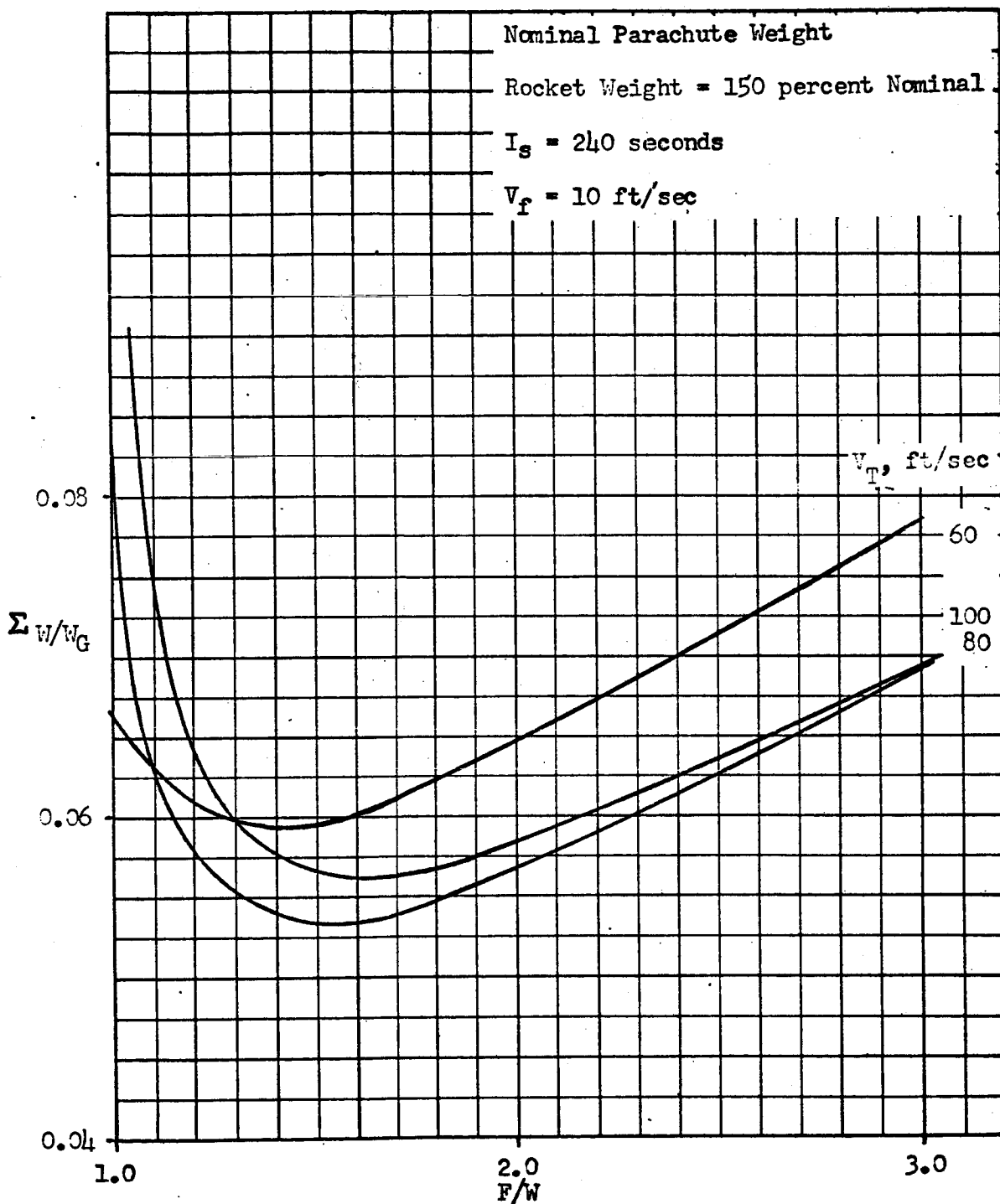


Figure 93 Variation of System Weight with Parachute Terminal Velocity and Rocket Thrust-to-Weight Ratio

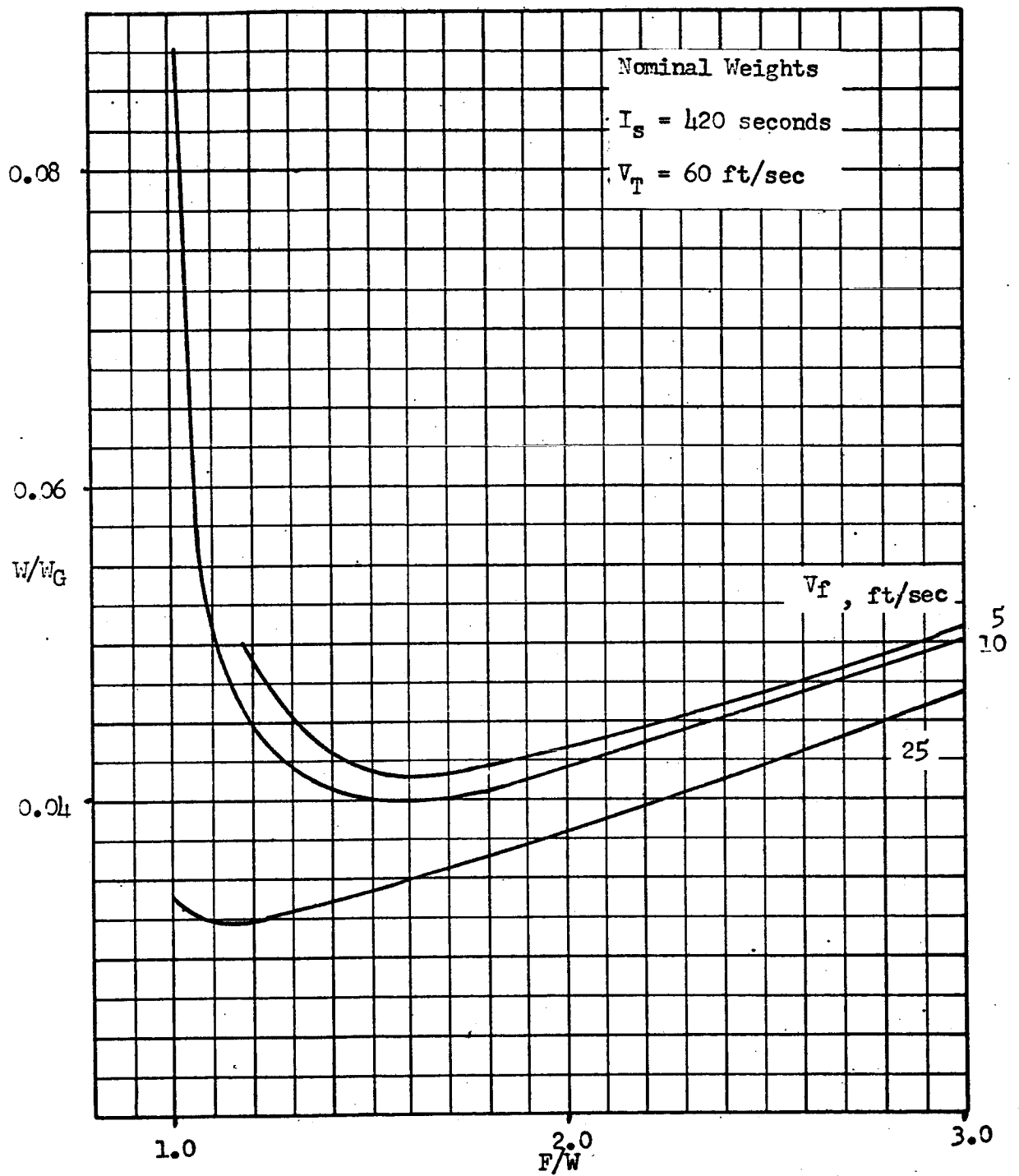


Figure 94 Effect of Design Impact Velocity on Thrust-to-Weight Optimization

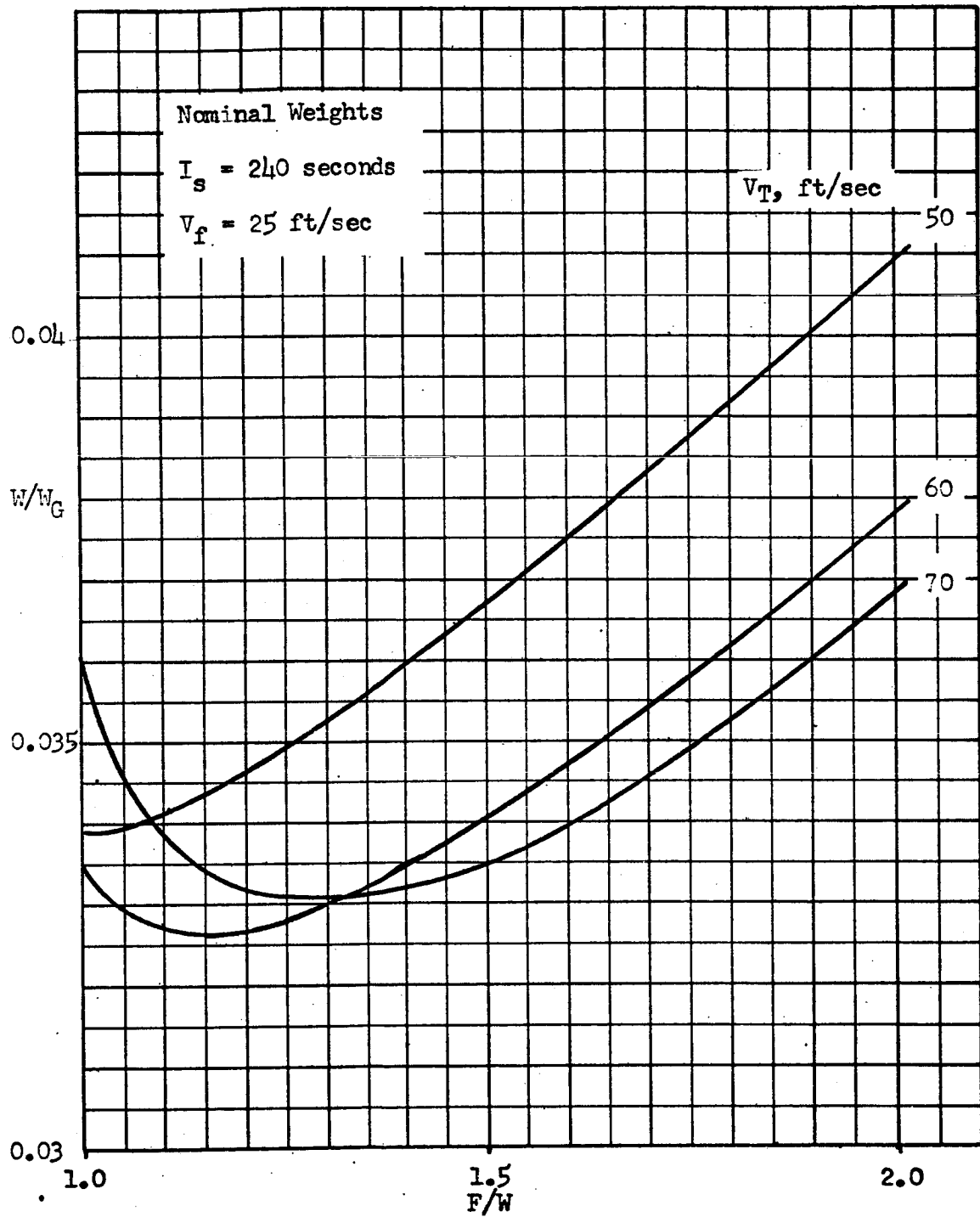


Figure 95 Variation of System Weight with Parachute Terminal Velocity and Rocket Thrust-to-Weight Ratio

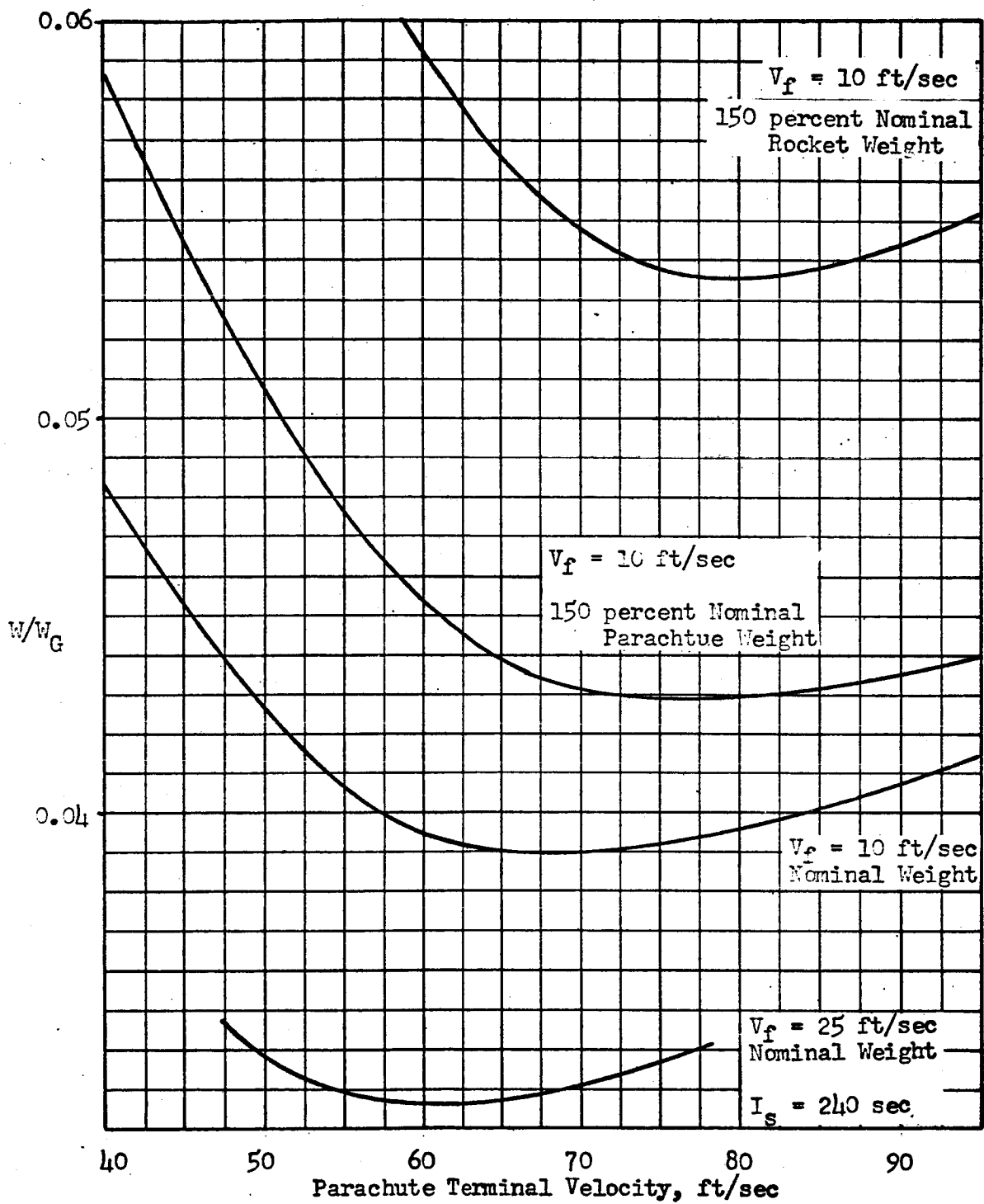


Figure 96 Optimum Pararocket System Weight vs Parachute Terminal Velocity for Earth Landing

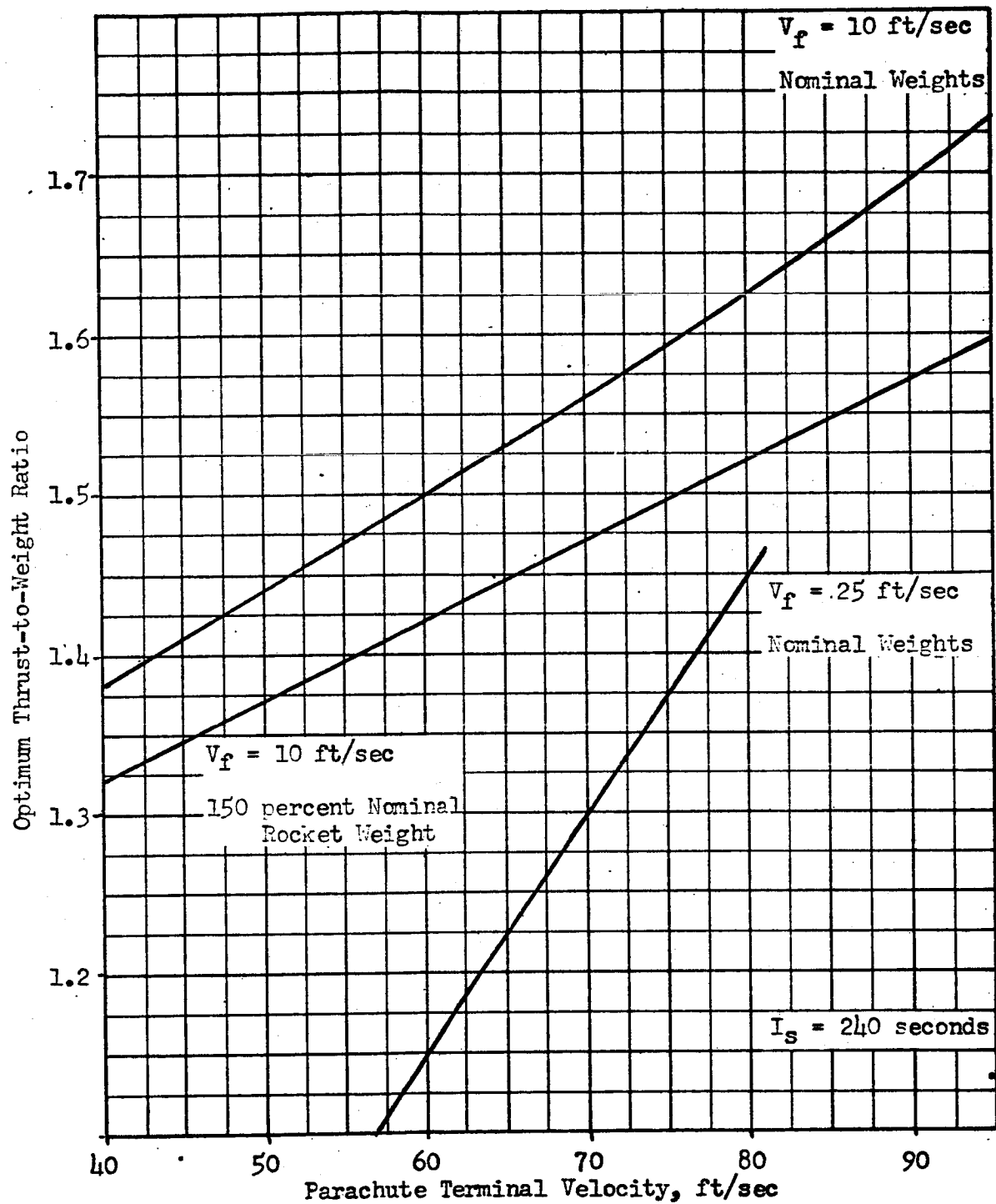


Figure 97 Optimum Thrust-to-Weight Ratio vs Parachute Terminal Velocity for Earth Landing

therefore the optimum F/W curve of Figure 97 for an impact velocity of 10 ft/sec and nominal system weights is also applicable to the case where 150 percent nominal parachute weight is used. The optimum parachute terminal velocity does, however, shift to a higher value for the higher parachute-weight case.

Parachute/Retrorocket/Impact Device System

In the study described above, discrete values of impact velocity were selected on the basis of stability criteria; the optimization analysis involved only the parachute and rocket employed prior to impact. An investigation optimization of a combined system employing a parachute, a retrorocket, and an impact energy-absorbing device was conducted to determine optimum overall terminal deceleration phase systems.

The weight percentage of an impact energy-absorbing device is dependent on the impact velocity (V_F). Therefore, for an optimization curve based on a constant V_F , adding a constant impact device weight does not change the optimum parachute terminal velocity (V_T) and rocket F/W . Only the system weight (which now includes the energy-absorbing device) is increased. For a range of V_F values, the optimum V_T values and the optimum rocket F/W values are presented in Figure 98.

The minimum pararocket weight, the parachute weight, and the weight of a frangible tube impact device* are presented in Figure 99 as a function of V_F . The frangible tube data is from Reference 5. For the pararocket system weight, the impact velocity refers to the velocity at which the vehicle strikes the surface immediately after rocket burnout. For the parachute (only) system, the impact velocity is the parachute terminal velocity.

The combined system weight for Earth is presented in Figure 100. For a nominal weight case, at impact velocities above approximately 40 ft/sec, the parachute system is lighter than a pararocket system. Adding the impact energy-absorbing device does not alter this trend; the lowest combined system weight (approximately 3.0 percent of the

*The indicated impact device weight essentially reflects only the weight of the velocity-dependent portion of the overall landing gear. A detailed landing gear study presented in the Appendix indicates that most of the weight is devoted to items which are not dependent on impact velocity.

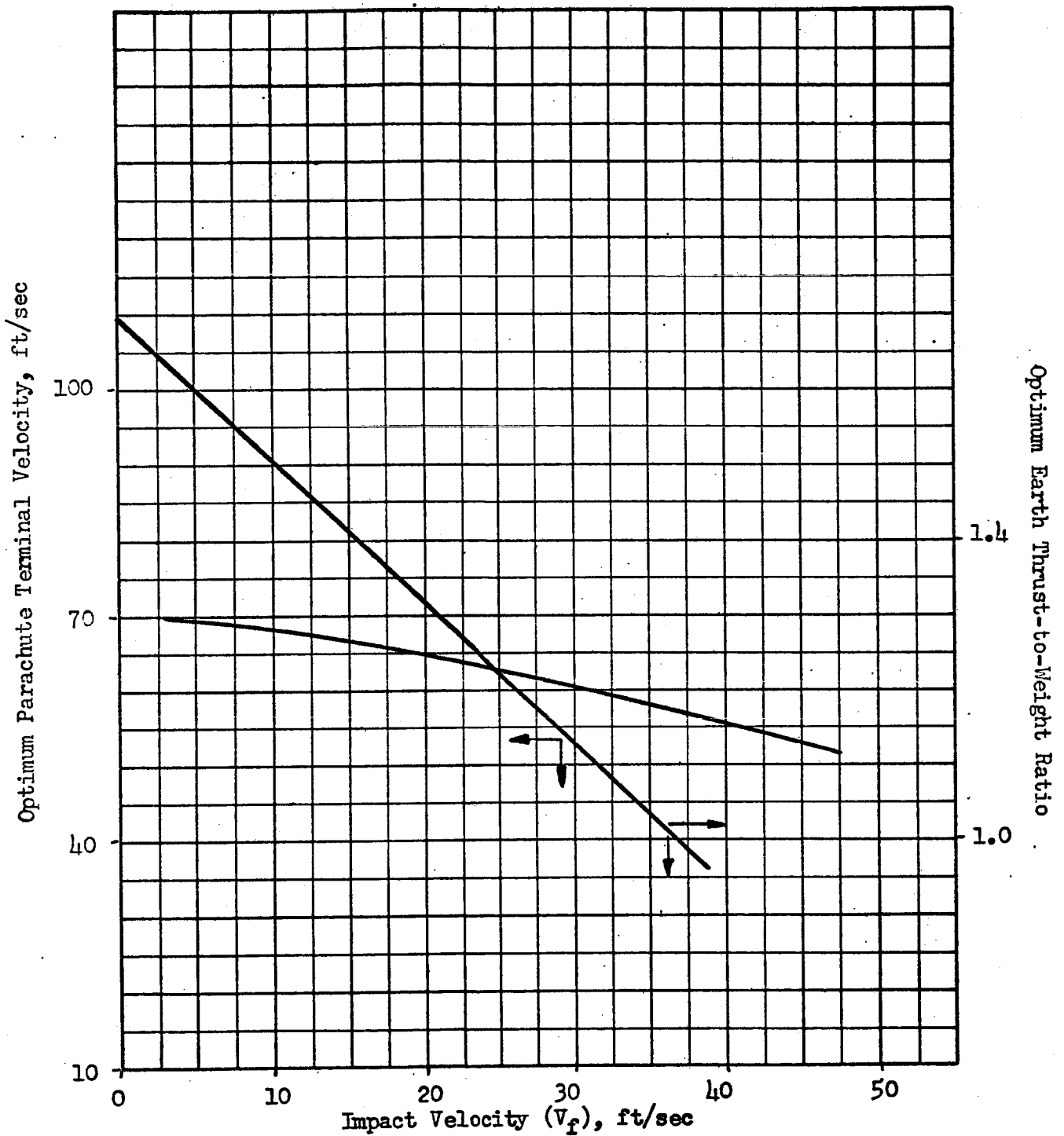


Figure 98 Optimum Terminal Velocity and Rocket Thrust-to-Weight Ratio for Pararocket Retro System (Earth)

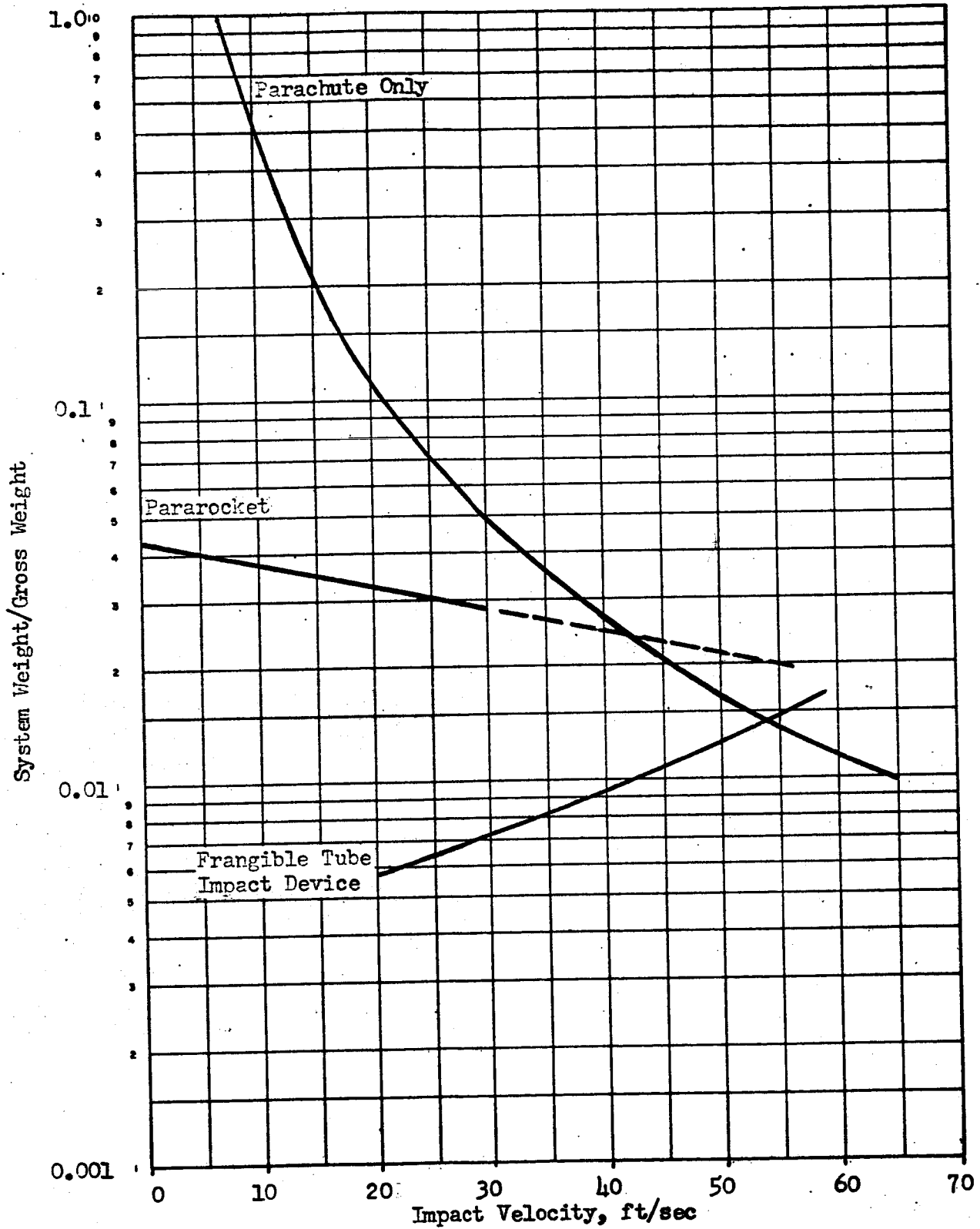


Figure 99 Landing System Weights (Earth)

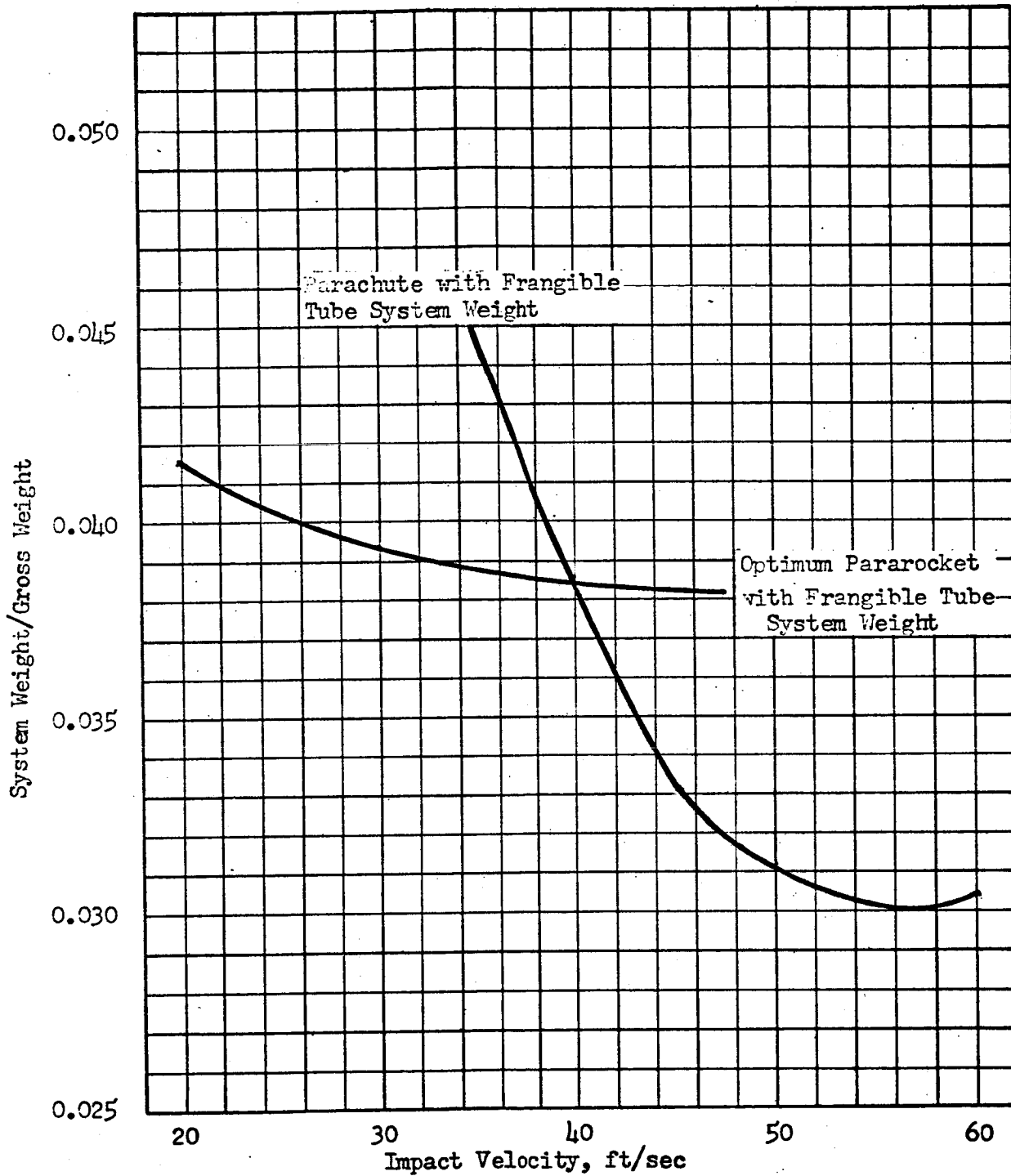


Figure 100 Optimization of Combined Earth Landing Systems

vehicle gross weight) is obtained by the use of a parachute to reduce the descent velocity to 55 ft/sec and then a frangible-tube system to absorb this velocity. If 55 ft/sec exceeds the impact velocity that assures touchdown stability, a nonoptimum parachute system would be employed to provide a lower impact velocity; if a velocity below 40 ft/sec is desired, the pararocket is more efficient than the parachute system. The fact that at zero impact velocity, the pararocket-system weight (no frangible-tube impact system) does not equal the optimum combined pararocket and frangible-tube system weight implies that some allowance is made for impact-device weight at zero impact velocity.

Analysis results using parachute weight increased by 50 percent are presented in Figure 101, and where the impact energy-absorbing device weight is increased 50 percent are presented in Figure 102. The former condition tends to increase the optimum impact velocity; the latter has little effect other than a reduction in payload.

System Selection

The results indicate that for design impact velocities below 40-45 ft/sec, the pararocket system (parachute plus retrorocket) results in a lower system weight than use of only a parachute. Approximate values of the optimum thrust-to-(Earth) weight ratio for the retrorocket and parachute design terminal velocity, based on a design impact velocity of 10 ft/sec, are 1.5 and 70 ft/sec, respectively, and the pararocket system constitutes 3.9 percent of the gross weight; including the frangible tube system raises this to 4.4 percent.

System optimization including an impact energy absorbing device, results in the minimum overall system weight occurring at high design impact velocities, where the parachute (only) system is lighter than the pararocket system. The combined system weights at optimum V_F , and for 25 ft/sec and 10 ft/sec V_F values are presented in Table 17.

The general results of the study indicate that if high impact velocities are allowable, the desirable system from a weight and minimum complexity standpoint is the parachute and impact energy absorbing device system. If it is necessary to limit the impact velocity to 10, or possibly 25 ft/sec, the addition of the retrorocket results in lower system weights.

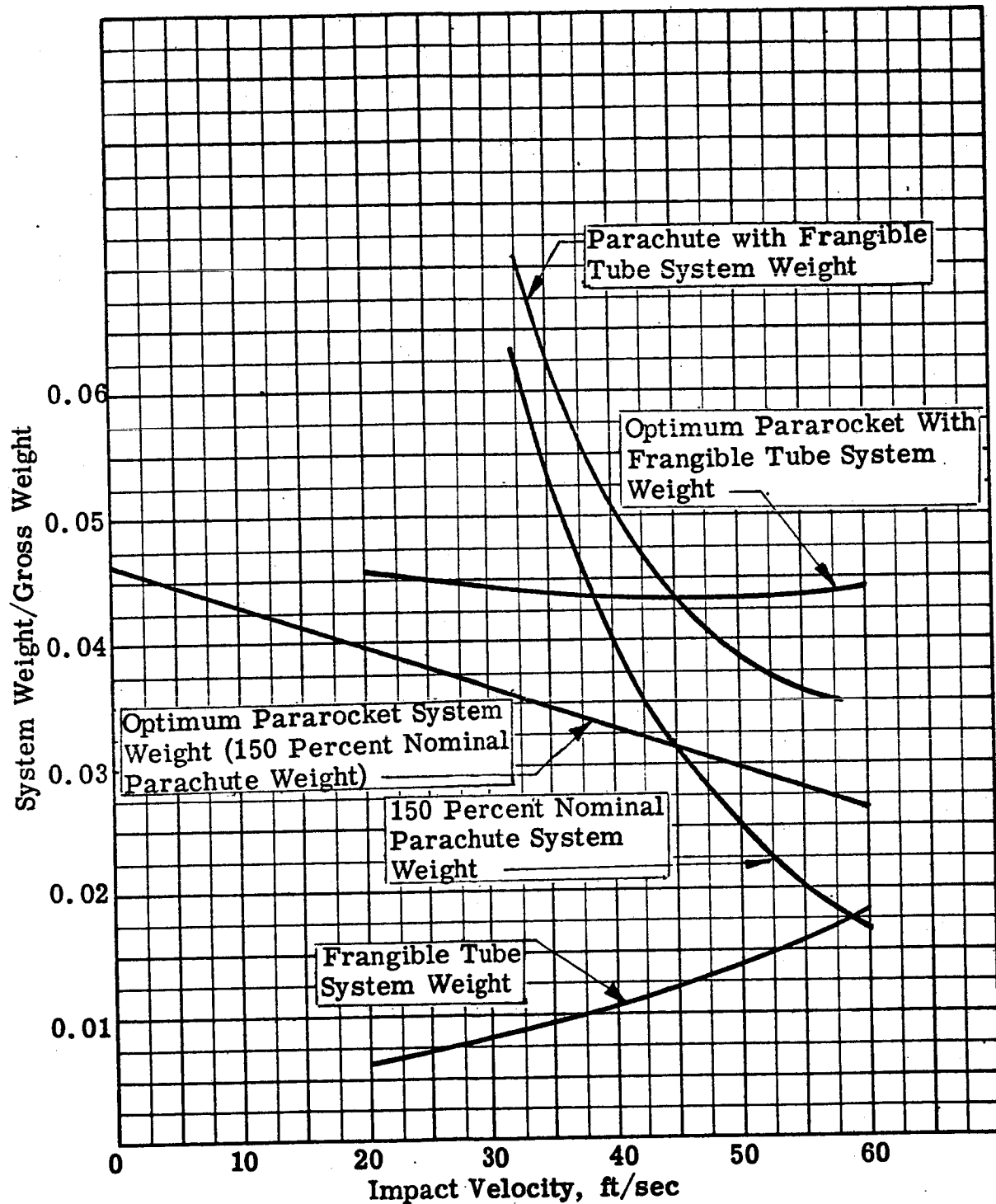


**Fig. 101 Optimization of Combined Earth Landing System.
150 Percent Nominal Parachute Weight**

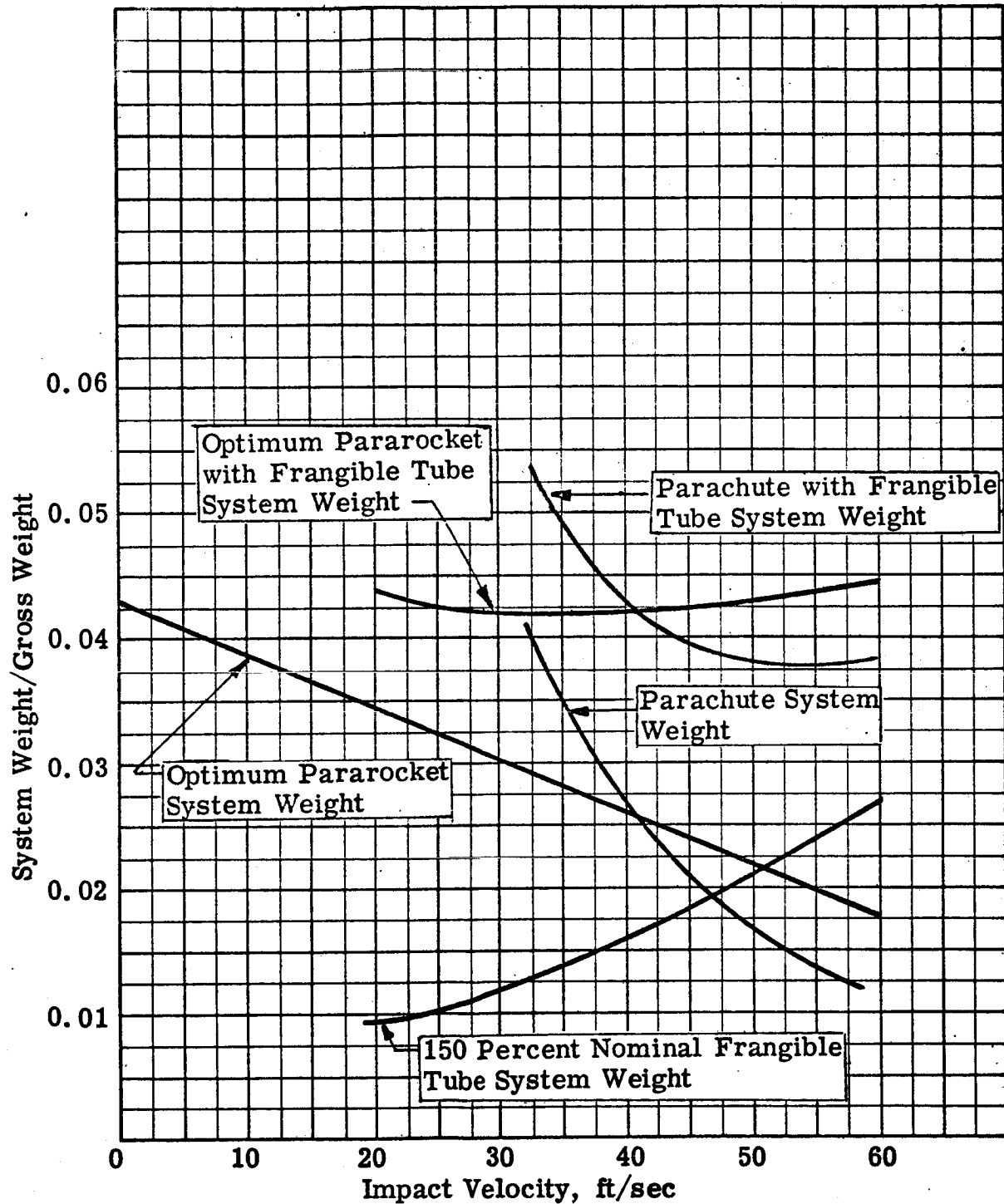


**Fig. 102 Optimization of Combined Earth Landing Systems.
150 Percent Nominal Impact Energy Absorbing
Device Weight**

TABLE 17

COMBINED SYSTEM WEIGHTS

Minimum Weight Configuration	Optimum V_F^* = 55 ft/sec	V_F = 10 ft/sec	V_F = 25 ft/sec
	<u>Parachute</u> Impact Device	<u>Pararocket</u> Impact Device	<u>Pararocket</u> Impact Device
Percent Gross Weight	3.1	4.4	4.1

* V_F = Impact Velocity

EARTH - MARS MISSIONS

MARS TRAJECTORY SELECTION

The propulsion requirements for a round-trip mission to Mars are strongly dependent upon the launch dates and transfer durations selected for the outbound and return legs of the journey. Optimum round-trip trajectory characteristics are determined by analysis of the trade-off between propulsion system ideal velocity requirements, which increase as total trip duration decreases below approximately 950 days, and the weight requirements imposed by life support, meteorite and radiation shielding, and propellant storage, all of which increase with increasing trip time. The latter factors are, at present exceedingly difficult to ascertain precisely; as a result, a parametric approach is utilized where necessary in subsequent studies.

A variety of Earth-Mars trips are described in Table 18; the data presented were obtained from References 6 and 7. It should be noted that the indicated hyperbolic velocities vary cyclically, and repeat (except for a change on the order of 1000 ft/sec from one period to the next, caused by the eccentricity and inclination of the Mars orbital plane) each synodic period, or 780 days. Specific trips are generally characterized as slow, such as items (1) and (2) in Table 18, or fast, as represented by items (7) and (8).

The propulsive energy requirements for each leg of a slow trip are minimized separately, without regard for the resulting planetary stay-time, which in the illustrative case is 465 days. The implication of selecting a slow trip is that the propellant required to provide additional velocity capability exceeds the weight of additional life-support, vehicle shielding and insulation; in the light of continuing developments in closed-cycle ecological systems, nuclear or solar power sources, insulation technology (and other methods of temperature control) and in-flight vehicle repair techniques, this possibility exists, but it is presently doubtful. The choice of launch dates and trip times in this instance is straightforward, and essentially unaffected by considerations such as the use of aerodynamic braking on arrival or propellant shielding and storage during transit.

Fast trips are difficult to optimize. For a typical specific total duration of 352 days, of which 12 days are for surface exploration (items (7) and (11) of Table 18), the selection of launch date and Earth-Mars trip time is not simply a case of minimizing the total hyperbolic velocity requirements. First, arrival conditions at Mars and later at Earth are less consequential

TABLE 18

MARS MISSIONS

Trajectory Number	Phase	Destination Stay, days	Launch Date Gregorian, Julian	Trip Time days	Hyperbolic Departure Excess Velocity ft./sec	Hyperbolic Arrival Velocity, ft/sec	Total Mission Time, days
(1)	Earth-Mars	---	5 December 1964 2438734.5	240	11,590	12,000	240
(2)	Mars-Earth	465	10 November 1966 2439439.5	240	9,800	14,900	945
(3)	Earth-Mars	---	19 May, 1971 2441090.5	170	9,700	11,000	170
(4)	Mars-Earth	5	10 November 1971 2441265.5	255	22,000	38,000	430
(5)	Earth-Mars	---	19 April 1971 2441060	160	16,000	19,000	160
(6)	Mars-Earth	8	14 October 1971 2441228	246	19,500	29,400	414
(7)	Earth-Mars	---	6 June 1971 2441108.5	80	20,500	34,400	80
(8)	Mars-Earth	2	26 August 1971 2441190.5	110	41,300	29,200	192
(9)	Mars-Earth	12	6 September 1971 2441200.5	110	44,000	30,000	202
(10)	Mars-Earth	12	6 September 1971 2441200.5	125	39,000	29,000	217
(11)	Mars-Earth	12	6 September 1971 2441200.5	260	18,000	27,000	352

since deceleration will be accomplished principally by aerodynamic means. This factor indicates that system optimization entails minimizing the sum of the departure velocity requirements. However, the Mars takeoff propulsion system must be shielded and insulated until it is used; the Earth-departure propulsion system has no such requirement. This condition suggests that for an optimum system the minimum total-departure velocity stipulation cited above should be biased toward higher Earth-departure velocity (i.e., a short outbound trip) in return for a subsequent lower Mars-departure velocity requirement. Though precise design data are not currently available in all pertinent areas (in particular, meteorite shielding), the round trip described by items (7) and (11) of Table 18 is a reasonable estimate of an optimum mission profile, and thus provides general requirements, where needed, for analysis of Mars landing phases.

TERMINAL CORRECTIONS FOR EARTH-MARS TRAJECTORIES

Landing on the surface of Mars can be performed in several ways. The vehicle can enter an orbit about the planet and then descend wholly or in part to the surface. This concept would be of value for early missions where it was not deemed possible to rely on a direct aerodynamic entry without surveillance, equipment checkout, etc. Alternately, the space vehicle can employ atmospheric braking for direct descent to the surface. In either case, since midcourse correction analyses for the missions studied have shown that the vehicle approach trajectory accuracy is inadequate, there is a requirement for terminal corrections. The terminal correction propulsion requirements for both landing concepts were analyzed since both concepts may be used for Mars systems.

Propulsive Orbit Establishment

An analysis of terminal corrections required for missions which utilize a propulsion phase to establish a 300-n mi circular orbit has been performed in conjunction with another study.* The method of analysis is presented in Reference 2. The Earth-Mars trajectory used in the analysis is summarized in Table 19.

TABLE 19

EARTH-MARS TRAJECTORY FOR ORBIT-ESTABLISHMENT MISSION

Launch Date	Transfer Time, days	Hyperbolic Arrival Velocity, ft/sec	Nominal Asymptotic Approach Distance, n mi	Actual Asymptotic Approach Distance, n mi
6 Dec. 1964	250	12,000	3,400	5850

* NASA contract NAS 7-88 conducted by Rocketdyne

The actual asymptotic approach distance resulting from midcourse correction inaccuracies was 5850 n mi, a deviation of 2450 n mi from the desired value. The relatively long transfer mission with its low arrival velocity was selected as representative of propulsive orbit-establishment missions since faster missions result in excessive propulsive ΔV and propulsion system weight requirements.

The terminal correction velocity requirements for the selected mission, and an alternative trajectory with a hyperbolic approach velocity of 15,000 ft/sec, are presented in Figure 103 for various asymptotic approach distances. A crossplot is presented in Figure 104 to indicate the decrease in correction velocity increment with reduction in asymptotic approach distance deviation.

An analysis of the effects of errors in position and velocity measurements and in correction maneuver execution was performed to evaluate the subsequent altitude deviations in the propulsively established orbit. The measurement errors were range dependent, and execution errors were ΔV dependent (where the ΔV was indirectly range dependent); therefore the deviations in apses altitude caused by the errors were plotted as a function of range (Figure 105). A tolerance of 10-percent (30 n mi) in the deviation of apoapsis altitude of the orbit was utilized for selecting the range for making the terminal correction.

For terminal corrections, the magnitude of execution error is a function of F/W ratio; the results presented for terminal correction requirements corresponded to a 0.3 F/W ratio, which is also the F/W value employed for the subsequent orbit-establishment maneuver. For F/W ratios between 0.1 and 0.5, the execution errors vary negligibly, and the investigation is therefore valid for any F/W in this range of values.

The correction range obtained from Figure 105 and the magnitude of the correction velocity increment (Figure 103) for that range are given in Table 20.

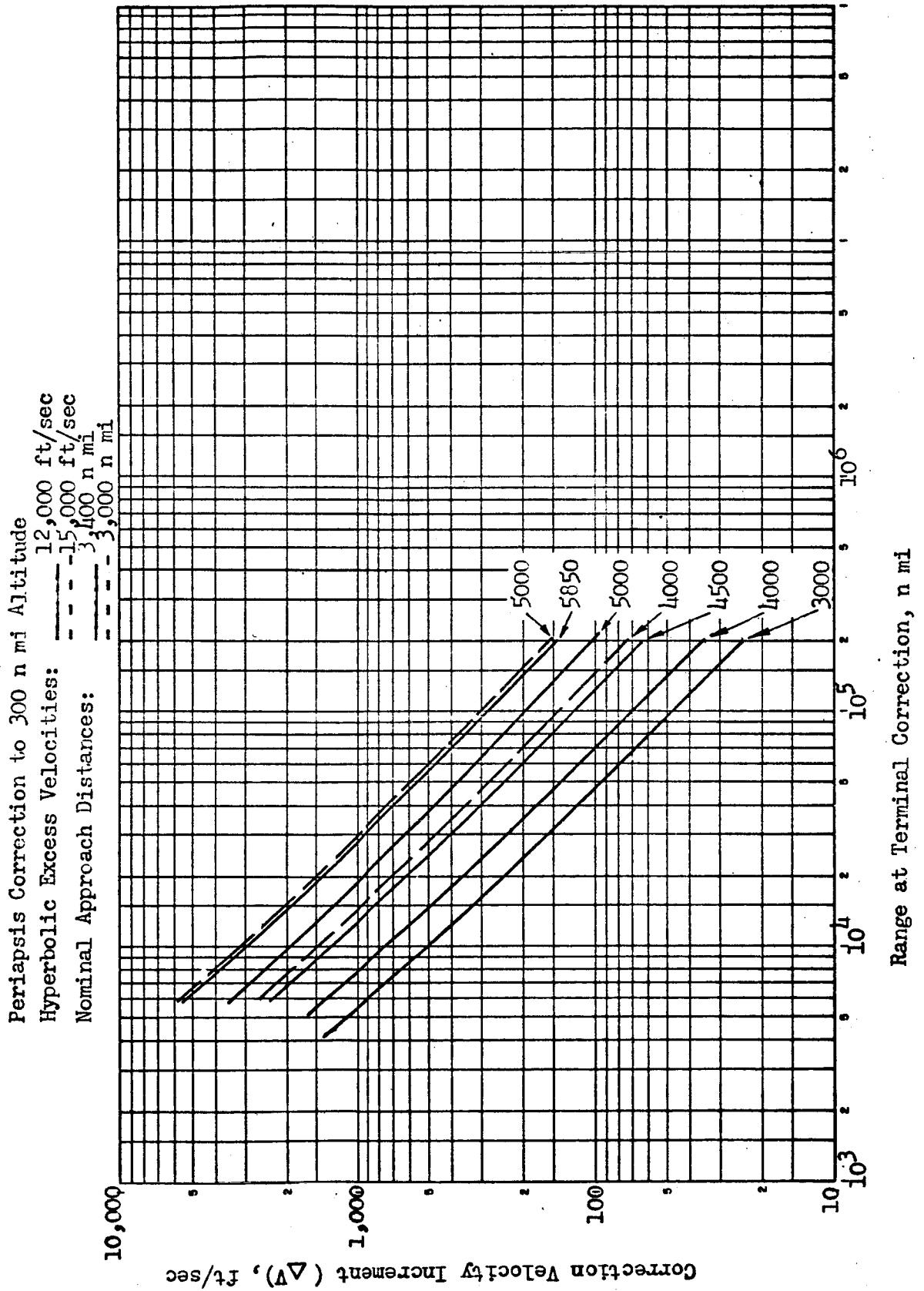


Figure 103 . Mars Terminal Correction Maneuver

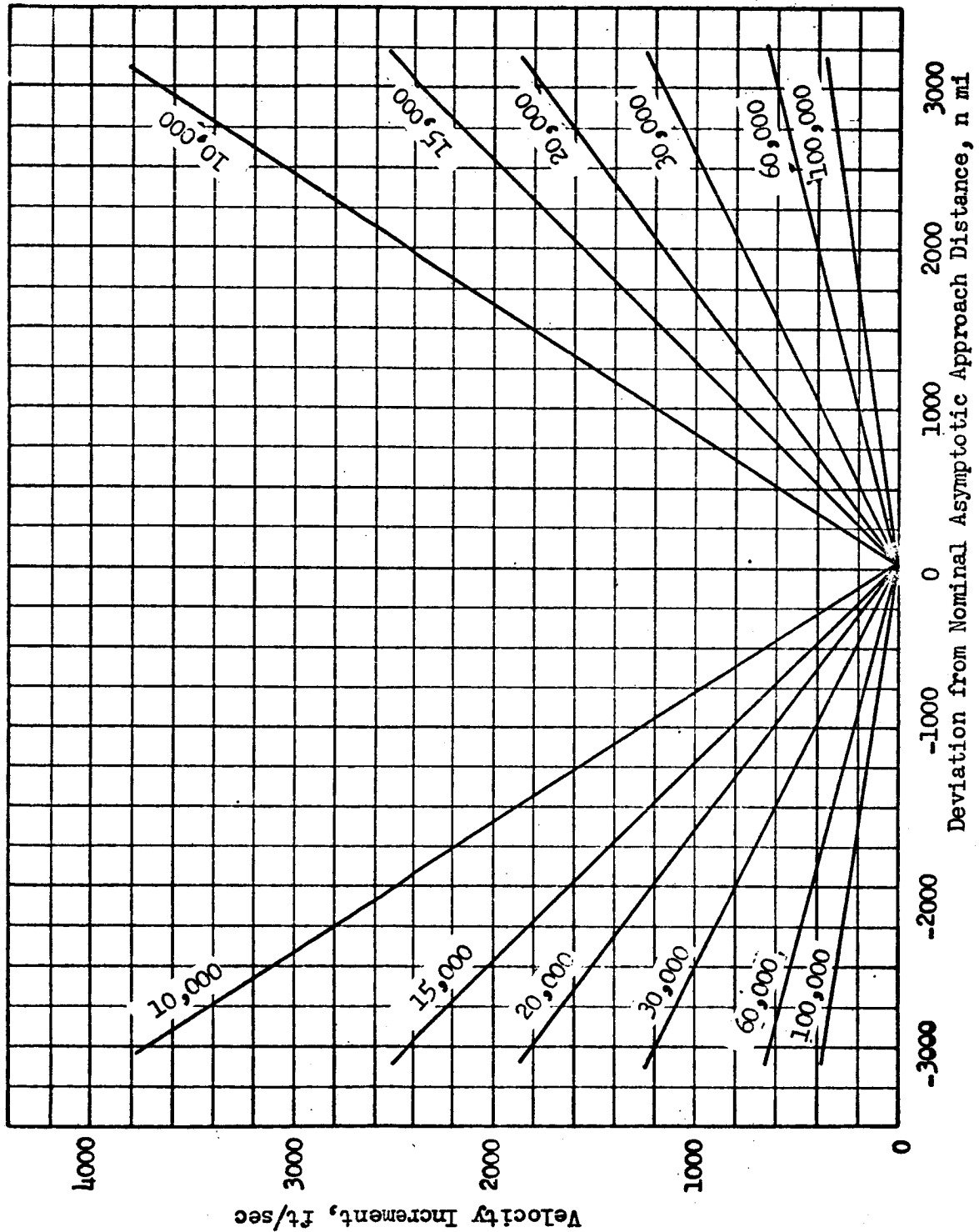


Figure 104. Mars Terminal Correction. Periaapsis Correction to 300 n mi Altitude
Hyperbolic Excess Velocity - 12,000 ft/sec. Nominal Asymptotic
Approach Distance - 3,400 n mi.

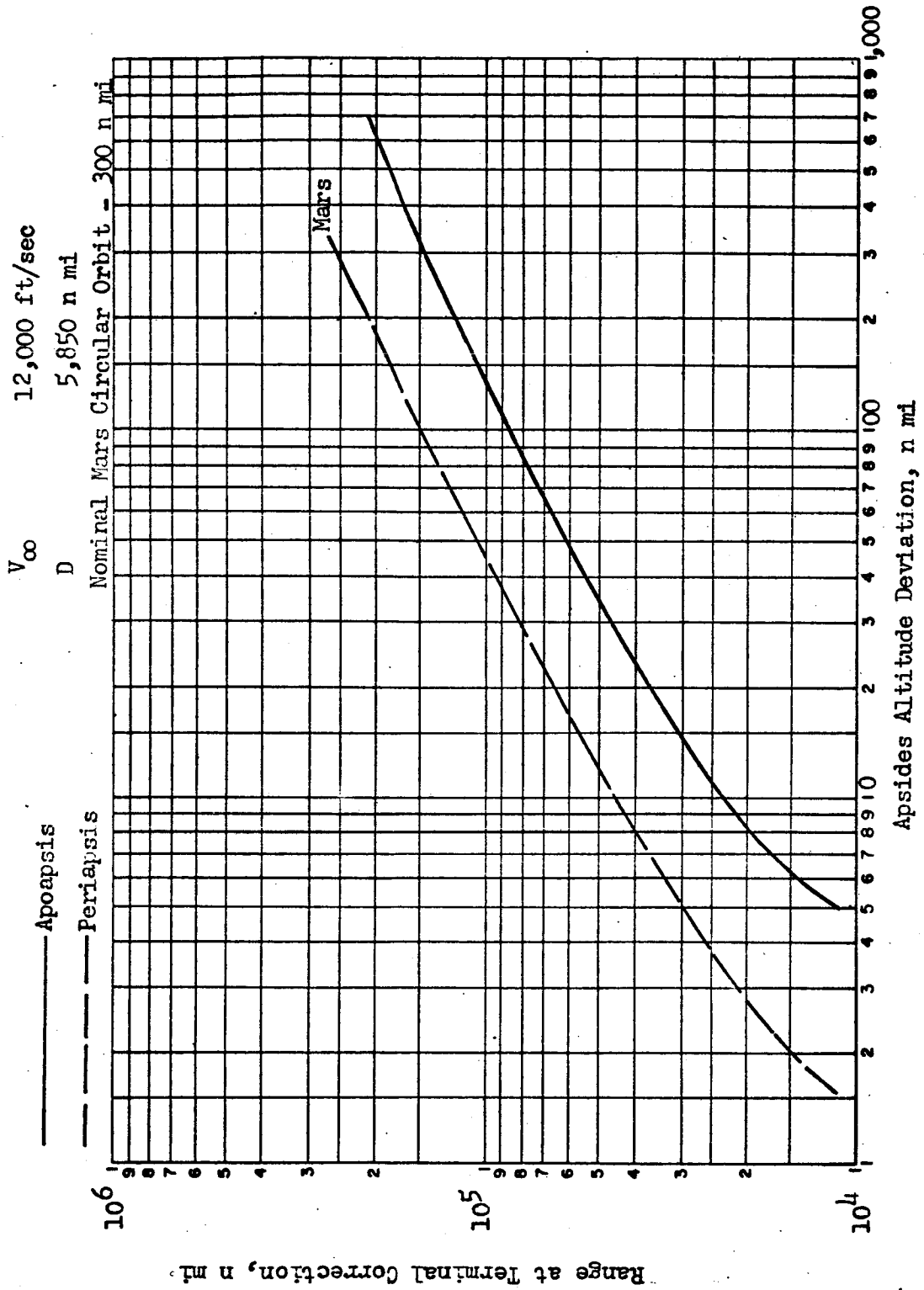


Figure 105 The Dependence of Apsides Altitude Deviation upon Range at Application of Terminal Correction.

TABLE 20

TERMINAL CORRECTION FOR MARS ORBIT ESTABLISHMENT MISSION

Mission	Nominal Orbital Altitude, n mi	Apoapsis Tolerance, n mi	Correction Range, n mi	Terminal Correction ΔV , ft/sec
Earth-Mars	300	30	46,000	630

Atmospheric Entry

Terminal Corrections required for atmospheric braking missions were investigated for the two Earth-Mars transfers presented in Table

TABLE 21

EARTH-MARS TRAJECTORIES FOR ATMOSPHERIC ENTRY MISSIONS

Trajectory Number (see Table 4)	Launch Date	Trip Time, days	Hyperbolic Arrival Velocity, ft/sec
1	19 May 1971	170	11,000
3	6 June 1971	80	34,400

An analysis of midcourse corrections for these two trajectories (discussed under Earth re-entry) was made to determine the deviation in asymptotic approach distance which existed at conclusion of the midcourse correction maneuvers. These results are shown in Table 22 .

TABLE

MARS ARRIVAL CONDITIONS

Trajectory Number (see Table 4)	Hyperbolic Arrival Velocity, ft/sec	Nominal Asymptotic Approach Distance (D), n mi	Deviation in D (ΔD), n mi	Actual Asymptotic Approach Distance (D_a), n mi
1	11,000	3190	2460	6650
3	34,000	2025	475	2500

The entry corridor (Figure 106) defines limits of entry conditions suitable for performance of aerodynamic landing maneuvers to the surface of Mars using a drag vehicle configuration. The corridor for this type vehicle is narrower than corridors for other vehicle configurations. Therefore, trajectories satisfying this corridor will be valid for other configurations.

The combinations of V_a and D_a from Table 22 represent trajectories with atmospheric entry conditions outside the Mars-entry corridor. Therefore, terminal corrections were necessary. The objectives of the terminal corrections are given in Table 23.

TABLE 23

NOMINAL ENTRY CONDITIONS INTO THE ATMOSPHERE OF MARS

Trajectory Number	Entry Altitude (h_E), feet	Entry Velocity (V_E), ft/sec	V_E/V_{CO}	Entry Trajectory Elevation Angle (α_E), degrees
1	1,425,000	19,090	1.73	-24.9
3	1,425,000	37,760	3.42	-24.9

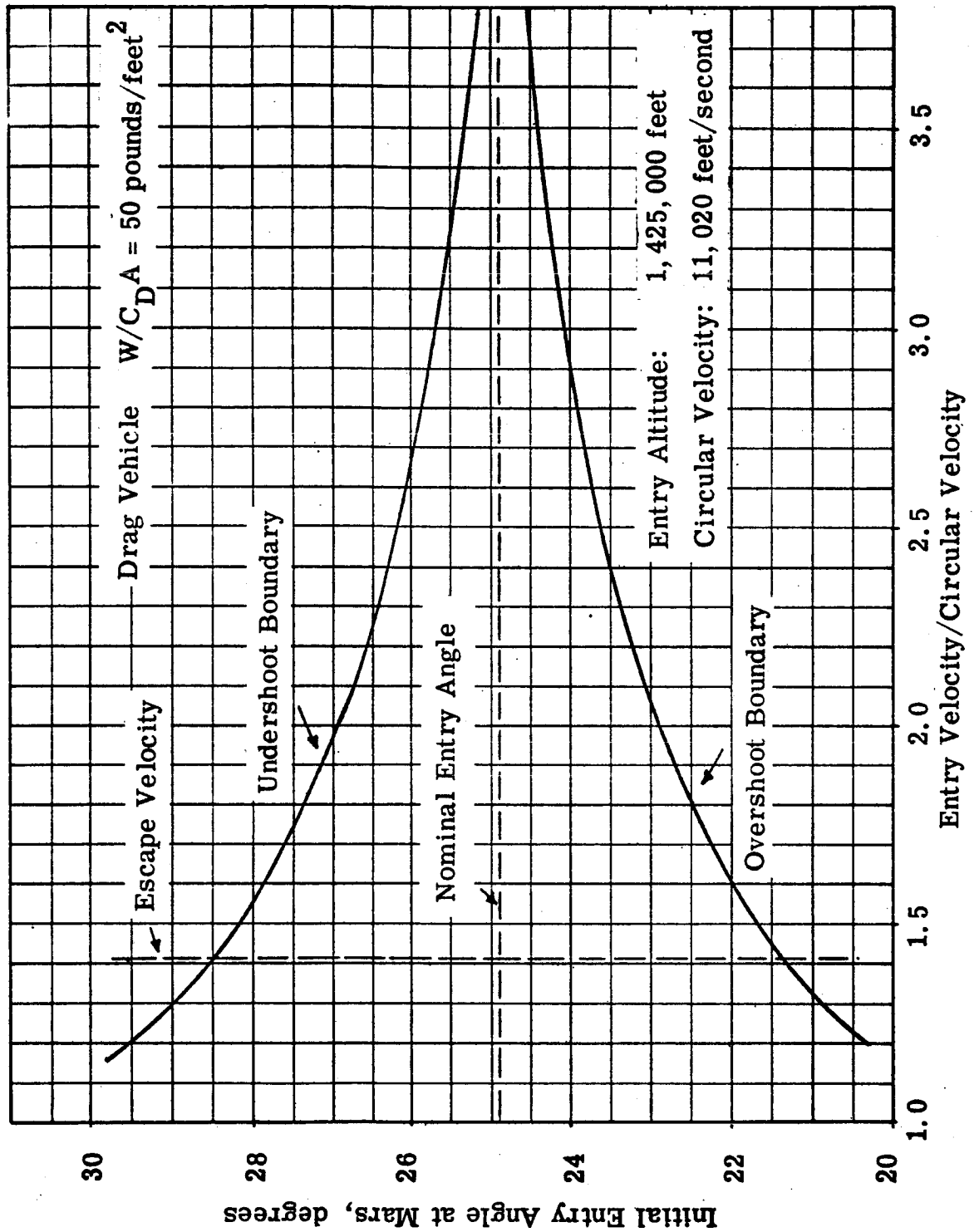


Fig. 106 Mars Entry Corridor

The magnitudes of the terminal corrections are plotted in Figures 107 and 108 , as functions of correction range. Correction velocity magnitudes are presented for several values of deviation in asymptotic approach distance to indicate the influence of that parameter.

Errors encountered in terminal corrections affect the selection of a range for making the correction. Measurement errors are range dependent. Correction execution errors are dependent on ΔV and F/W ratio. Since the magnitude of correction errors varied only slightly for F/W ratios between 0.1 and 0.5 (Reference 2), errors corresponding to a F/W of 0.3 were used.

The rms deviations in entry velocity and entry trajectory elevation angle are indicated in Figure 109 and 110 . The deviation in entry velocity is insignificant. The allowable deviation in trajectory elevation angle at entry establishes the range for terminal correction. For the applicable conditions, the required correction range and the corresponding velocity increment are shown in the summary of terminal corrections presented in Table 24 .

TABLE 24

SUMMARY OF TERMINAL CORRECTIONS FOR MARS ATMOSPHERIC

ENTRY MISSIONS

Trajectory Number	Entry Corridor Half-band Width, degrees	Entry Angle Deviation, degrees	Correction Range, n mi	Correction Velocity Increment, Ft/sec
1	2.5	± 2.5	72,000	380
3	0.5	± 0.5	44,000	360

Conclusions

The analyses conducted have indicated a need for terminal corrections in missions using orbit-establishment maneuvers prior to landing and in missions using atmospheric deceleration entry maneuvers for direct landing. The magnitude of the velocity requirements have been determined and presented for propulsion systems with a nominal 0.3 initial F/W ratio. However, the velocity requirements analysis indicated that for a F/W range from 0.1 to 0.5, the change in results is negligible.

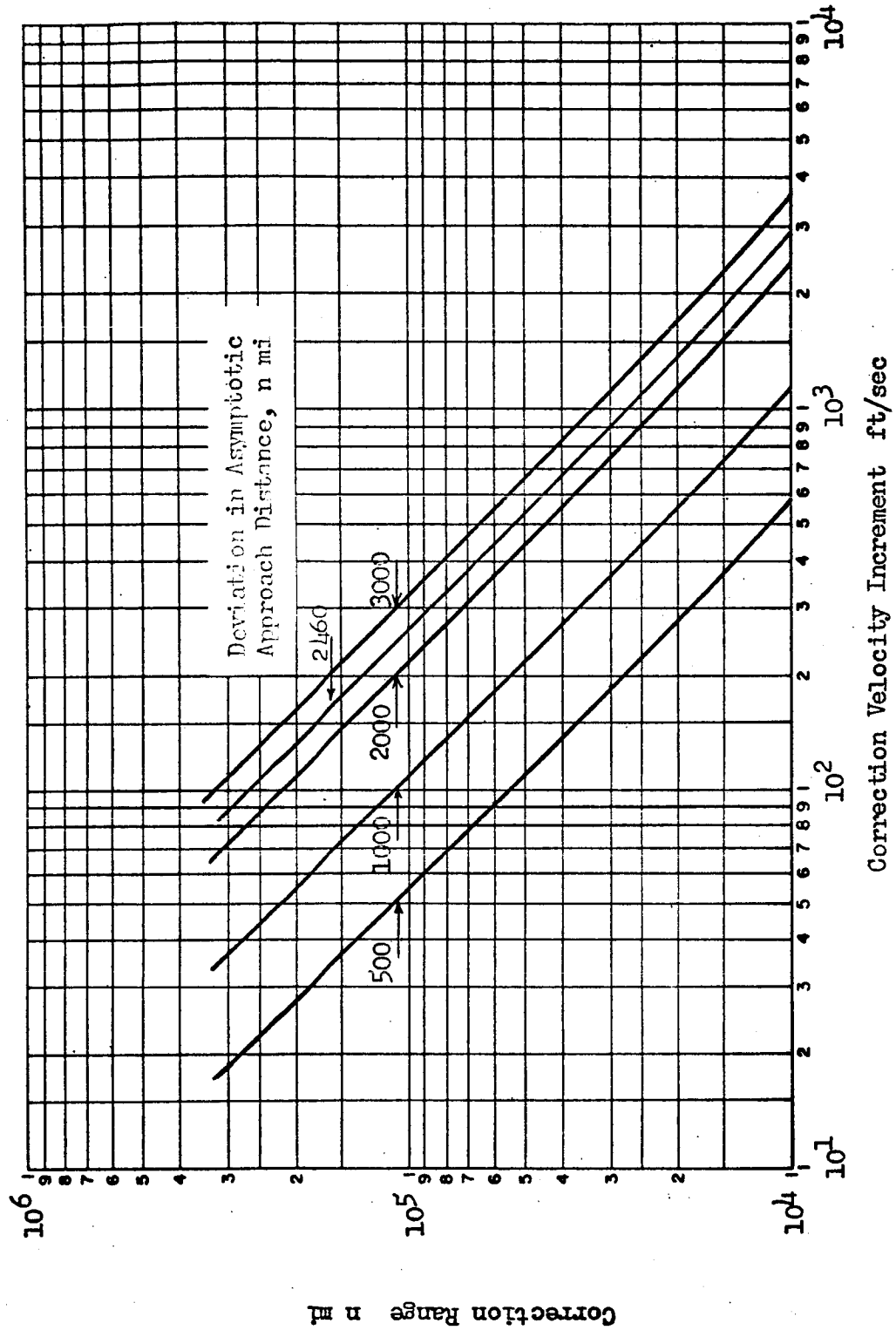


Fig. 107 The Effect of a Deviation in Asymptotic Approach Distance on the Terminal Correction Velocity Increment for Mars Atmospheric Entry. (Trajectory /)

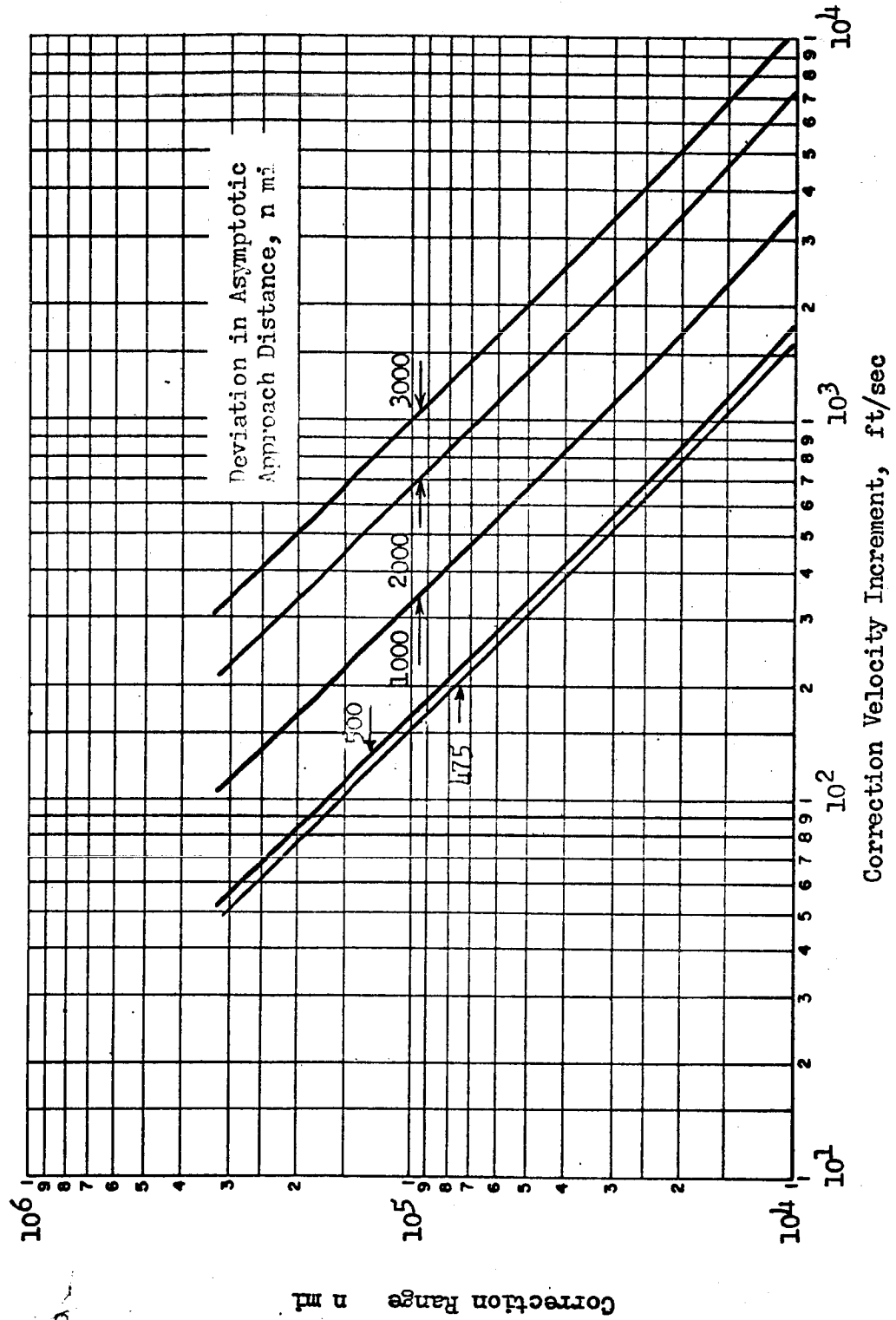


Fig. 108 The Effect of a Deviation in Asymptotic Approach Distance on the Terminal Correction Velocity Increment for Mars Atmospheric Entry. (Trajectory 3)

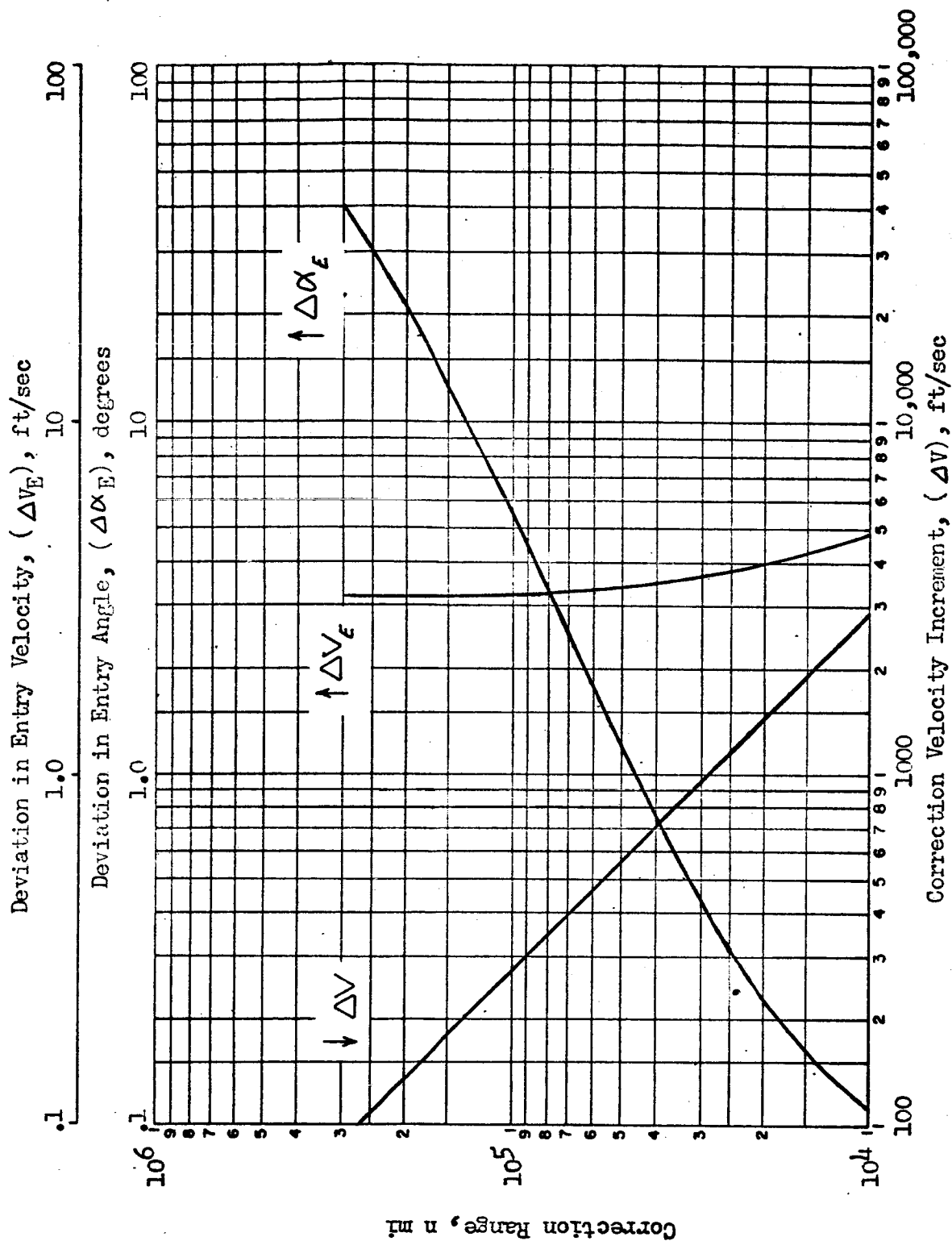


Fig. 109 Terminal Correction for Mars Atmospheric Entry. (Trajectory 1)

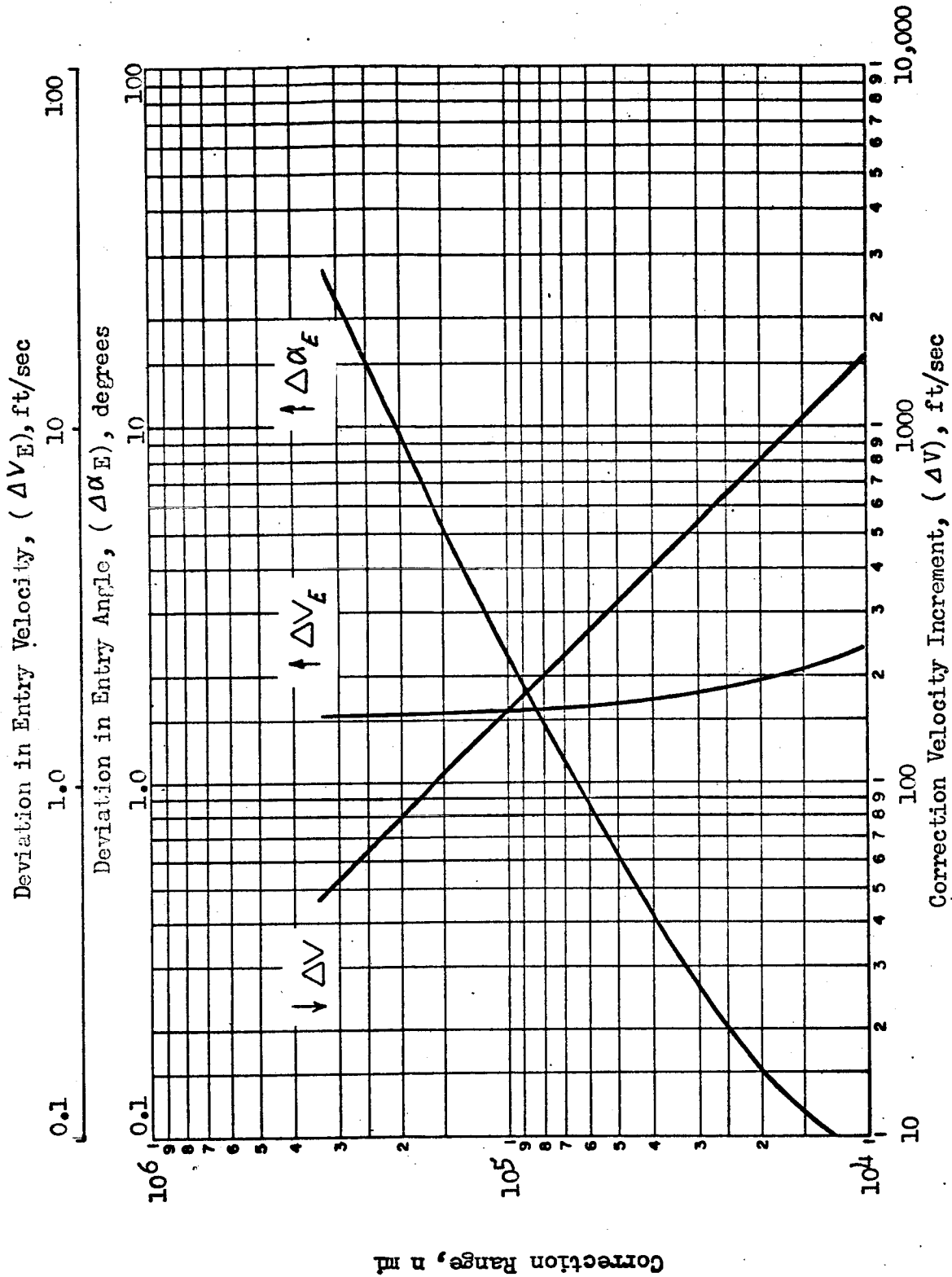


Fig.110 Terminal Correction for Mars Atmospheric Entry. (Trajectory 3)

The results indicate that for aerodynamic direct-landing maneuvers, the use of terminal correction will permit successful entry into the entry corridor and a propulsive phase for deceleration is not a requirement.

The nominal trajectory conditions and required corrections for the selected orbit-establishment and aerodynamicentry missions are summarized in Table 25 .

TABLE 25

NOMINAL CORRECTIONS FOR MARS MISSIONS

Mission	Hyperbolic Arrival Velocity, ft/sec	Deviations from Nominal Asymptotic Miss Distance, n mi	Correction Range, n mi	Correction Velocity Increment, ft/sec
Orbit Estab- lishment	12,000	2450	46,000	630
Direct Entry	11,000	2460	72,000	380
Direct Entry	34,400	475	44,000	360

The magnitudes of the required velocity increments are sufficiently small to preclude the need for dual correction schemes as were used for Earth terminal corrections.

PROPULSIVE MARS ORBIT ESTABLISHMENT AND DEPARTURE MANEUVERS

Optimization of thrust-to-weight ratios (F/W) for propulsive orbit establishment and departure maneuvers at Mars was conducted by means of the nomograph technique described earlier for Earth missions. The propulsion requirement nomograph is presented in Figure 111, and the applicable factors for introducing F/W effects are presented in Figure 112.

The variables considered were the thrust-dependent weight factor, K_E , the propellant-dependent weight factor, K_T , and specific impulse. A nominal value of hyperbolic excess velocity, corresponding closely to a minimum-energy transfer, was utilized; optimum F/W was demonstrated previously to be relatively insensitive to hyperbolic excess velocity, and it was, therefore, not treated as a variable in the present analysis.

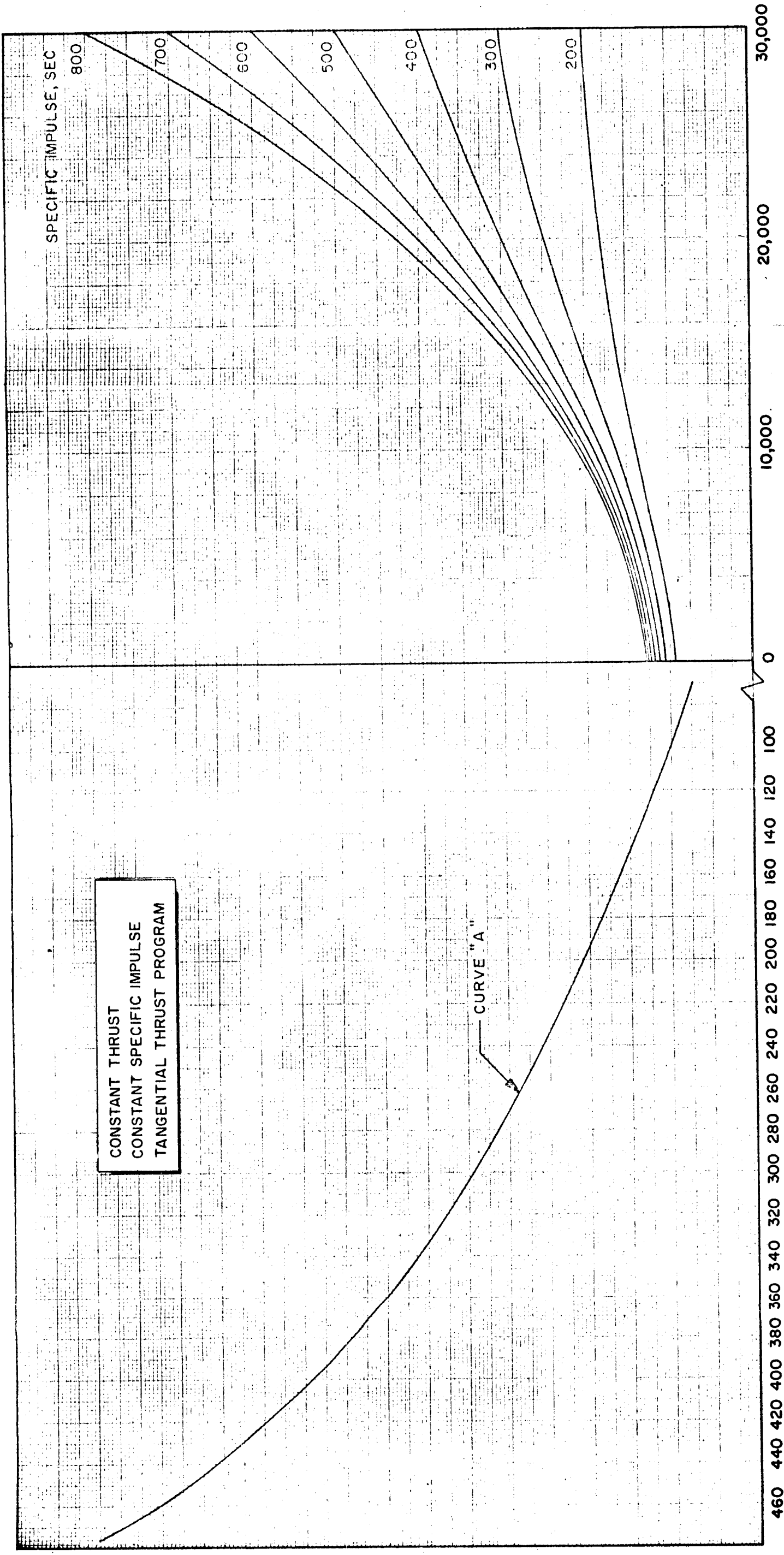
Results are presented in Figures 113, 114, 115 and 116. As in previous studies, the most significant result is the relative flatness of the payload curve in the neighborhood of the optimum point, resulting in a wide range of F/W values over which payload is close to its maximum value. This result is emphasized by the data presented in Figure 117.

The effect of hyperbolic excess velocity on payload for a Mars orbit-establishment mission is presented in Figure 118. The rapid dropoff to zero payload indicates that for high values of hyperbolic excess velocity, i.e., short Earth-Mars trips, aerodynamic braking should be employed to provide at least a portion of the total required deceleration.

MARS ORBIT ESTABLISHMENT FOLLOWING AN ATMOSPHERIC GRAZE

The feasibility of establishing a Martian orbit using an atmospheric grazing maneuver followed by a propulsive maneuver has been investigated in a similar manner to the analysis performed for Earth. The entry and exit altitude for the Martian atmosphere is 1,425,000 feet and the entry and exit angles range from 10 to 30 degrees. Three impulsive techniques for establishing an orbit following the graze maneuver have been investigated: 1) two impulse direct-to-orbit, 2) coast to apoapsis, then two impulse to orbit, and 3) a three impulse maneuver. These three schemes are discussed in further detail in the section dealing with Earth orbit-establishment maneuvers.

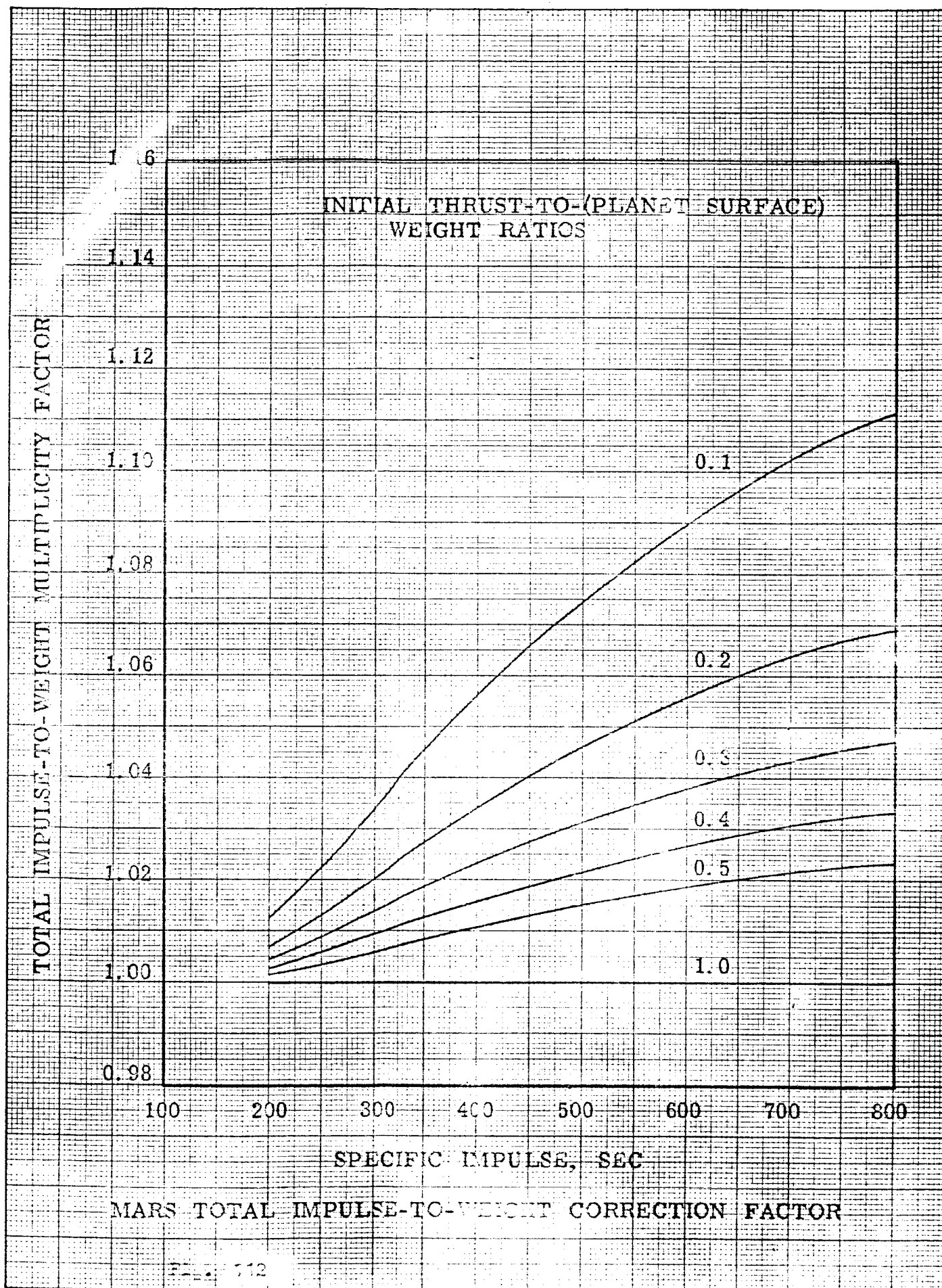
The impulsive velocity requirements for the three schemes are presented in Figures 119 through 123. A summary of the three schemes is given in Figure 124 for an exit angle of 20 degrees. The figures indicate a trend similar



MARS HYPERBOLIC EXCESS VELOCITY (V_0), FT/SEC

Figure 111 Mars Nomograph





ROCKETDYNE
A DIVISION OF NORTH AMERICAN AVIATION, INC.

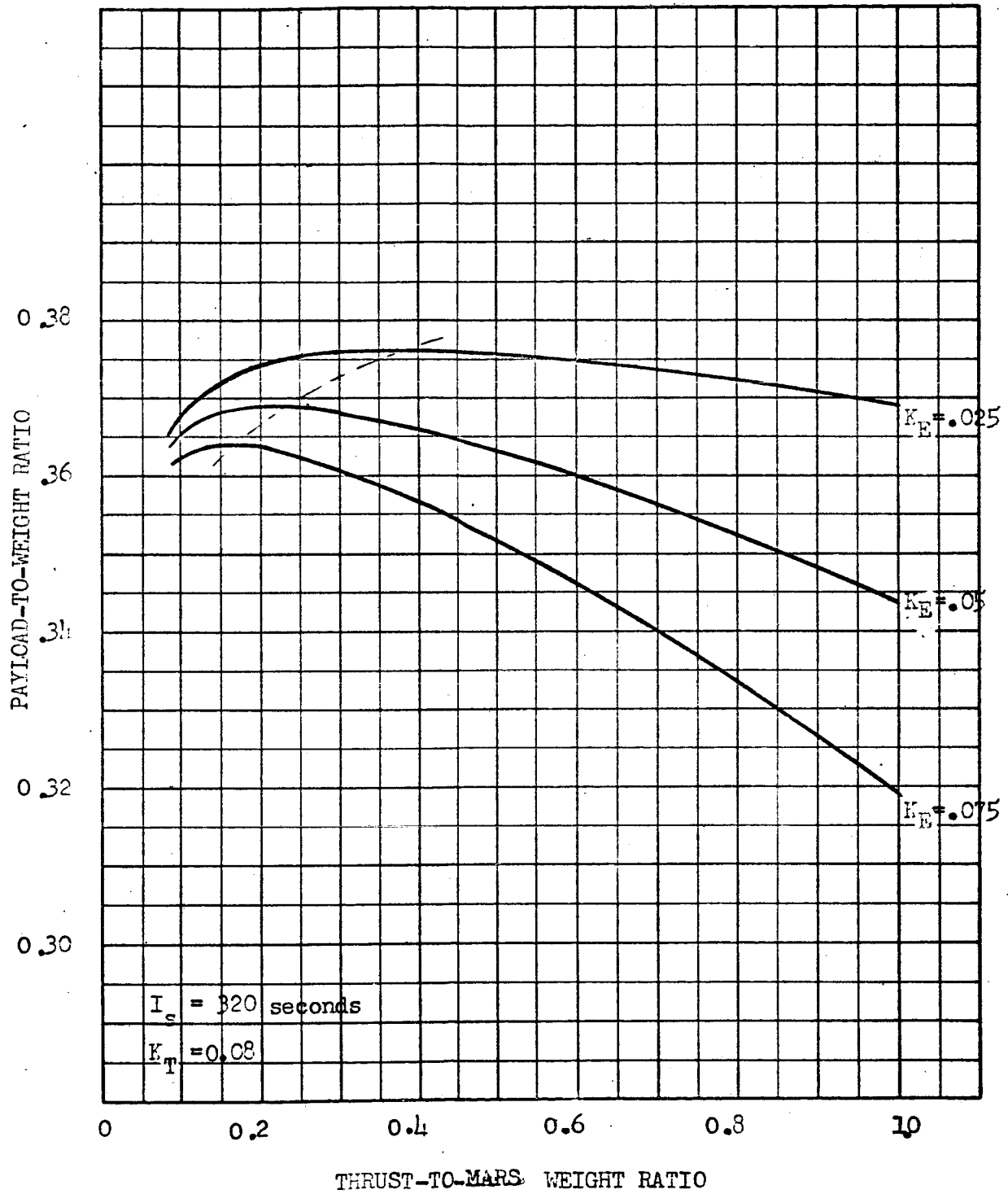


Figure 113

MARS - HYPERBOLIC EXCESS = 12,000 ft/sec

ROCKETDYNE
A DIVISION OF NORTH AMERICAN AVIATION, INC.

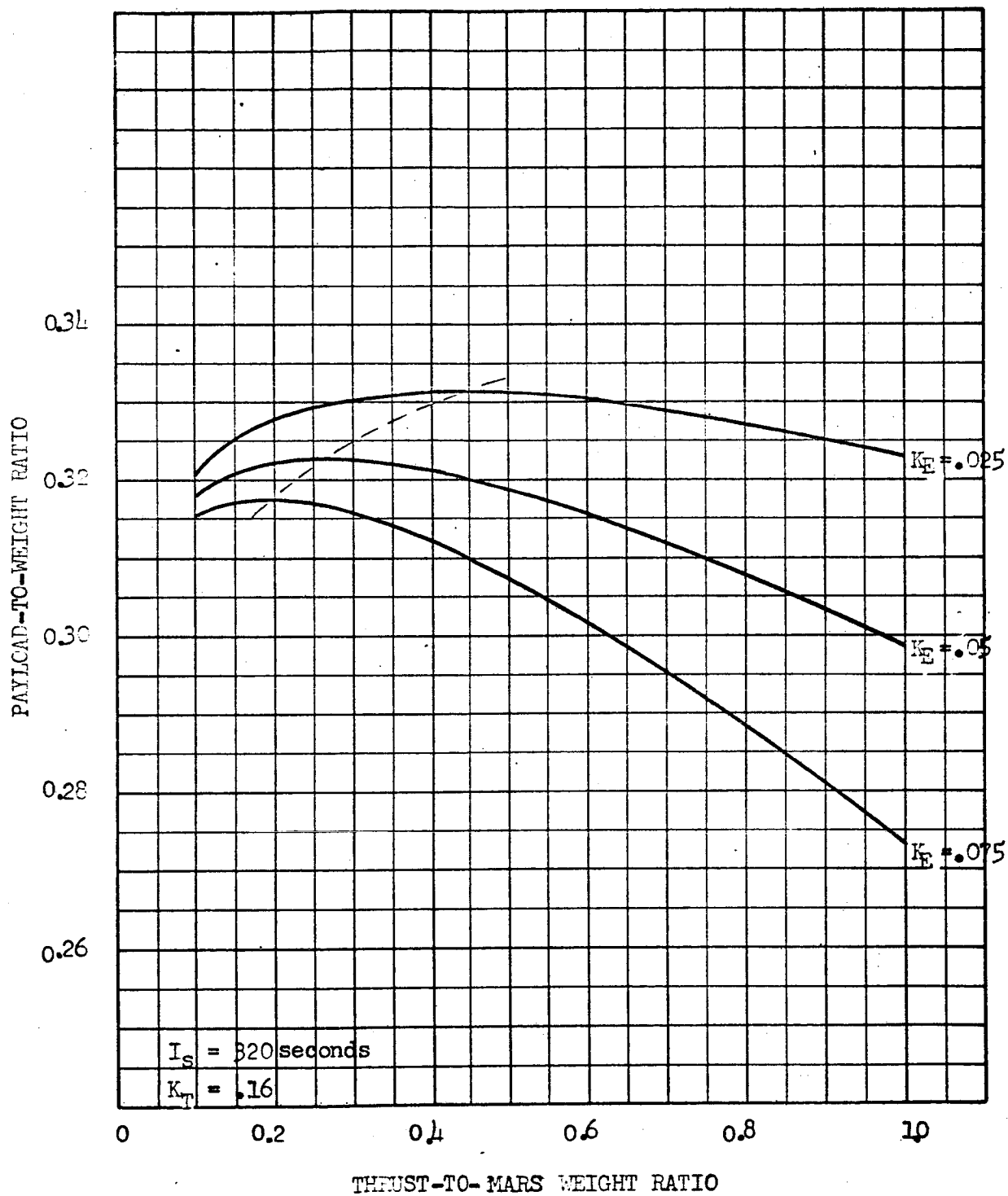


Figure 114

MARS - HYPERBOLIC EXCESS = 12,000 ft/sec

ROCKETDYNE
A DIVISION OF NORTH AMERICAN AVIATION, INC.

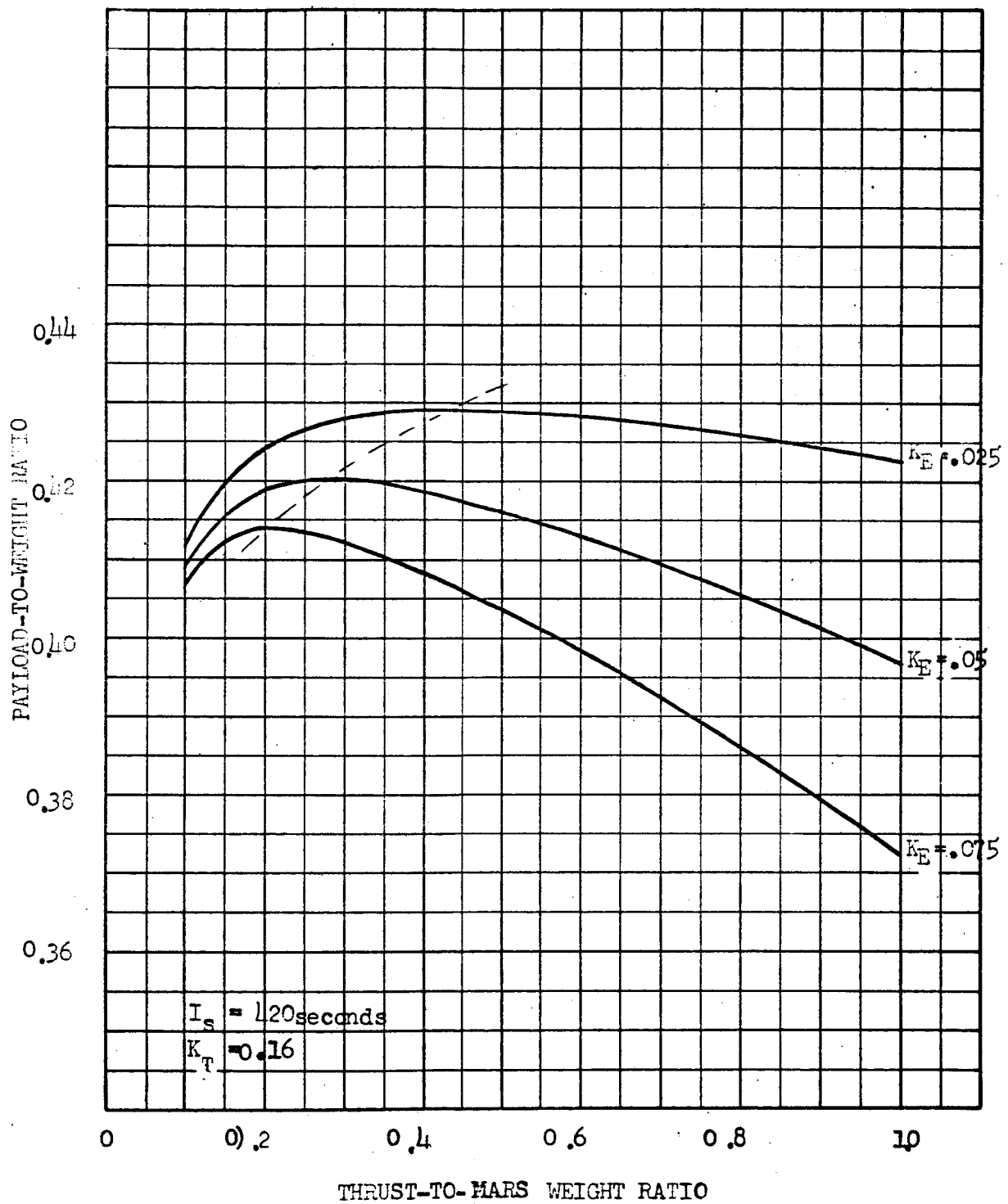


Figure 115

MARS - HYPERBOLIC EXCESS = 12,000 ft/sec

ROCKETDYNE
A DIVISION OF NORTH AMERICAN AVIATION, INC.

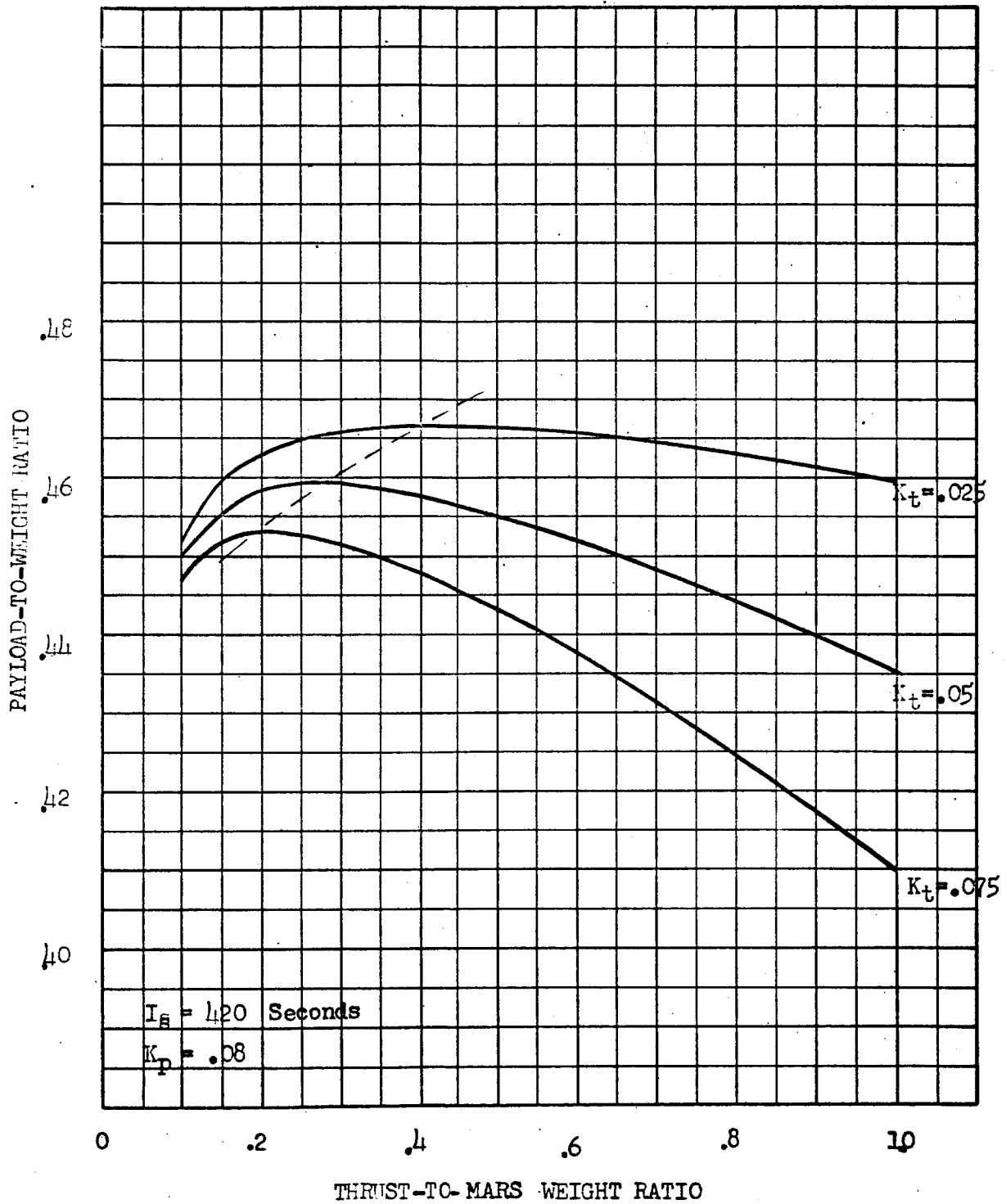


Figure 116

MARS - HYPERBOLIC EXCESS = 12,000 ft/sec

Nominal Vehicle: $I_s = 420 \text{ sec}$, $K_T = 0.16$,
 $K_E = 0.05$, $V_h = 12,000 \text{ ft/sec}$

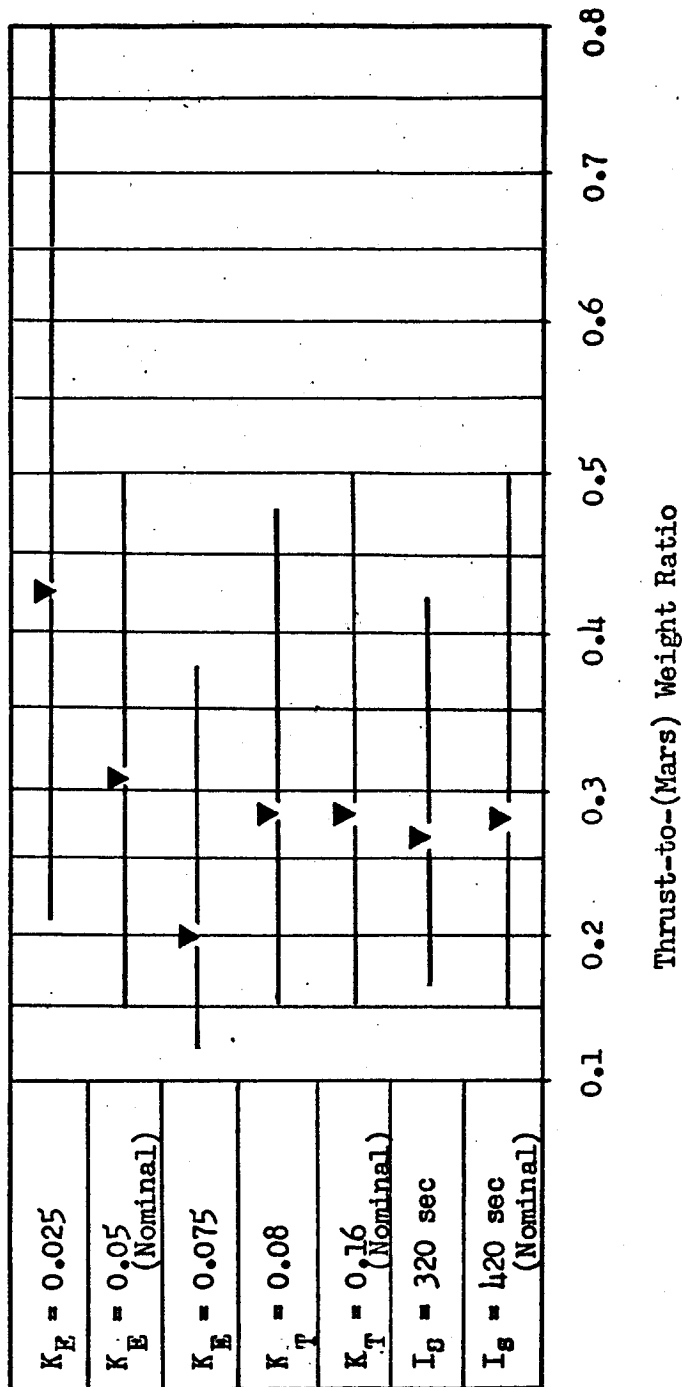


Figure 117 Thrust-to-Weight Ratio Variation for a One-Percent Change in Payload for Mars Orbit Establishment or Departure Maneuver.

ROCKETDYNE
A DIVISION OF NORTH AMERICAN AVIATION, INC.

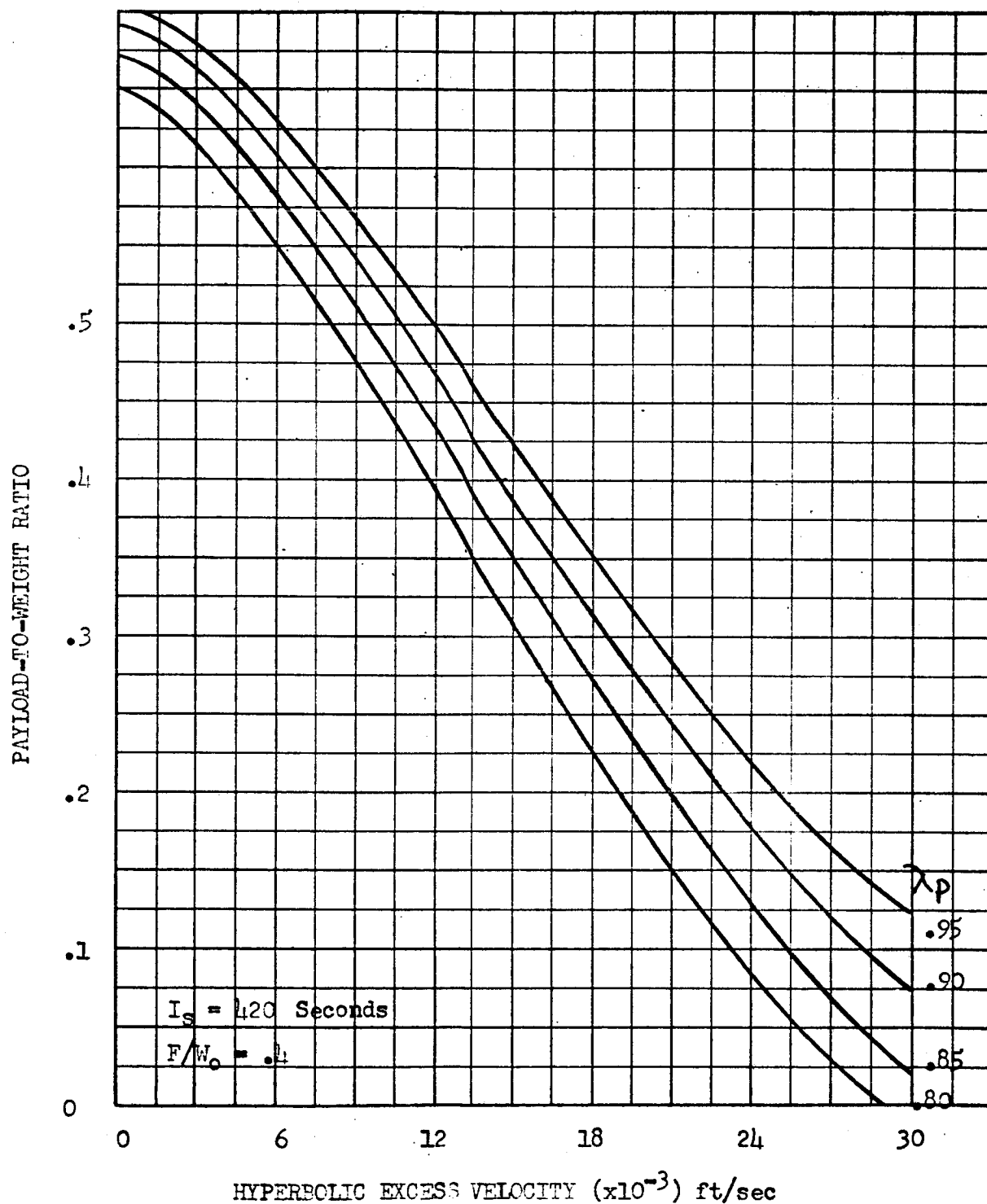


Figure 118
MARS PAYLOAD VS. HYPERBOLIC EXCESS

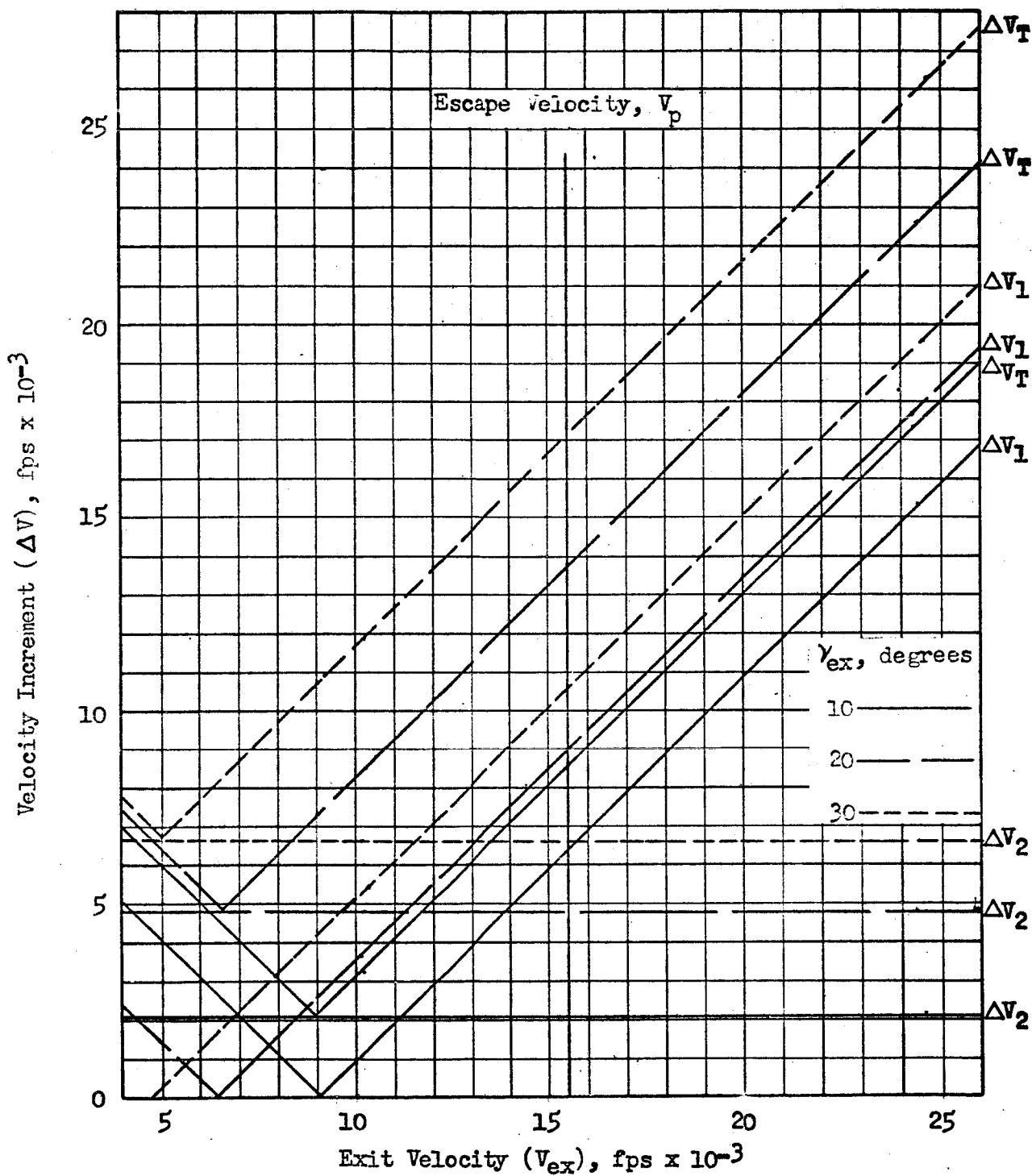


Fig.119 Velocity Requirements for Establishing a 300 n mi Orbit at Mars, Scheme 1.

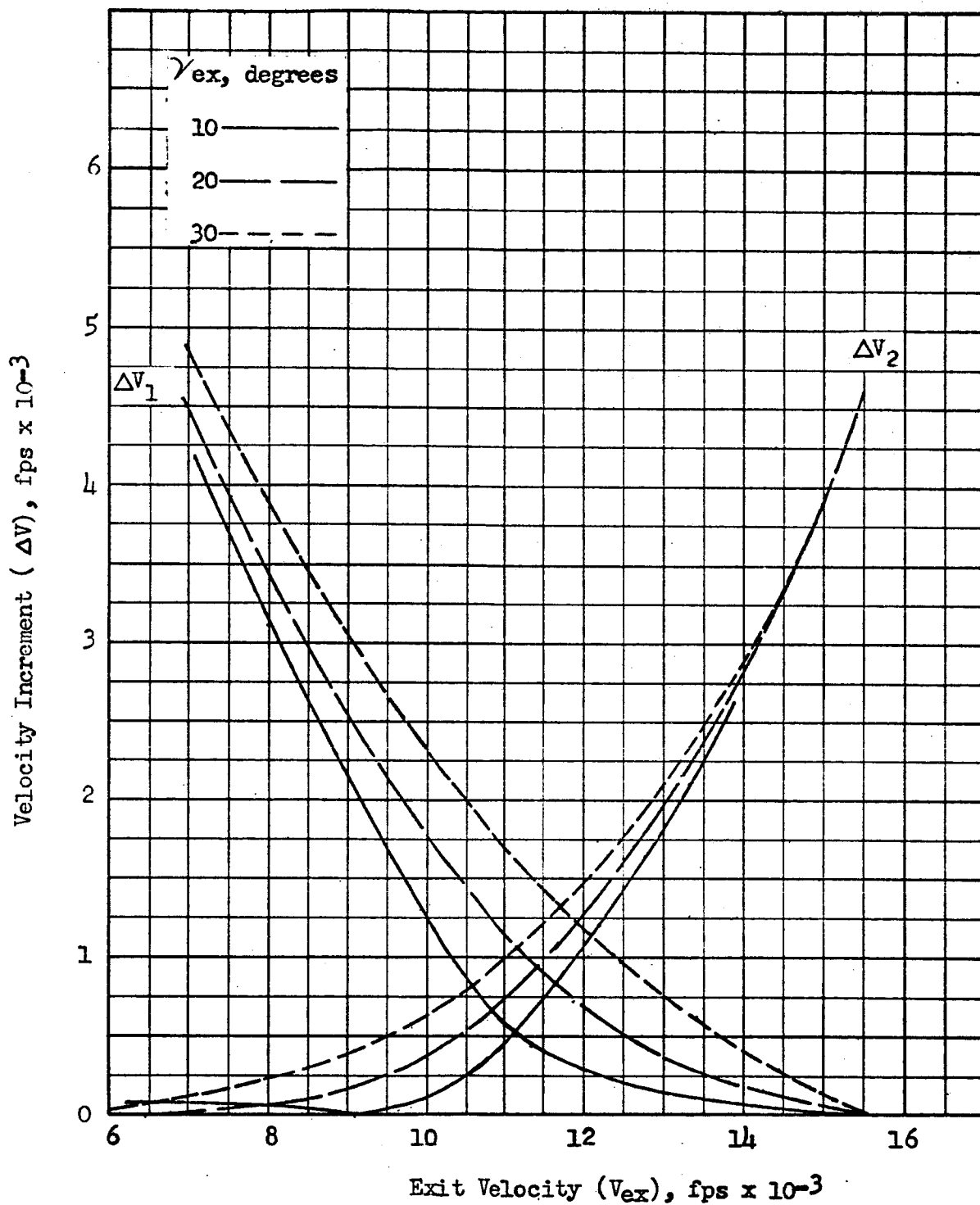


Fig. 120 Velocity Increments for Establishing a 300 n mi Orbit at Mars, Scheme 2.

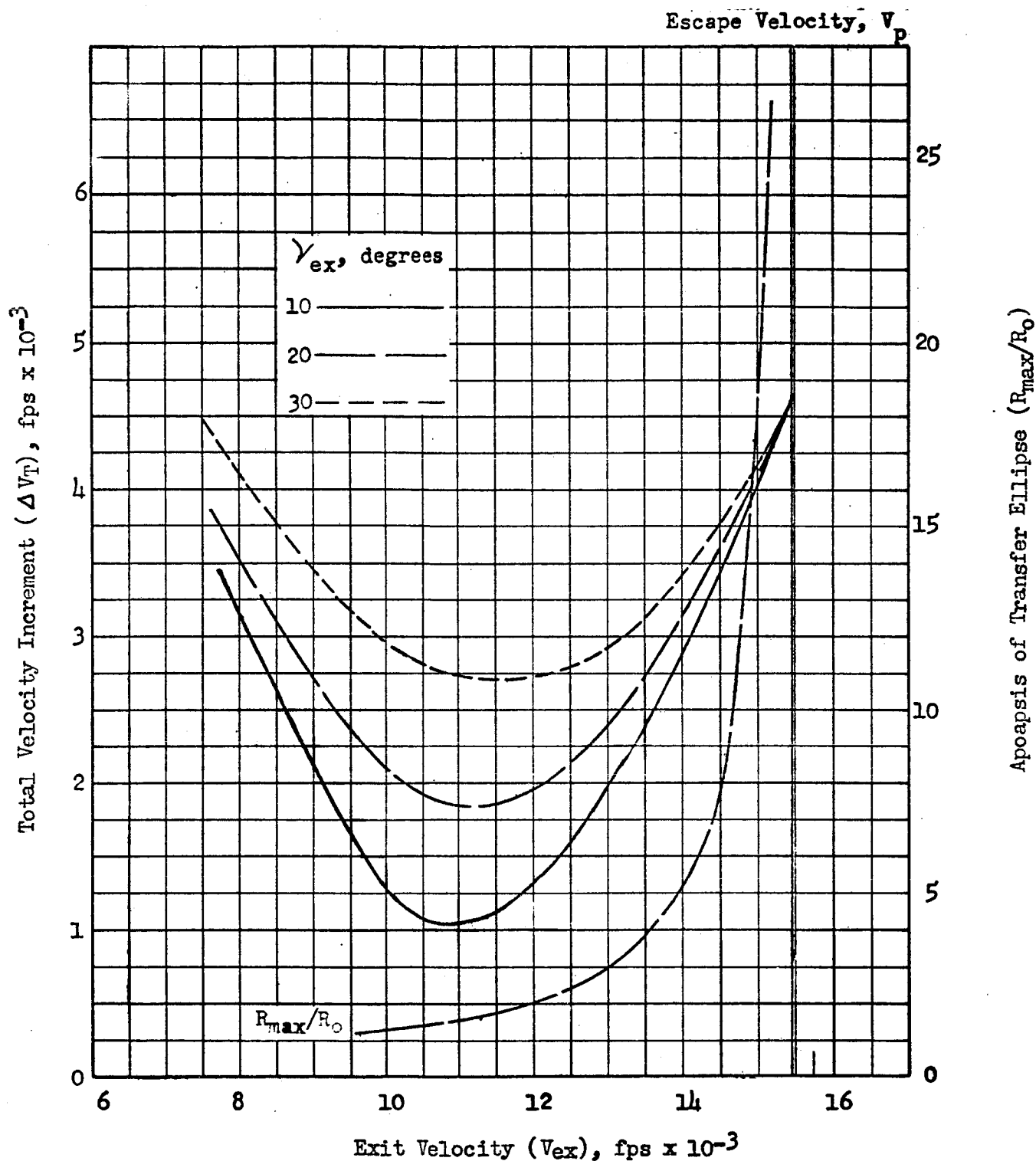


Fig. 121 Total Velocity Requirements for Establishing a 300 n mi Orbit at Mars, Scheme 2.

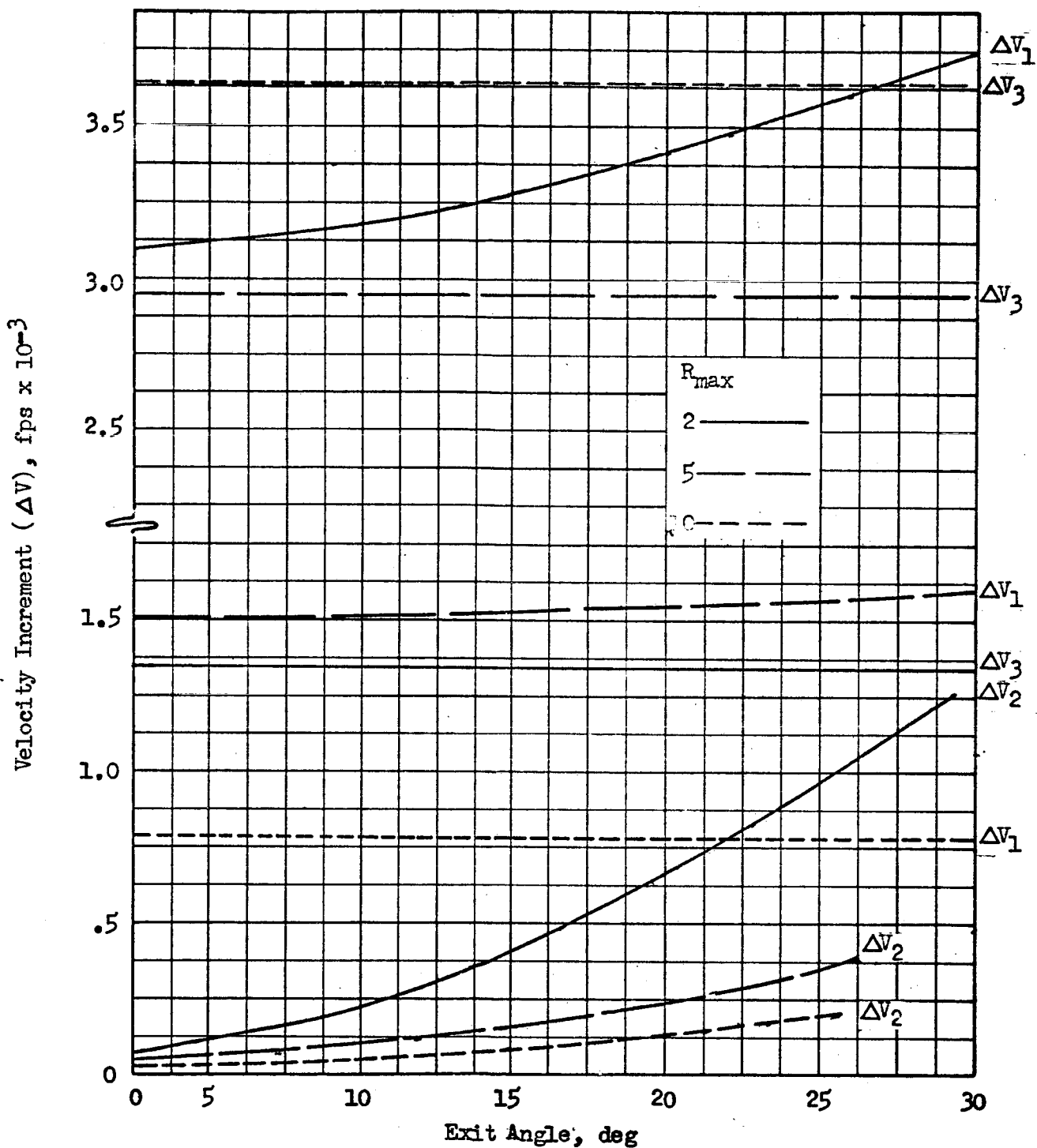


Fig. 122 Velocity Increments for Establishing a 300 n mi Orbit at Mars, $V_{ex} = V_p = 15,462$ fps, Scheme 3.

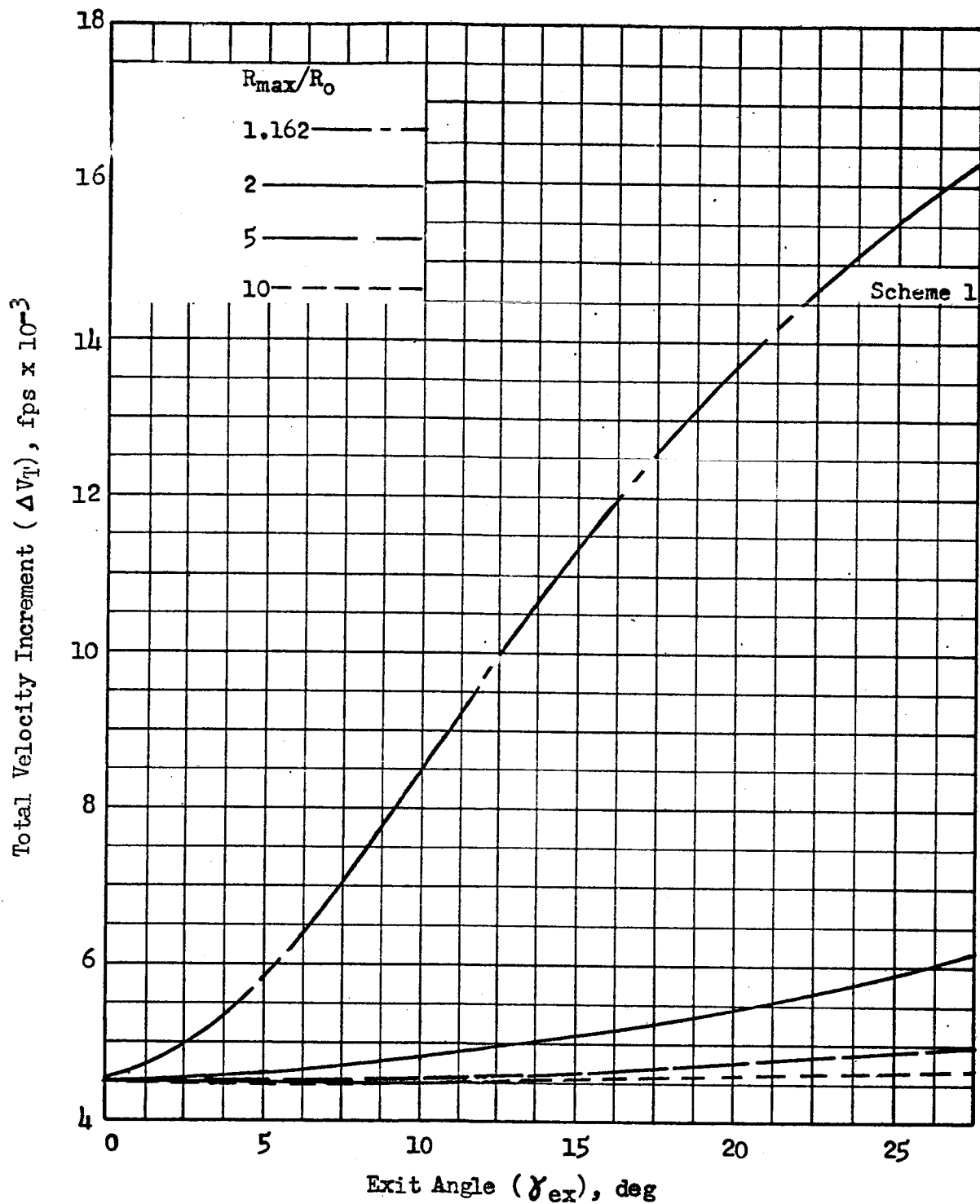


Fig. 123 Total Velocity Requirements for Establishing a 300 n mi Orbit at Mars, $V_{\text{ex}} = V_p = 15,462$ fps, Scheme 3.

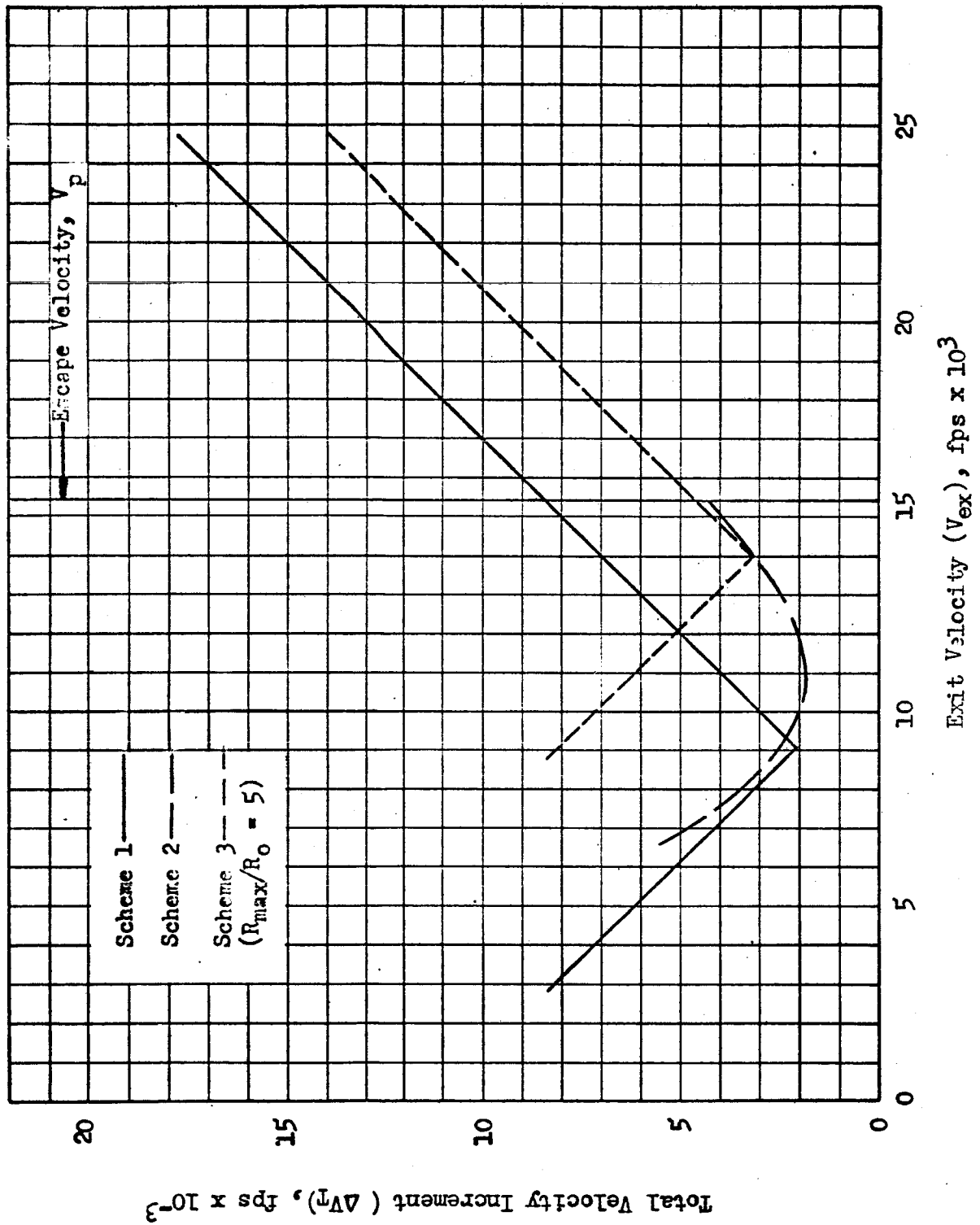


Fig.124 Summary of Impulsive Velocity Requirements for Establishing a 300 n mi Orbit at Mars, $\gamma_{ex} = 20$ degrees

to that noted in the Earth analysis in that schemes 2 and 3 yield the lowest velocity requirements over most of the range of exit velocities. Scheme 2 for exit velocities less than 14,000 ft/sec and Scheme 3 for exit velocities greater than 14,000 ft/sec.

The applicability of the atmospheric graze maneuver to a given mission will depend on the vehicle configuration and constraints (i.e., maximum g limit, heat shielding, etc.). If the vehicle is capable of executing the graze maneuver, considerable saving in propulsive energy can be realized over a direct orbit establishment maneuver. Since the velocity requirements for orbit establishment following the graze may be approximated by the difference between exit (from the graze) and orbital velocities, the propulsion requirements for a combined graze and propulsion maneuver are less than that of the direct propulsive maneuver by approximately the amount of velocity reduction achieved by the graze.

PROPULSIVE/AERODYNAMIC BRAKING MANEUVER FOR MARS ENTRY

The analytical techniques and assumptions required for the analysis of propulsive/aerodynamic landings were described in detail for Earth re-entry systems, and do not warrant additional discussion at this juncture. In general, the results can be stated in a manner similar to the Earth re-entry results: if the resulting ablation weight characteristics agree with the current estimates, propulsive deceleration is not required for achievement of maximum payload.

The results of a parametric study of a Mars entry vehicle are presented in Figure 125. The optimum propulsive ΔV for a mission characterized by a particular hyperbolic excess velocity is equal to the vertical distance between the arrival velocity curve and the optimum entry velocity curve for the appropriate ablation characteristic.

MARS TERMINAL DECELERATION PHASE SYSTEMS

The presence of an atmosphere about Mars indicates that parachute/retro-rocket/impact device systems such as those described earlier for Earth landings are applicable to the terminal deceleration phase of a Mars landing. Appropriate expressions for parachute and retrorocket weights were obtained from previous results by replacing values of the Earth gravitational constant and atmospheric density with the corresponding Mars values.

Pararocket System

For a Mars landing, a parachute system is not as efficient as for Earth since the atmospheric density at the surface of the planet is considerably less than that of Earth. The combination of the less dense atmosphere and the smaller gravitational force shifts the optimum parachute terminal velocity to a higher value.

The same system parameters were varied as in the case for the Earth landing system. The effect of parachute terminal velocity and rocket F/W on system weight for impact velocities of 10 and 25 ft/sec respectively are presented in Figures 126 and 127. The optimum pararocket system weights and optimum F/W values obtained from Figures 126 and 127 are presented in Figures 128 and 129 respectively.

For a design impact velocity of 10 ft/sec and nominal weight assumptions, the optimum V_T is 120 ft/sec (Figure 128) and the optimum rocket F/W is 0.925 (Figure 129). Under these conditions, the pararocket system is 4.4 percent of the vehicle weight. The corresponding data for a 25 ft/sec impact velocity are 120 ft/sec, 0.85 and 4.0 percent for V_T , F/W and percent of vehicle weight respectively.

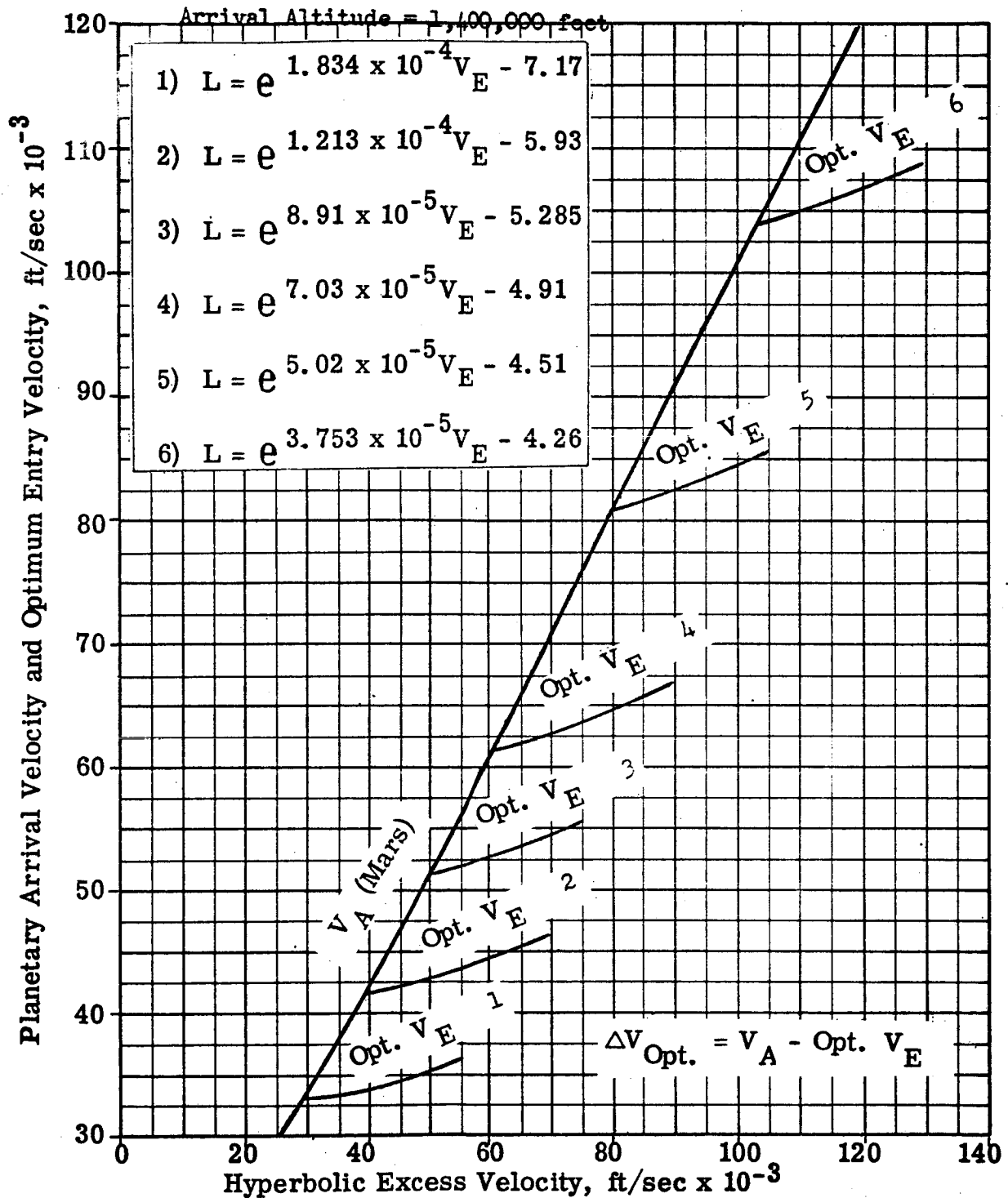


Fig. 125 Optimum Propulsive ΔV (Impulsive) for Mars Entry of Propulsive/Aerodynamic Systems.

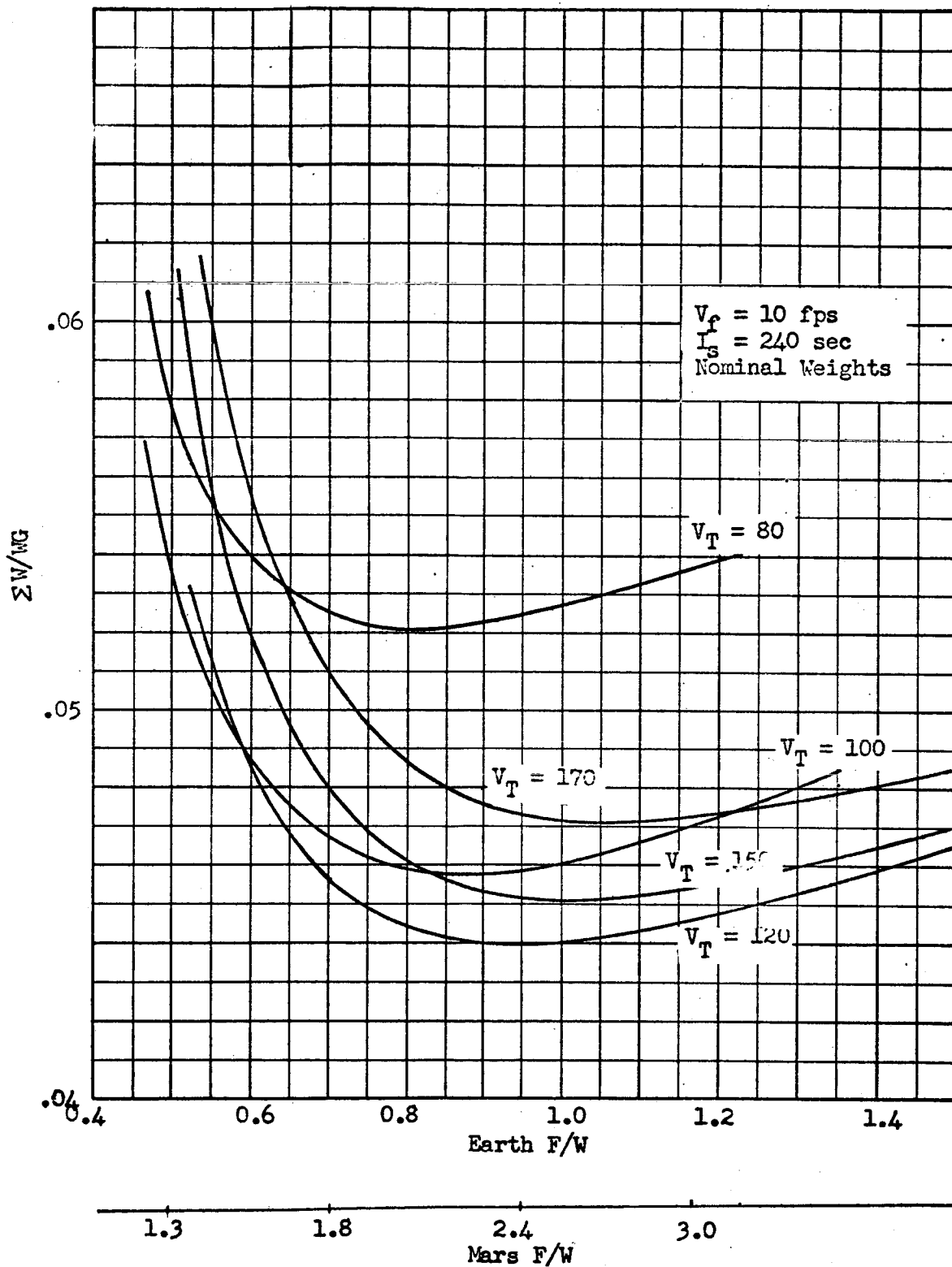


Figure 126. Effect of Parachute Terminal Velocity and Rocket F/W on Pararocket System Weight for a Mars Landing.

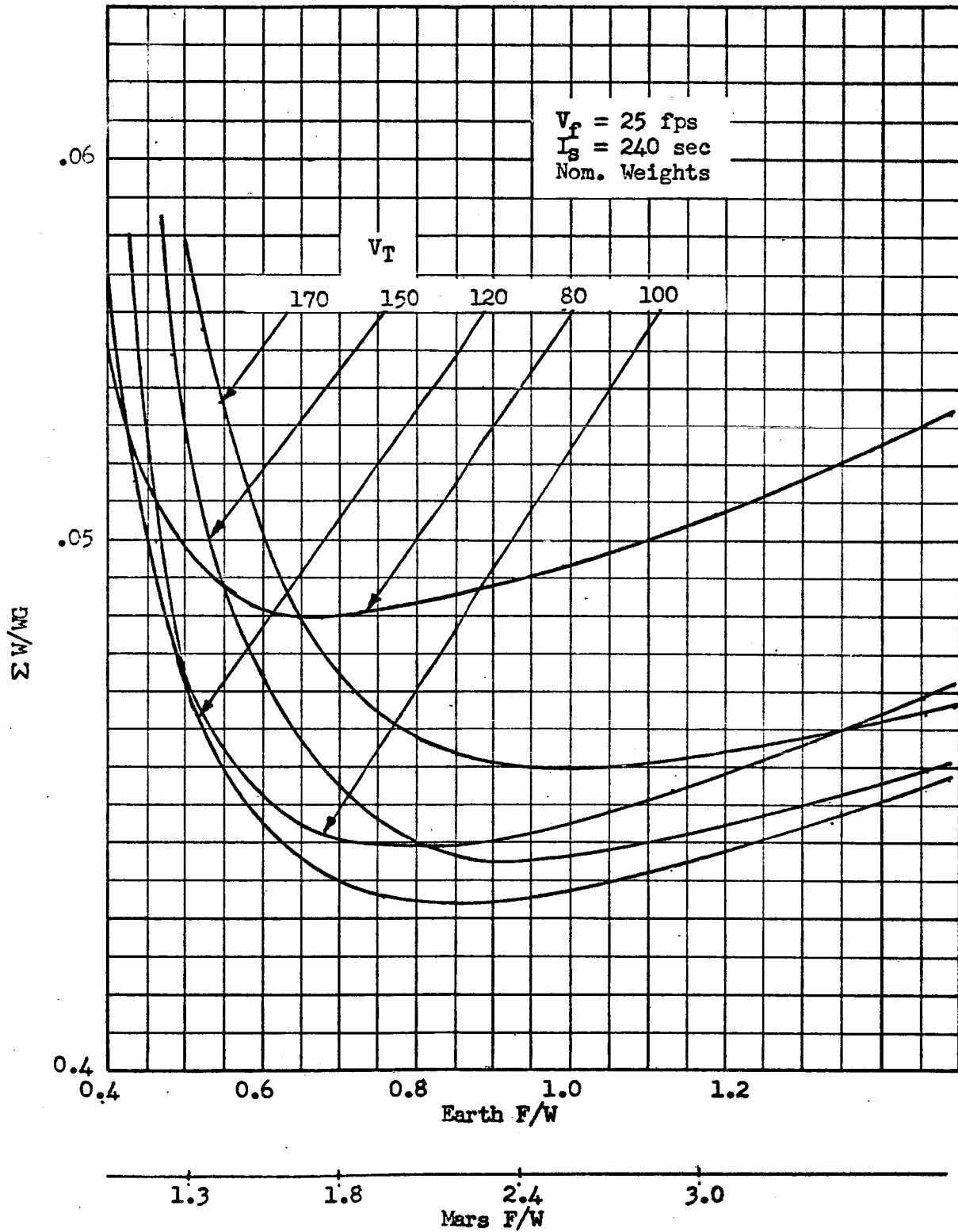


Figure 127 . Effect of Parachute Terminal Velocity and Rocket F/W on Pararocket System Weight for a Mars Landing

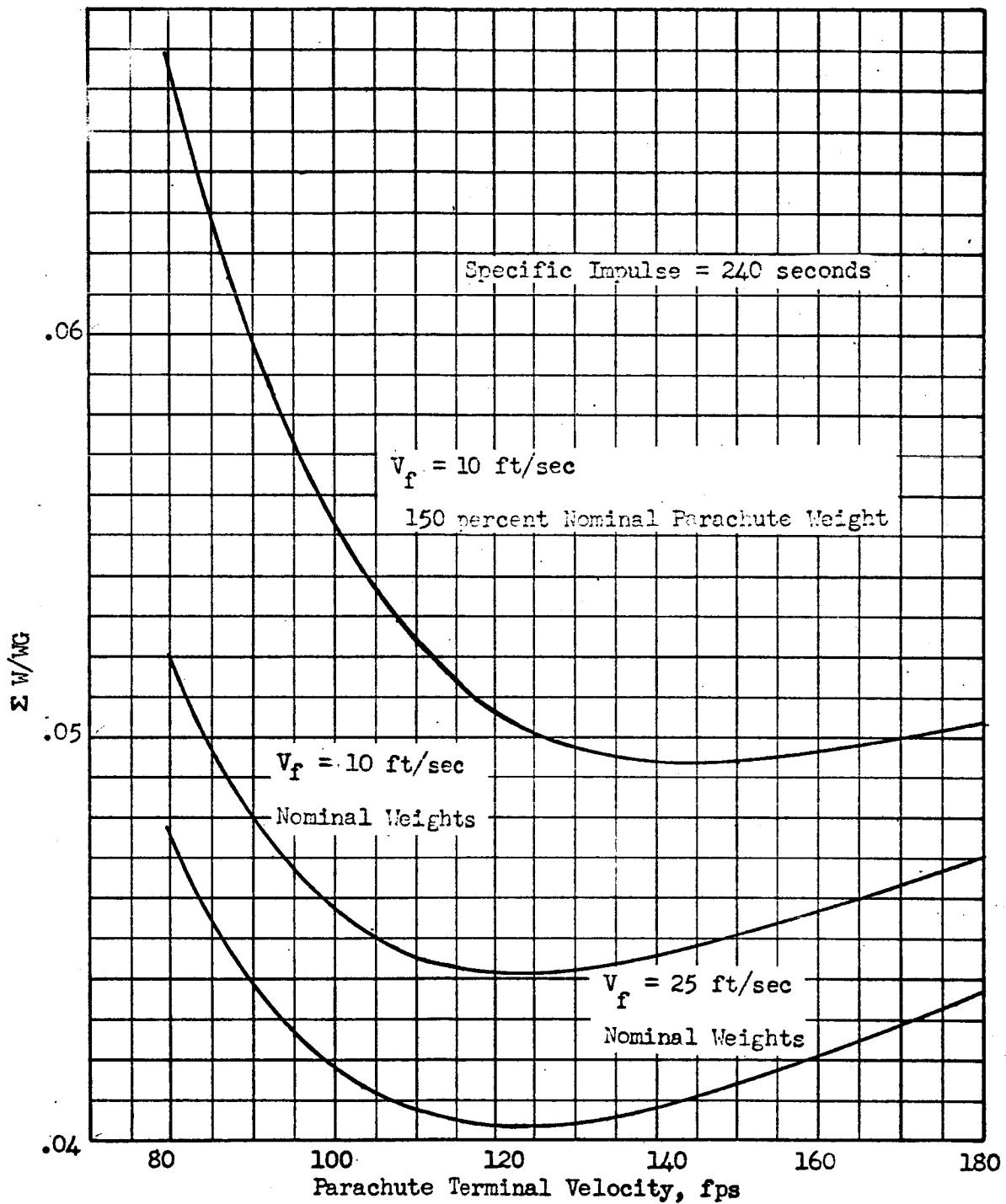


Figure 128 . Optimum Pararocket System Weight vs Parachute Terminal Velocity for Mars Landing.

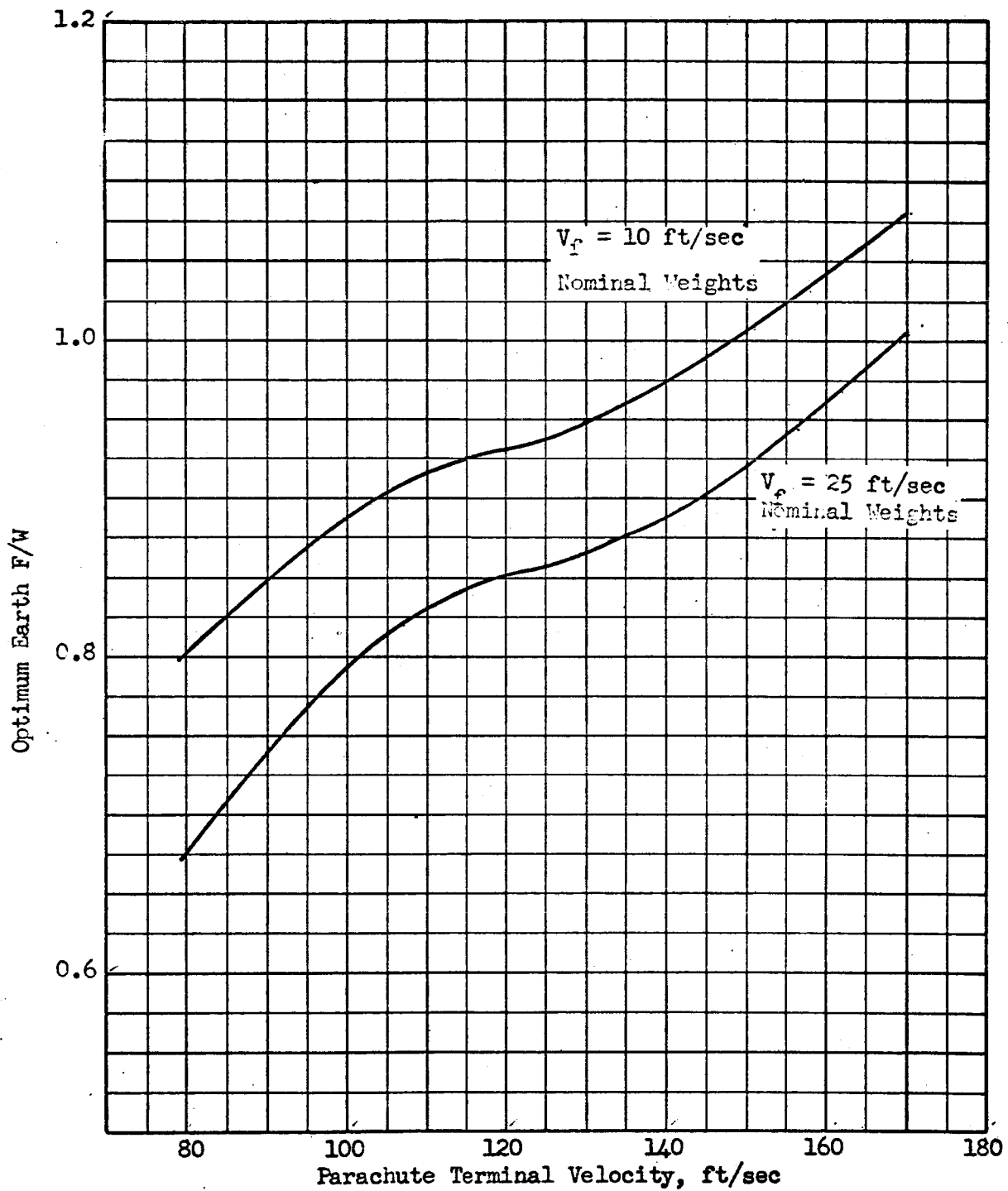


Figure 129. Optimum F/W vs Parachute Terminal Velocity for a Mars Landing

Parachute/Retrorocket/Impact Device System

The optimum parachute terminal velocity and rocket F/W of a pararocket system for a Mars landing are presented in Figure 130 as a function of impact velocity. The weights of these optimum systems, along with the weights of parachutes and frangible-tube impact devices alone, are shown in Figure 131. The low density of the Martian atmosphere results in excessively heavy parachutes for possible parachute/impact device systems. This combination was therefore examined only briefly for use in the Mars landing application. The pararocket/impact device weights were combined to obtain the overall weight of the terminal deceleration system as a function of impact velocity. The results, presented in Figure 132, indicate an optimum impact velocity of 35 ft/sec, though a variation of ± 15 ft/sec can be applied without significantly penalizing the weight of the landing system. The optimum combined pararocket/impact device system constitutes approximately 4.7 percent of the landing vehicle weight.

Effect of Off-Optimum Operation of the Retrorocket. For a Mars landing, the optimum system (a pararocket and a frangible-tube impact device) has an impact velocity of 35 ft/sec. The optimum parachute V_T is approximately 120 ft/sec and the optimum rocket F/W is approximately 0.80. If the retro-rocket operates under nominal conditions, the ignition occurs 256 feet above the surface and the burning time is 3.3 seconds. For this preliminary analysis, the deceleration during retrorocket operation was assumed to be constant.

If the rocket thrust is increased 5 percent, and it fires until touchdown, the impact velocity will be 25 ft/sec assuming 5 percent additional propellant is available. If the thrust is decreased by 5 percent, the vehicle will strike the ground at 45 ft/sec, before the 3.3 firing time has elapsed.

If ignition occurs 1 second early (4.3 seconds before touchdown), the desired impact velocity will occur above the surface. Assuming that the rocket operates at design thrust, the vehicle will continue to decelerate to an impact velocity of 9 ft/sec at touchdown, again providing sufficient propellant is available. If the ignition occurs 1 second early, and the engine fires for the nominal 3.3 second period, the design impact velocity (35 ft/sec), and burnout, will occur 48 feet above the surface. The vehicle will then have a parachute-drag force acting on it and the impact velocity will be slightly higher than 35 ft/sec.

If ignition occurs 1 second late, the vehicle will not decelerate to the desired impact velocity and would strike the surface at approximately 60 ft/sec. Design of the frangible-tube system for 60 ft/sec rather than 35 ft/sec impact would increase its weight from 0.9 to 1.6 percent of the gross weight.

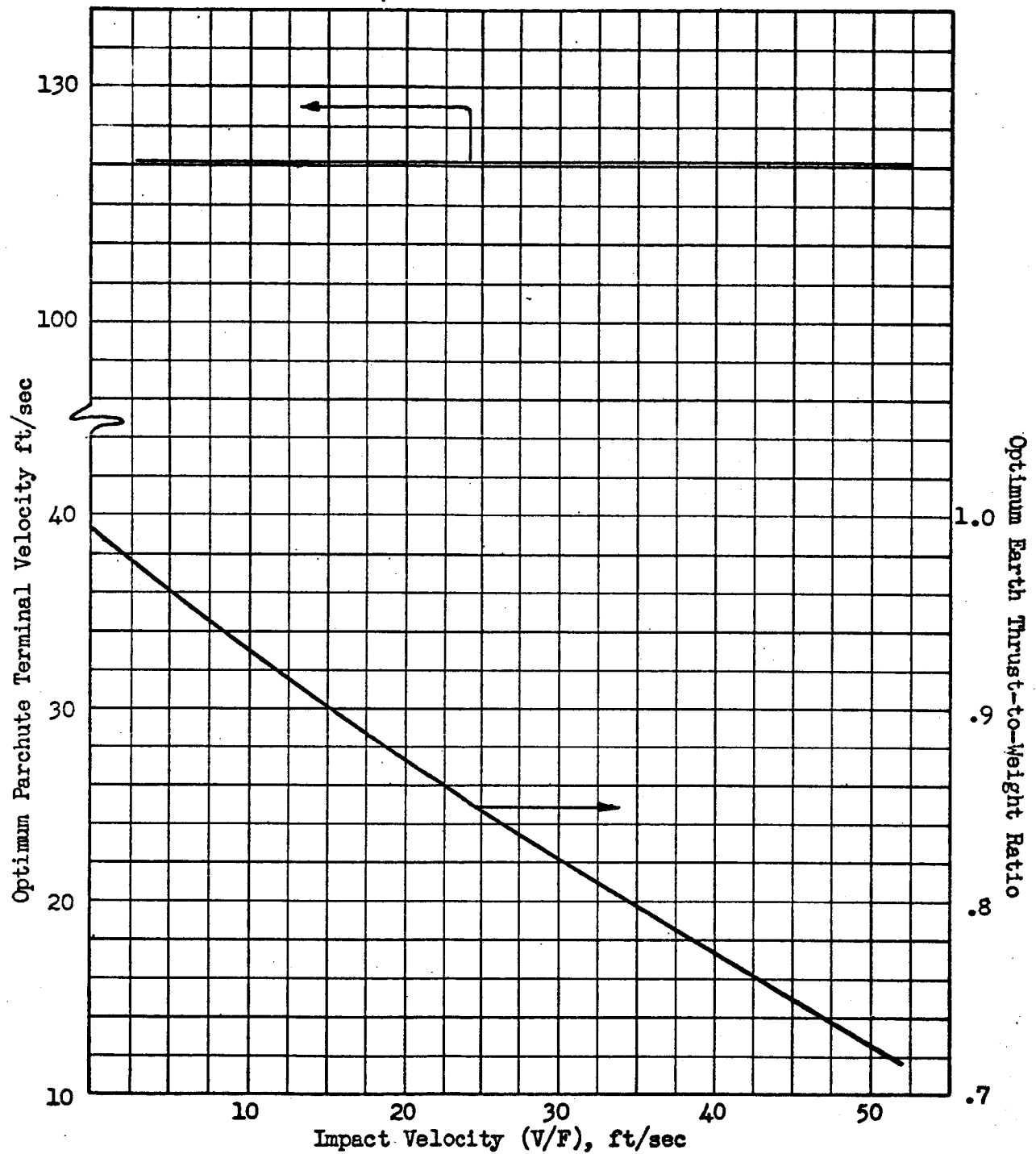


Figure 130 . Optimum Terminal Velocity and Rocket Thrust-to-Weight Ratio For Pararocket System (Mars)

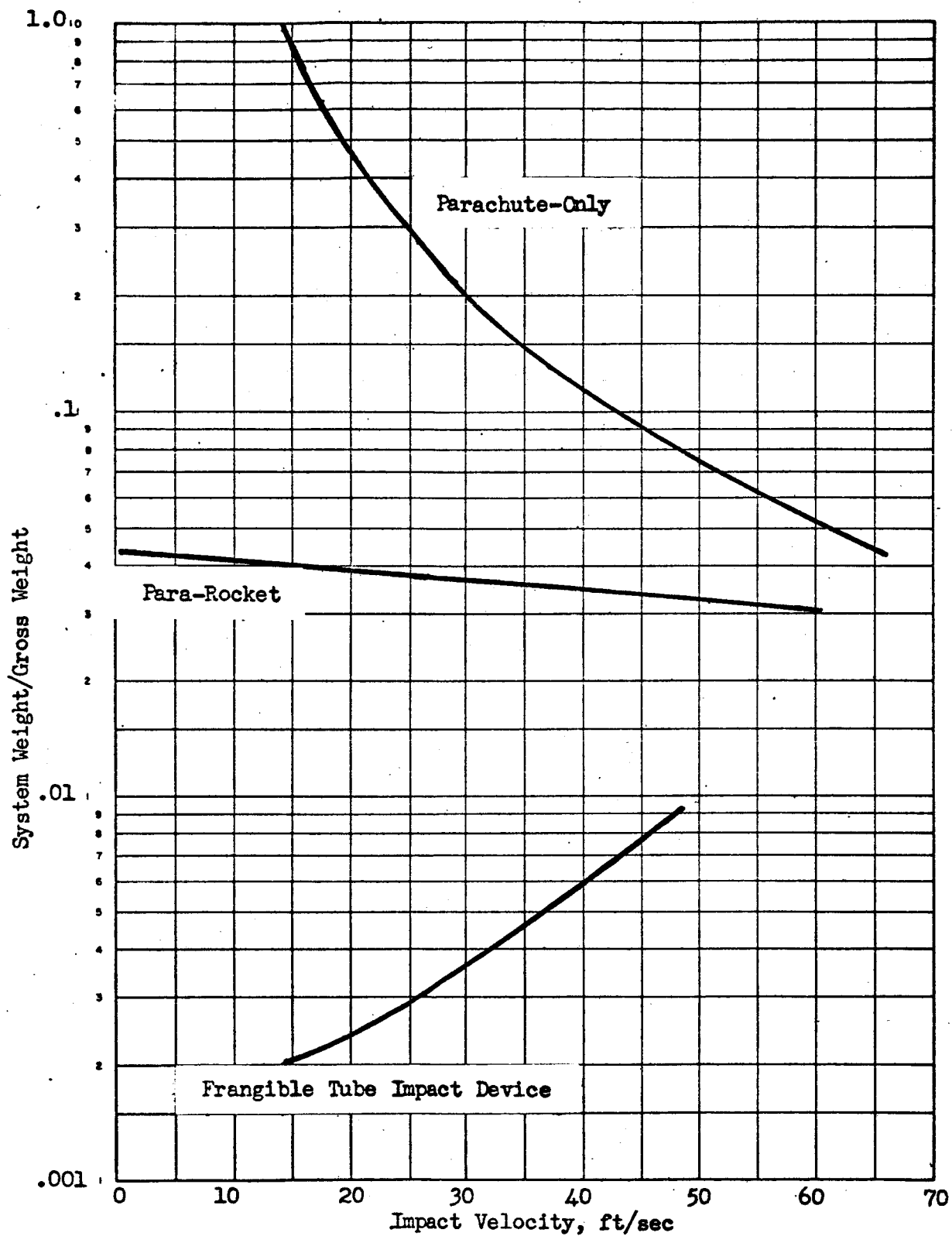


Figure 131. Landing System Weights (Mars)

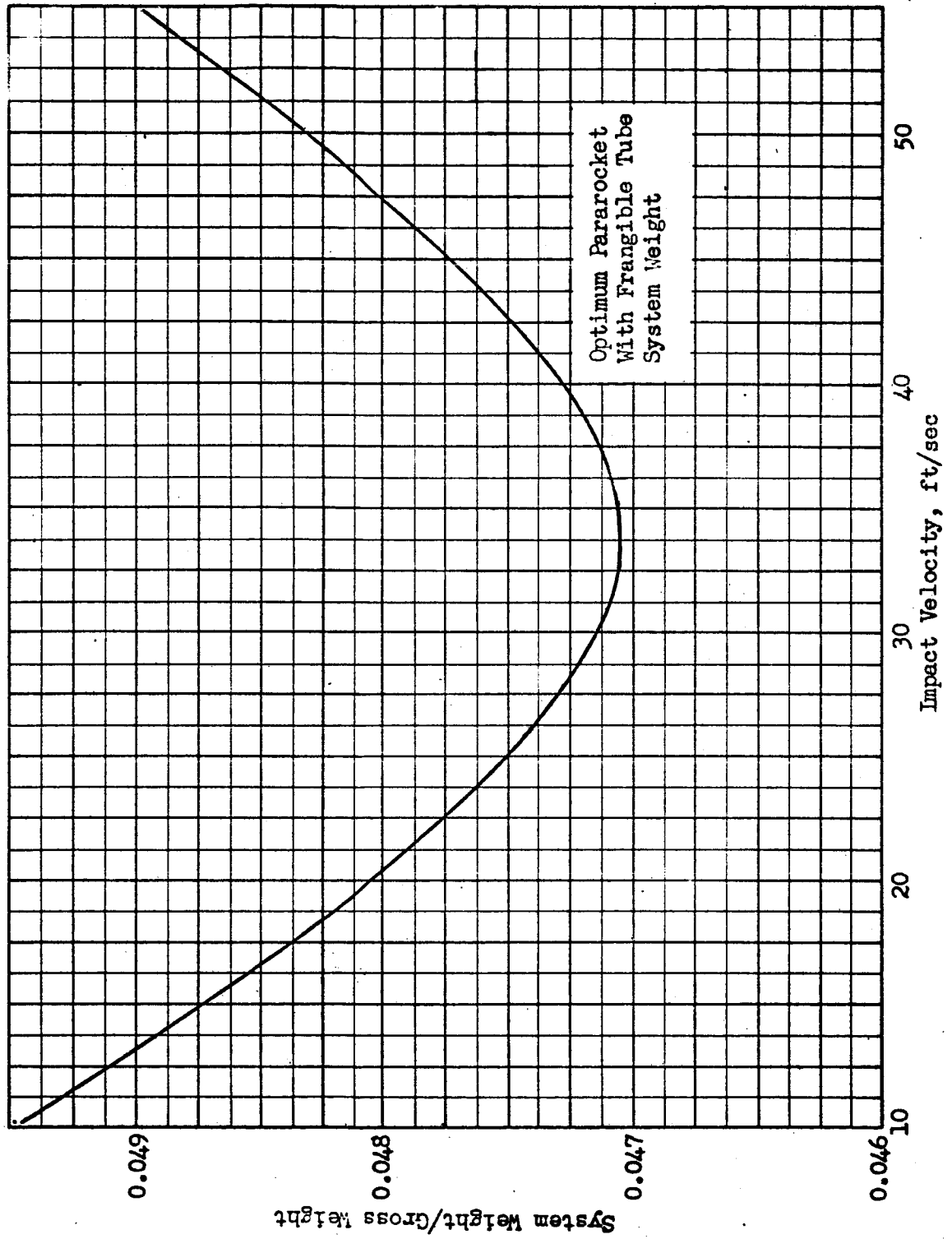


Figure 132 . Optimization of Combined Pararocket and Frangible Tube Mars Landing System

Thus, actual overall system weight would be 5.6 percent of gross weight rather than the 4.7 percent gross weight shown previously. The 1-second variation in time used in this analysis is probably somewhat high, but the preliminary results emphasize the fact that late ignition is a critical item.

System Selection

The results indicate that for design impact velocities below 75 ft/sec, the pararocket system (parachute plus retrorocket) results in a lower system weight than use of a parachute only. (This result was computed but is not shown in the figures presented.) Approximate optimum values of the thrust-to-(Earth) weight of the retrorocket and the terminal velocity of the parachute, based on a design impact velocity of 10 ft/sec, are 0.9 and 120 ft/sec respectively; the optimum pararocket represents 4.4 percent of the landed gross weight. The lightest overall system obtained was a pararocket/impact device combination with an impact velocity of 35 ft/sec, a rocket F/W of 0.8, and a parachute terminal velocity of 120 ft/sec; the system constituted 4.7 percent of the landed weight .

A summary of the minimum-weight systems for the optimum impact velocity, and for impact velocities of 10 ft/sec and 25 ft/sec, is presented in Table 26 .

TABLE 26
COMBINED SYSTEM WEIGHTS

	Optimum $V_F = 35$ ft/sec	$V_F = 10$ ft/sec	$V_F = 25$ ft/sec
Minimum Weight Configuration	Pararocket/Impact device	Pararocket/Impact device	Pararocket/Impact device
Percent Gross Weight	4.7	5.0	4.8

Preliminary analysis of the retrorocket indicates that the most critical conditions are low thrust level operation or late ignition. Both these conditions result in impact velocities considerably above the expected value. Thus in the actual design, the impact energy absorbing device must be designed with an adequate margin for errors in impact velocity.

MARS PROPULSIVE TAKEOFF AND LANDING

Advanced planetary missions include landings on, and takeoffs from, the planet Mars. The takeoffs must be propulsive maneuvers. Although the propulsive aerodynamic braking analysis has shown that aerodynamic deceleration is, in general, more efficient, early missions may, because of atmospheric uncertainties or mission philosophy, use a propulsive landing. Therefore, propulsive landings and takeoffs were investigated. Integrated trajectories for a Mars takeoff to a 300-n mi circular orbit and for a Mars propulsive landing from a 50-n mi circular orbit were determined in the present study. An O_2/H_2 vehicle was assumed in all cases. Both the launches and the landing were assumed to take place in the direction of planetary rotation at the planetary equator.

Trajectory Characteristics

Takeoff Maneuvers. In the type of simulated takeoff trajectory considered, the vehicle first rises vertically. The vehicle then turns, and the flight continues with thrust parallel to velocity. If necessary, in order to prevent negative flight path angles, the thrust parallel-to-velocity maneuver is terminated and a constant-altitude, variable thrust-orientation-angle maneuver is used for the remainder of this propulsive phase. The maneuver is terminated when the vehicle has sufficient velocity to coast to the desired orbital altitude. After the coast-to-orbit altitude, a constant-altitude, variable thrust-orientation-angle maneuver increases the vehicle velocity to orbital velocity. The angle through which the vehicle turns to initiate the thrust parallel-to-velocity maneuver is optimized to determine the maximum payload the vehicle will deliver.

Landing Maneuvers. In the simulated continuous-powered landing trajectory considered for the Mars propulsive landing, the vehicle first decelerates from orbital velocity using a constant altitude, variable thrust-orientation-angle maneuver. Following this maneuver, the vehicle enters a thrust parallel-to-velocity maneuver which continues until the vehicle is near the planet surface with a low velocity. The vehicle then turns and descends vertically to the surface.

The planetary landing considered in this study takes the vehicle to a point near the surface with zero velocity. The final hover-translation phase of the landing was not included.

Vehicle Description

A single stage vehicle was selected for both the Mars landing and takeoff, since velocity requirements are in the range efficiently performed by a single stage. Vehicle thrust-to-Mars weight ratios between 1.2 to 2.0 were considered. For the Mars takeoff, which was considered to be the maneuver of primary interest, the stage jettisoned weights were determined using thrust-dependent (K_P) and propellant-dependent (K_T) weight factors. This allowed the selection of an optimum thrust-to-weight ratio for this maneuver. Propellant-dependent jettisoned weight was assumed equal to 0.10 times the propellant weight and thrust-dependent jettisoned weight was assumed equal to 0.02 times the thrust level. For the Mars landing, an integrated trajectory was determined only for an initial thrust-to-(Mars) weight ratio of 0.855. This resulted in a thrust-to-(Mars) weight of about 2.0 at touchdown. For the landing stage, the stage propellant fraction was assumed to be 0.90.

The characteristics of the engine systems used in this study are presented in the following table. The engine systems considered are representative of pump-fed designs using O_2/H_2 propellants.

TABLE 27
ENGINE PERFORMANCE

	Mars Takeoff and Landing Engine
Chamber Pressure	650 psia
Nozzle Expansion Area Ratio	50:1
Vacuum Specific Impulse	432 seconds
Surface Specific Impulse	411 seconds

The drag coefficients used in the study are presented in Figure 133. Curve A is similar to the characteristic for conventional, Earth-launched ballistic missiles, and was used in both the landing and takeoff analyses. Curve B has C_D values twice those of curve A, and was introduced to illustrate the effect of vehicle drag characteristics on the takeoff maneuver.

Results

From the integrated trajectories computed, a curve of ideal velocity requirement versus takeoff thrust-to-weight ratio was determined for a Mars takeoff to a 300-n mi circular orbit. This information is presented in

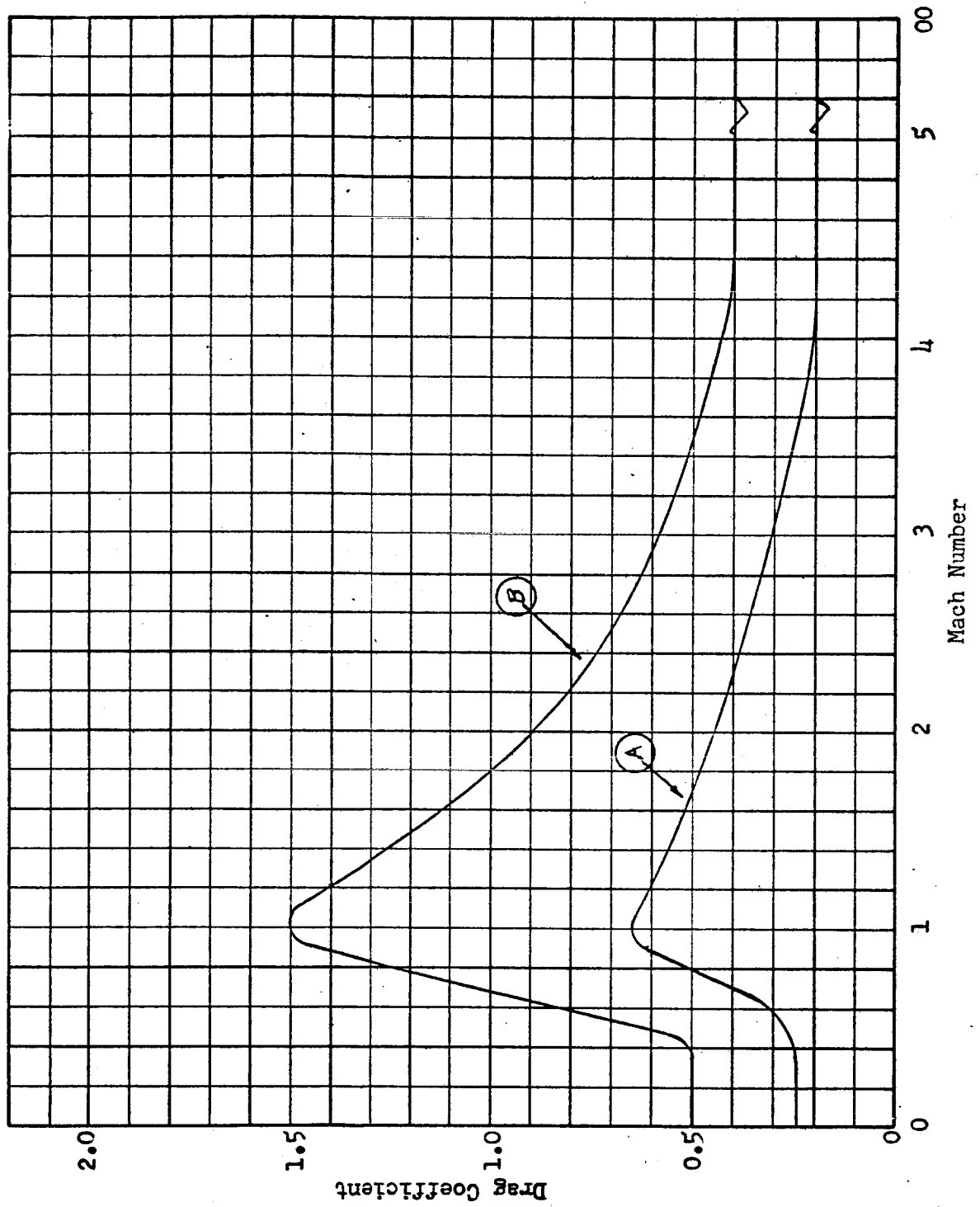


Fig. 133 • Assumed Stage Drag Coefficients

Figure 134 . The payload-to-gross weight ratio for the assumed Mars takeoff stage is presented in Figure 135 . A takeoff thrust-to-(Mars) weight of about 2.0 provides the highest vehicle payload for a given vehicle gross weight as indicated in Figure . A lower thrust-to-weight ratio would be selected if the maximum payload for a given thrust was desired. The two drag curves considered yield payloads which differ by about 7 percent.

The Mars landing from a 50-n mi orbit required a stage-ideal velocity increment of 12,430 ft/sec. This ideal velocity is significantly different from the ideal velocity requirements for the takeoffs, which range from about 14,000 to 16,000 ft/sec. Part of this difference (about 750 ft/sec) is due to the difference in orbit height. The landing ideal velocity requirement is also lower because of the effect of drag. The drag force, which acts to slow the vehicle, assists the propulsive thrust during the landing but opposes the thrust during takeoff. The landing vehicle has a payload -to-gross weight ratio of 0.34 for a stage propellant fraction of 0.90.

Only one type of trajectory was considered for each maneuver in this study. Other trajectory types might result in a more optimum flight path and consequently higher payloads than those presented. In addition, the effect of thrust-to-weight ratio was not considered for the Mars landing. The ideal velocity requirements presented in this study therefore are not necessarily as low as those that might be obtained by more detailed analysis, but they do indicate the approximate velocity magnitude required.

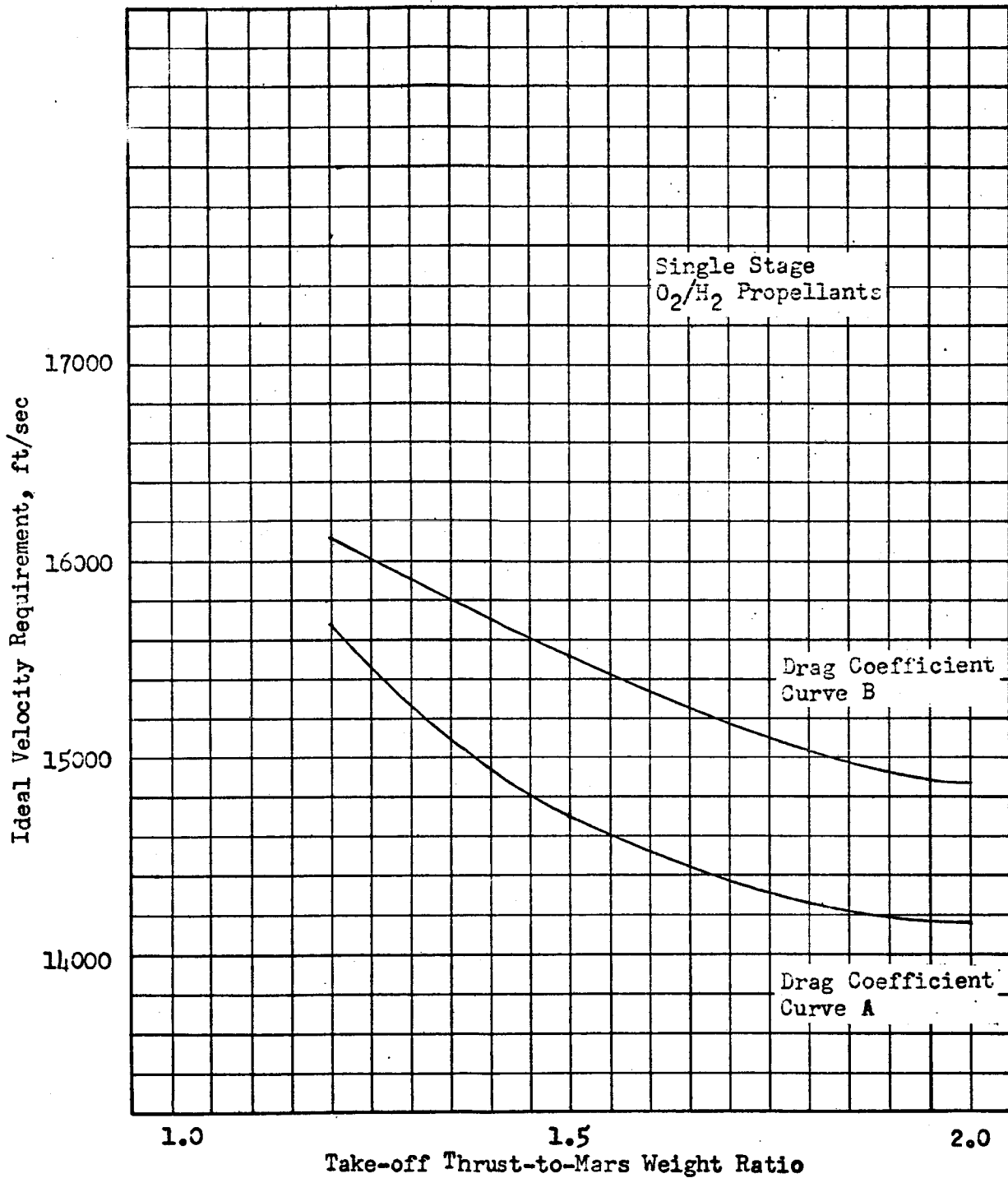


Fig. 134 Ideal Velocity Requirement Mars Take-Off to 300 n mi Circular Orbit.

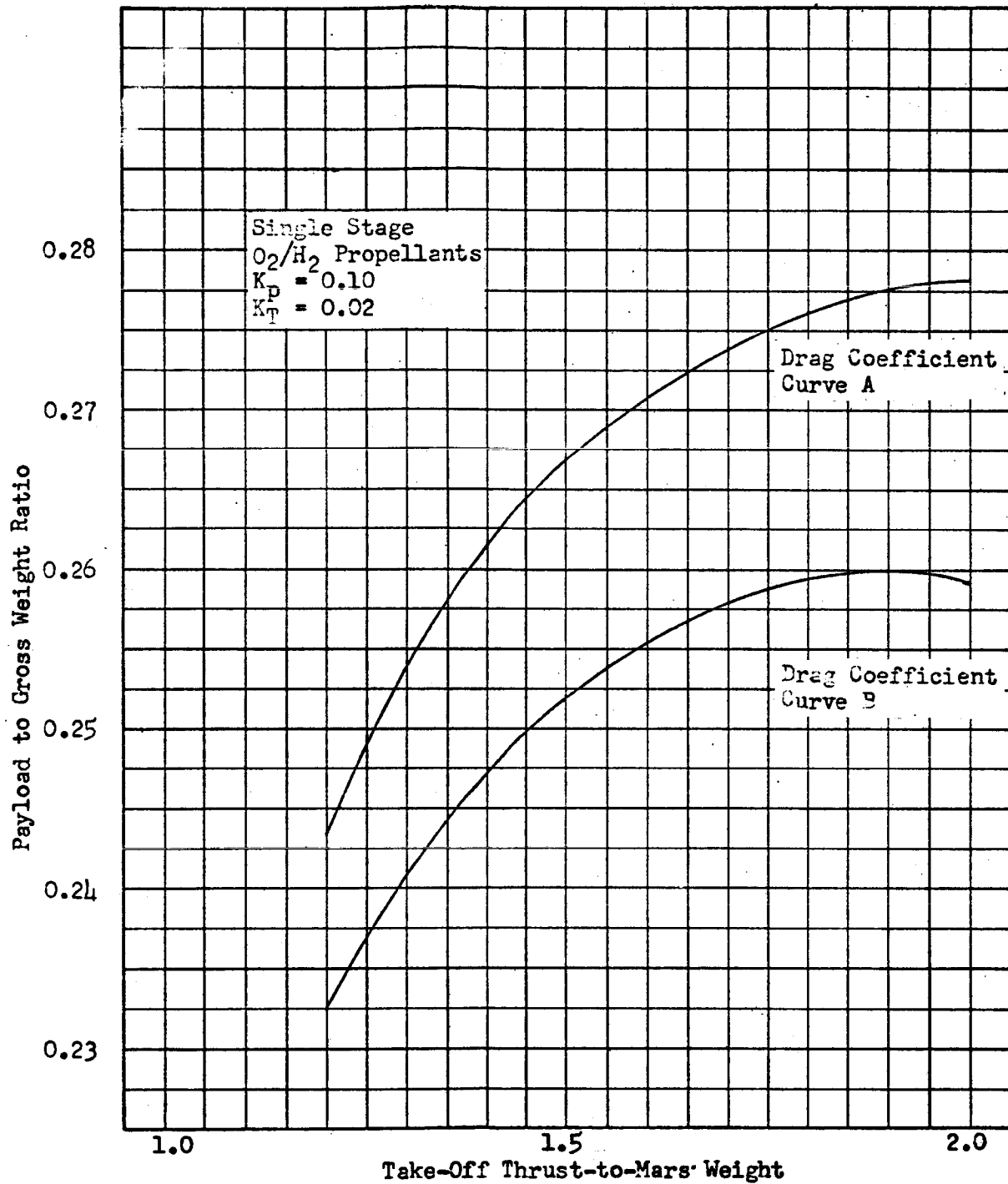


Fig. 135 Payload Mars Take-Off to 300 n m circular orbit

EARTH-VENUS MISSIONS

TRAJECTORY SELECTION

The trajectory characteristics of several Earth-Venus missions are presented in Table 28 . The indicated missions are repeated every 584 days. Because the orbit of Venus is very nearly circular (eccentricity of 0.007 as compared to Mars-orbit eccentricity of 0.093), the cycle-to-cycle repeatability of Venus missions is close to exact.

The minimum-energy mission, items (3) and (5), resembles the minimum-energy Mars mission described earlier in that a long (457 day) Venus stay-time is required while awaiting the appropriate Earth-return launch date. For shorter trips, the optimum mission might be selected by minimizing total velocity requirements; this is approximated by the 356 day trip represented by items (1) and (2); alternatively, it might be more effective to increase the Earth-departure propulsion requirements, item (6), since the limited space exposure of the system greatly reduces shielding and insulation requirements for propellant tanks, resulting in a higher propellant fraction in comparison to Venus maneuver propulsion systems . The resulting high Venus arrival velocity is relatively unimportant since aerodynamic braking is likely to be employed. A reasonably favorable Earth-return phase, item (7), is obtained. Equally, or perhaps more, important than the modest reduction in Venus-departure velocity requirements, as compared to item (2), is the 80-day reduction in required propellant-storage duration for the Venus-departure propulsion system.

As in the previous case of Mars trajectories, there is insufficient design information available to warrant a firm preference for one mission profile over another. On the basis of available evidence, the 300-day mission described in items (6) and (7) may be suited to a manned Venus expedition.

TERMINAL CORRECTIONS FOR EARTH-VENUS TRAJECTORIES

There are alternate landing concepts applicable to Venus landing missions. The vehicle can first enter an orbit about the planet, and from there descend to the surface. Alternately, the space vehicle can employ atmospheric braking for direct descent to the surface. In either case, there is a necessity for terminal corrections since midcourse correction analyses

TABLE 28

VENUS MISSIONS

Trajectory Number	Phase	Destination Stay, days	Launch Date Gregorian, Julian	Trip Time days	Hyperbolic Departure Excess Velocity ft./sec	Hyperbolic Arrival Velocity, ft./sec	Total Mission Time, days
(1)	Earth-Venus	—	5 April 1965 2438855.5	265	23,800	15,900	265
(2)	Venus-Earth	5	31 December 1965 2439125.5	86	20,300	12,650	356
(3)	Earth-Venus	—	10 November 1965 2439074.5	150	9,650	10,950	150
(4)	Venus-Earth	6	15 April 1966 2439230.5	300	19,000	32,000	456
(5)	Venus-Earth	457	10 June 1967 243968.5	140	11,950	8,590	747
(6)	Earth-Venus	—	24 June 1965 2438935.5	185	27,000	29,000	185
(7)	Venus-Earth	5	31 December 1965 2439125.5	110	19,500	10,000	300
(8)	Earth-Venus	—	30 November 1968 2440190.5	125	21,000	31,000	125
(9)	Venus-Earth	5	9 April 1969 2440320.5	145	29,000	20,000	275

for the missions studied have shown that the vehicle will not approach the planet within allowable accuracy tolerances. The propulsion requirements for the terminal corrections have been evaluated in a manner similar to the Earth and Mars studies.

Propulsive Orbit Establishment

An analysis of terminal corrections required for missions which include establishment of a 300-n mi circular orbit by propulsive maneuvers has been performed in conjunction with another study. The method of analysis is presented in Reference 2. The Earth-Venus trajectory used in the analysis is summarized in Table 29.

TABLE 29

EARTH-VENUS TRAJECTORY FOR ORBIT ESTABLISHMENT MISSION

Launch Date	Transfer Time, days	Hyperbolic Arrival Velocity, ft/sec	Nominal Asymptotic Approach Distance, n mi	Actual Asymptotic Approach Distance, n mi
20 Nov. 1965	150	12,500	10,000	12,850

The actual asymptotic approach distance resulting from midcourse correction inaccuracies was 12850 n mi, a deviation of 2850 n mi from the desired value. The relatively long transfer mission and related low hyperbolic arrival velocity was selected as representative of propulsive orbit-establishment missions since faster missions usually result in excessive propulsive ΔV and propulsion system weight requirements.

The terminal correction velocity requirements for the mission are presented in Figure 136 along with the equivalent requirements for several values of asymptotic approach distance. A crossplot of the curves is shown in Figure 137 to indicate the decrease in correction velocity increment with reduction in asymptotic approach distance deviation.

Additional analysis of terminal correction errors was performed to evaluate deviations in altitude of the propulsively-established orbit. The errors encountered were range-dependent, and therefore their effects were evaluated

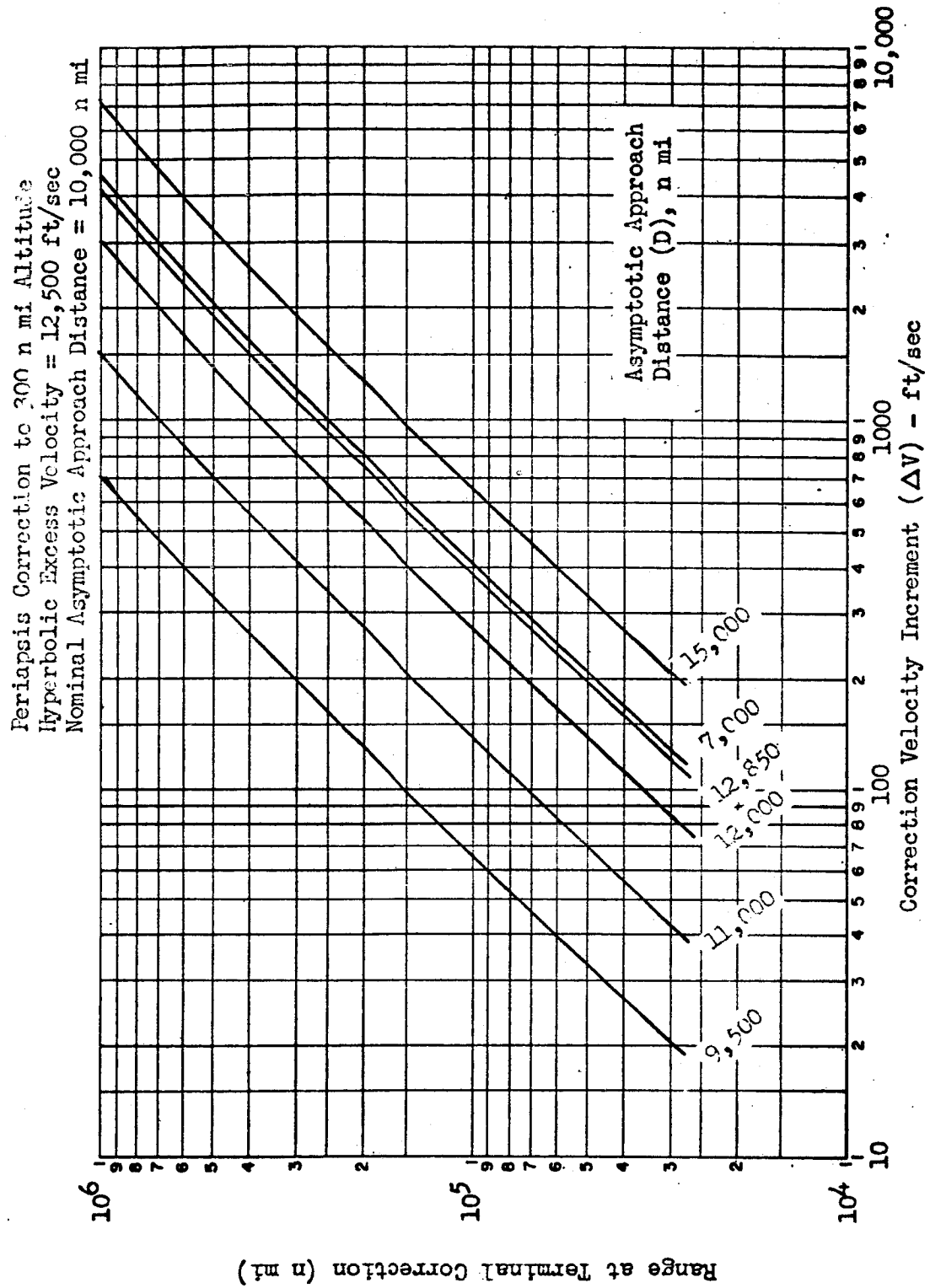


Figure 136. Versus Terminal Correction Maneuver

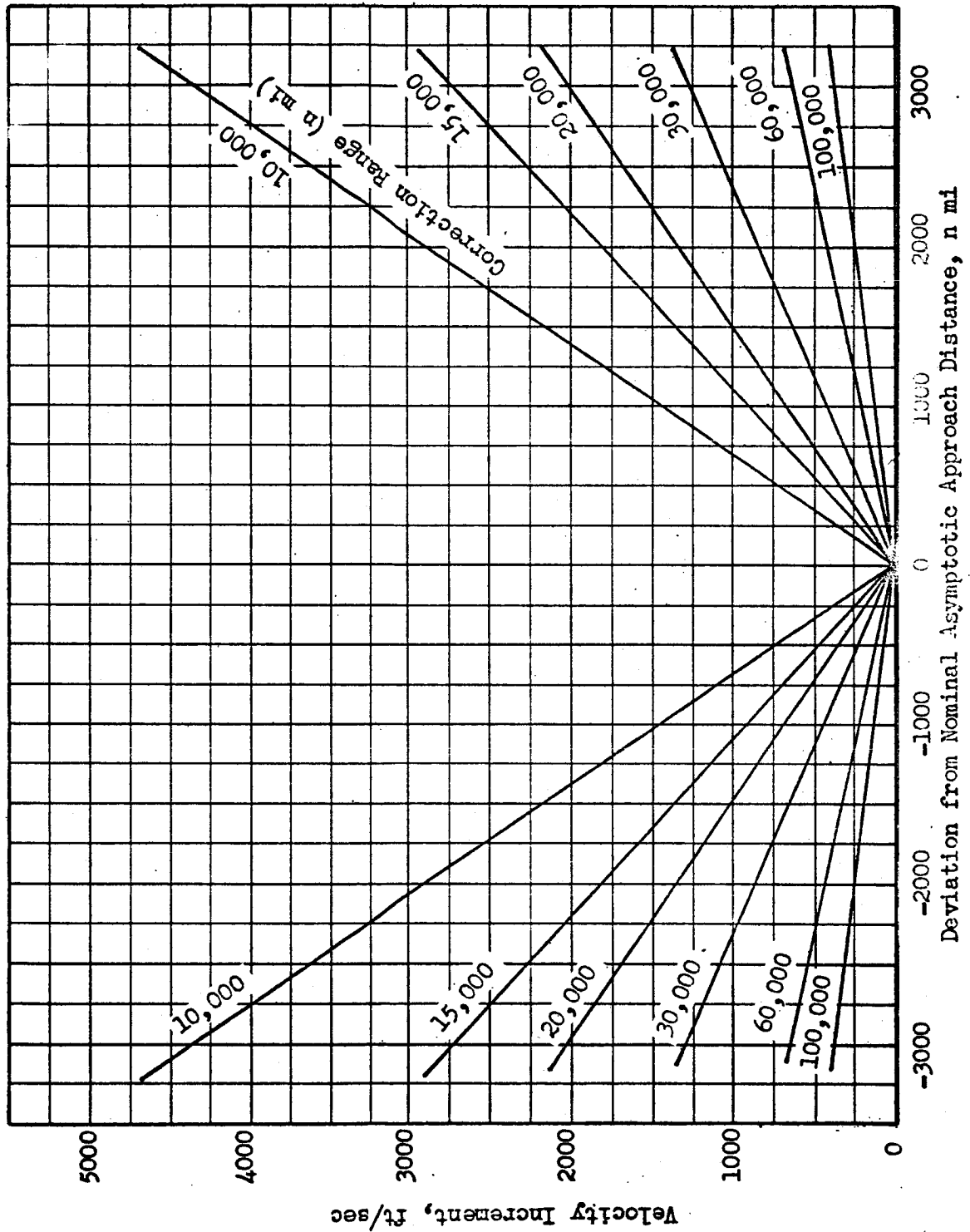


Figure 137. Venus Terminal Correction. Periaapsis Correction to 300 n mi Altitude
Hyperbolic Excess Velocity - 12,500 ft/sec. Nominal Asymptotic Approach
Distance - 10,000 n mi.

as a function of range (Figure 138). An allowable tolerance of 10 percent (30 n mi) in the deviation of apoapsis altitude of the orbit was selected for determining the appropriate range for applying the terminal correction.

The correction range obtained from Figure 138 and the magnitude of the correction velocity increment (Figure 136) corresponding to that range are given in Table 30 .

TABLE 30

TERMINAL CORRECTION FOR VENUS ORBIT-ESTABLISHMENT MISSION

Mission	Nominal Orbital Altitude, n mi	Apoapsis Altitude Tolerance, n mi	Correction Range, n mi	Terminal Correction ΔV , ft/sec
Earth-Venus	300	30	61,000	550

Atmospheric Entry

Terminal corrections required for direct aerodynamic entry into the Venusian atmosphere were analysed in a manner similar to previous Earth and Mars studies. The Earth-Venus transfer is described in Table 31 .

TABLE 31

EARTH-VENUS TRAJECTORY FOR ATMOSPHERIC ENTRY MISSION

Trajectory Number (see Table 4)	Launch Date	Trip Time, days	Hyperbolic Arrival Velocity, ft/sec
5	5 April 1965	265	15,900

The study was based on a nominal initial thrust-to-(Earth) weight ratio of 0.3; however, a wide range of F/W values can be utilized without changing the results obtained.

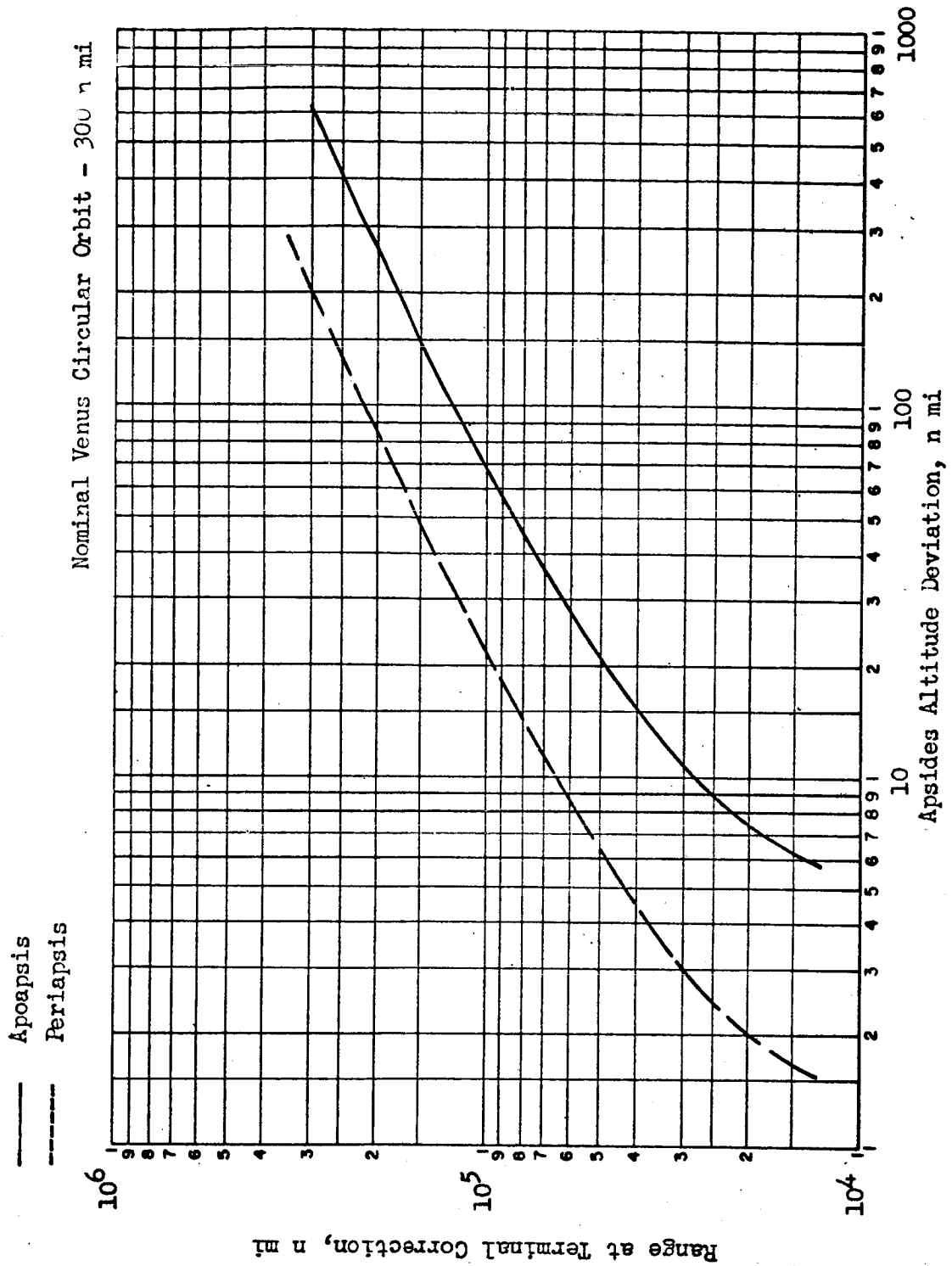


Figure 138. The Dependence of Apsides Altitude Deviation Upon Range at Application of Terminal Correction.

The deviation from nominal asymptotic approach distance which existed at conclusion of the midcourse correction maneuvers is indicated in Table

TABLE 32

VENUS ARRIVAL CONDITIONS

Trajectory Number (See Table 4)	Hyperbolic Arrival Velocity, ft/sec	Nominal Asymptotic Approach Distance (D), n mi	Deviation in D (ΔD), n mi	Actual Asymptotic Approach Distance (D_a), n mi
5	15,900	7780	3150	10,930

The combination of V_∞ and D_a from Table 32 represents a trajectory with atmospheric entry conditions outside the allowable Venus entry corridor described in Figure 139. Therefore, terminal corrections were applied to modify the trajectory. The terminal correction objectives are given in Table 33.

TABLE 33

NOMINAL ENTRY CONDITIONS INTO THE ATMOSPHERE OF VENUS

Trajectory Number	Entry Altitude (h_e), feet	Entry Velocity (V_E), ft/sec	(V_E/V_{co})	Entry Trajectory Elevation Angle (α_E), degrees
5	435,000	36,870	1.57	-7.55

The magnitudes of terminal corrections are plotted in Figure 140 as a function of correction range. Correction velocity magnitudes are presented for several values of deviations in asymptotic approach distance to indicate the influence of that parameter.

The study of measurement and execution errors encountered in terminal corrections produced the rms deviation in entry velocity and entry trajectory elevation angle indicated in Figure 141. The deviation in entry velocity is insignificant. The allowable deviation in trajectory elevation

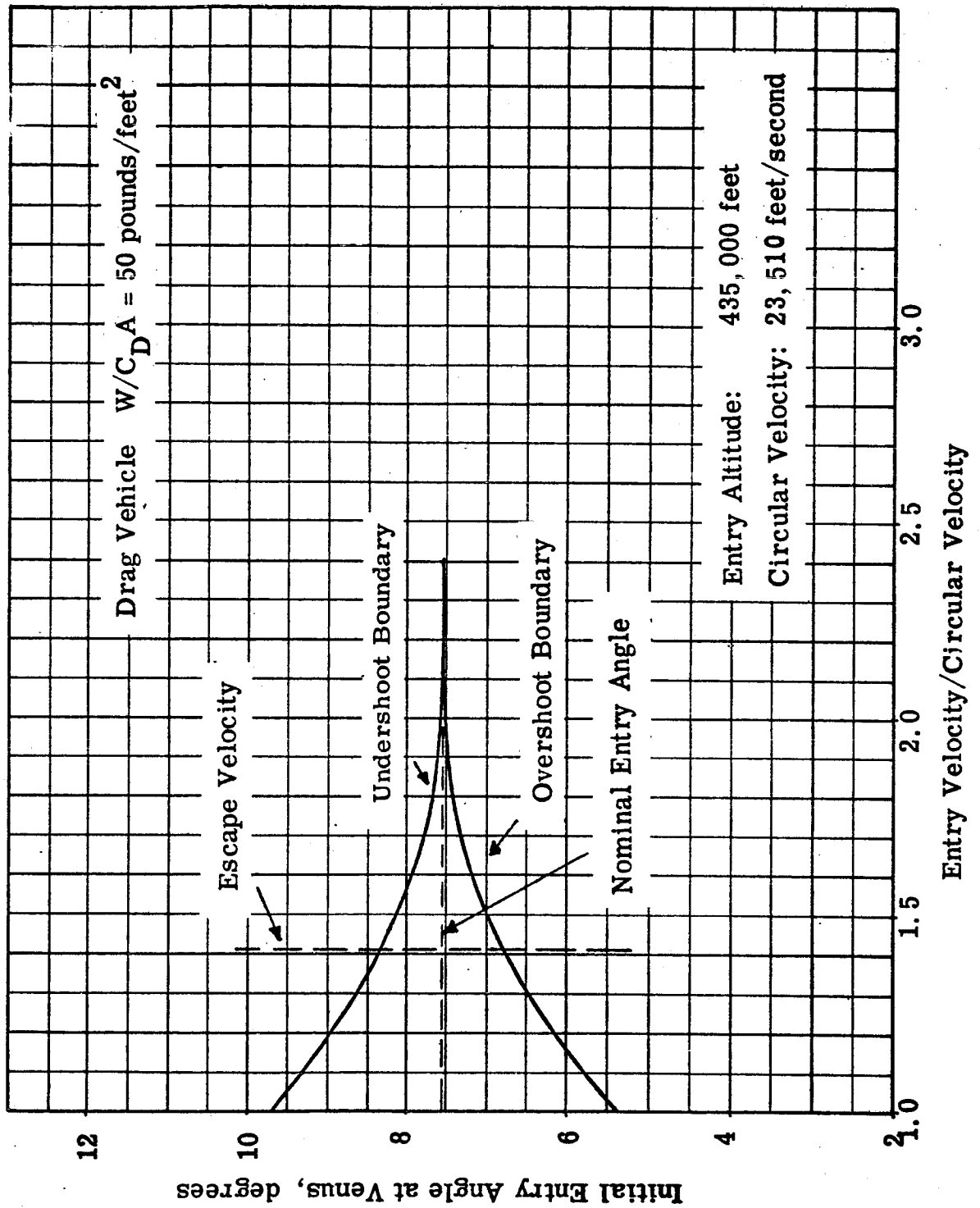


Fig. 139. Venus Entry Corridor

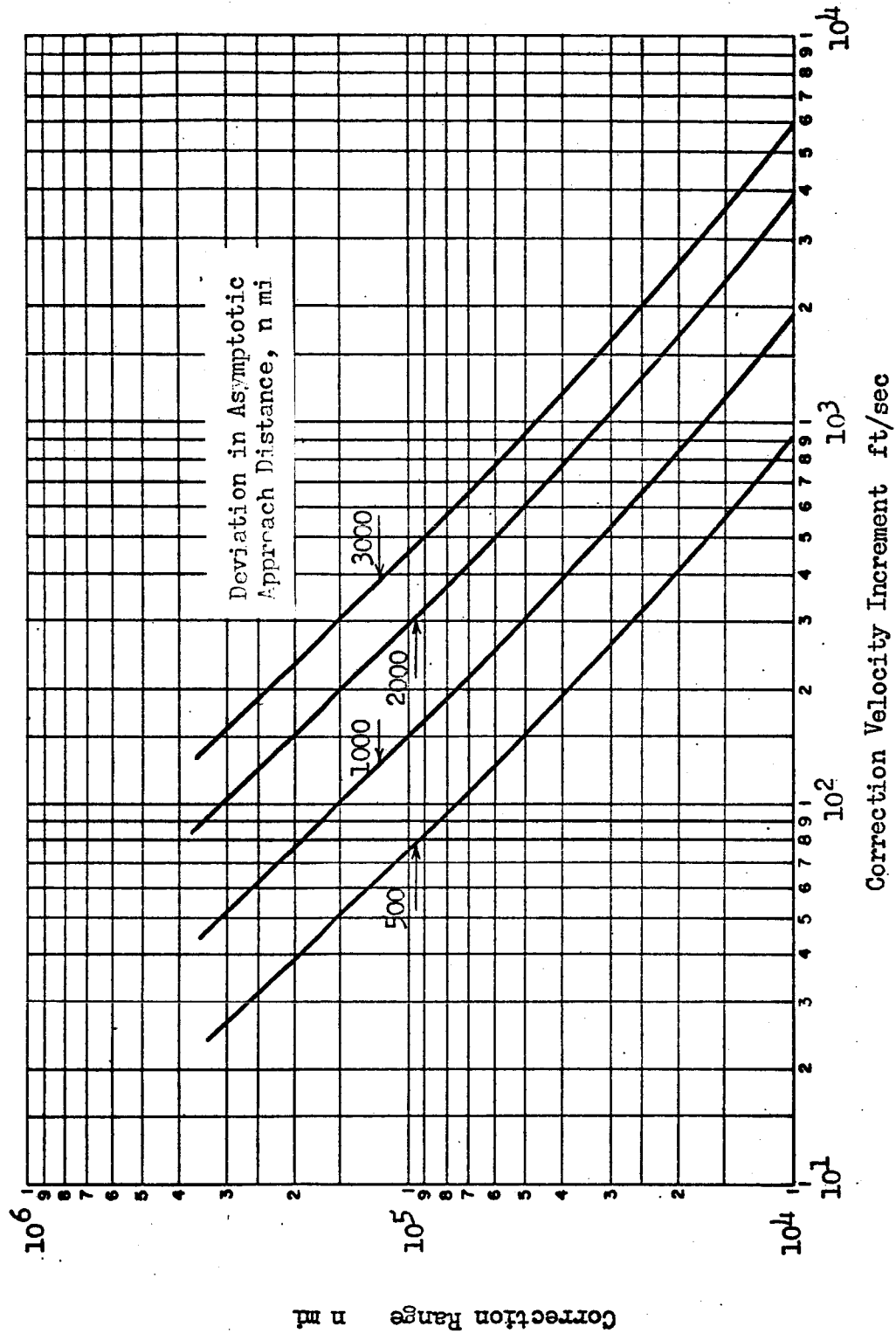


Fig. 140. The Effect of a Deviation in Asymptotic Approach Distance on the Terminal Correction Velocity Increment for Venus Atmospheric Entry. (Trajectory 5)

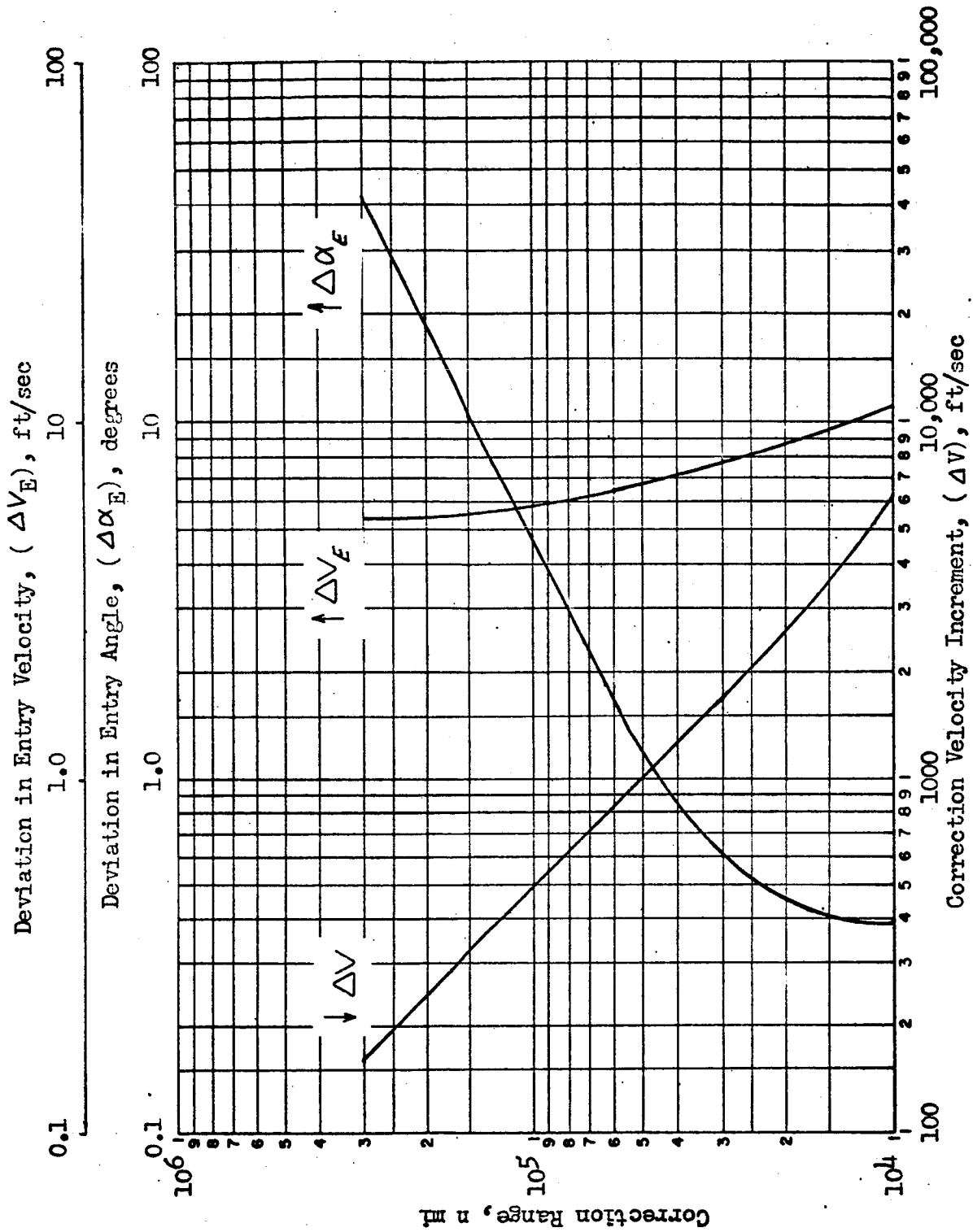


Fig. 141. Terminal Correction for Venus Atmospheric Entry. (Trajectory 5)

angle at entry establishes the required range for application of the terminal correction. For a single correction, the range and the corresponding velocity increment are shown in Table 34 .

TABLE 34

SINGLE TERMINAL CORRECTION FOR VENUS ATMOSPHERIC ENTRY

Trajectory Number	Entry Corridor Half-Band Width, Degrees	Entry Angle Deviation, Degrees	Correction Range, n mi	Correction Velocity Increment, ft/sec
5	0.4	± 0.4	14,000	3,800

The velocity requirements for a single terminal correction were considered excessive; therefore, the use of two corrections was investigated. In the dual correction scheme, the first correction was applied at 100,000 n mi. An error analysis study of a second correction applied to this corrected trajectory gave the resulting rms deviations in entry parameters shown in Figure 142. The entry angle was the predominant factor to be considered. A second correction range was determined to give an entry angle deviation which satisfied the entry corridor requirement. .

The dual correction scheme is summarized in Table 35 .

TABLE 35

SUMMARY OF TERMINAL CORRECTIONS FOR VENUS ATMOSPHERIC

ENTRY MISSION

Trajectory Number	Entry Corridor Half-Band Width, degrees	Correction	Correction Range, n mi	Entry Angle Deviation, degrees	Correction Velocity Increment, ft/sec	Total Terminal Correction ΔV , ft/sec
5	0.4	1st	100,000	± 4.7	490	620
		2nd	16,000	± 0.4	130	

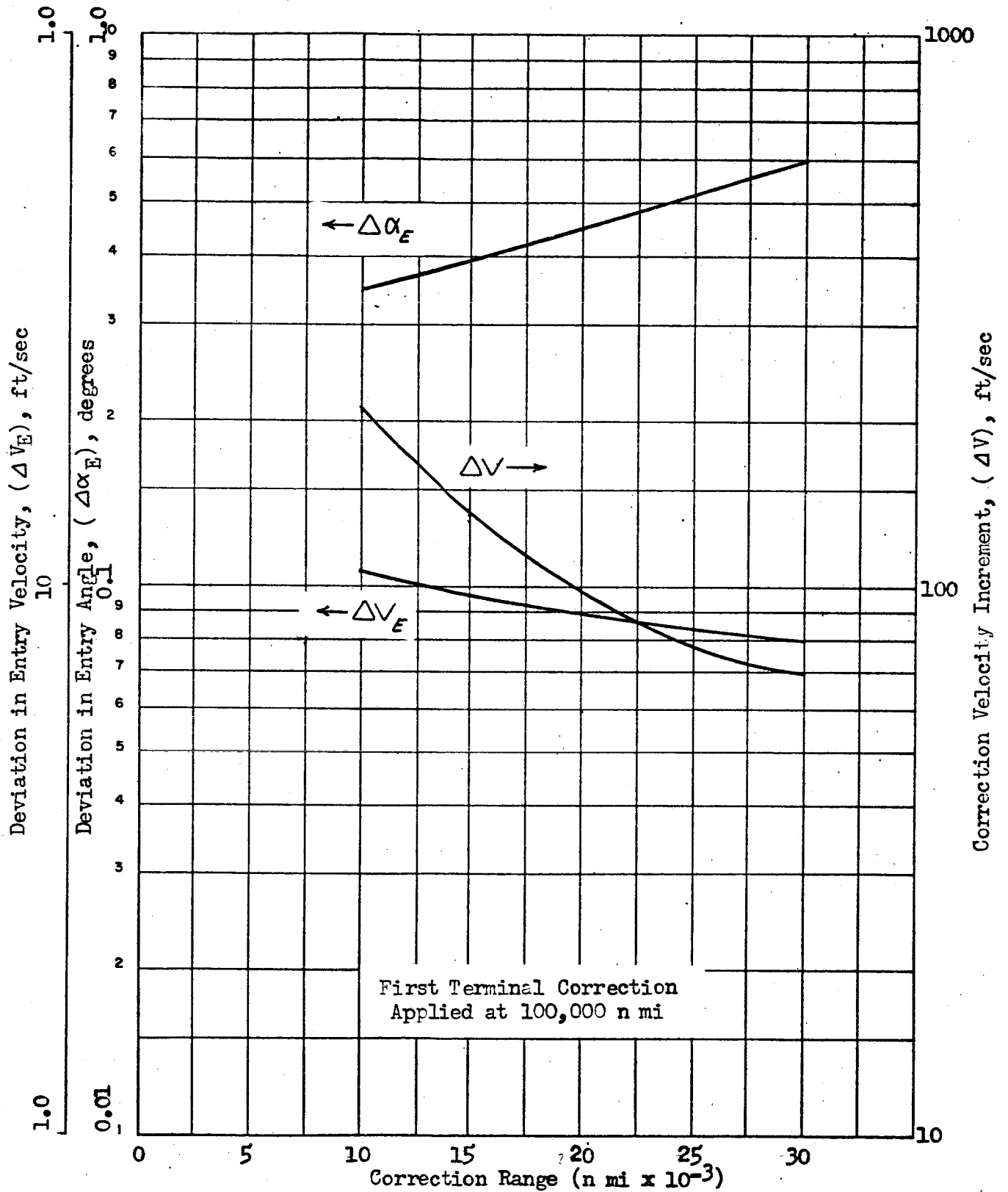


Fig. 142. Second Terminal Correction for Venus Atmospheric Entry.
(Trajectory 5)

The use of dual correction schemes greatly reduced the velocity requirements of terminal corrections for atmospheric entry at Venus. The magnitude of the saving, 3180 ft/sec, clearly warrants the use of a dual correction scheme, despite the addition of a requirement for engine restart capability. With the terminal corrections, the required entry corridor can be successfully established, as in the case of Earth and Mars, without an additional propulsive deceleration phase.

PROPULSIVE VENUS ORBIT ESTABLISHMENT AND DEPARTURE MANEUVERS

The propulsion requirement nomographs utilized in the thrust-to-weight (F/W) optimization analysis for Venus orbit establishment and departure maneuvers are presented in Figures 143 and 144. The techniques described previously were employed to determine the optimum F/W values for representative non-cryogenic and cryogenic systems.

The results presented in Figures 145 and 146 considered in conjunction with earlier results for other planets, indicate a consistent optimum thrust-to-planet-weight ratio for orbit establishment maneuvers. This is demonstrated in Figure 147; corresponding values of thrust-to-Earth-weight ratio are presented for comparison.

The effect of hyperbolic arrival velocity on payload capabilities for a Venus orbit establishment maneuver is shown in Figure 148 for a cryogenic propulsion system. It is evident that combinations of sufficiently high excess velocity and sufficiently low propellant fraction can result in zero payload capability; this result, however, is for all-propulsive orbit-establishment maneuvers, and does not consider the possibility of aerodynamic braking.

VENUS ORBIT ESTABLISHMENT FOLLOWING AN ATMOSPHERIC GRAZE

The feasibility of establishing a Venusian orbit using an atmospheric grazing maneuver followed by a propulsive maneuver has been investigated in a similar manner to the analysis performed for Earth. The entry and exit altitude for the Venusian atmosphere is 435,000 feet, and the entry and exit angles range from 5 to 10 degrees.

Three impulsive techniques for establishing an orbit following the graze maneuver have been investigated: 1) two-impulse, direct-to-orbit, 2) coast-to-apoapsis, then two-impulse-to-orbit, and 3) a three-impulse maneuver. These schemes are discussed in the section dealing with Earth orbit-establishment maneuvers.

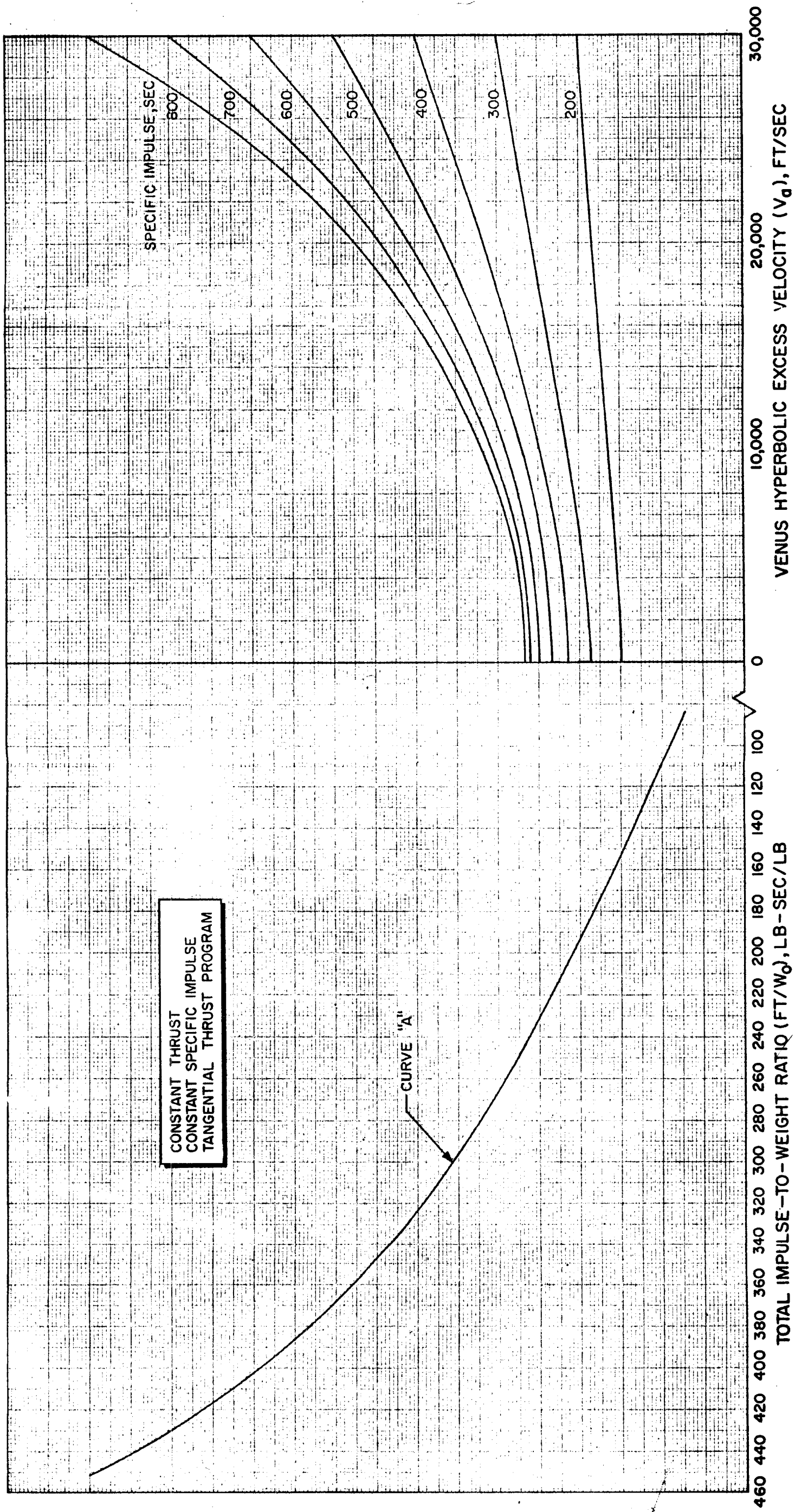


Figure 113. Venus Nomograph

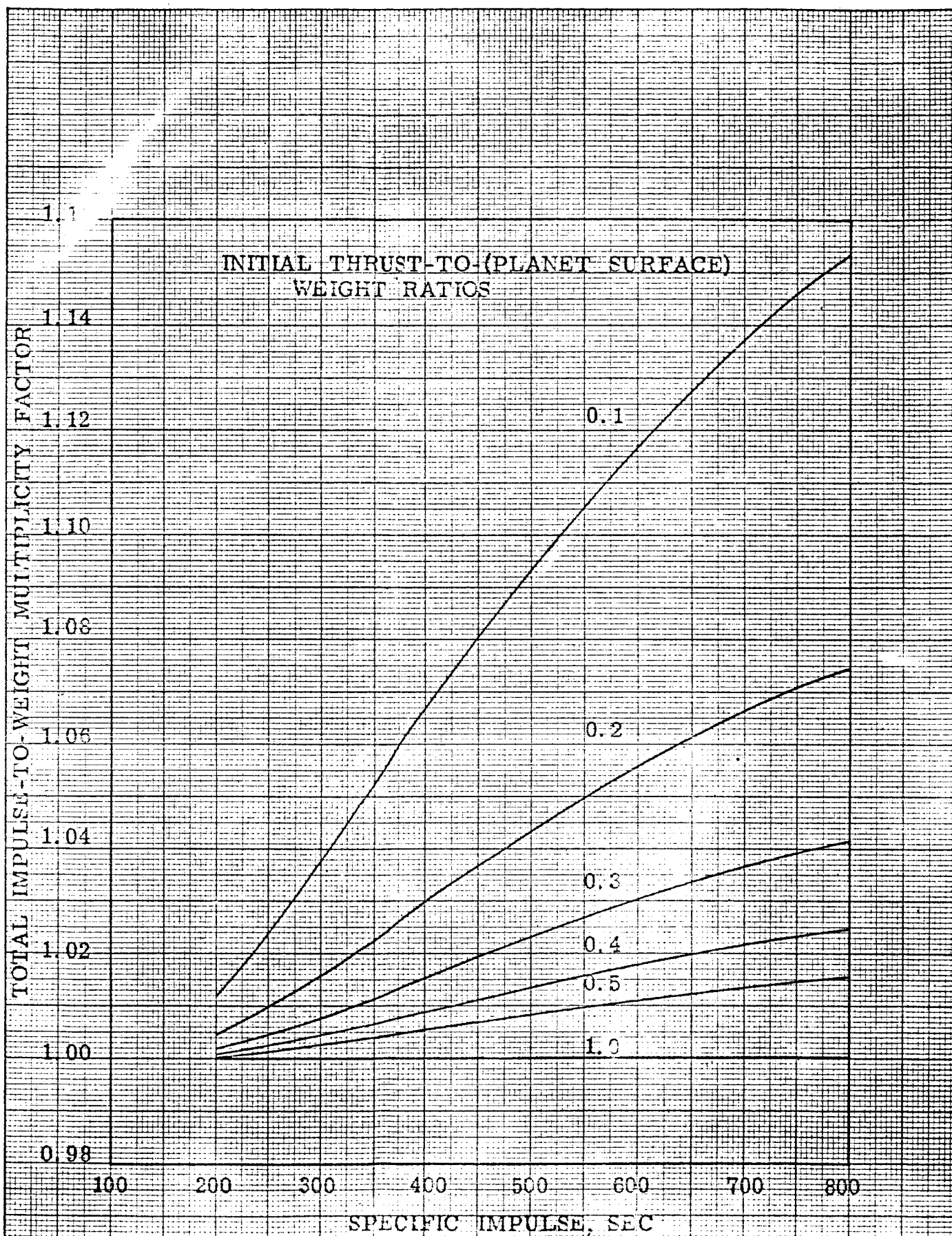


FIGURE 2-11. VENUS TOTAL IMPULSE-TO-WEIGHT CORRECTION FACTOR

ROCKETDYNE
A DIVISION OF NORTH AMERICAN AVIATION, INC.

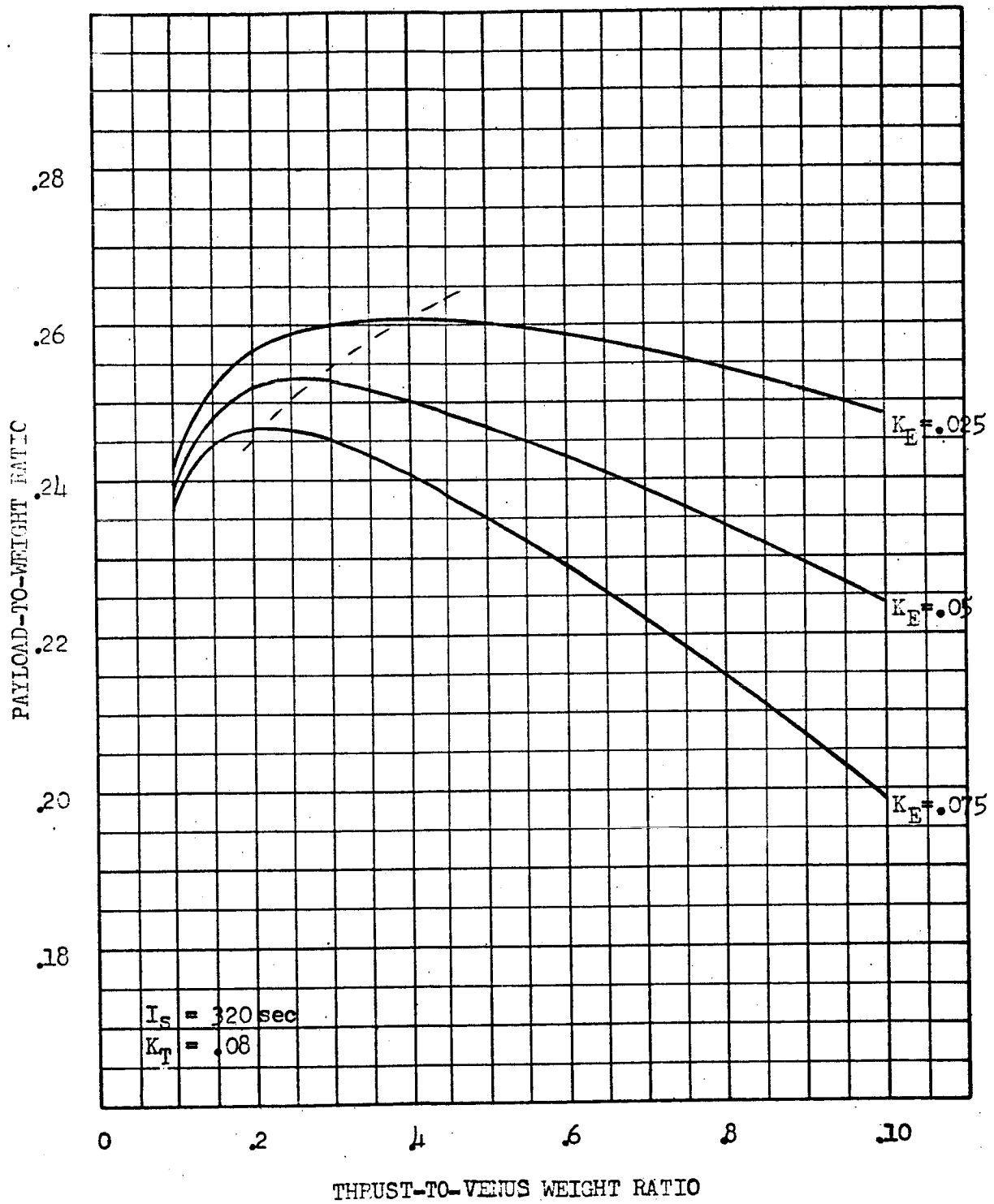


Figure 1h5.
VENUS - HYPERBOLIC EXCESS = 12,000 ft/sec

ROCKETDYNE
A DIVISION OF NORTH AMERICAN AVIATION, INC.

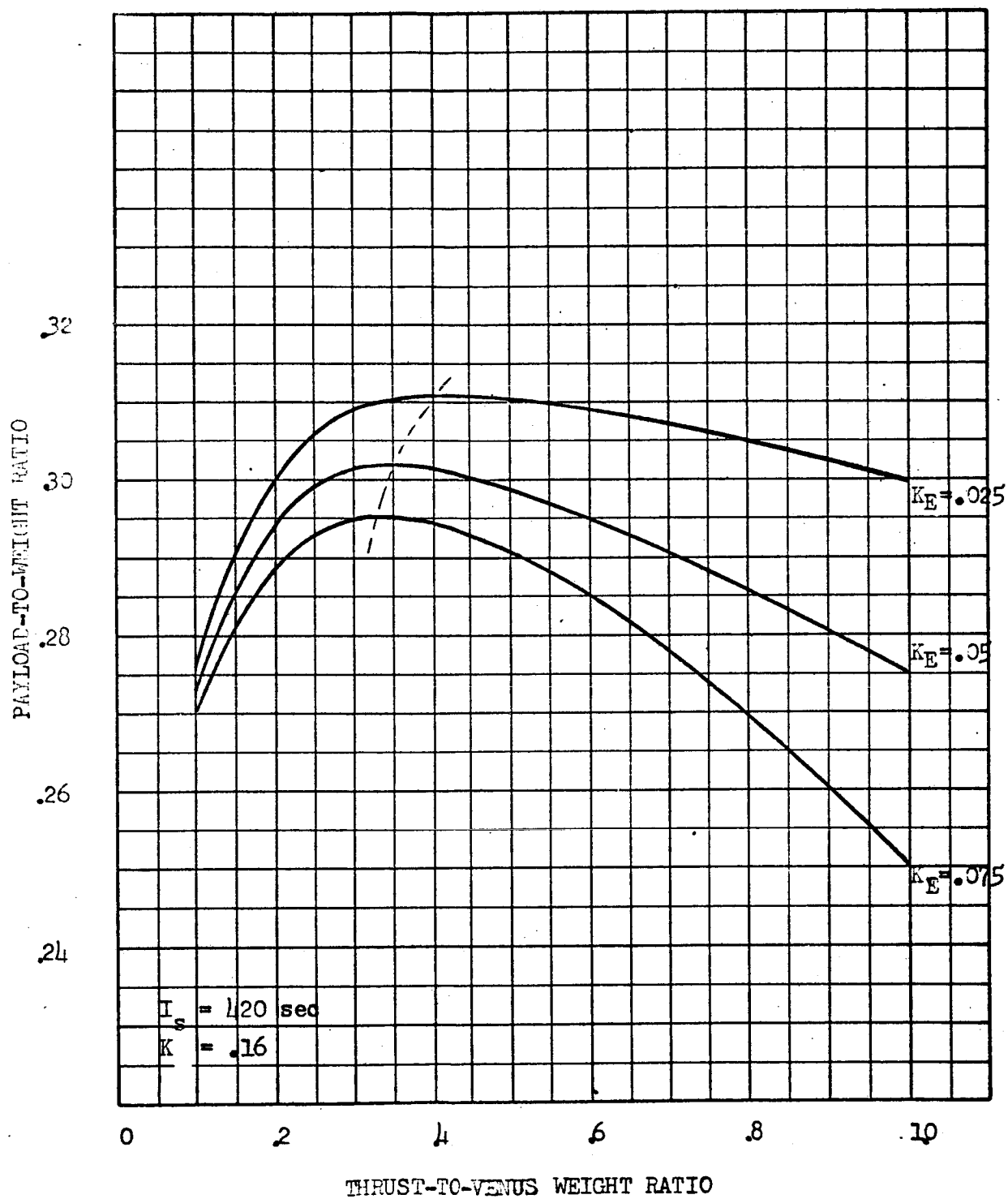


Figure 146
VENUS - HYPERBOLIC EXCESS = 12,000 ft/sec

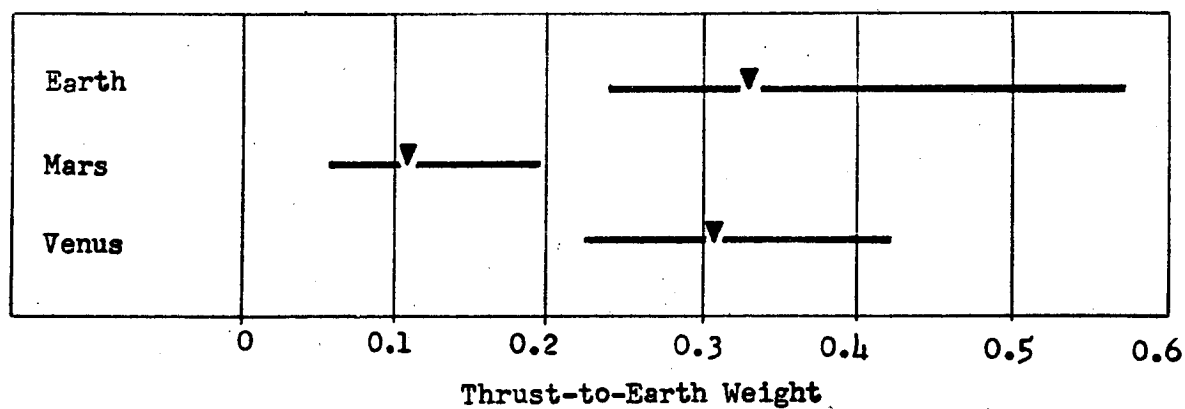
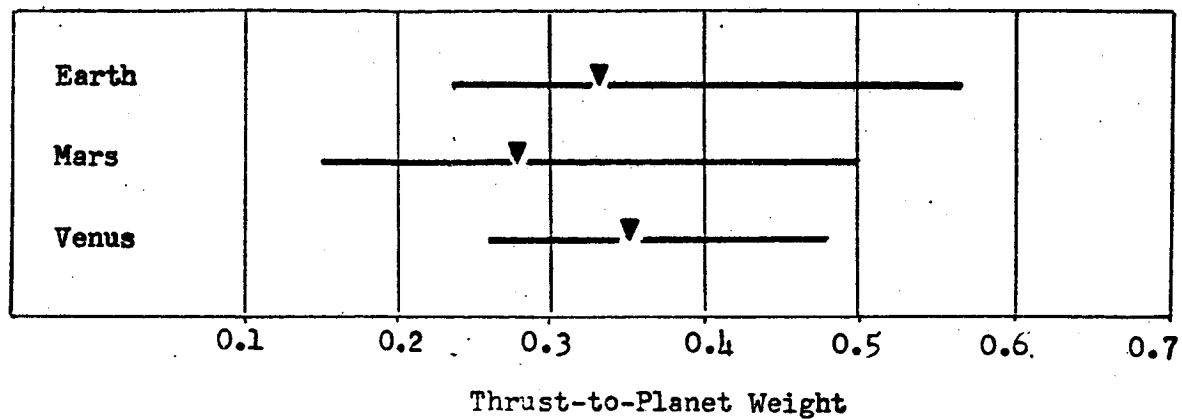


Fig. 147. Thrust-to-Weight Comparison for Nominal Planetary Vehicles

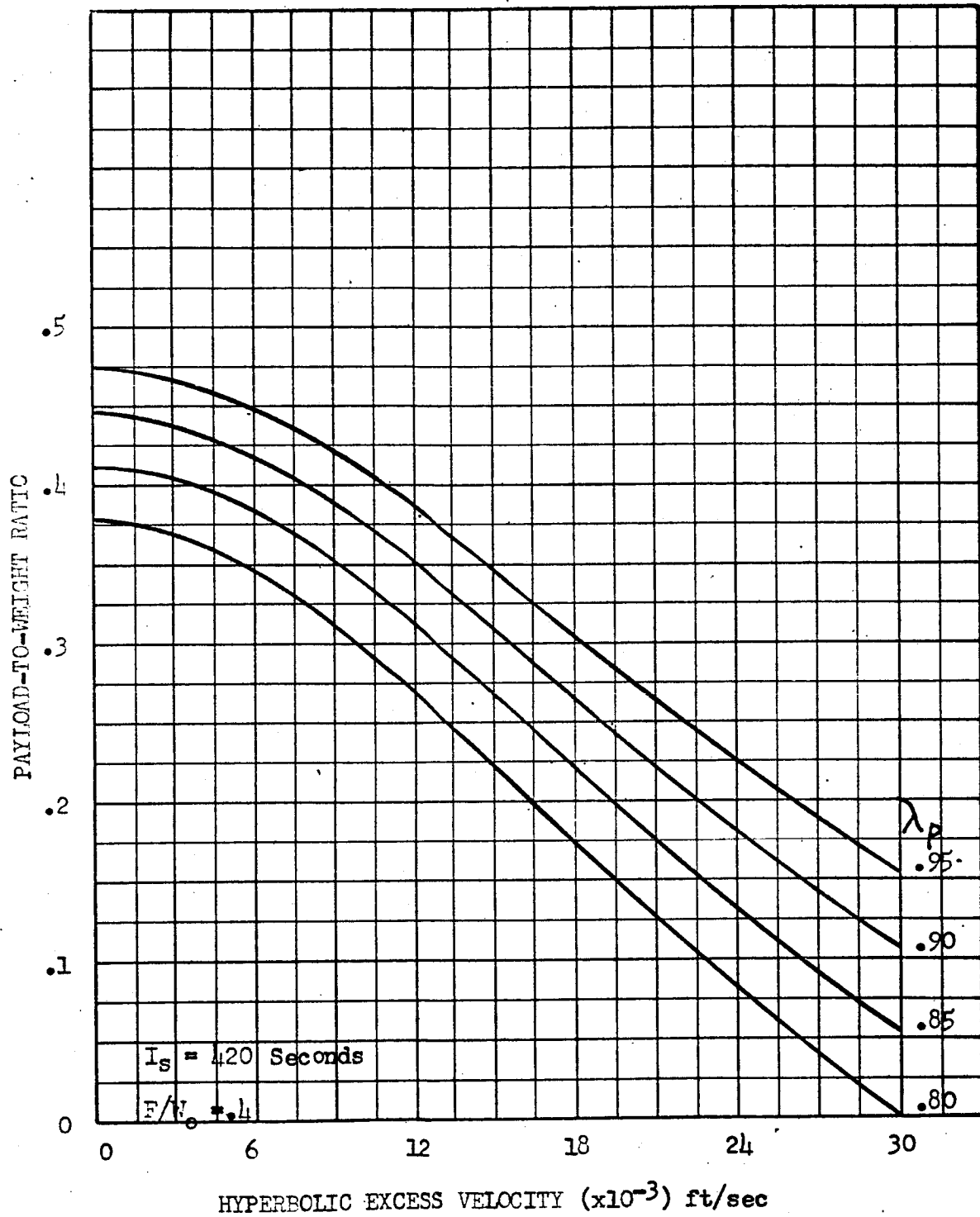


Figure 148.

VENUS PAYLOAD VS. HYPERBOLIC EXCESS

The impulsive velocity requirements for the three schemes are presented in Figures 149 through 153. A summary of the three schemes is given in Figure 154 for an exit angle of 5 degrees. A trend similar to that noted in the Earth analysis is indicated in these figures in that Schemes 2 and 3 yield the lowest velocity requirements over most of the range of exit velocities, Scheme 2 for exit velocities less than 30,000 ft/sec and Scheme 3 for exit velocities greater than 30,000 ft/sec.

For vehicles capable of executing a graze maneuver, a propulsion savings, as in the case of Earth and Mars, can be achieved.

PROPULSIVE/AERODYNAMIC BRAKING MANEUVER FOR VENUS ENTRY

The analytical techniques and assumptions required for the analysis of propulsive/aerodynamic landings were described in detail for Earth re-entry systems. The results for a parametric study of a Venus entry vehicle are presented in Figure 155. The results show that for current ablative heat shield weight estimates, the heat shield is more efficient than a propulsion system. The optimum propulsive ΔV for a mission characterized by a particular hyperbolic excess velocity is equal to the vertical distance between the arrival velocity curve and the optimum entry velocity curve for the appropriate ablation characteristic. (See Figure 82 for the ablation weight curves.)

VENUS TERMINAL DECELERATION PHASE SYSTEMS

The high density of the atmosphere at the surface of Venus suggests that for parachute/retrorocket/impact device systems, the optimum parachute terminal velocity will be substantially lower than it is for Earth or Mars landing systems. The present analysis was similar to those conducted for Earth and Mars, and was directed at optimization of parachute terminal velocity (V_T) and rocket F/W for fixed impact-velocity systems, and optimization of V_T , F/W and impact velocity (V_F) for parachute/retrorocket/impact device systems.

Pararocket System

The effect of F/W and V_T on the weight of pararocket systems for Venus landings is presented in Figure 156. The optimum parachute terminal velocity is 40 ft/sec, as compared to 70 ft/sec for Earth and 120 ft/sec for Mars. The effect of increasing parachute weight by 50 percent is shown

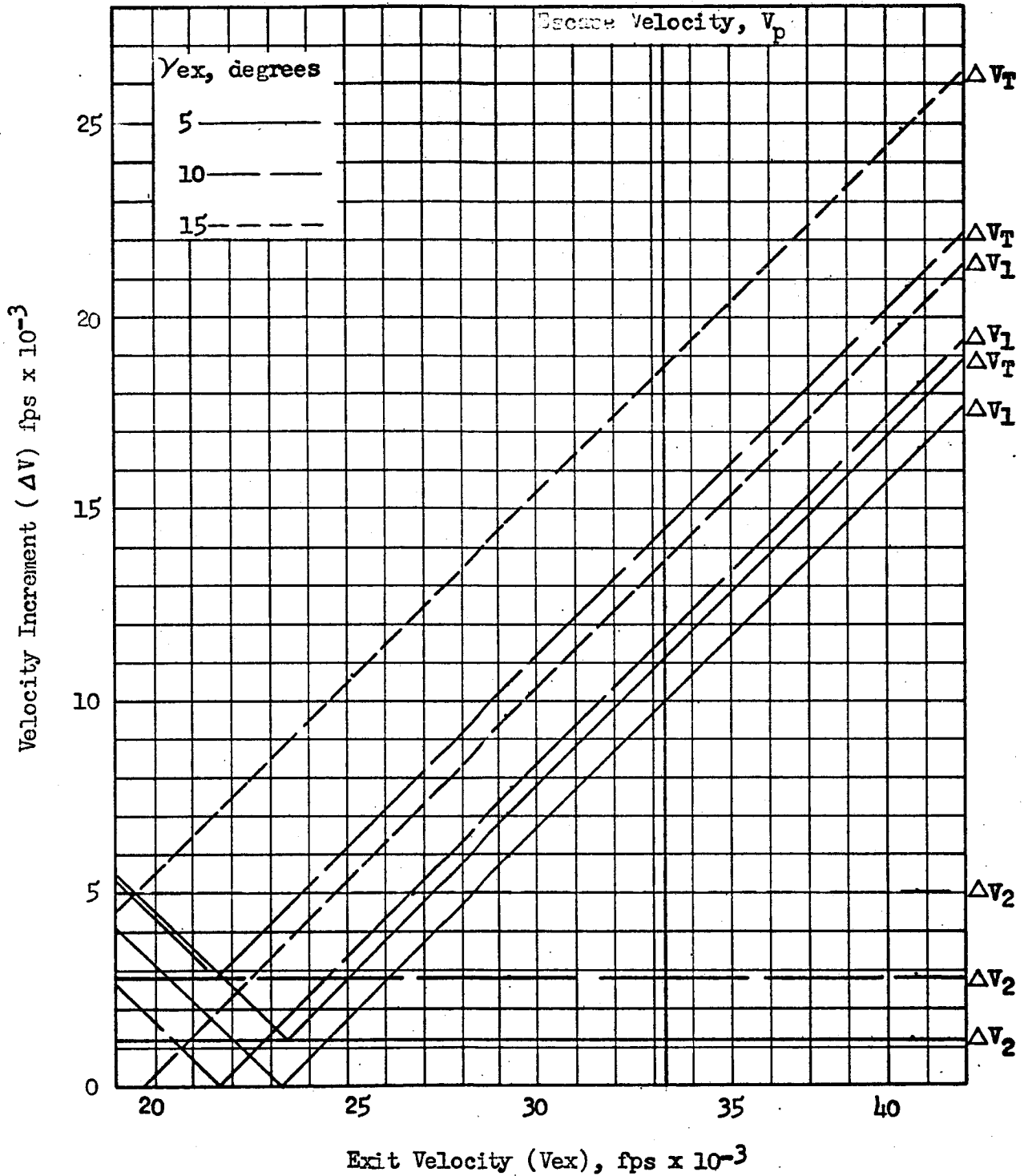


Fig. 149. Velocity Requirements for Establishing a 300 n mi Orbit at Venus, Scheme 1.

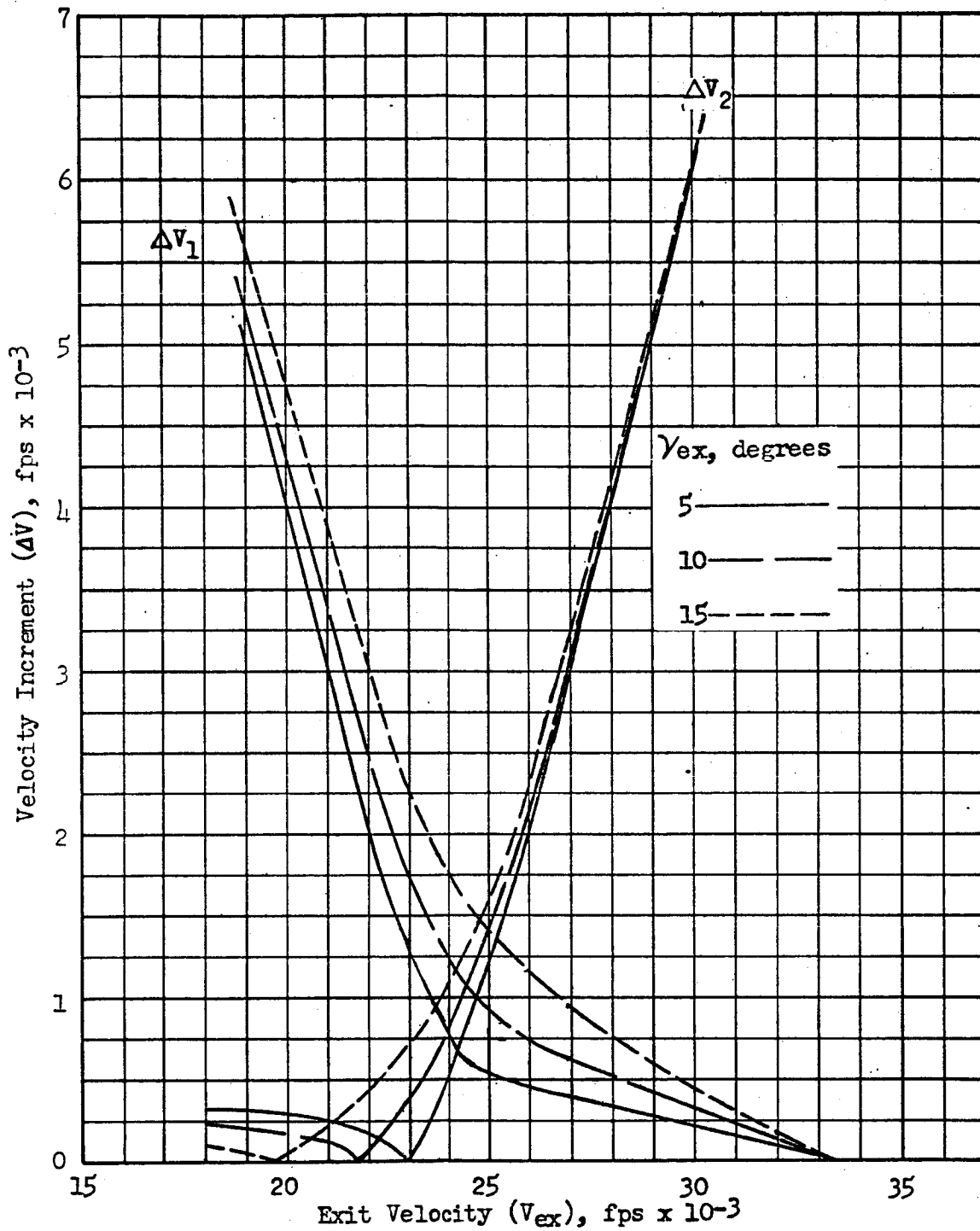


Fig.150. Velocity Increments for Establishing a 300-n mi Orbit at Venus, Scheme 2

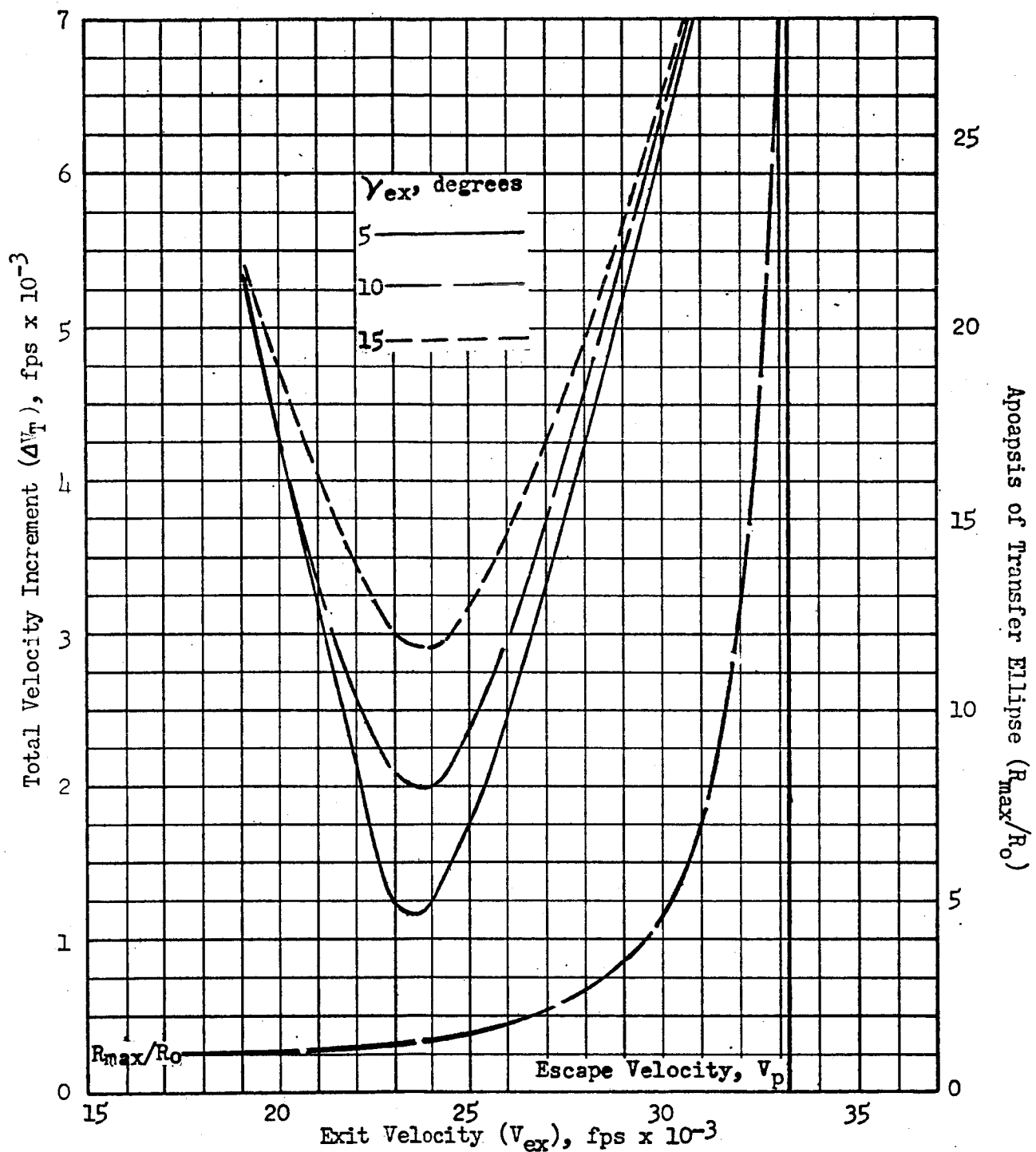


Fig.151. Total Velocity Requirements for Establishing a 300-n mi Orbit at Venus, Scheme 2

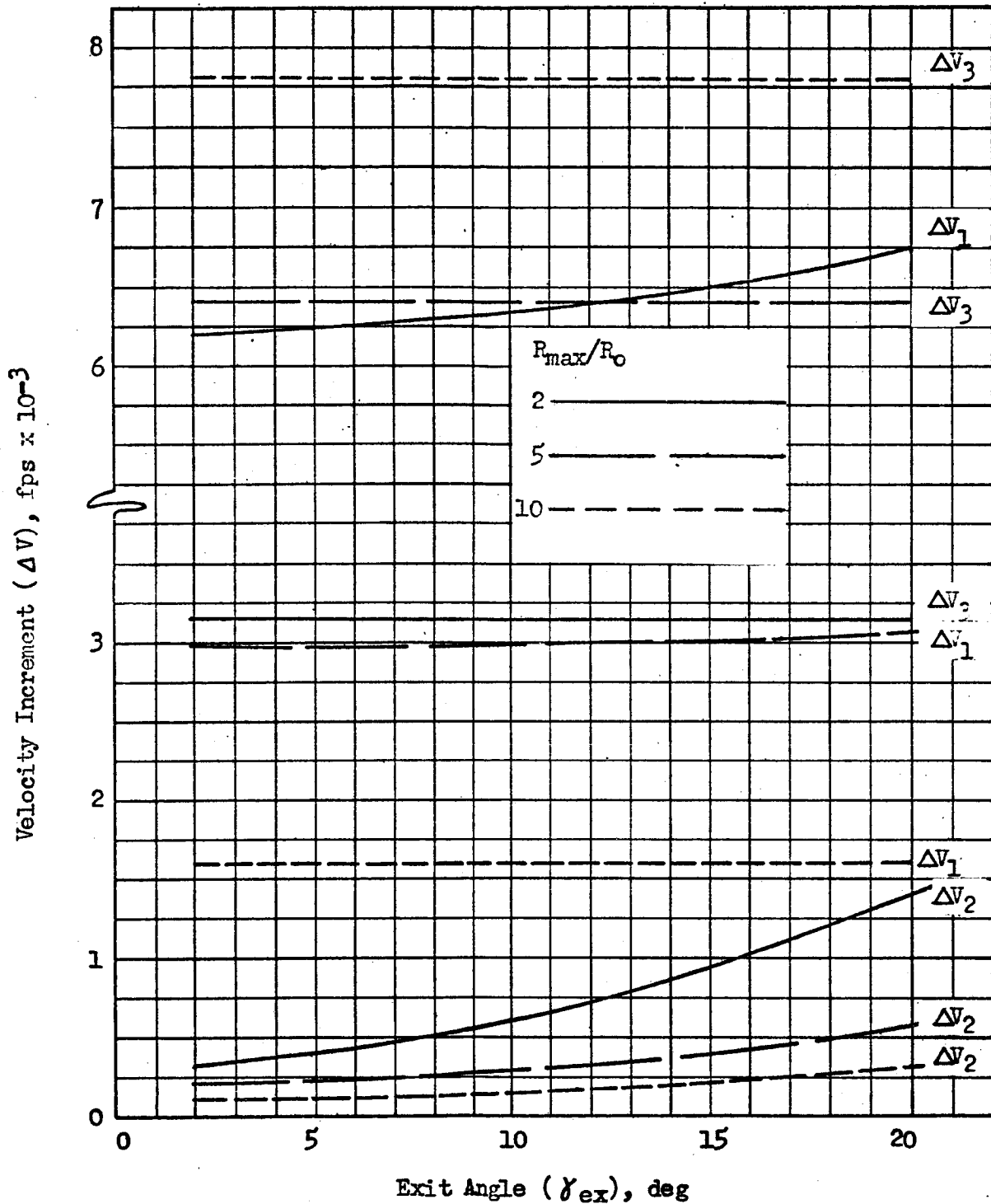


Fig. 152. Velocity Increments for Establishing a 300-n mi Orbit at Venus, $V_{ex} = V_p = 33,217$ fps, Scheme 3.

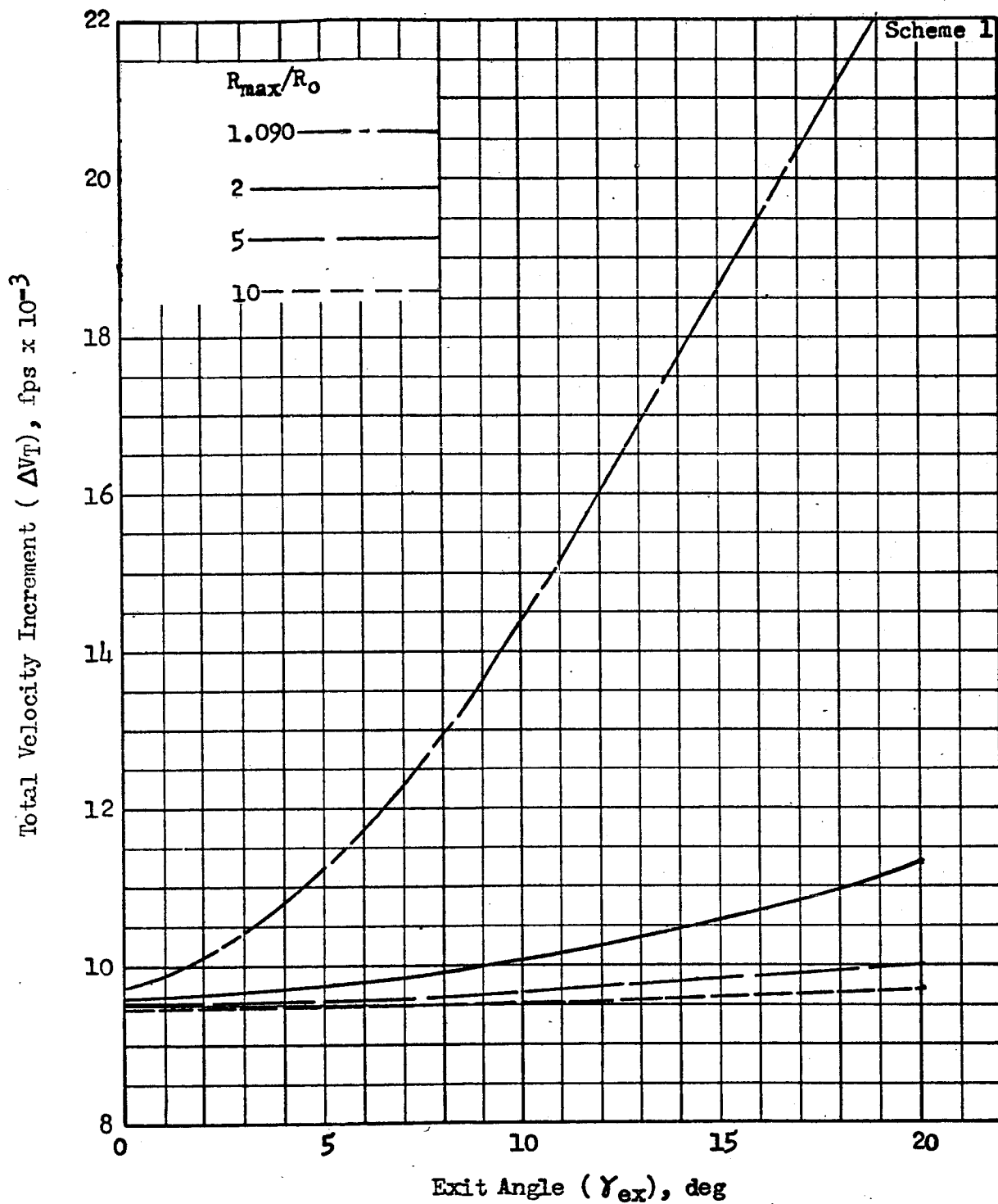


Fig. 153. Total Velocity Requirements for Establishing a 300-n mi Orbit at Venus, $V_{ex} = V_p = 33,217$ fps, Scheme 3.

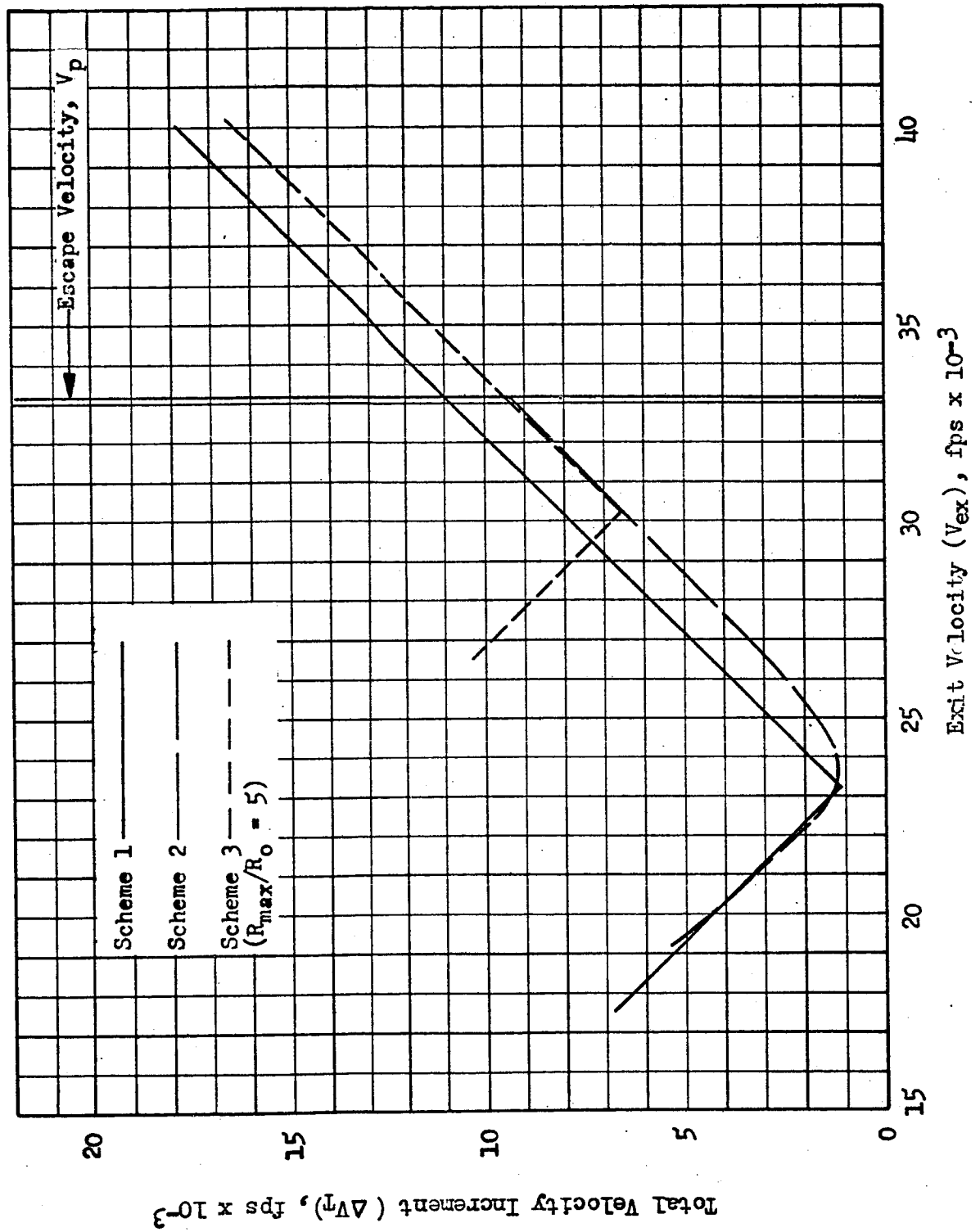


Fig. 1.15, Summary of Impulsive Velocity Requirements for Establishing a 300-n mi Orbit at Venus, $\gamma_{ex} = 5$ degrees

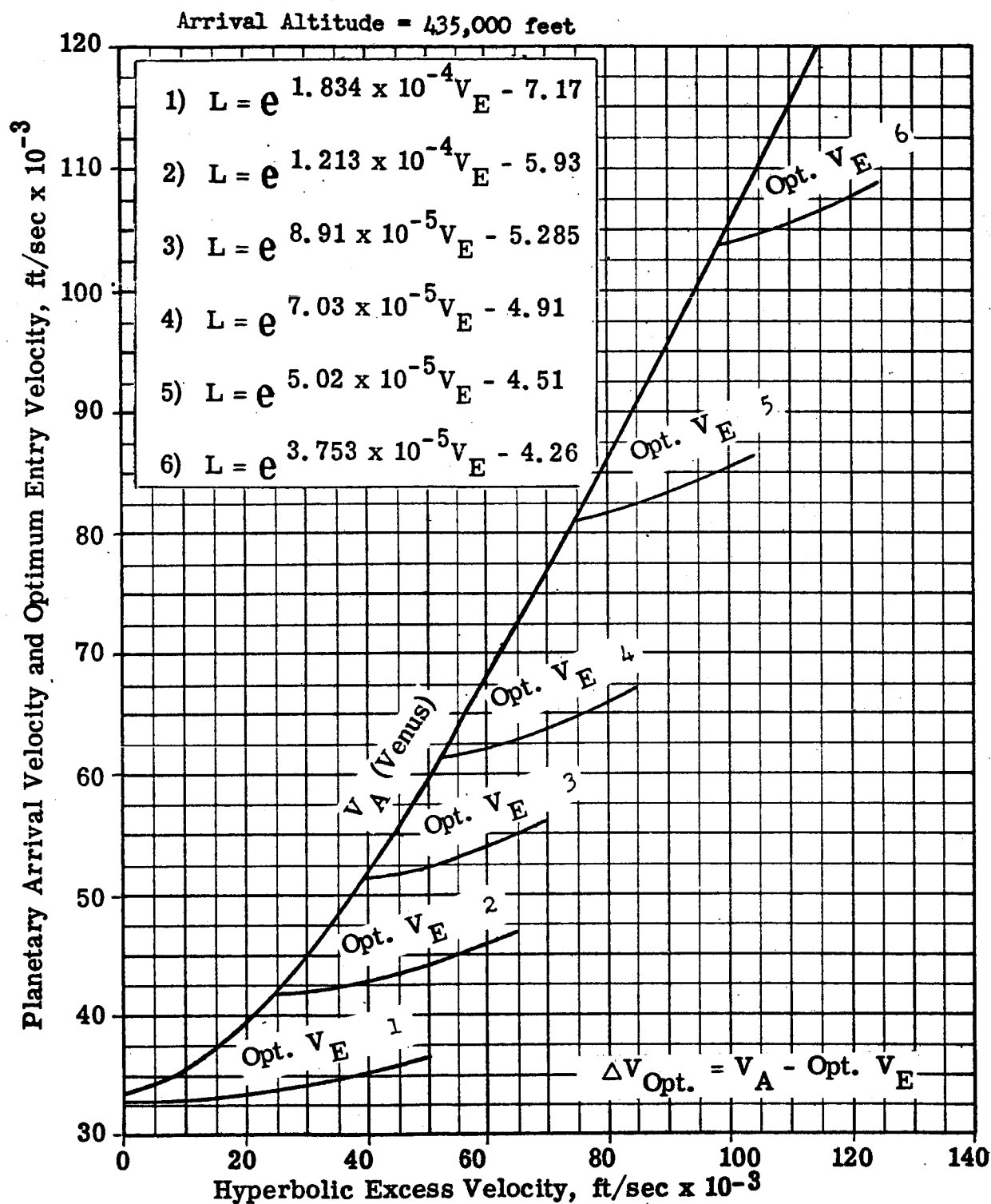


Fig.155. Optimum Propulsive ΔV (Impulsive) for Venus Entry of Propulsive/Aerodynamic Systems.

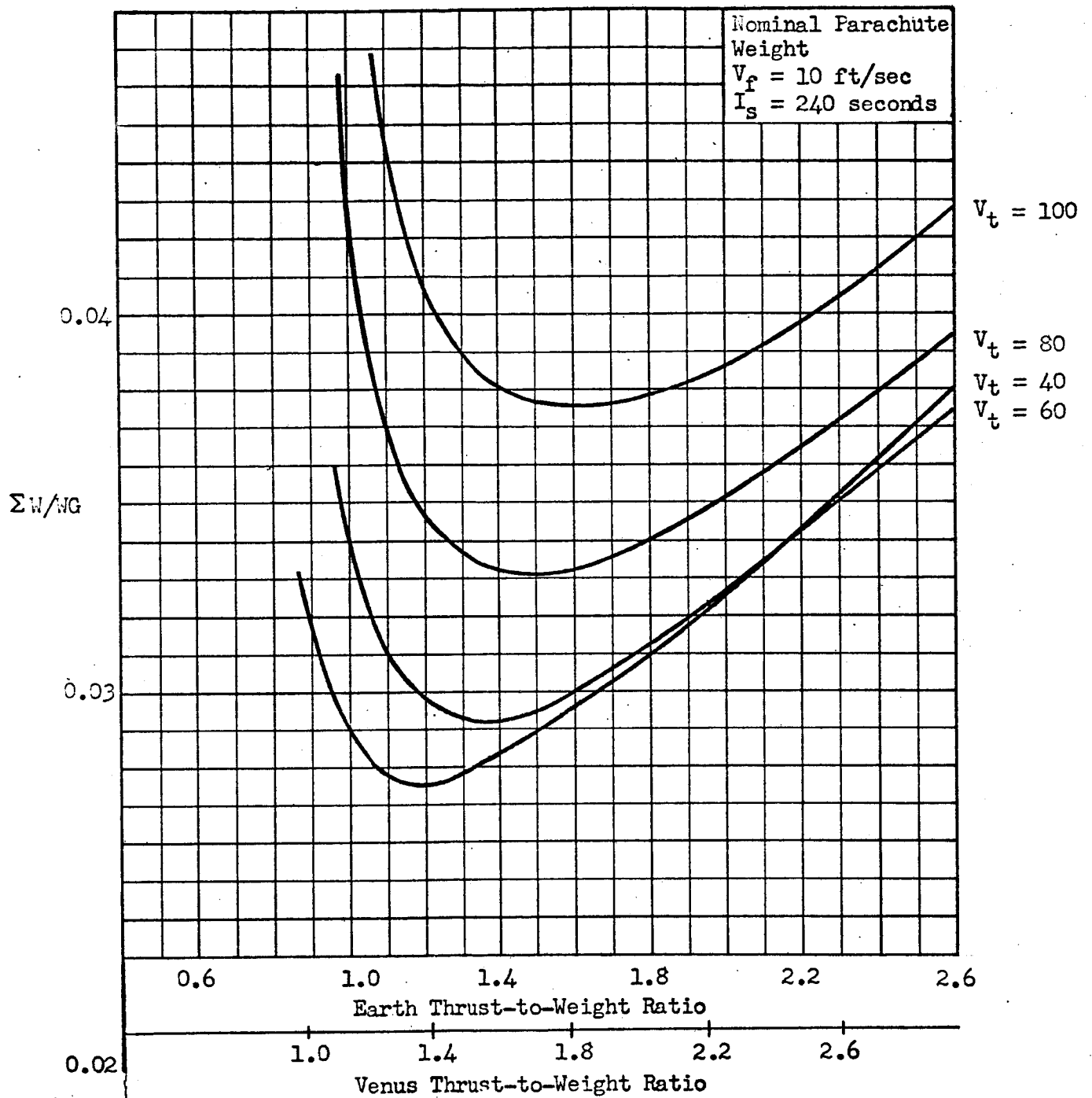


Figure 156 . Effect of Parachute Terminal Velocity
and Rocket Thrust-to-Weight On Pararocket
System Weight For a Venus Landing

in Figure 157, and the effect of raising the impact velocity to 25 ft/sec is illustrated in Figure 158. If the parachute system weight is increased by 50 percent, the system is only slightly heavier, and optimizes at a terminal velocity of 50 ft/sec and a slightly higher F/W.

In Figure 159, the optimum total system weights are presented as a function of V_T . In Figure 160, the optimum Earth F/W values are given. For a design impact velocity of 10 ft/sec and nominal weight assumptions, the optimum V_T and F/W values are 42 ft/sec and 1.22 respectively as shown in Figure 159 and 160.

If the design impact velocity is increased to above 25 ft/sec, the optimum terminal velocity shifts to below 40 ft/sec and the optimum F/W is less than one. (The computer program analysis utilized in this study was restricted to a local $F/W \geq 1$; therefore, the optimization of 25 ft/sec impact velocity system was not completed.) With the optimum terminal velocity below 40 ft/sec, and a 25 ft/sec impact velocity, the ΔV requirement of the rocket is small. It would seem more reasonable to allow the parachute to perform the entire retro task since the weight penalty for this nonoptimum system would be very small.

Parachute/Retrorocket/Impact Device System

The parachute terminal velocities and F/W values for optimum Venus landing pararocket systems are presented in Figure 161. The weights of these systems, along with the weights of parachutes and frangible-tube impact devices, are shown in Figure 162. The weights of two types of overall landing systems, one comprised of a parachute and impact device, and the other, of a pararocket and impact device, are presented in Figure 163.

The results indicate that the pararocket and frangible-tube system is lighter for design impact velocities up to 25 ft/sec; for a higher design V_F , the parachute and frangible-tube system is lighter. The minimum-weight system has an impact velocity of approximately 40 ft/sec, uses the parachute and frangible-tube device, and has an approximate system weight of 1.8 percent of the landing vehicle gross weight.

System Selection

For impact velocities below approximately 25 ft/sec, a pararocket combination is lighter than a parachute. The optimum system for a Venus landing, based on a 10 ft/sec impact velocity, is a pararocket with the rocket F/W at 1.2

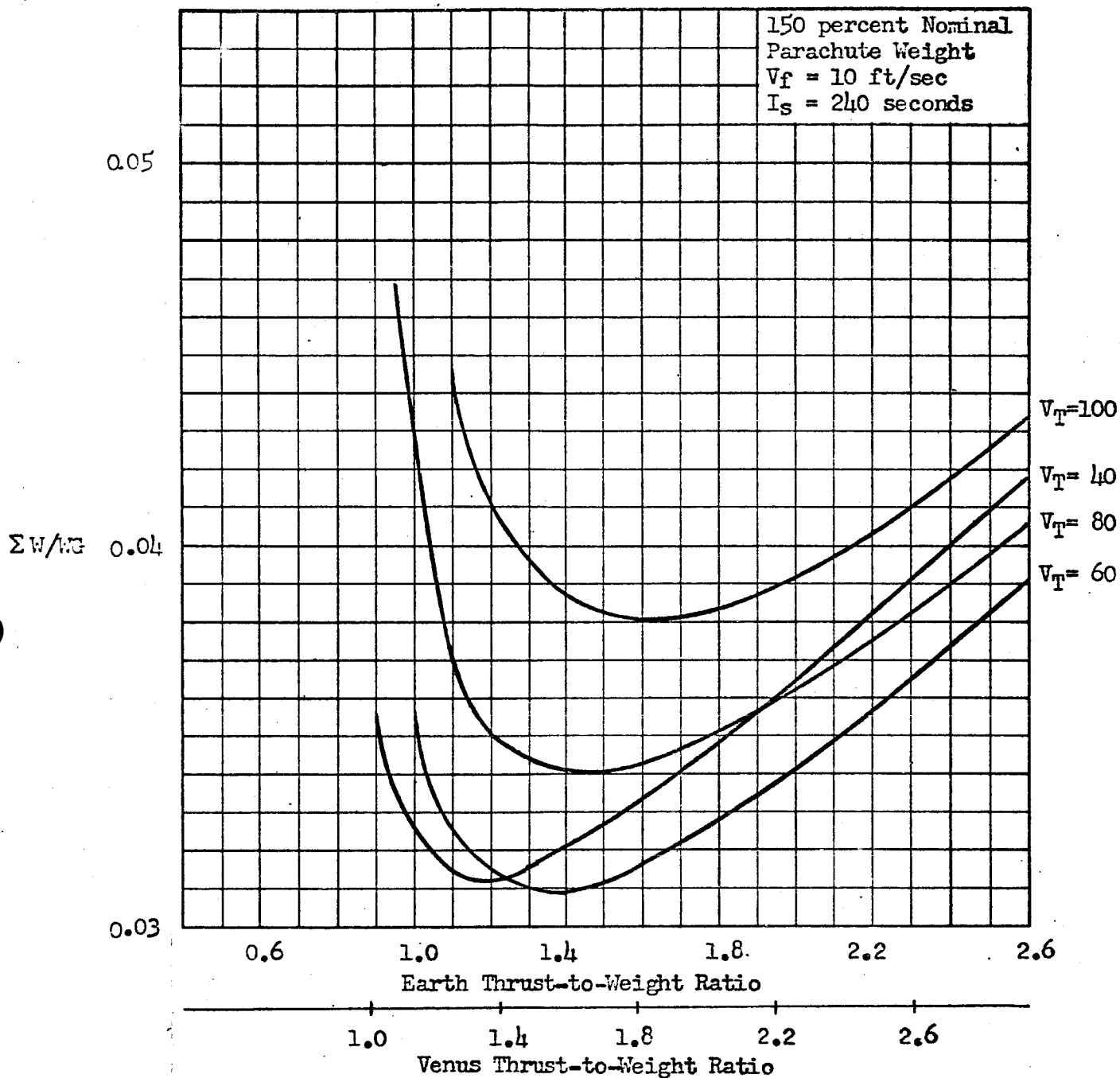


Figure 157. Effect of Parachute Terminal Velocity and Rocket Thrust-to-Weight on Pararocket System Weight for a Venus Landing

ROCKETDYNE
A DIVISION OF NORTH AMERICAN AVIATION, INC.

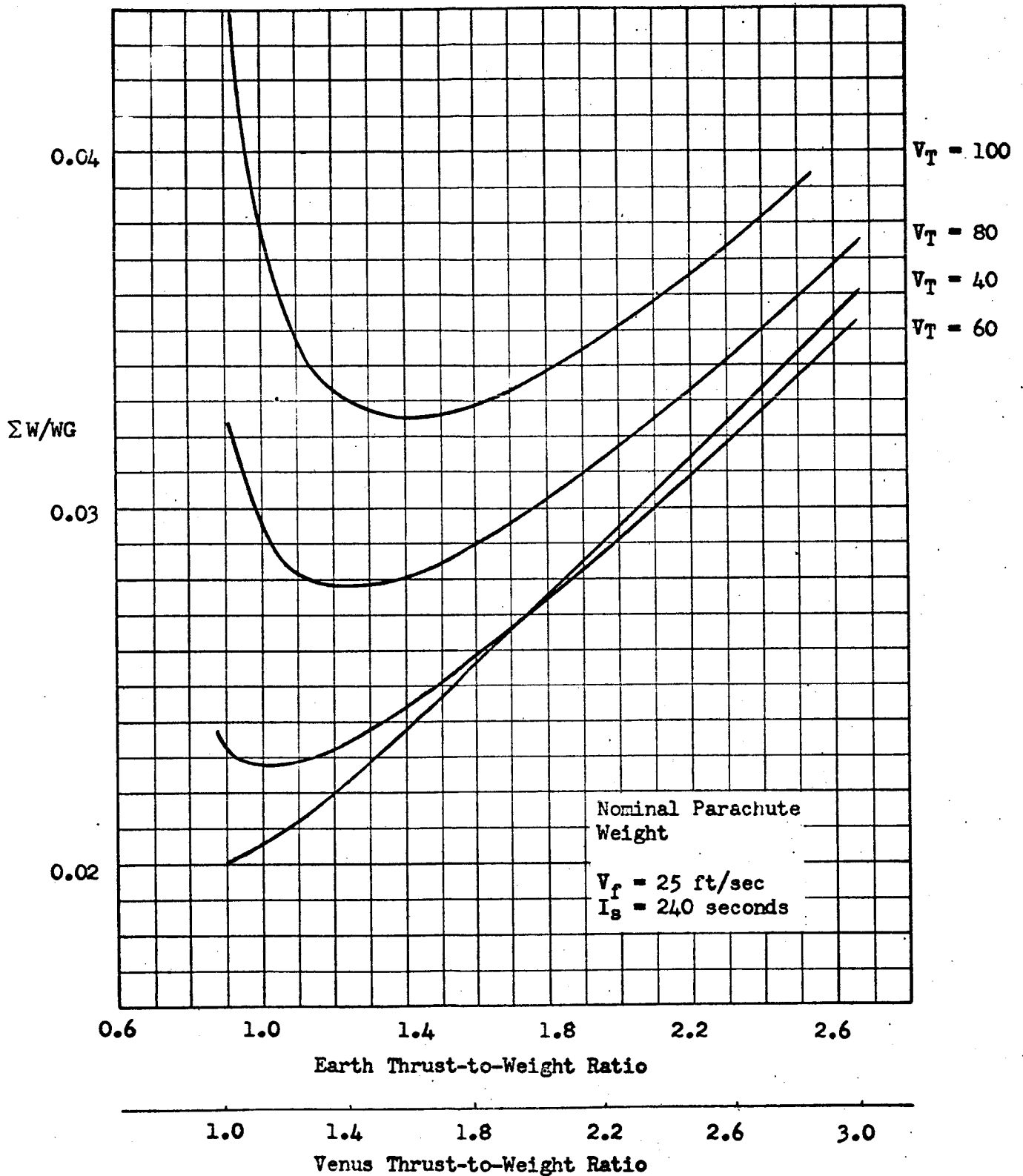


Figure 158. Effect of Parachute Terminal Velocity and Rocket Thrust-to-Weight Ratio on Pararocket System Weight for a Venus Landing

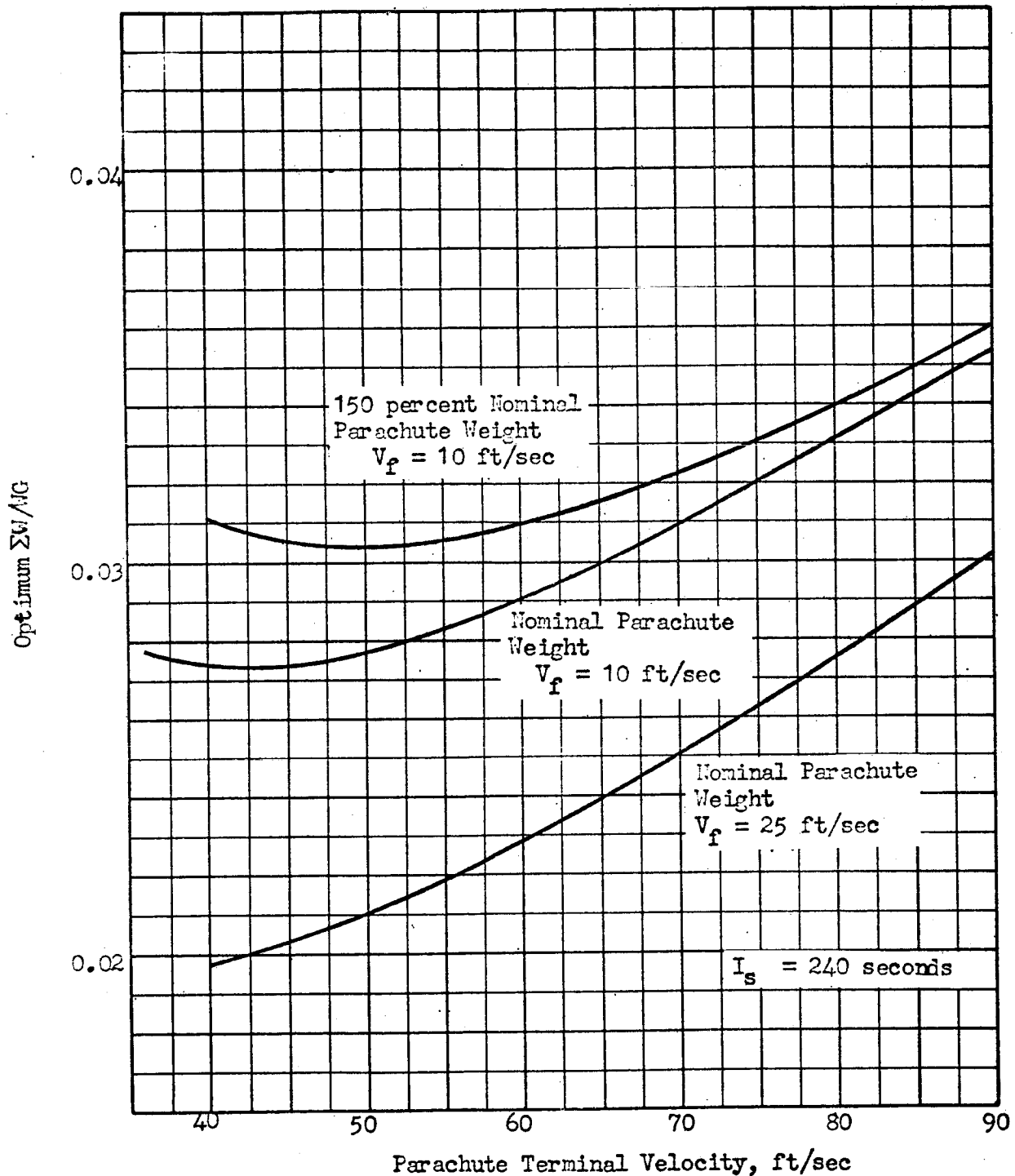


Figure 159. Optimum Pararocket System Weight Versus Parachute Terminal Velocity for a Venus Landing

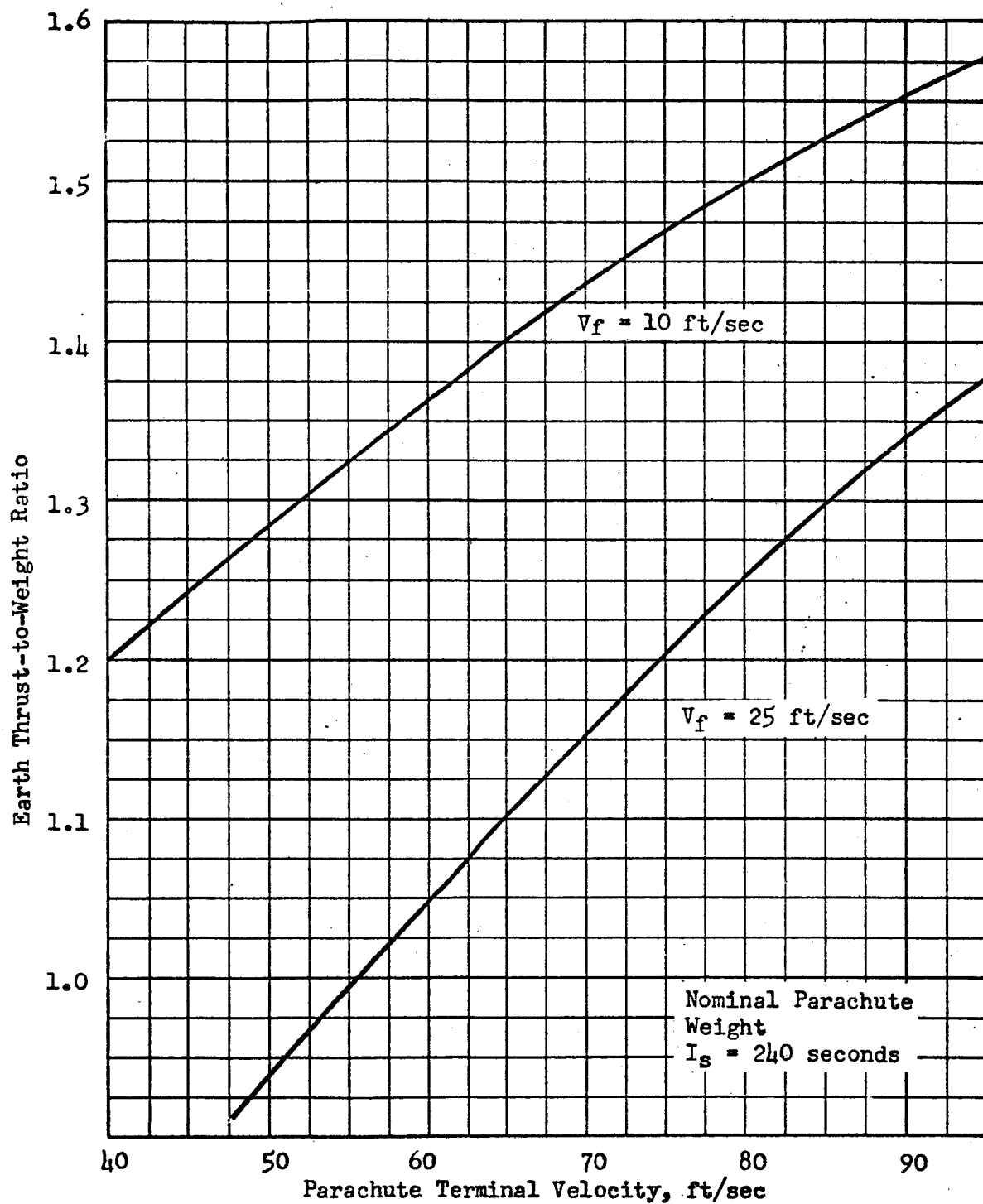


Figure 160. Optimum Earth Thrust-to-Weight Ratio Vs. Parachute Terminal Velocity for a Venus Landing

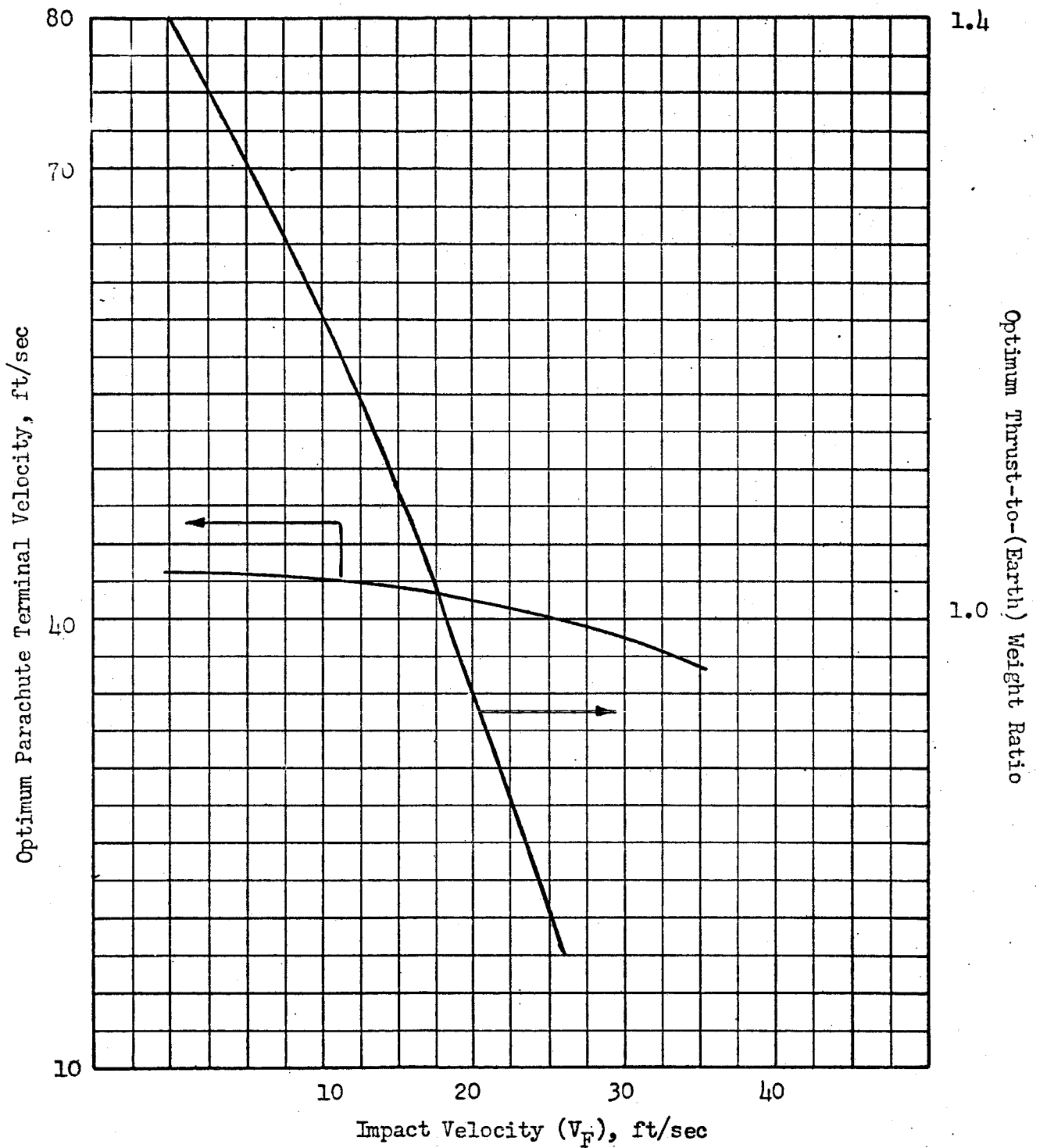


Figure 161. Optimum Terminal Velocity and Rocket Thrust-to-Weight Ratio: Pararocket Retro System (Venus)

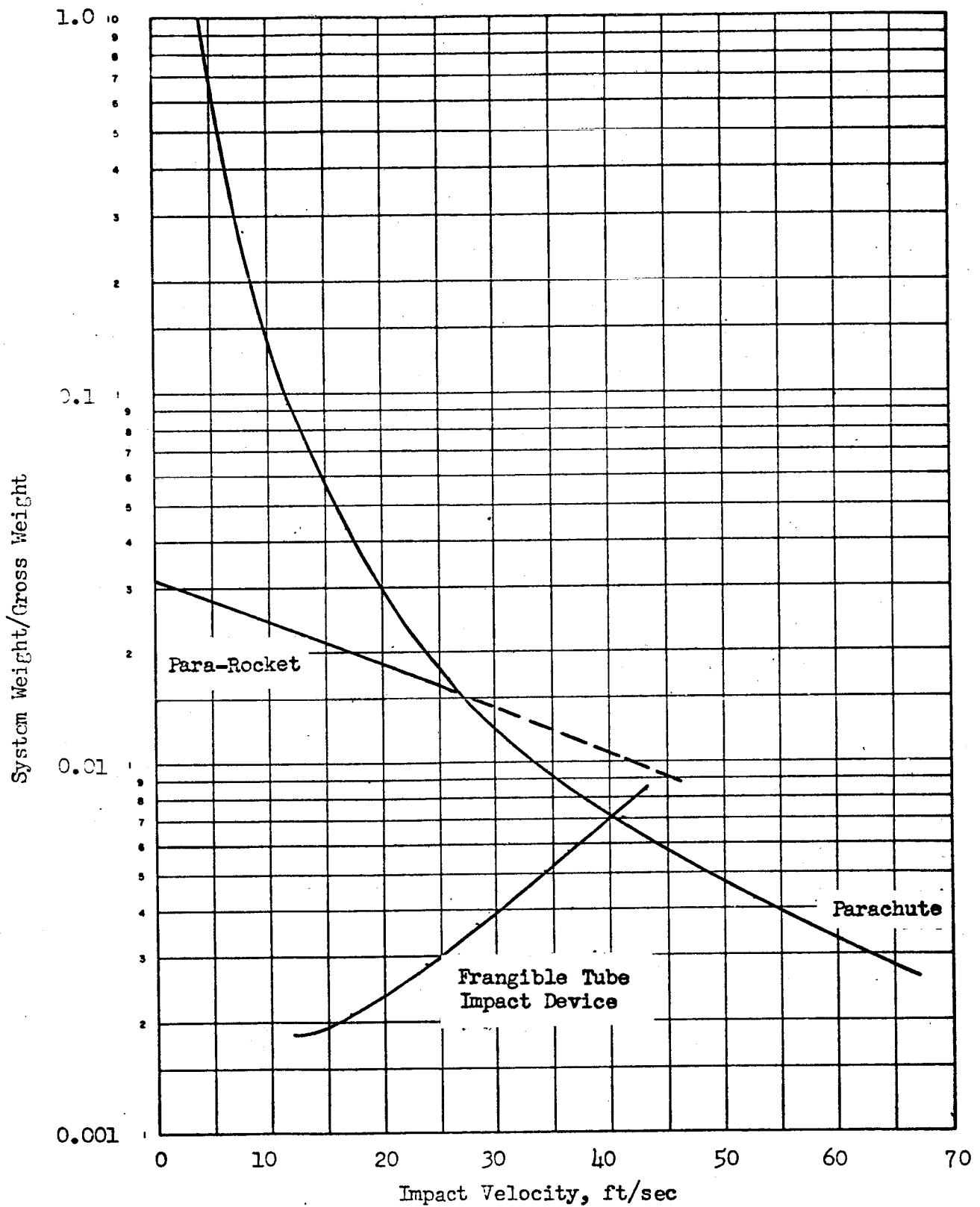


Figure 162. Landing System Weight (Venus)

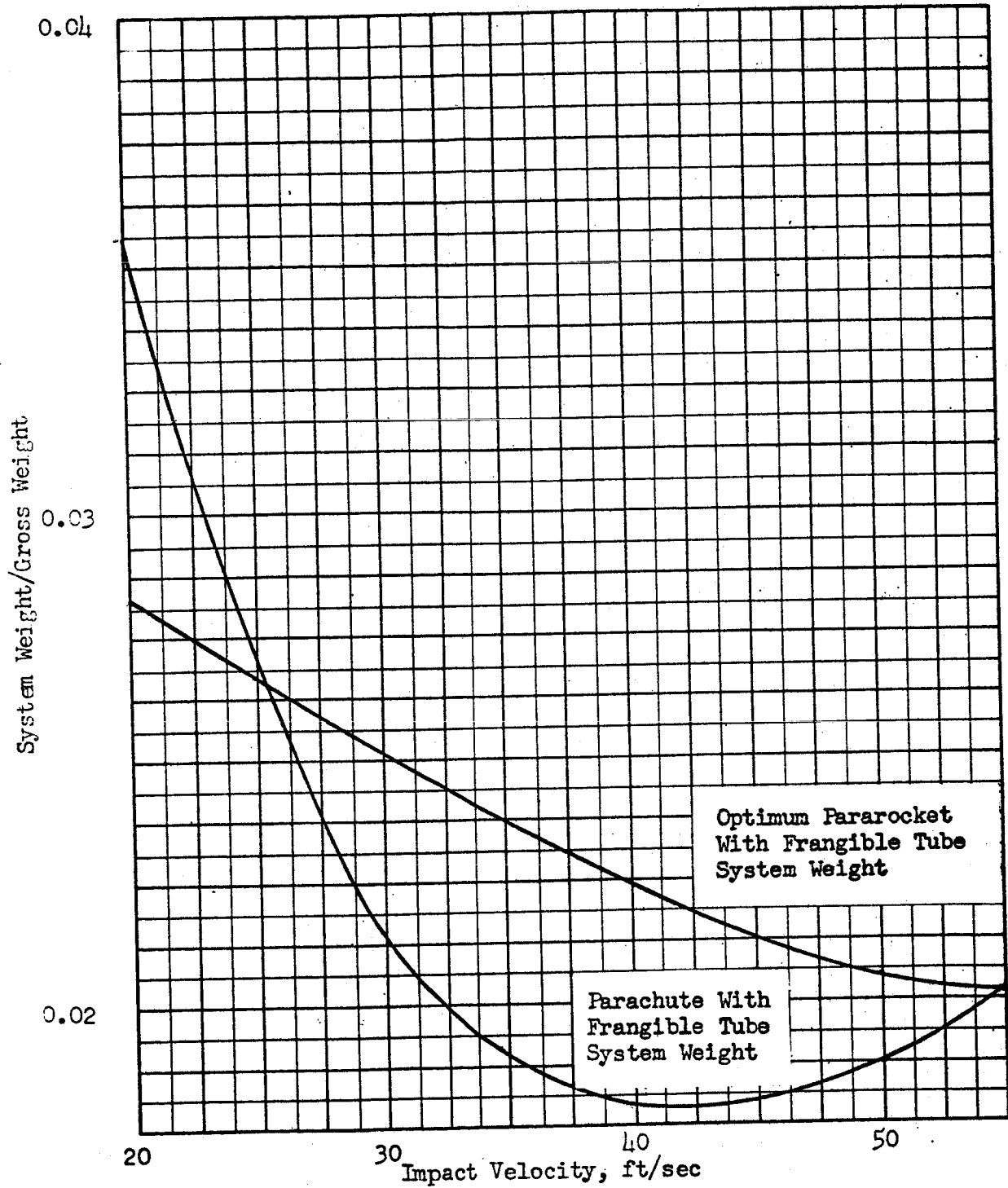


Figure 163. Optimization of Combined Venus Landing System

and the parachute terminal velocity at 40 ft/sec. The optimum pararocket constitutes 2.7 percent of the landed gross weight.

If impact velocity is unrestricted, the optimum landing system is a parachute, with terminal velocity equal to 42 ft/sec, in conjunction with a frangible-tube impact device. The overall system represents 1.8 percent of the landed weight.

A summary of the minimum-weight systems for the optimum impact velocity, and for impact velocities of 10 ft/sec and 25 ft/sec, is presented in Table 36.

TABLE 36

COMBINED SYSTEM WEIGHTS

System	Configuration	Impact Velocity (V_F), ft/sec	Percent Gross Weight
Minimum Weight	Parachute/Impact Device	42	1.8
Limited V_F	Pararocket/Impact Device	10	3.2
Limited V_F	Pararocket/Impact Device	25	2.7
Limited V_F	Parachute/Impact Device	10	5.0
Limited V_F	Parachute/Impact Device	25	2.7

VENUS TAKEOFF PROPULSION REQUIREMENTS

Takeoff from the planet Venus is a propulsive maneuver made particularly difficult by the high drag resistance and poor rocket performance experienced at low altitudes in the dense Venusian atmosphere. Integrated trajectories

for Venus takeoff to a 300-n mi circular planetary orbit were computed to determine the propulsion requirements for performing the takeoff maneuver. An O_2/H_2 vehicle was assumed in all cases, and the launch was assumed to take place in the direction of planetary rotation at the planetary equator. A conventional, thrust-parallel-to-velocity maneuver, described in greater detail in an earlier discussion of Mars takeoffs, was employed; the vehicle drag characteristic, shown as Curve A of Figure 134, was also obtained from the previous analysis.

Because of the high ideal velocity requirement of the mission, 2, 3, and 4 stage vehicles were utilized for the Venus takeoff. First stage thrust-to-(Venus) weight ratios of 1.3 to 1.7 were considered. In most cases, upper stage thrust-to-weight ratios were set equal to first stage thrust-to-weight ratios. For the two stage vehicle, however, alternate second stage thrust-to-weight ratios were also considered. The stage propellant fraction was assumed to be 0.90.

The characteristics of the engine systems used in this study are presented in Table 37. The engine systems considered are representative of pumped designs using O_2/H_2 propellants.

TABLE 37
ENGINE PERFORMANCE

	Venus Takeoff Engines		
	First Stage	Upper Stages	
Chamber Pressure, psia	1000	1000	1000
Nozzle Expansion Area Ratio	5:1	50:1	10:1
Vacuum Specific Impulse, seconds	381	435	403
Surface Specific Impulse, seconds	310	-277	260

The 50:1 expansion area ratio engine was used in the second stage of the 2-stage vehicles, the third stage of the 3-stage vehicles, and the third and fourth stages of the 4-stage vehicles. The 10:1 expansion area ratio engine was used as a second stage engine in both the 3 and 4-stage vehicles.

The results for the analysis of Venus takeoff to 300 n mi orbit are presented in Table 38. This table shows the thrust-to-weight ratio of each stage and the corresponding ideal velocity requirement necessary for mission accomplishment. The payload which would result if each stage had a propellant fraction of 0.9 is also presented.

A particularly interesting result which emphasizes the influence of the dense Venusian atmosphere is that the ideal velocity requirement for the 4-stage vehicle is the lowest value of the entire list. Generally, the presence of a large number of stages, because it implies a comparatively low time-averaged thrust-to-weight ratio, yields a high ideal velocity requirement for a given mission. In this case, however, high acceleration increases drag losses so rapidly that it is more efficient to operate at lower thrust-to-weight ratios and to tolerate higher gravity losses. The result suggests that a throttleable engine (operated regressively until the vehicle passes above the dense portion of the atmosphere) might be best suited to the Venus takeoff mission.

It should be emphasized that only one type of trajectory was considered in this study. Other trajectory types might result in a more optimum flight path and consequently higher payloads than those presented. The ideal velocity requirements presented in this study therefore are not necessarily as low as those that might be determined by more detailed analysis.

TABLE 38

VENUS TAKE-OFF VEHICLE PERFORMANCE

Gross Weight = 100,000

	Thrust-to-Weight				Mission Ideal Velocity Requirement - ft/sec	Payload - LB ($\Delta P_{all\ stages} = 0.90$)
	1st Stage	2nd Stage	3rd Stage	4th Stage		
2 Stages	F/W = 1.3	F/W = 0.77	---	---	39,800	1510
	F/W = 1.3	F/W = 1.30	---	---	39,000	1670
	F/W = 1.3	F/W = 2.20	---	---	39,200	1620
	F/W = 1.5	F/W = 0.87	---	---	40,100	1460
	F/W = 1.5	F/W = 1.50	---	---	39,800	1510
	F/W = 1.5	F/W = 2.49	---	---	40,100	1450
3 Stages	F/W = 1.3	F/W = 1.3	F/W = 1.3	---	40,000	2170
	F/W = 1.5	F/W = 1.5	F/W = 1.5	---	39,700	2250
	F/W = 1.7	F/W = 1.7	F/W = 1.7	---	40,000	2180
4 Stages	F/W = 1.5	F/W = 1.5	F/W = 1.5	F/W = 1.5	39,800	2940

REFERENCES

1. Eggers, A. J., and Wong, T. S., "Motion and Heating of Lifting Vehicles During Atmosphere Entry", ARS Journal, Volume 31, No. 10, October 1961.
2. R-3923, Space Transfer Phase Propulsion Systems Study, Final Report, Rocketdyne, A Division of North American Aviation, Inc., Canoga Park, California, February 1963.
3. Kirby, F. M., Propulsion for Interplanetary Space Missions, I.A.S. Paper No. 62-85, I.A.S. Meeting, New York, New York, January 1962.
4. R-3208, Propulsion Requirements for Space Missions, Rocketdyne, A Division of North American Aviation, Inc., May 1961.
5. Fisher, L. J., Landing Impact Dissipation Systems, NASA TND 975, December 1961.
6. LAPM 62-104, Propulsion Requirements for Soft Landing in Extraterrestrial Environments, First Quarterly Progress Report, Rocketdyne, A Division of North American Aviation, Inc., July 1962.
7. A Study of Interplanetary Transportation Systems, Lockheed, Missiles and Space Division; Sunnyvale, California, June 1962.